The University Of Sheffield.

Thesis Title:

Endothelial HIF2-α at the crossroads of obesity and atherosclerosis.

By:

Daniela Pirri

A thesis submitted in partial fulfilment of the requirements for the degree of Doctor of Philosophy

The University of Sheffield
Faculty of Medicine, Dentistry & Health
Department of Infection, Immunity and Cardiovascular Disease

Submission Date
September 2020

Acknowledgments

I would like to thank my supervisors, Professor Paul Evans and Dr Maria Fragiadaki for all their support, advice and encouragement during my PhD. I would also like to thank Professor Weiping Han for all the support during my year of attachment at the A*STAR in Singapore. I also thank Dr Mark Ariaans and Carl Wright from the technical staff of the Royal Hallamshire Hospital in Sheffield for their help with animal works. I would like also to thank Dr Scott Allen for its inestimable help and support for the experiments performed at SITraN.

I thank all the present and past members from the Paul Evans lab in Sheffield for all the technical and emotional support they offered me during the past four years. A special thank goes to Celine, Jovana, Blanca, Hannah, Kajus, Ziqi and George. A very special thanks to Merete and Lindsay for being good colleagues in first instance and then great and lovely friends. You girls truly meant so much to me during these years. A special thank also to all the other Sheffield friends that made this experience truly amazing; particularly thank to Laura, Ruggero, Chiara, Anjana, Oliver, Andreas and Margo. I also thank all the member of the Han's laboratory in Singapore for how they welcomed me and made me feel beloved in Singapore. They made of Singapore a fantastic experience. Thanks to the Makan Kakis group: Joy, QianYi, Zhi Whi, Raymond and Shawn.

I also thank all my friends in Italy for always being next to me, for supporting me in the most complicated times and for always believing in me.

Finally, I thank my family in Italy for all the love given to me and for never letting me give up on my dreams.

Abstract

Obesity and related metabolic abnormalities are drivers of atherosclerosis and major contributors to worldwide cardiovascular disease and mortality. Atherosclerosis is a chronic inflammatory disease of the vascular wall that preferentially develops at bends and curvatures of the arteries. At these sites, endothelial cells (ECs) are exposed to flowing blood generating low wall shear stress (WSS). The transcription factor hypoxia-inducible factor 2- α (HIF2-α) controls vascular development but its potential role in cardiovascular disease is unknown. Here I investigated the potential role of HIF2-α in the crosstalk between obesity and focal atherosclerosis. En face staining of murine aorta and immunoblotting of cultured porcine aortic endothelial cells (PAECs) show that HIF2-α is activated by both high and low WSS. Inducible deletion of HIF2-α from ECs significantly increased lesion formation in a murine model of hypercholesterolemia, indicating an atheroprotective function. At a mechanistic level, HIF2-α maintained mitochondrial function in ECs which prevented the accumulation of pro-atherogenic senescent cells. This protective pathway was lost in obese mice (leptin knockout or high fat diet) via triglyceride-mediated inhibition of HIF2-α. In conclusion, endothelial HIF2-α protects from atherosclerosis by promoting endothelial cell metabolism which reduces cellular senescence at sites of disturbed flow. This novel protective pathway is inhibited in obesity. My results have important implications for therapeutic strategies to reduce endothelial dysfunction and atherosclerosis in obesity.

Table of Contents

List of figures

List of table

List of abbreviation

2-OG - 2-oxoglutarate
AAV - adeno associated virus
ACE - angiotensin converting enzyme
ACER2 – alkaline ceramidase 2
ADM - adrenomedullin
AF - alexa fluor
AGE - advanced glycated end products
AKT – protein kinase B
ANGPTL4 - angiopoietin-like 4
AP1- activator protein 1
ApoE - apolipoprotein E
ARNT – aryl hydrocarbon receptor nuclear translocator
B2M - beta-2-microglobulin
bHLH – basic helix loop helicx
BL6J - C57Black6/J mice
C-TAD – C-terminus domain
CB - carotid body
CCND1- cyclin D1
CCNG2- cyclin G2
CD31 - cluster of differentiation 31
CDH5 - cadherin 5 (VE-Cadherin)
cDNA – complementary DNA
CFD - computational fluid dynamics
CO2 - corbon dioxide
CoA – coenzyme A
COX – cytochrome oxidase
CPT1 – carnitine palmitoyltransferase I
CTGF - cellular communication network factor 2
CVDs - cardiovascular diseases
D.F. - dilution factor
DAP - diastolic blood pressure
DAPI - 4′,6-diamidino-2-phenylindole
DEAE – diethylaminoethyl
DLL4- Delta Like Canonical Notch Ligand 4
DMEM - Dulbecco's Modified Eagle's Medium
DMOG - N-(methoxyoxoacetyl)-glycine methyl ester
dNTP – deoxynucleoside triphosphates
E2F1 – retinoblastoma-associated protein 1
ECAR - extracellular acidification rate
ECGF - endothelial cells growth factor
ECs - endothelial cells

EDTA – ethylenediaminetetraacetic acid
EFNB2- ephrin B2
EGFR – epidermal growth factor receptor
EGLN1 – egl-9 family hypoxia-inducible factor 1
EndMT - endothelial to mesenchymal transition
eNOS - endothelial nitric oxide synthase
EPAS1 - endothelial PAS 1
EPCs - endothelial progenitor cells
EPO - erythropoietin
ESELE- selectin E
FABP – fatty acid binding protein
FAO - fatty acid oxidation
FATP – long-chain fatty acid transporter protein
FBS - fetal bovine serum
FFAs - free fatty acids
FIH - factor inhibiting Hypoxia-inducible factor
FISH - fluorescent in situ hybridization
FITC - fluorescein isothiocyanate
Flk1 – vascular endothelial growth factor receptor 2
Flt1 – vascular endothelial growth factor receptor 1
GATA4- Gata binding protein 4
GLS1 - glutaminase
GSEA - gene set enrichment analysis
HCC – hepatocelluar carcinoma cells
HDAC – histone deacetylase
HDL - high density lipoprotein
HEK293 - Human embryonic kidney 293 cells
HFD - high fat diet
HIF-α - Hypoxia-inducible factor alpha
HIF2-$\alpha^{fl/fl}$ - Hypoxia-inducible factor 2-alpha flox/flox
HRE – hypoxia responsive element
HRGP - histidine-rich glycoprotein
HSS -high shear stress
HUVECs - human umbilical vein endothelial cells
IDT - integrated DNA technologies
IgG - immunoglobulin G
IL-6 - interleukin 6
IL-8 – interleukin 8
KD - knock-down
KLF2 - kruppel-like factor 2
KO - knock-out
LDL - low density lipoproteins
LOSS - low oscillatory wall shear stress

LSS - low shear stress
MAP - mean blood pressure
MCP1 – monocyte chemoattractant protein 1
MFI - mean fluorescent intensity
MI - myocardial infarction
MOI - multiplicity of infection
mRNA - messanger RNA
MSigDB - molecular signature database
mTORC - mammalian target of rapamycin complex
N-TAD - N-terminus domain
NAFLD - non-alcoholic fatty liver disease
NDUFA4L2- NADH dehydrogenase 1 alpha subcomplex 4l2
NF-κB - nuclear factor- κB
NIDDM - insulin-independent diabetes mellitus
NLS – nuclear localization signal
NMR – nuclear magnetic resonance
NO - nitric oxide
NQO1- NAD(P)H Quinone Dehydrogenase 1
Nrf2 -Nuclear factor erythroid 2- related factor
OA - oleic acid
Ob/+ - heterozygous mice with leptin deletion
Ob/ob - obese/obese, mice with leptin deletion
OCR - oxygen consumption rate
ODDD – oxygen dependent degradaton domain
ORO - Oil red O
oxLDL - oxidised low density lipoproteins
OXPHOS - oxidative phosphorylation
P53 – tumour protein 53
PAECs -porcine aortic endothelial cells
PAI1 – endothelial plasminogen activator inhibitor
PAS – Period/ARNT/Single-minded
PBS - phosphate buffer saline
PBST - phosphate buffer saline-tween 20
PCC - pheochromocytoma
PCSK9 – proprotein convertase subtilisin/kexin type 9
PFA – paraformaldehyde
PFKFB3- 6- phosphofructo-2-kinase/fructose-2,6-biphosphatase 3
PGL - paraganglioma
PHDs - prolyl hydroxylases
PI3K -phosphatidylinositol-4,5-biphosphate 3-kinase
POMC - pro-opiomelanocortin
qRT-PCR – quantitative real time-polymerase chain reaction
RBC - red blood cell

RCC – renal cell carcinoma
RNA – ribonucleic acid
ROS - reactive oxygen species
SAP - systolic blood pressure
SASP - senescent-associated secretory phenotype
SDH – succinate dehydrogenase
SDS – sodium dodecyl sulfate
SEM - standard error mean
SFN - sulforaphane
shRNA - small hairpin RNA
SIN3A – hystone deacetyase complex subunit Sin3a
SINHCAF – SIN3A-HDAC complex associated factor
siRNA - small interfering RNA
SMA - smooth muscle cells
SNAIL- snail family transcriptional repressor
SNP – single nucleotide polymorphism
SP1- Sp1 transcription factor
STZ - streptozotocin
T1DM - type 1 diabetes mellitus
T2DM - type 2 diabetes mellitus
TAE – tris acetate-EDTA
TAZ - transcriptional co-activator with PDZ-binding motif
TBST – tris buffered saline 0.1% tween
TCA - tricarboxylic acid
TFPI – tissue factor pathway inhibitor
TFs - transcription factors
Tie-2 – angiopoietin 1 receptor
TU - transducing units
TWIST1-Twist Basic Helix-Loop-Helix Transcription Factor 1
VCAM1- Vascular cell adhesion molecule 1
VEGFR - vascular endothelial growth factor receptor
VHL - von Hippel Lindau protein
VLDL - very low density lipoprotein
VSMC - vascular smooth muscle cells
WBCs - white blood cells
WSS - wall shear stress
YAP - Yes-associated protein

Chapter 1. Introduction

Atherosclerosis

Pathogenesis

Atherosclerosis is a chronic inflammatory disease characterised by thickening of the arterial wall with the formation of a lipid-enriched plaque. It is a major cause of cardiovascular diseases (CVDs) and epidemiological studies estimate that around 17 million deaths are caused by CVDs each year (WHO, 2018). Atherogenesis, the generation of atheroma or plaque, silently begins when the monolayer endothelial cells (ECs) lining the inner arterial wall, undergo pathogenic changes leading to higher permeability and an inflammatory phenotype that allows leukocytes to adhere on their surface of the vessel wall and penetrate underneath the EC layer (Libby, 2012). For instance, white blood cells (WBCs) and lipoproteins particles usually do not associate with the ECs as they are carried through blood flow. When a multiplicity of risk factors coexist - such as diabetes, hyperlipidaemia and hypertension - arterial ECs express surface adhesion molecules that can interact with and capture the WBCs (Cybulsky and Gimbrone, 1991). Additionally, lipoproteins can pass through the EC layer and, by interacting with apolipoproteins from the apoB family, remain trapped underneath the endothelium where they are oxidized (Tabas, Williams and Borén, 2007), to form oxidised low density lipoproteins (ox-LDL). In addition to passive diffusion, a recent *in vivo* work showed that LDL actively access to the endothelium via the scavenger receptor class B type 1 (SR-B1). SR-B1 binds the LDL and recruits the guanine nucleotide exchange factor dedicator of cytokinesis 4 (DOCK4), which promotes LDL/SR-B1 internalisation (Huang *et al.*, 2019).

Meanwhile, vascular smooth muscle cells (VSMC) from the tunica media migrate into the sub-endothelial tunica intima, further contributing to inflammation while also produce collagen to form a fibrous cap, figure 1.1 (Lutgens *et al.*, 1999), which delays plaque rupture.

As the inflammatory process progresses over time, infiltrating macrophages engulf ox-LDL and eventually turn into large foam cells (Goldstein and Brown, 1977), which give rise to a fatty streak. Furthermore, the foam cells can die, exacerbating the inflammatory process to result in a hypoxic highly pro-inflammatory environment with a central necrotic core (Tabas, 2010).

All these cell types contribute to the atheromatous plaque (or atheroma), and plaque stability is determined by the relative abundance of these constituents. Plaques can rupture, the

release of their content into the bloodstream followed by the activation of platelet coagulation confers a high risk of thrombosis. Despite the risk of an atheroma partially or fully occluding the vascular lumen, thrombosis remains the main complication in plaque progression (Kolodgie FD, Burke AP, Farb A, Gold HK, Yuan J, Narula J, 2001). Nevertheless, sometimes thrombi can occur in the presence of fissures of the plaque, without plaque rupture (Van Der Wal *et al.*, 1994). Plaque with high content of smooth muscle cells and proteoglycans can erode on their luminal surface by endothelial denudation (Kolodgie *et al.*, 2004; White, Newby and Johnson, 2016). However, this process remains enigmatic and requires further investigation.

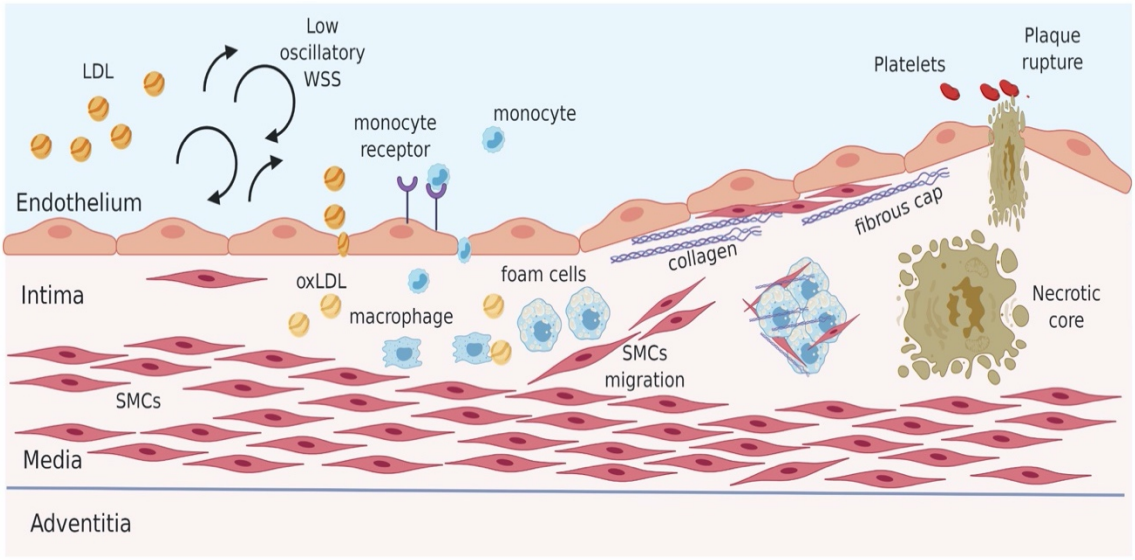

Figure 1. 1 The cellular basis of atherogenesis

Atherogenesis occurs at site of the vasculature exposed to disturbed flow (low oscillatory WSS). Low density lipoproteins (LDL) particles penetrate the endothelium and accumulate in the subendothelial layer. LDL undergo qualitative changes by oxidation (oxLDL). *In situ*, activated inflammatory process recruit monocytes from the blood flow. Monocytes differentiate into tissue resident macrophages and initiate the digestion of oxLDL, transforming into foam cells. During this inflammatory process, smooth muscle cells (SMCs) from the tunica media migrate into the intima and produce collagen to form a fibrous cap. Plaque components can undergo necrosis, creating an highly inflammatory necrotic core. Plaques can break, releasing their content into the blood stream and activating platelets to initiate the coagulation cascade. Illustration was created using Biorender.com

Co-morbidities

Atheroma formation develops focally within arteries, yet endothelial dysfunction is induced by a multitude of systemic hormonal and molecular abnormalities. While some risk factors can be modified or prevented with lifestyle changes, others cannot, such as gender and ageing. Women have a lower risk of cardiovascular disease than men, an effect that is attributed to the endogenous oestrogens that protect women throughout life until the menopause (Iorga *et al.*, 2017). Nevertheless, both gender are exposed to the same classic risk factors and interestingly; smoking, hypertension and hypercholesterolaemia seem to have a more deleterious effect in women's cardiovascular health (Maas and Appelman, 2010). In addition, ageing is associated with a progressive loss of cardiovascular functions and with an increased risk in cardiovascular complications (North and Sinclair, 2012). Ageing results in an increased arterial thickening and endothelial dysfunction (Lakatta and Levy, 2003; Brandes, Fleming and Busse, 2005). The ageing of the endothelium is characterised by a decrease in nitric oxide (NO) production, thus impairing its protective effects on reducing proliferation and preventing cellular senescence (Vasa *et al.*, 2000; Collins and Tzima, 2011).

Among the risk factors that can be prevented by life style changes, smoking is one of the most important and it causes 10% of the deaths for CVD (Ezzati *et al.*, 2005). Interestingly, even in the presence of low cholesterol levels, cigarette smoking increased the risk of coronary heart disease (Blanco-Cedres *et al.*, 2002). Furthermore, despite women having a lower absolute risk of atherosclerosis and cardiovascular disease, cigarette smoking has an independent effect on increasing their cardiovascular risk (Kawachi *et al.*, 1994). Cigarette smoking contributes to cardiovascular disease via mechanisms that accelerate platelets turnover, promoting endothelial dysfunction and lipid oxidation (Yamaguchi *et al.*, 2000; Wolf and Baynes, 2007; Salahuddin, Prabhakaran and Roy, 2012).

Together with smoking, hypertension is one of the most potent risk factor for cardiovascular disease (Fuchs and Whelton, 2020). Hypertension promotes endothelial dysfunction via the generation of excessive reactive oxygen species, and the induction of inflammatory responses and mitochondrial dysfunction (Vecchione *et al.*, 2009; Widder *et al.*, 2009).Nevertheless, multiple drug therapies are now available for treating raised blood pressure; treatments that can effectively reduce cardiovascular events (Law, Morris and Wald, 2009).

To date, over 4 millions of people in the UK have been diagnosed with diabetes, of whom 90% have an obesity-associated type of diabetes (T2DM)(González *et al.*, 2009; Whicher, O'Neill and Holt, 2020). Over the past two decades, the prevalence of obesity has drastically increased in both the adult and the child population in the UK (Capehorn, Haslam and Welbourn, 2016). Diabetes induced dyslipidaemia with the greatest changes in lipidemic profile seen in the increased in triglyceride levels and the lowered HDL (Athyros *et al.*, 2018). In this scenario, hypertriglyceridemia always coexists with the presence of other lipid alterations (Hegele *et al.*, 2014; Rosenson *et al.*, 2014). Anti-dyslipidaemic therapeutic interventions act on lowering both LDL and TG, thus leading to inconclusive data on the direct effect of TG levels with CVD (Bansal *et al.*, 2007; Freiberg *et al.*, 2008; Faergeman *et al.*, 2009). However, patients with a low LDL profile and with hypertriglyceridemia have high risk of CVD (Bansal *et al.*, 2007; Freiberg *et al.*, 2008; Faergeman *et al.*, 2009). In addition, because of the complexity in lipid profile of obese and diabetic patients, epidemiological studies have shown a weaker association of TG to CVD when TG levels were adjusted for the total cholesterol and HDL values (Di Angelantonio *et al.*, 2009). In conclusion, despite dyslipidaemia being a hallmark for atherosclerosis, the complexity of the lipid profiles led to some degree of uncertainty in the relative risk associated with the different lipid fractions.

In addition, the inflammatory process characterising every step of atherogenesis, is associated with other co-morbidities such as obesity and diabetes (Beckman, Creager and Libby, 2002; Libby, 2012). Both type 1 diabetes mellitus (T1DM) and type 2 diabetes mellitus (T2DM) are associated with increased cardiovascular risk, myocardial infarction (MI), heart failure and macrovascular complications (Kannel and McGee, 1979; Stratton *et al.*, 2000; Bell, 2003). When T2DM clusters together with other pathologies such as dyslipidaemia, visceral obesity, insulin resistance and raised blood pressure among others, it is defined as metabolic syndrome. On one hand, it is known that diabetes participates in endothelial dysfunction and exacerbates atherosclerosis. As an example, hyperglycaemia contributes to endothelial pro-inflammatory signalling via activation of the NF-κB transcription factor, as well as by a PKC-mediated mechanism. Furthermore, hyperglycaemia increases the formation of reactive oxygen species (ROS) and the formation of advanced glycated end-products (AGE). On the other hand, obesity alters the physiology of the leptin signalling, an essential hormone in regulating the sensation

of hunger. Multiple studies have suggested that leptin enhances atherosclerosis (Bouloumie *et al.*, 1998; Loffreda *et al.*, 1998; Nakata *et al.*, 1999; Konstantinides *et al.*, 2001; Yamagishi *et al.*, 2001; Zarkesh-Esfahani *et al.*, 2001; Wu *et al.*, 2005; Wendt *et al.*, 2006; Chiba *et al.*, 2008; Kennedy *et al.*, 2010). Whilst, insulin resistance also contributes to cardiovascular risk, its role in participating in atherosclerosis is more complex (Nigro *et al.*, 2006). Insulin was shown to have a protective role in endothelial physiology, while in VSMC insulin has pro-inflammatory and pro-atherogenic function (Banskota *et al.*, 1989; Kuboki *et al.*, 2000). Taken together multiple studies have identified a contribution for diabetes and obesity to atherosclerosis, however the exact mechanisms, and importantly the master regulators underpinning these changes, remained incompletely elucidated.

Vascular endothelium

The endothelium is a monolayer of cells that is derived from mesoderm via haemangioblast or angioblast precursors (Pardanaud *et al.*, 1996). Then, depending on the environmental stimuli they adopt arterial or venous characteristics (Marcelo, Goldie and Hirschi, 2013). In both arteries and veins, ECs exhibit multiple functions. ECs modulate the vascular tone, regulate the blood tissue exchange and control the permeability of the vessel. These homeostatic functions depend on the integrity of the layer (Michiels, 2003). Integrity of the ECs relates to cell-cell interactions which are mediated by tight junctions, adherents junctions, and gap junctions (Dejana, E. ; Corada, M. ; Lampugnani, 1995).

Intact and healthy ECs are usually in a quiescent state, which promotes tight cell-cell interactions thereby reducing the permeability of the vessel to lipoproteins and preventing leukocyte infiltration of the vessel wall. The initiation of atherosclerosis is associated with enhanced rates of EC proliferation and apoptosis (Chaudhury *et al.*, 2010; Warboys *et al.*, 2014). This can contribute to atherosclerosis because apoptosis and proliferation of ECs monolayers increases their permeability (Cancel and Tarbell, 2010, 2011). Indeed, both *in vitro* and *in-vivo* models showed that apoptosis in ECs can contribute itself to vascular injury and dysfunction (Hansson *et al.*, 1985; Foteinos and Xu, 2009; Chaudhury *et al.*, 2010).

Furthermore, EC metabolism has been implicated in the development of atherosclerosis (Michael A. and Guillermo, 2016). When compared to other cells, ECs have a very low mitochondrial content and the main source of energy is glycolysis (Oldendorf, Cornford and

Brown, 1977; Falkenberg *et al.*, 2019a). When compared to other mechanisms, this process is inefficient for the production of ATP. Nevertheless, it might be evolutionarily conserved for several possible reasons, including: *i.* reduction of ROS production (generated by mitochondrial respiration), *ii.* maximized transport of oxygen carried from the blood to the perivascular cells, *iii.* the presence of hypoxic surroundings for the sprouting of cells (which requires glycolysis) and, *iv.* the presence of increased lactate production from glycolysis for promoting angiogenesis (Ghesquière *et al.*, 2014).

Different glycolytic rates are associated with EC quiescence and proliferation, and the latter requires an increase in glycolysis (Vizán *et al.*, 2009). On the other hand, fatty acid oxidation (FAO) and amino-acid utilization as metabolic fuel are much less studied and understood. Nevertheless, FAO fuels the tricarboxylic acid (TCA) cycle for de novo synthesis of deoxyribonucleotides, instead of for ATP production (Schoors *et al.*, 2015). Furthermore, during atherosclerosis, a process of endothelial to mesenchymal transition (EndMT) is associated with a reduction of FAO levels, which in turn it is essential to maintain ECs identity both *in vitro* and *in vivo* (Xiong *et al.*, 2018). To this end, frictional forces exerted by the flowing blood play a critical role in driving site specific expression of metabolic enzyme and receptors for the metabolic switch required from an healthy endothelium to a proliferating and/or dysfunctional one.

Role of shear stress in vascular physiology

Atherosclerosis develops focally within the arterial trees (CARO, FITZ-GERALD and SCHROTER, 1969). Haemodynamic forces are essential in regulating EC homeostasis, vascular tone and integrity (Nerem, 1993). However, flowing blood generates frictional forces (wall shear stress) which directly determine the susceptibility of ECs to atherogenesis (Cheng *et al.*, 2006). Within the vasculature, regions exposed to low wall shear stress (LSS) are atheroprone while sites exposed to high wall shear stress (HSS) are atheroprotected (Gimbrone *et al.*, 2000). Plaques will develop preferentially at regions where frictional forces (LSS) induce a pro-inflammatory phenotype with increased expression of leukocyte adhesion molecules (Walpola *et al.*, 1995; Davies *et al.*, 2013).

Endothelial cells morphology changes in shape and orientation according to blood flow dynamics, figure 1.2 (Wang *et al.*, 2013). For example, a characteristic elongated shape is

observed under HSS caused by laminar flow, with the cells aligned with the direction of blood flow. On the contrary, ECs exposed to LSS from disturbed flow show a cobblestone morphology with no fixed directionality and a decrease in intercellular junctions (Davies *et al.*, 1986). Furthermore, it has been shown that shear stress induced changes in cell proliferation rate. On one hand, HSS promotes cell cycle arrest (Lin *et al.*, 2000) while on the other hand, LSS promotes endothelial cell cycle progression (Zhou *et al.*, 2012).

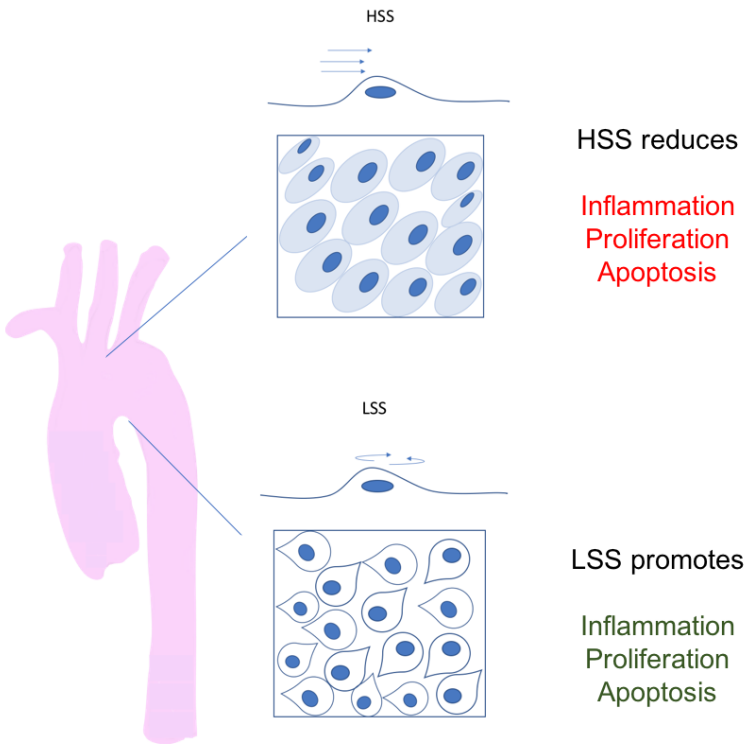

Figure 1. 2 Endothelial cells morphology and function at HSS and LSS sites.

Murine aorta is here shown to represent vessels. The inner layer, ECs exposed to atheroprotective HSS (outer curvature of the arch) or atheroprone LSS (inner curvature of the arch) exhibit a different morphology and function. ECs at HSS are elongated and aligned. ECs at LSS have a cobblestone shape. HSS reduces inflammation, proliferation and apoptosis. LSS promotes inflammation, proliferation and apoptosis.

For these reasons, atherosclerotic plaques are observed mostly at sites of branching and bends in the vasculature where LSS occurs. This intimate connection between mechanical forces and endothelial response is regulated by a mechanosensory system composed by a wide range of surface receptors that integrate the signal from the apical surface to the basal and lateral junctions of the endothelial cells (Tzima *et al.*, 2005), figure 1.3.

Mechanotransduction pathways are still not completely understood. However, in the last couple of decades, many seminal works have contributed to dissecting the complicated network of interactions connecting blood flow to gene activation to cellular responses. Ion channels, integrins, cavaolae, cytoskeleton and apical membrane receptors have been shown to be involved in the transduction of the wall shear stress signals and were recently reviewed by Baratchi et al. 2017. For instance, the glycocalyx can communicate with both junctional and basal mechanoreceptors by transmitting signals via the cytoskeleton (Jing Zhou, Yi-Shuan Li, 2014). At the basal membrane, conformational changes in integrins constitute another check-point for mechanotransduction (Schwartz and DeSimone, 2008). Lateral mechanosensors, such as VE-cadherin/VEGFRs, are also connected to basal integrin via a pathway mediated by phosphatidylinositol-4,5-bisphosphate 3-kinase (PI3K)/protein kinase B (AKT) activation (Coon *et al.*, 2015). The Hippo pathway has also been recently implicated in mechanotranduction (Mehta and Tzima, 2016). The transcriptional coactivators Yes-associated protein (YAP) and transcriptional co-activator with PDZ-binding motif (TAZ) (YAP/TAZ) are increased at the LSS region and inhibited by HSS magnitudes, and YAP/TAZ activation is relevant to atherosclerosis development (Wang *et al.*, 2016). Additionally, Notch1 has been shown to be atheroprotective, and the activation of the Notch pathway by HSS is crucial for maintenance of EC junctions and vessel integrity (Mack *et al.*, 2017; Mack and Iruela-Arispe, 2018). Multiple intracellular signalling cascades induced by flow end with the activation of transcription factors. Therefore, mechanotransduction of shear stress from blood flow controls gene expression in endothelial cells. Physiological and pathological responses to shear stress are mediated by multiple TFs, such as nuclear factor-κB (NF-κB), Hypoxia-inducible factor 1-α (HIF1-α), TWIST1, NF-E2-related factor 2 (NRF2) and Kruppel-like factor 2 (KLF2), table 1. NF-κB, HIF1-α and TWIST are activated by LSS and are associated with increase in inflammation, proliferation and atherosclerosis initiation (Gareus *et al.*, 2008; Mahmoud *et al.*, 2016; Feng *et al.*, 2017; Wu *et al.*, 2017). In contrast, KLF2 and NRF2 are commonly activated by HSS and exert an

atheroprotective effect by increasing the expression of anti-inflammatory molecules, such endothelial nitric oxide synthase (eNOS), as well as anti-oxidative signalling (Parmar *et al.*, 2005; Wu *et al.*, 2006; Chien, 2008; Zakkar *et al.*, 2009; White *et al.*, 2011; Satta *et al.*, 2017).

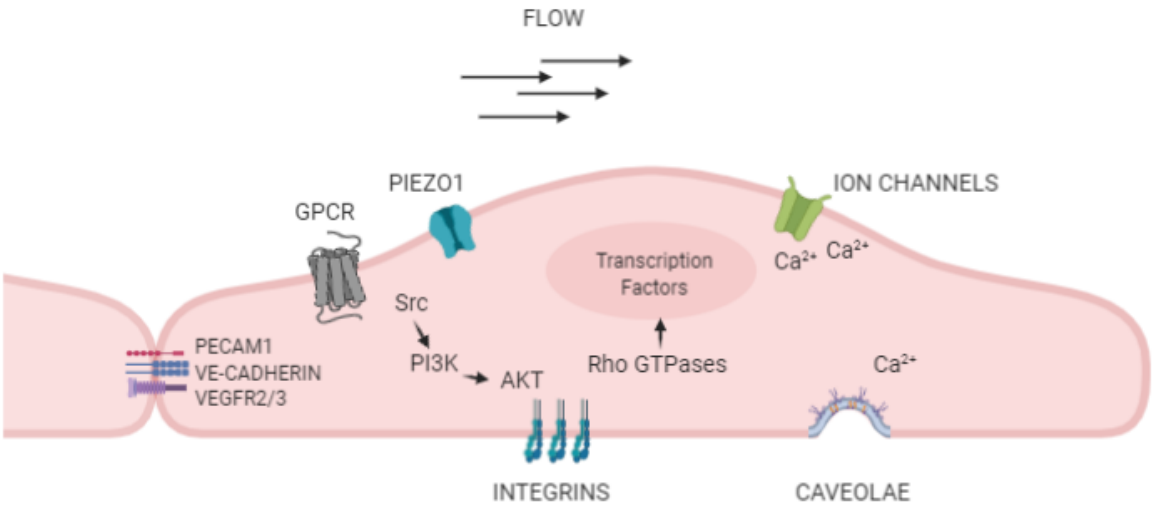

Figure 1. 3 Mechanotransduction signaling

Endothelial mechanotransduction is mediated by multiple molecules located at the later junctions or at the apical and basal surfaces of the cells. The lateral mechanosensory complex is composed by the platelet endothelial cell adhesion molecule (PECAM-1), VE-cadherin and vascular endothelial growth factor receptor (VEGFR)-2/3. Activation of the Src-dependent phosphatidylinositol-4,5-bisphosphate 3-kinase (PI3K)/ protein kinase B (AKT) lead to integrins activation. Integrins in turn activate Rho-GTPases and downstream activation of transcription factors. Activation of integrins can also trigger caveolae. At the apical membrane, cationic channels, such as calcium (Ca^{2+}) channels, transmembrane G proteins (GPCR) and PIEZO contributes to transduce shear stress forces. Illustration adapted from Baratchi et al. 2017 and created using Biorender.com.

Table 1. Mechanosensitive transcription factors.

Shear stress	Transcription factors	Downstream target	Effects
High WSS	KLF2, KLF4	eNOS	Anti-inflammatory, Anti-oxidant, Anti-proliferative, Cell alignment and integrity of ECs junctions.
	NRF2	PAI1, ET1	
	Notch1	CCND1, EFNB2	
Low WSS	NF-κB	VCAM1, ESELE, MCP1	Inflammation and proliferation, Pro-thrombotic, EndoMT, Glycolysis
	AP-1	NQO1	
	YAP/TAZ	CTGF	
	TWIST1/GATA4	CCND1, CCNG2, SNAIL	
	HIF1-α	PFKFB3	

Endothelial mechanosensitive transcription factors: Kruppel-like factor 2 (KLF 2), Kruppel-like factor 4 (KLF4), NF-E2-related factor 2 (NRF2), Notch homolog 1 (Notch1), nuclear factor-κB (NF-κB), Activator Protein 1 (AP-1), Yes-associated protein (YAP) and transcriptional co-activator with PDZ-binding motif (TAZ) (YAP/TAZ), Twist Basic Helix-Loop-Helix Transcription Factor 1 (TWIST1), GATA binding protein 4 (GATA4) and Hypoxia-inducible factor 1-alpha (HIF1-α). Downstream targets: endothelial nitric oxide synthase (eNOS), endothelial plasminogen activator inhibitor (PAI1), endothelin-1 (ET1), cyclin D1 (CCND1), ephrin B2 (EFNB2), Vascular cell adhesion molecule 1 (VCAM1), Selectin-E (ESELE), monocyte chemoattractant protein 1 (MCP1),NAD(P)H Quinone Dehydrogenase 1 (NQO1), Cellular Communication Network Factor 2 (CTGF), Cyclin G2 (CCNG2), Snail Family transcriptional repressor (SNAIL), 6-phosphofructo-2-kinase/fructose-2,6-biphosphatase 3 (PFKFB3).

Hypoxia-inducible factor (HIF)

The family of the HIF transcription factors

In 2019 the Nobel Prize in Physiology or Medicine was awarded jointly to Professors Peter Ratcliffe, Gregg Semenza and William Kaelin for the discovery of how cells sense and adapt to low oxygen availability (hypoxia). The hypoxia-inducible factor (HIF) family of heterodimeric transcription factors respond to oxygen availability, which was discovered by the Semenza's group (Wang and Semenza, 1993). HIFs have mainly been studied in the context of cancer progress and growth (Masson and Ratcliffe, 2014), and only later has been recognized as important in the cardiovascular disease scenario (Vink *et al.*, 2007). This heterodimeric transcription factor is composed of two subunits, which together create the active form of HIF, one HIF alpha (HIFα) subunit, which is sensitive to hypoxia, and the HIF beta (HIFβ) subunit which is constitutively expressed and not responsive to oxygen availability. Three alpha isoforms are known, HIF-1α and HIF-2α that shares 48 % amino acid sequence with the HIF-1α. The last isoform to be discovered and studied was HIF-3α (Gu *et al.*, 1998). HIFα subunits are transcription factors linked to the PAS family (Per/ARNT/Sim), whose name is derived from Period, Aryl hydrocarbon nuclear transport, Single minded sequences, figure 1.4. The other component of the heterodimer is the HIF-β subunit which also belongs to the PAS family. HIF-1α and HIF1-β have characteristic domains involved in DNA binding and protein dimerization (Wang *et al.*, 1995). The basic helix-loop-helix (bHLH) and PAS domains are necessary for heterodimer formation between subunits alpha and beta, and to allow specific binding to the hypoxia-responsive element (HRE) DNA sequence (Crews, 1998). Two independent domains N-TAD and C-TAD, can activate transcription. Furthermore, the HIF β subunit is constitutively expressed and it is not influenced by O_2 tension because it lacks the oxygen-dependent degradation domain (ODDD). All the main isoforms have a nuclear localization signals (NLS)), which allows them to move to the nucleus and act as canonical transcription factors.

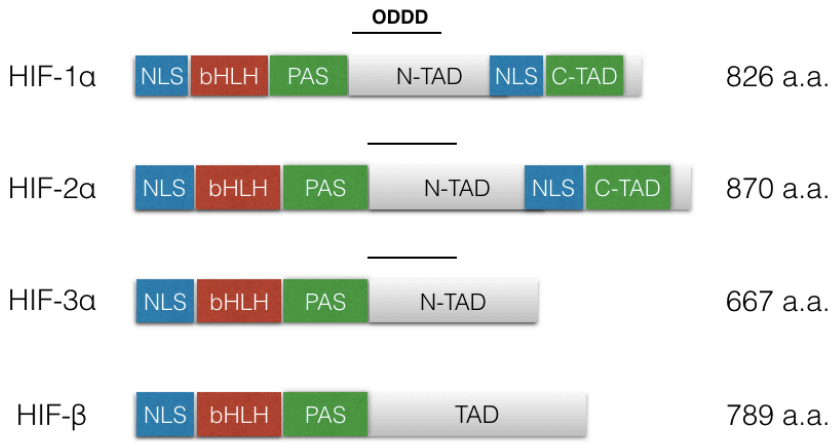

Figure 1. 4 HIF family

HIF is a heterodimeric transcription factor composed by alpha subunit (HIF-1α, HIF-2α, HIF-3α) and a beta subunit (HIF-β). Nuclear localization signals (NLS), basic helix-loop-helix (bHLH), Per-ARNT-Sim homology domains (PAS), transactivation domains (TAD), N- and C-terminal TAD (N-TAD and C-TAD), oxygen dependent degradation domain (ODDD).

Regulation of HIF

All the HIF-α subunits are rapidly degraded in the presence of O_2. HIF-α is highly unstable in normoxia (20% oxygen tension) and with a half time life of about 5 minutes. HIFs are regulated at the level of transcription, translation, post-translation and by microRNAs. It was shown that HIF1-α and HIF2-α stabilization and activation was observed after direct phosphorylation mediated by ERK1/2 (Conrad *et al.*, 1999; Richard *et al.*, 1999; Sang *et al.*, 2003; Mylonis *et al.*, 2006, 2008; Triantafyllou *et al.*, 2006). However, other studies have shown that PI3K/PKB (Akt) pathway-mediated phosphorylation of HIFs may be secondary to the activation of an intermediate molecule such as mTOR (Treins *et al.*, 2002). Interestingly, mTORC2 also regulates both HIF2-α transcriptional level and activity in a model of neuroblastoma (Mohlin *et al.*, 2015). At the transcriptional level, HIF-α isoforms are further regulated by the NF-κB transcription factors. NF-κB is direct modulator of HIF1-α expression as well as HIF2-α protein levels and HIF1-β mRNA and protein levels (Rius *et al.*, 2008; van Uden, Kenneth and Rocha, 2008). A recent work from Paul Evans's laboratory further confirmed transcriptional regulation of the HIF1-α by NF-κB in a model of endothelial cells exposed to physiological shear stress (Feng *et al.*, 2017). In addition, the role of the short non-coding RNAs (microRNAs) on HIF regulation in hypoxia has been extensively studied, although many aspects of their dynamic regulation are still unsolved (Chan *et al.*, 2009; Ho *et al.*, 2012; Araldi and Suárez, 2015; Janaszak-Jasiecka *et al.*, 2016). Several studies have provided evidence for microRNA mediated-switch of HIFs isoforms during hypoxia (Camps *et al.*, 2014; Janaszak-Jasiecka *et al.*, 2016). Moreover, multiple works have shown microRNA-mediated HIFs regulation in endothelial cells (reviewed in (Serocki *et al.*, 2018). Furthermore, microRNAs are affected by shear stress and have a relevant function in the modulation of vascular remodelling and endothelial cells physiology (Davies *et al.*, 2013; Schober, Nazari-Jahantigh and Weber, 2015).

From these mechanisms of HIF regulation, specifically, the post-translational level is a key regulator of HIFs stability, Figure 1.5. Proline hydroxylase enzymes (PHDs) promote degradation of HIFs via hydroxylation of key proline residue of HIFs (Epstein *et al.*, 2001). This hydroxylated form is then recognised by the Von Hippel Lindau protein (VHL), which ubiquitinates HIF-α subunits, and ubiquitinated-HIFs are targeted to the proteosome for degradation (Maxwell *et al.*, 1999). PHDs require oxygen and 2-oxoglutarate as substrates, thus when O_2 tension is low, PHDs are inhibited. Reduction in hydroxylated proline residues cause

HIFs to escape VHL recognition and thus become stabilised. Next the stabilised HIFs translocate into the nucleus to activate gene promoters containing the 'HRE' hypoxia response elements. Furthermore, HIF transcriptionally activates its regulators PHD 2 and 3 to generate a negative feedback loop (Berra *et al.*, 2003). HIF-Ubiquitination can be reversed by ubiquitin editing enzymes, with de-ubiquitinating activity (DUBs). Recently, our group identified Cezanne (OTU7B) as a novel DUB of HIFs in endothelial cells (Feng *et al.*, 2017).

In addition to the post-translational regulation of HIFs, the HIF promoter is sensitive to epigenetic modification (Cui *et al.*, 2016; Nakazawa *et al.*, 2016; Cruzeiro *et al.*, 2018). A recent work identified an *in vitro* novel negative regulator of HIF2-α. The HIF2-α promoter was inhibited by the interaction of the histone deacetylase complex subunit Sin3a (SIN3A) and HDAC associated factor complex (SINHCAF) with the transcription factor Sp1 (SP1). SINHCAF caused histone deacetylation and HIF2-α gene silencing, thereby inhibiting cellular viability, angiogenetic functions and proliferation in multiple cancer cells and primary endothelial cells (Biddlestone *et al.*, 2018). Furthermore, in cancer cells, Cezanne indirectly regulated HIF2-α at the transcriptional level by modulating the expression of E2F1 transcription factor, which enhances HIF2-α promoter activity (Moniz *et al.*, 2015). Overall, HIFs transcriptional levels can be regulated by many other mechanisms, including response to reactive oxygen species and inflammatory stimuli mediated by the nuclear factor- κB (NF-κB) transcription factors (Frede *et al.*, 2006; Bonello *et al.*, 2007; Rius *et al.*, 2008; van Uden, Kenneth and Rocha, 2008; Biddlestone *et al.*, 2018).

In addition to PHD-mediated regulation of protein stability, the activity of another 2-oxoglutarate-dependent enzyme was shown to regulate the interaction of the HIFs transactivation domain (C-TAD) with the transcriptional co-activator p300 (Ema *et al.*, 1999; Lando *et al.*, 2002). HIF transcriptional activity is suppressed under normoxia by modification of an asparagine residue in C-TAD is mediated by the factor inhibiting HIF (FIH) hydroxylase (Lando *et al.*, 2002). FIH activity is abrogated during hypoxia allowing HIFs to initiate transcriptional responses.

Taken together these studies suggest that non-canonical HIFs regulation via transcriptional and post-transcriptional mechanisms, add complexity to an already intricate network of molecules that connects HIFs to endothelial responses.

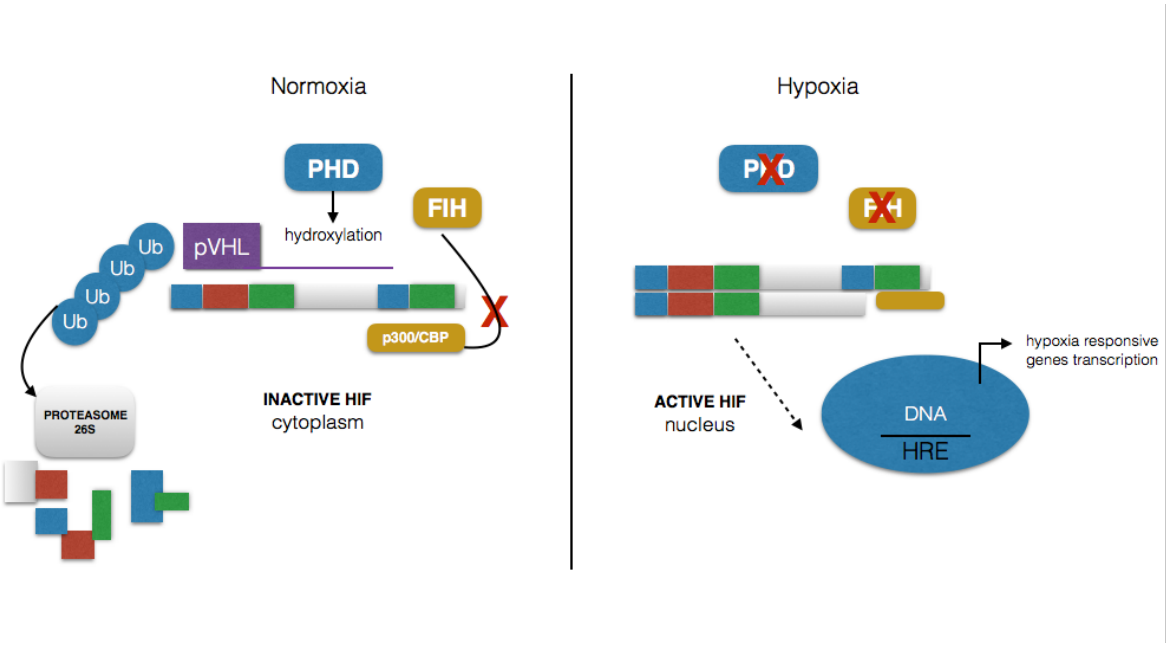

Figure 1. 5 HIF post-translational regulation

HIFs are mainly regulated by post-translational control. HIFα subunits are rapidly degraded under normoxia (21% O_2), left panel. Prolyl hydroxylase enzymes (PHD) hydroxyalates two proline residues on the HIF1-α and HIF2-α. Hydroxylated HIFs are recognised by Von Hippel Lindau (pVHL), ubiquinated and then degraded by the proteasome. Factor inhibiting the HIF (FIH) block the recruitment for the cofactors (p300/CBP). Under hyxpoxia (<5% O_2), right panel, PHDs and FIH activity are inhibited and HIFα subunits bind the remaining heterodimeric part (HIF-β). Active HIFs translocate into the nucleus and bind the hypoxia response elements (HREs) on DNA, thus activating the transcription of multiple downstream targets.

HIF2-α localisation and functions

HIF2-α tissue expression

HIF-2α is also named Endothelial PAS Domain-Containing Protein 1 (EPAS1) or Member Of PAS protein 2 (MOP2); it was initially characterized in late 1990s by fluorescent *in situ* hybridization (FISH) and was demonstrated to be located on the short arm of the chromosome 2 (2p16-p21) (Tian, Mcknight and Russell, 1997). Even if it shares many similarities, HIF2-α has a different gene locus from HIF1-α, which is located on chromosome 14 q21-q24 (Semenza *et al.*, 1996). Highly vascularized tissues, such as heart, lung and placenta, showed higher concentrations of HIF2-α mRNA rather than the HIF1-α isoform (Tian, Mcknight and Russell, 1997). Furthermore, in chicken embryos HIF2-α was present at the early stages of development at the endothelium of the dorsal aorta as well as at the extra-embryonic ectoderm. However, HIF2-α was absent in cardinal veins but present in almost all the other vessels and co-localized with the tyrosine hydroxylase in the sympathetic nervous system (Favier *et al.*, 1999).

HIF2-α in health and disease

HIF-2α is critical during developmental stages. Several initial attempts to generate HIF2-$\alpha^{-/-}$ mice failed during the embryonic stages or resulted in perinatal lethality. It was later found that HIF2-$\alpha^{-/-}$ mice exhibited various phenotypes including severe bradycardia (i.e. slow heart rate) due to reduced catecholamine production (Tian *et al.*, 1998), vascular defects in the yolk sack and embryos (Peng *et al.*, 2000), and reduced surfactant production (Compernolle *et al.*, 2002). In 2003, Scortegagna et al. generated HIF2-$\alpha^{-/-}$ mice on a C57Black/6J and 129S6/SvEvTac background. New-born HIF2-$\alpha^{-/-}$ mice had a smaller stature and multiple organ pathology, including cardiac hypertrophy, hepatosteatosis and an overall shorter lifespan. This multi-organ pathology was attributed to a mitochondrial disorder and in agreement with that, several enzymes like succinate dehydrogenase (SDH) or cytochrome oxidase (COX) were found to be increased in the HIF2-$\alpha^{-/-}$ tissues. Furthermore, by generation of adult mice lacking HIF2-α it was also possible to elucidate its role in erythropoiesis (Scortegagna *et al.*, 2003). HIF2-α is also involved in development of blood vessels and lung (Peng *et al.*, 2000; Favier *et al.*, 2001).

In adult tissues, HIF2-α is involved in several processes, such as angiogenesis, proliferation, endothelial cell integrity and inflammation, Figure 1.6. HIF2-α has recently emerged as a major

regulator of erythropoiesis both *in vitro* and *in-vivo* (Scortegagna *et al.*, 2005; Rankin *et al.*, 2007; Pangou *et al.*, 2016), however the ability to activate erythropoietin (EPO) gene expression is shared with the paralogue HIF-1α (Wang and Semenza, 1993; Wang *et al.*, 1995). Postnatal deletion of HIF2-$\alpha^{-/-}$ using an inducible Ubiquitin-CreER^{T2} driver caused anaemia and this phenotype was recovered by EPO administration (Gruber *et al.*, 2007), highlighting the crucial role for HIF2-α in red blood cell production. EPO is a hormone produced by the kidneys which regulates red blood cells mass. Postnatally it is produced by the liver as well as the kidney, whilst in adults it is produced by the kidneys. Fibroblast like cells in the kidney and hepatocytes in the liver produce EPO in response to hypoxic stimuli (Schuster *et al.*, 1989; Maxwell *et al.*, 1993; Rankin *et al.*, 2007). EPO activates progenitors cells to maturate into red blood cells (RBC) from the bone marrow. Clinically, overproduction of EPO lead to polycythaemia (overproduction of RBC) and a certain type of erythrocytosis (Hussein, Percy and McMullin, 2012), whilst lack of EPO causes anaemia.

Multiple mutations occurring in the members of HIF pathways are associated with erythrocytosis, including mutations in the HIF2-α gene (Lee and Percy, 2011). Therefore, mutations in the HIF2-α gene were associated with erythrocytosis. Single amino acid mutation located nearby the sites of prolyl hydroxylation of HIF-2α (Proline 405 and Proline 531) led to decreased recognition of the protein for proteasomal degradation, thus causing prolonged protein stability and gain of function.

Interestingly, erythrocytosis is also observed in populations living at high altitude, thereby exposed to hypobaric hypoxia. Nevertheless, inhabitants of the high plateau of Central Asia (e.g. Tibetans) have developed a blunted response to hypoxia. Genome wide analysis revealed that SNPs of the HIF2-α gene are recurrent in those populations (Beall *et al.*, 2010). Tibetans have adapted to high altitude by minimising the red blood cells mass, thus avoiding stroke and other complications usually occurring in the presence of high blood viscosity due to high erythrocytosis. Therefore, mutation of HIF2-α was evolutionary beneficial and quickly spread throughout the Tibetan population. HIF2-α Tibetan variants (loss of function) alongside with gain of function mutation of the gene encoding for the PHD2 enzyme (EGLN1), built the mechanistic fundaments of such adaptation (Lorenzo *et al.*, 2014; Peng *et al.*, 2017).

High altitude inhabitants have also an increase in pulmonary pressure (ARIAS-STELLA and KRUGER, 1963). Thus, chronic exposure to low oxygen tension causes remodelling of the pulmonary arteries and it is a driving factor for pulmonary hypertension development (Stenmark, Fagan and Frid, 2006). Inactivation of PHD2 in endothelium, which led to sustained HIF1-α and HIF2-α expression, also led to increased pulmonary hypertension mediated by HIF2-α (Dai *et al.*, 2016; Kapitsinou *et al.*, 2016). Deletion of HIF2-α, but not HIF1-α, in the pulmonary endothelium of mice prevented the development of pulmonary arterial hypertension via the regulation of arginase (Cowburn *et al.*, 2016). However, mice with vascular endothelial HIF2-α deletion developed increased pulmonary arterial pressure and cardiac hypertrophy (Skuli, Liu, Runge, Wang, Yuan, Patel, Iruela-arispe, *et al.*, 2009). Interestingly, HIF2-α heterozygous mice exposed to chronic hypoxia were protected from pulmonary vascular remodelling and hypertension (Brusselmans *et al.*, 2003).

Similarly, HIF2-α transcript is also highly expressed in the carotid body (*glomus caroticum,* CB), a multi-cell type structure that senses variations in the oxygen and carbon dioxide content of blood (Tian *et al.*, 1998; Zhou *et al.*, 2016; Gao *et al.*, 2017). HIF2-α is essential for the CB development and ventilatory responses to hypoxia (Macias *et al.*, 2018; Moreno-Domínguez *et al.*, 2020). In the CB, HIF2-α induces expression of the cytochrome c oxidase subunit 4i2 (*Cox4i2)*, the NADH dehydrogenase 1 alpha subcomplex 4l2 (*Ndufa4l2)* and the cytochrome c oxidase subunit 8b *(Cox8b)* mitochondrial genes that allow oxygen sensitivity of the carotid body (Bishop and Ratcliffe, 2020; Moreno-Domínguez *et al.*, 2020). Therefore, HIF2-α is considered a major regulator of haematic pH homeostasis, erythropoiesis and high-altitude acclimatisation.

In the liver, HIF2-α regulates a hepatokine named histidine-rich glycoprotein (HRGP) that promotes inflammation by inducing M1 polarization of hepatic macrophages (Morello *et al.*, 2018). HIF2-α is highly expressed in liver tissues from patients with non-alcoholic fatty liver disease (NAFLD), as well as in murine NAFLD tissues. NAFLD is common in subjects with T2DM and obese individuals, and it is characterised by an abnormal accumulation of fat in the liver (steatosis), which may subsequently evolve into a chronic liver inflammation state and fibrosis. Ablation of hepatic HIF2-α in mice ameliorated liver fibrosis and steatohepatosis (Rankin *et al.*, 2009). Therefore, HIF2-α was shown to promote inflammation, fibrosis and increase lipid accumulation with consequent steatohepatosis (Rankin *et al.*, 2009; Qu *et al.*, 2011).

Whilst HIF2-α has a role in fibrotic events associated with obesity and diabetes, its role in this pathology is not fully elucidated. Stabilization of HIF2-α in PHD3-deficient hepatocytes, led to amelioration of the hepatic glucose metabolism (Taniguchi *et al.*, 2013). Furthermore, in adipocytes, loss of HIF2-α increased insulin resistance (Lee *et al.*, 2015). Whereas loss of function of HIF2-α in neurons expressing pro-opiomelanocortin (POMC), which regulate hunger, led to increased obesity (Zhang *et al.*, 2011). Controversially, stabilisation of HIFs signalling via pharmacological inhibition of PHDs led to an amelioration of obesity and dyslipidaemia (Rahtu-Korpela *et al.*, 2014). Collectively these data suggest that different peripheral tissues require different levels of HIF2-α and HIF1-α, in which their transient activation may be beneficial; whereas at the nervous system, HIF2-α may have a more central role in the metabolic control of obesity by regulating POMC neurons.

In conclusion, while HIF2-α is an essential regulator of metabolic and haematopoietic functions, collectively these data suggested that chronic activation of HIF2-α might be harmful.

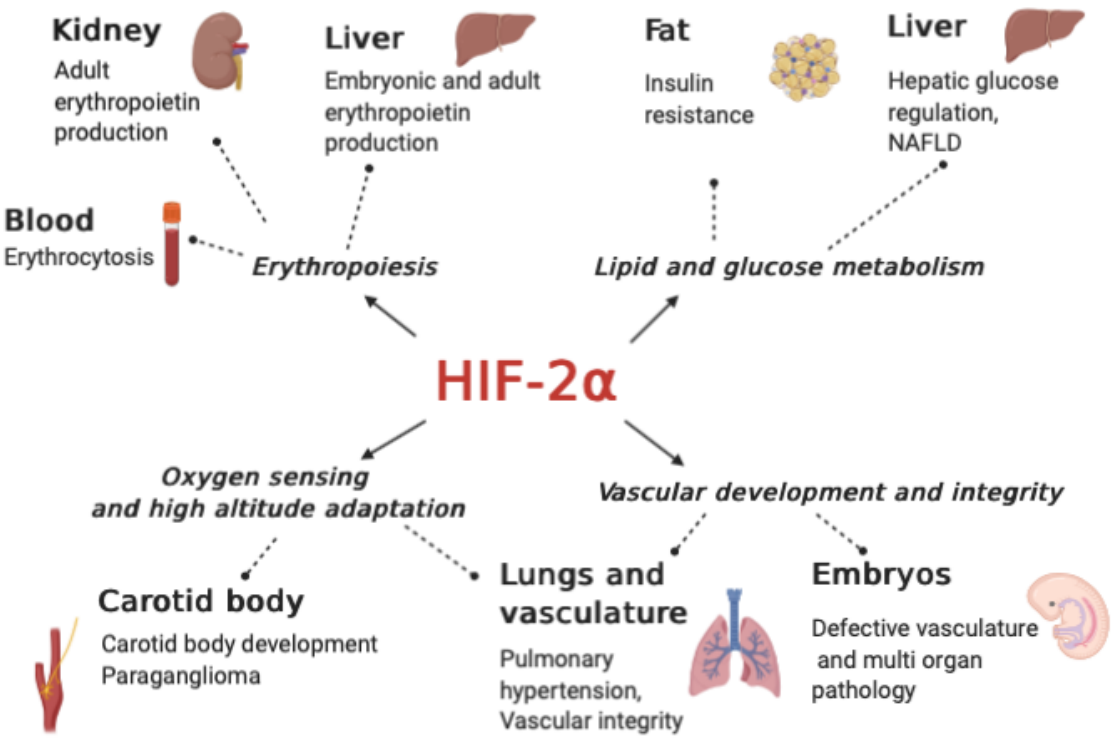

Figure 1. 6 HIF2-α in health and disease

Graphical summary of the main functions of HIF2-α in health and disease. Illustration created using Biorender.com

HIF2-α in cancer

Solid tumours are often associated with a hypoxic environment and both HIF1-α and HIF2-α are highly expressed in cancer tissue. HIF2-α has been investigated in multiple cancer cell types and its activation upon hypoxia led to the identification of several key downstream targets such as Epo (Ema *et al.*, 1997), VEGF (Forsythe *et al.*, 1996), Tie-2 (Takeda *et al.*, 2004) and plasminogen activator inhibitor (PAI-1) (Sato *et al.*, 2004). These molecules are key regulators of cancer progression and growth. Several cancer tissues exhibited higher levels of HIF2-α compared to HIF1-α. For instance, in renal cell carcinoma (RCC), a tumour associated with mutations of the Von Hippel Lindau (VHL) gene (Gnarra *et al.*, 1994), HIF2-α and VEGF were abundant (Maxwell *et al.*, 1999; Xia *et al.*, 2001). Furthermore, in RCC, HIF2-α was shown to enhance c-Myc transcriptional activity and to promote cancer proliferation (Gordan *et al.*, 2007).

Paragangliomas (PGL) and phaeochromocytomas (PCC) are rare, highly vascularised neuroendocrine tumours arising from extra-adrenal medulla and adrenal medulla, respectively (Dahia, 2014). PGL and PCC are generally associated with germline mutation of VHL, egl-9 family hypoxia-inducible factor 1 (EGLN1) and succinate dehydrogenase (SDH) genes. However, recent findings have shown that a somatic mutation with gain-of-function of HIF2-A was identified in patients with multiple paragangliomas and erythrocytosis (Zhuang *et al.*, 2012; Toledo *et al.*, 2013), or with development of cancer alone (Comino-Méndez *et al.*, 2013). Carotid body PGL is observed in individuals living at high altitude (Saldana, Salem and Travezan, 1973). Recently, the HIF2-α-PHD2 axis was identified as an essential regulator of the expansion and proliferation of Type I cells in the carotid body (Fielding *et al.*, 2018). Thus confirming the predominant role of HIF2-α, over HIF1-α isoform in this tissue. Furthermore, in human hepatocellular carcinoma cells (HCC) HIF2-α showed a positive correlation with tumour size (Bangoura *et al.*, 2007). Similarly, HIF2-α promoted colorectal cancer progression and growth by increasing YAP1 activity (Xue *et al.*, 2012; Ma *et al.*, 2017). In conclusion, multiple studies showed the predominant expression of HIF2-α over HIF1-α in certain malignant tissues and its ability to modulate cancer progression and tumour angiogenesis.

HIF2-α in vascular endothelium

Early after its discovery HIF2-α was determined as a critical regulator of the vasculature via modulation of angiopoietin-1 receptor tyrosine kinase (Tie-2) expression (Tian *et al.*, 1998; Duan, Zhang-Benoit and Fong, 2005). Initial conditional studies of HIF2-α employed a Tie-1 inducible Cre for genetic deletion (Yamashita *et al.*, 2008). However, Tie1 is expressed at early stages in the embryo and also in haematopoietic progenitor cells (Gustafsson *et al.*, 2001). To overcome this issue, the generation of a vascular endothelial Cre recombinase model using cadherin-5 (CDH5) was developed (Alva *et al.*, 2006). Thus, the generation of a CDH5-HIF2-α knock-out model gave further insight of HIF2-α function in vascular endothelium with greater confidence. Vascular endothelial deletion of HIF2-α in mice led to pulmonary hypertension, increased permeability in the lung and adipose tissues, as well as to increased red blood cell extravasation, lymphocyte infiltration and plasma protein leakage (Skuli, Liu, Runge, Wang, Yuan, Patel, Iruela-arispe, *et al.*, 2009; Skuli *et al.*, 2012). Thus, HIF2-α appeared to be a central regulator of endothelial cell integrity. Nevertheless, mice harbouring a gain of function mutation (G536W) for HIF2-α presented erythrocytosis and pulmonary hypertension (Tan *et al.*, 2013). Confusingly, miss-sense mutation and vascular endothelial deletion of HIF2-α lead to the same results. This may suggest that an optimal amount of HIF2-α level is required for endothelial physiology, in which both deletion or gain of function may be detrimental for the erythropoiesis and the vascular integrity.

Furthermore, the pivotal role of HIF2-α in angiogenesis was confirmed in the CDH5-Cre model. HIF2-α ECs knock-out mice exhibited reduction in tumour size and tumour growth in xenograft experiments and decreased formation of luminised vessels (Skuli, Liu, Runge, Wang, Yuan, Patel, Iruela-arispe, *et al.*, 2009; Skuli *et al.*, 2012). Whereas, Tie-2 driven endothelial cells deletion of HIF2-α causes increased tumour area and number of metastatic foci in the lungs (Branco-Price *et al.*, 2012). Furthermore, vascular endothelial HIF2-α protects from inflammation associated with ischaemic injury in kidneys (Kapitsinou *et al.*, 2014). Finally, genetic deletion studies found that HIF2-α is required for maintaining a physiological level of ANGPT1/Tie2 signalling which promotes EC survival and vessel integrity by a Notch-mediated pericyte recruitment (Jiang *et al.*, 2019). This might suggest an endothelial-selective cytoprotective function for HIF-2α, which diverges from its systemic function.

HIF2-α in angiogenesis

Angiogenesis is mediated by HIF-2α transcriptional control of growth factors and genes active in vascular formation, such as VEGF, ANGPTL4, cyclin D1 and G2, and the epidermal growth factor, EGFR (Xia *et al.*, 2001; Keith, Johnson and Simon, 2011). HIF2-α also promotes transcriptional activity of Tie-2. Tie-2, as well as Tie-1, and several receptors of the VEGF family (Flk-1, Flt-1) are involved in endothelial specification. In a murine model, disruption of the Flk-1 gene led to abnormalities in vascular formation and haematopoiesis, while Flt-1 disruption led to defects in vascular endothelium assembly (Dumont *et al.*, 1995; Fong *et al.*, 1995; Sato *et al.*, 1995; Shalaby *et al.*, 1995). These data suggest that HIF2-α is a regulator of vascular and haematopoietic development. Direct evidence for the role in angiogenesis was obtained by Skuli et al. who showed that HIF2-α is essential for vessel integrity and leads to decreased expression of HIF2-α downstream targets, such as Ang2, Delta Like Canonical Notch Ligand 4 (Dll4) (Skuli, Liu, Runge, Wang, Yuan, Patel, Iruela-Arispe, *et al.*, 2009). Although HIF1-α has been previously demonstrated to increased VEGFs expression, drive ECs angiogenesis and proliferation (Tang *et al.*, 2004); purified lung ECs lacking of HIF2-α increased migration and tube formation *in vitro* (Skuli, Liu, Runge, Wang, Yuan, Patel, Iruela-Arispe, *et al.*, 2009). Furthermore, endothelial deletion of HIF2-α controls angiogenic genes of the Dll4/Notch pathway. Interestingly, chemical inhibition of Dll4/Notch signalling *in vitro* phenocopied the loss of HIF-2α. Therefore, a link between the two pathways has been suggested in vascular angiogenesis (Skuli *et al.*, 2012). Recently, in an *in vitro* study in human umbilical vein endothelial cells (HUVEC) it was reported that HIF2-α may orchestrate angiogenic migration and tube formation via production of the inflammatory cytokines IL-6 and IL-8 (Endler *et al.*, 2013). HIF2-α has also been suggested to mediate ECs barrier integrity (Gong *et al.*, 2015). HIF2-α has also been implicated in tumour vascularization (Iliopoulos *et al.*, 1996; Maxwell *et al.*, 1999; Gordan *et al.*, 2007). HIF2-α EC null mice exhibit decreased tumour growth and angiogenesis (Skuli, Liu, Runge, Wang, Yuan, Patel, Iruela-Arispe, *et al.*, 2009). Thus, HIF2-α is an essential regulator of both physiological and tumour angiogenesis.

The role of HIF transcription factors in atherosclerosis

HIF1-α in atherosclerosis

The role of HIFs in atherosclerosis is not yet clear, although low oxygen tension is found in human and murine plaque cores (Sluimer *et al.*, 2008; Parathath *et al.*, 2011). Hypoxia might participate to atheromatous plaque by increasing inflammatory signals, promoting lipid uptake and plaque angiogenesis (Sluimer and Daemen, 2009). Furthermore, HIF1-α expression and level correlate to the progression of a plaque (Sluimer *et al.*, 2008). HIF1-α in macrophages aggravates inflammatory signals, partially modulates the lipid metabolism and thus may contributes to atherosclerosis (Jiang *et al.*, 2007; Sluimer *et al.*, 2008; Parathath *et al.*, 2011; Aarup *et al.*, 2016).

Although, HIF1-α is expressed in atheroma, contrasting evidence has emerged about its possible roles in pathology. As an example, reduced re-stenosis and neointimal formation were evidenced after local siRNA-mediated silencing of HIF1-α at the left common carotid of an ApoE$^{-/-}$ mice model (Karshovska et al. 2007). Furthermore, adenoviral inhibition of HIF1-α led to reduced neointimal formation whereas adenoviral overexpression of HIF1-α augmented re-stenosis in a wire-induced injury of the femoral artery in the ApoE$^{-/-}$ mice model (Christoph *et al.*, 2014). In contrast to this, HIF1-α overexpression in experimental atherosclerotic mice led to reduced plaque size and lipid core (Ben-Shoshan *et al.*, 2009). The latter study, however, analysed plaque development at the aortic sinus site, whereas the work from Christoph et al. investigated the effects of HIF1 overexpression at the femoral aortae of ApoE mice. The difference in anatomical sites analysed between the two studies may explain their contradictory findings.

Cell specific deletion studies have provided some clarity. Akhtar et al. found using ApoE$^{-/-}$ mice that endothelial HIF1-α promotes atherosclerosis, as its deletion in ECs reduces macrophage abundance in lesions, via the expression of miR-19a (Akhtar *et al.*, 2015). Furthermore, deletion of HIF1-α reduces the expression of (C–X–C motif) ligand 1, which usually promotes monocyte adhesion (Zhou *et al.*, 2011; Akhtar *et al.*, 2015). A study conducted in ApoE$^{-/-}$ mice with low WSS induced by carotid partial ligation, showed that HIF transcripts increase after 2 and 4 weeks, after an initial decline (Akhtar *et al.*, 2015). Thus, HIF

expression is elevated by low WSS, which is a predisposing factor for focal atherosclerosis. Further evidence linking HIF with atherosclerosis was obtained by studying the genes that are induced by HIF. They include Snail and Twist, and Notch (Sahlgren *et al.*, 2008; Yang *et al.*, 2008) which are drivers of EndMT, which is a key process in atherosclerosis (Chen *et al.*, 2015; Moonen *et al.*, 2015; Mahmoud *et al.*, 2016). A summary of the animal works investigating the effects of HIF1-α in atherosclerosis is presented in table 2.

While animal studies suggested that hypoxia is associated with cardiovascular risk and atherosclerosis (Savransky *et al.*, no date; Nakano *et al.*, 2005), epidemiological studies of highlander populations acclimatized to environmental hypoxia suggest such individuals are protected from atherosclerosis (Mortimer, Monson and MacMahon, 1977; Faeh, Gutzwiller and Bopp, 2009; Cao *et al.*, 2020). Interestingly, ApoE$^{-/-}$ mice with chronic exposure to low oxygen tension displayed increased anti-inflammatory IL-10 signals and reduced atherosclerosis (Kang *et al.*, 2016). These studies suggest that genetic variation in human and mice contribute to the different cardiovascular response to hypoxia.

In conclusion, these data suggest that activation of HIF pathway, via HIF1-α mediated mechanisms, is detrimental by accelerating atherosclerosis. Time and spatial distribution of HIF isoforms might have differing effects and be the cause of the different response to chronic hypoxia observed in human and mice.

HIF2-α in atherosclerosis

While HIF1-α promotes atherogenesis, the role of HIF2-α in this process is unknown as yet. However, since HIF2-α is suggested to be a regulator of endothelial cell homeostasis and it is known to be involved in vessel integrity and maturation, a role in atherogenesis is plausible. *In vitro*, exposure of arterial and venous endothelial cells lines to hypoxia showed a time-dependent expression of HIF1-α and HIF2-α isoforms (Bartoszewski *et al.*, 2019). Similarly to HIF-1α, HIF-2α was found upregulated in human carotid plaques (Sluimer *et al.*, 2008) . Furthermore, macrophages of advanced carotid lesion also expressed HIF2-α mRNA (Sluimer *et al.*, 2008). A potential role for HIF2-α in late stages of atherosclerosis has been suggested, but not completely confirmed, by Stavik et al who found that siRNA knock down of HIF-2α

rescued antithrombotic tissue factor pathway inhibitor (TFPI) in endothelial cells (Stavik *et al.*, 2016), implicating this HIF isoform in plaque rupture. HIF2-α overexpression led to reduction of neointimal formation and augmented re-stenosis in a wire-induced injury of the femoral artery in ApoE$^{-/-}$ mice model (Christoph *et al.*, 2014). Whereas Zhang et al. showed that expression of HIF2-α is enhanced by cold temperature (16°C) in adipocytes and by pharmacological stabilisation using FG-4592. HIF2 protects from atherosclerosis via activation of alkaline ceramidase 2 (ACER2), thereby inhibiting ceramide catabolism and by reducing cholesterol levels (Zhang *et al.*, 2019). Therefore, Zhang et al. showed a role for HIF2-α in regulating atherosclerosis via an indirect mechanism of regulation of lipid levels. On the contrary, activation of HIF-2α in SMCs of ApoE$^{-/-}$ mice promotes atherosclerosis (Qi *et al.*, 2017). A summary of the studies investing the role of HIF2-α in atherosclerosis is presented in Table 2. Collectively, these studies suggest that HIF isoforms may play different roles in atherosclerosis, participating in disease initiation, progression and resolution.

Table 2. HIFs in atherosclerosis.

Isoform	Model	Findings	Reference
HIF1-α	Human carotid plaque	Hypoxia colocalised with HIF1-α expression. HIF1-α levels increased with plaque progression	Sluimer et al. 2008
	Wire-induced injury of left carotid artery in ApoE mice	HIF1-α levels increased in the SMCs of the media	Karshovska et al. 2007
	HIF1-α siRNA (local application) after wire-induced injury in ApoE mice	Inhibition of HIF1-α reduced neointimal formation	
	Adenoviral inhibition of HIF1-α after wire-induced injury of femoral artery in ApoE mice	Reduction of neointimal/media ratio and increase in lumen/vessel-wall ratio	Christoph et al. 2014
	Adenoviral OE of HIF1-α after wire-induced injury of femoral artery in ApoE mice	Increase in intima/media ratio and decrease in lumen/vessel-wall ratio	
	Intravenous injection of Adenoviral OE of HIF1-α in ApoE mice	reduction of plaque size at the aortic sinus	Ben-Shoshan et al. 2009
	HIF1-α $CDH5^{ERT2}$/ApoE mice in presence of HFD and partial ligation at the carotid artery	Reduction in plaque area and macrophage accumulation	Akthar et al. 2015

Continued Table 1. HIFs in atherosclerosis.

HIF2-α	human carotid plaque	HIF2-α levels increased with plaque progression	Sluimer et al. 2008
	Adenoviral OE of HIF2-α after wire-induced injury of femoral artery in ApoE mice	Increase in intima/media ratio and decrease in lumen/vessel-wall ratio	Christoph et al. 2014
	HIF2-$\alpha^{\Delta Adipo}$/ApoE mice in presence of HFD and exposed to 16°C or 22°C	Increased atherosclerosis plaque and macrophage infiltration, these effects are enphasised when mice were exposed to 22°C	Zhang et al. 2019
	HIF2-$\alpha^{\Delta Adipo}$/ApoE mice and controls HIF2-$\alpha^{fl/fl}$/ApoE mice injected with FG-4592	FG4592 reduced atherosclerotic plaque in controls mice but not in HIF2-$\alpha^{\Delta Adipo}$/ApoE mice	Zhang et al. 2019
	HIF2-$\alpha^{\Delta SMC}$/ApoE mice and controls fed a HFD	Reduction of atherosclerotic plaque	Qi et al. 2017
HIF1-α and HIF2-α	Oral administration of FG-4497 in LDLR mice fed a HFD	Reduction in plaque area	Rahtu-Korpela et al. 2014, 2016

Targeting HIF for atherosclerosis therapeutic intervention

Atherosclerosis has been subject of extensive research with the aim to find new drug targets. Currently pharmacological approaches rely on three major concepts: (i) lower lipid levels, (ii) antagonise the inflammatory process to slow down the progression of the atheroma, and (iii) block or prevent thrombotic events using anti-coagulant therapy (Bäck and Hansson, 2015; Bergheanu, 2017). Over the past decades the HIF pathway has been therapeutically targeted for multiple pathologies, including cancer, chronic kidney disease, inflammatory bowel disease and peripheral arterial disease, as reviewed in (Chan *et al.*, 2016; Semenza, 2019). Thus, activation of the HIF pathways can be targeted to restore angiogenesis, prevent ischaemic events and to metabolically reprogram cells. Only recently, HIF activation has been associated with atherosclerosis development, thereby becoming an exciting target for atherosclerosis therapeutic intervention.

Therapeutically targeting HIF-activation

With the aim to enhance HIF activity, current therapeutic approaches for chronic kidney disease are based on the inhibition of PHD enzymes, that are responsible for the initiation of HIF degradation. As an example, Molidustat (BAY-3934) and Roxadustat (FG-4592), among others, are PHD2 inhibitors. However, PHD inhibition lead to the simultaneous activation of both major isoforms, HIF1-α and HIF2-α, thus possibly causing undesirable effects. Nevertheless, treatment of dyslipidaemic mice with the PHD2 inhibitor (FG-4497) ameliorated obesity, glucose and lipid metabolism in liver and white adipose tissue and reduced atherosclerotic plaque size (Rahtu-Korpela *et al.*, 2014, 2016).

Confusingly, although HIF1-α stabilisation has been suggested to promote atherosclerosis by a number of laboratories, its angiogenic effects may make this molecule an attractive target for treatment of limb-ischemia and claudication. Furthermore, adenoviral-HIF1-α gene therapy was shown to improve local wound healing and angiogenesis in diabetic mice (Botusan *et al.*, 2008). However, the administration of Adenovirus 2- HIF1-α overexpressing construct-VP16 was not effective in treating limb ischemia in a patient (Creager *et al.*, 2011).

Overall, the effects of long-term treatment with HIF stabilisers are currently unknown, and the contrasting activities of the HIFs isoform in various organs suggest that this aspect must be carefully and thoroughly investigated.

Therapeutically targeting HIF-inhibition

Selective HIF inhibitors are currently studied for cancer therapy and undergoing assessment in several clinical trials (available on https://clinicaltrials.gov). As an example, selective antagonists of HIF2-α have been recently developed (Chen *et al.*, 2016; Cho *et al.*, 2016; Wallace *et al.*, 2016), and shown to target HIF2-α specifically in kidney cancer models. These compounds, PT2385 and PT2399, inhibit heterodimerization with HIF1-β by binding to the PAS-B domain of HIF2-α.

Despite the co-existence of the two main isoforms in vascular endothelium, and the fact that HIF1-α and HIF2-α might have opposing roles, targeting the HIF pathway for atherosclerosis may be a great therapeutic option. It may however require an isoform specific and tissue specific drug development programme. A potential way of achieving subunit specificity is the coadministration of isoform specific HIF inhibitors together with HIF stabilisers to finely regulate the balance between HIF1-α and HIF2-α to suppress atherogenesis. In addition, site specific therapy (e.g. at the atheroma plaque) may be considered the key for aiming a selective activation or inhibition of these transcription factors, potentially with limited undesirable effects. Taken together HIF modulating drugs are an exciting therapeutic development that requires further study.

Hypothesis and project aims

In this PhD project, I hypothesised HIF2-α is a vital regulator of endothelial physiology in arteries and that it is regulated locally by shear stress and systemically by metabolic syndrome risk factors.

To test this hypothesis I aimed to:

- Assess the expression of HIF2-α in adult vascular endothelium and assess its response to shear stress using mice aorta.
- The response of HIF2-α to cardiovascular risk factors by assess its levels in adult vascular endothelium in mouse models of diabetes, high fat diet or leptin deletion to obtain obesity.
- Assess the expression of HIF2-α in cultured endothelial cells exposed to different patterns of flow.
- The function of HIF2-α in endothelium by inducing endothelial knock-out *in vitro* and generating endothelial specific KO mice.
- Finally, test the role of HIF2-α in response to PCSK9-induced atherosclerosis development using endothelial HIF2-α KO mice.

Summary

Atherosclerosis is an inflammatory disease that begins with the dysfunction of endothelial cells. The frictional force of the blood flow, the shear stress, primes the endothelial cell layer to physiological changes. Low wall shear stress results in atheroprone phenotype, while high wall shear stress drives atheroprotection.

At different shear stress magnitudes, endothelial cells change their gene expression profiles. For example, the transcription factor member of the HIFs family, HIF1-α is enhanced at the atheroprone regions, whilst the role of its siblings, including HIF2-α, is unknown.

This PhD will study whether the HIF2-α isoform is regulated by shear stress. To investigate this I will perform both *in vivo* and *in vitro* studies to characterize protein levels and gene expression. After showing this, I will investigate whether endothelial HIF2-α responds to cardiovascular risk factor, such as diabetes and obesity. Finally, I will investigate whether HIF2-α participates to the atherogenesis process. This will be assessed by functional studies, using both *in vivo* and *in vitro* models.

Chapter 2. Materials and Methods

Materials and suppliers

Materials and reagents used are listed in the following tables and presented in the appendix (Chapter 7):

- Tissue culture media (Tables 3 and 4), *In vitro* reagents (Table 5) , lentiviral particles (Table 6);
- RT-qPCR primers (Table 7);
- Western blotting reagents (Table 8) and buffer composition (Tables 9, 10, 11);
- *In vivo* reagents (Table 12) and genotyping reagents (Tables 13, 14, 15);
- *En face* staining reagents (Table 16);

In vitro studies

Collection of porcine aortas

Porcine aortas samples were collected from a local abattoir (N. Bramall and son Ltd, Oxspring, UK) and kept in cold Dulbecco's Modified Eagle Medium (DMEM) enriched with 10,000U/ml Penicillin-10,000 µg/ml Streptomycin antibiotics, 250 µg/ml Amphotericin B antifungal and 100 µg/ml Gentamycin. Samples were quickly brought to the lab and processed for primary endothelial cells or nucleic acid isolations as described in the following sections.

Porcine aortic endothelial cells (PAECs) isolation

PAECs were isolated from aortic arch or descending aorta of 6 months old pigs collected immediately after slaughter. Aortae were submerged in DMEM containing Penicillin and Streptomycin antibiotic mix, cleaned of fat and connective tissues excess and ostiae from intercostal arteries were sealed using cotton stitches (Ethicon). Brachiocephalic artery and carotid artery were closed using plastic surgical clips (Ethicon). Aortic arch and descending aorta compartments were isolated by closing the aortic lumen using a surgical clip. A three-way tap Luer lock (BD Connecta) was inserted at the extremity of the aorta, the ascending aorta and the lower extremity of the descending aorta. To allow endothelial cells digestion a solution

of collagenase IV was made up in FBS-free media at 1mg/ml final concentration and sterile filtered. Collagenase IV solution was pre-warmed at 37°C then flushed into the vessel and incubated for 10 mins under the tissue culture hood. After incubation, the solution containing PAECs was aspirated off from the aortic arch and descending aorta respectively. PAECs were pelleted by centrifugation at 250 g for 5 mins. Cell pellet was suspended into complete media (composition of media are listed on tables 1 and 2.) and seeded into a T25 flask (Thermo Fisher Scientific) pre-coated with 1% gelatin. PAECs were then tested for an endothelial cell marker and routinely subcultured as described in the following sections.

Primary cell culture

Primary PAECs were maintained at 37°C in a 5% CO_2 incubator. Cells were passaged before they reached 90% confluency, every 2-3 days. To dissociated cells from the flask, PAECs were washed twice with PBS and treated with pre-warmed trypsin 0.25% for 2-3 mins. Enzymatic activity was inhibited by adding complete media to the flask. Cell suspension was collected into a falcon tube and centrifuged at 250 g for 5 mins. PAECs were then resuspended into an appropriate volume of media and split in a ratio of 1:4 for routine subculture. PAECs that were between passage 3-6 were used for subsequent experiments.

Flow cytometry

CD31 (PECAM-1), a well-known endothelial cell marker was used to identify the isolated primary cells as cells derived from endothelium (van Mourik *et al.*, 1985). PAECs were suspended in PBS and stained using LCI-4 (PECAM-1) antibody at 10 µg/ml and gently rocking on ice for 20 mins. PAECs were pelleted by centrifugation 250 G for 5 mins and washed with PBS to remove any antibody excess. PAECs were then stained using a FITC-conjugated secondary antibody (Goat anti-mouse AF488, 6.6 µg/ml) and incubated on ice for 20 mins protected from light. Cells were then washed by centrifugation and then resuspended in PBS for analysis. Cells viability was assessed by TO-PRO-3 iodide reagent at the final concentration of 5 µg/ml for counterstaining. Cells were analysed on the LSRII flow cytometer (BD) using forward versus side scatter to gate on a population of living cells. Baseline fluorescence was

set established by a secondary antibody only control, then single cells where gated on and these were analysed for FITC fluorescence using the blue (488 nm) laser with 530/30A filter.

Flow studies

Orbital shaker system

A confluent 75cm^2 flask of endothelial cells was seeded onto gelatin pre-coated 6 well plates or on glass at 4x10^5 cells/well and kept in an incubator at 37°C and 5% CO_2 for 24h. The day after seeding, complete media was refreshed with 3mL in every well. The 6-well plate was placed onto an orbital shaker system (Grant-Bio PSU 10i) orbiting at 210rpm for 72h at 37°C and 5% CO_2. This system reproduces typical undisturbed flow signalling in the periphery of the well, exposed at high wall shear stress (HSS), whilst, at the centre, the orbital shaker reproduces low-oscillatory shear stress (LSS) (Figure 2.1) (Warboys *et al.*, 2014).

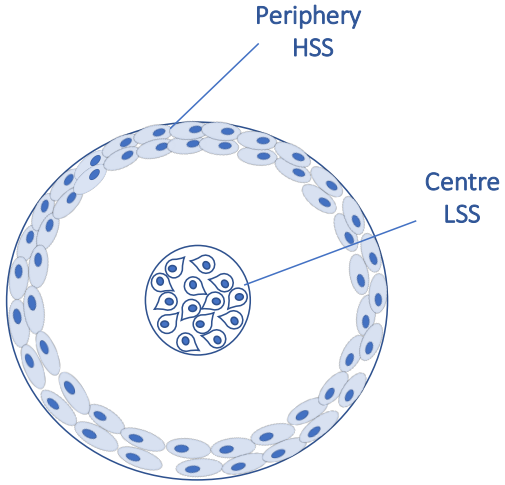

Figure 2.1 Orbital shaker system

ECs placed on the orbital shaker system for 72h experienced HSS in the periphery, and LSS in the centre of the well. ECs morphology and alignment varied depending on the shear stress experienced. Cells at the periphery aligned with the flow with an elongated shape. Cells in the centre experiencing LSS, are not aligned and cobblestone shaped. Cells between the periphery and the central region of the well (not shown) were not collected or examined during the experiments.

Ibidi system

Part of the *in vitro* flow experiments were performed using the Ibidi system (Ibidi GmbH, Munich, Germany). This system can produce different shear stress in vitro at biologically relevant magnitudes, as is seen in HSS and LSS areas of the vasculature. The Ibidi pump is set to 12 dyn/cm^2 to represent high unidirectional shear stress and 0 ± 4 dyn/cm^2 for low oscillating shear stress. Twenty-four hours prior to every experiment, PAECs were harvested from a T75 flask and seeded onto pre-gelatinised 1 % w/v gelatine 0.4 µm deep flow chambers (Ibidi µ-slide 1$^{0.4-}$ Luer) at the density of 2 x 10^5 cells in 100 µl of complete media. On the day of the experiment, Ibidi flow units were kept into an incubator at 37°C, 5% CO_2 to equilibrate and then cells were plugged to the Ibidi flow units containing 12 ml of complete media. Shear stress conditions were applied for 72h.

Viability assay

PAECs were suspended in an appropriate volume of media. An aliquot of cells suspension was mixed with Trypan blue 0.4% reagent in ratio 1:1 and cell viability was assessed by hemocytometry. Trypan blue is a charged dye that localised into the cytoplasm of cells when their membrane is compromised. Therefore, dead cells are more permeable and uptake trypan blue appearing stained of an intense blue under the microscope, while intact live cells excluded the dye and appeared to have a pale colour under the microscope. Dead cells and total cell number were counted and values were adjusted for dilution factor (d.f.). Percentage of dead cells was calculated as follow:

$$\%\, Dead\ cells = \frac{N°\ of\ dead\ cells}{N°\ of\ total\ cells\ counted} x\ d.f.x\ 100$$

Immunofluorescence staining

PAECs were blocked by treating them with 20% goat serum in 1XPBS with 0.1% tween-20 (PBST) for 1h at 4°C. Cells were then stained with HIF2-α antibody used at a final concentration of 6.6 µg/ml in PBST and kept at 4°C for 24h on a gentle rocking plate. To remove any excess antibody PAECs were washed twice with PBS for 5 mins. A secondary antibody (Goat anti Rabbit AlexaFluor (AF) 568) at 10 µg/ml diluted in 5% goat serum in PBST was applied for 5h at room temperature. PAEC were then washed with PBS and stained with the LCI-4 antibody which

recognises the endothelial cell marker PECAM-1. Samples were incubated with LCI-4 at the final concentration of 10 µg/ml diluted in 5% goat serum PBST overnight at 4°C, followed by 5h of incubation at room temperature with a secondary antibody (Goat anti mouse AF647) at 3.3 µg/ml diluted in 5% goat serum PBST. All procedures were performed away from light. Finally, glass coverslip were mounted onto microscopy slides using an antifade reagent, ProLong™Gold. Samples were imaged using Olympus FV1000 confocal microscope. Antibodies and reagents used in this section are listed on table 5.

RNA isolation from tissue

Aortae were submerged in DMEM containing Penicillin and Streptomycin antibiotic mix, cleaned of fat and connective tissues excess. Regions were identified by a shear stress map, which was previously developed in our laboratory (Serbanovic-canic *et al.*, 2016). During all the procedures of dissection, tissues were kept in ice cold PBS. Regions of HSS and LSS were isolated by a scalpel blade (Figure 2.2). Explanted regions were then place face down onto a drop of collagenase type IV 1 mg/mL suspended in FBS-free media and pre-warmed at 37°C . After ten minute of collagenase digestion, endothelial cells from selected areas were scraped with a scalpel into a 1.5 mL Eppendorf tube and collected by centrifugation.

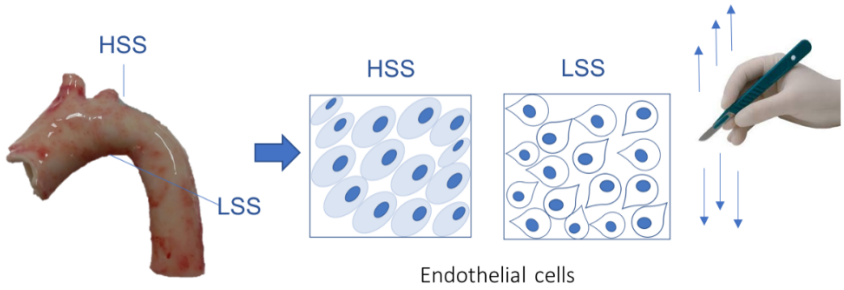

Figure 2.2 Porcine aorta dissection

The selected regions of porcine aorta experiencing either HSS or LSS were explanted and subjected to collagenase digestion for 10 min. After digestion, endothelial cell layer was gently scraped with a scalpel and collected for RNA isolation.

The endothelial cell pellet was suspended in 500 µL of Trizol®Reagent and homogenized by pipetting up and down 8 to 10 times with a 21 Gauge needle attached to a 1ml syringe. RNA isolation was performed according to manufacturer instruction and then the RNA pellet was

air dried for 5-10 minutes, and re-suspended with 35 µL of nuclease free water. RNA purity and quantification was assessed by Nanodrop spectrophotometer (Thermo Scientific).

In vitro HIF2-α functional study

HIF2-α silencing by lentivirus transduction

To study the function of HIF2-α in sheared endothelial cells, PAECs were seeded onto a pre-gelatinised Ibidi slide at the density of 2 x 10^4 cells in 100 µl of complete media and incubated for 1-2h until complete attachment. PAECs were then treated with Dharmacon™ SMARTvector Human Lentiviral shRNA pool composed by three shRNAs against human HIF2-α sequence built under non fluorescent reporter human CMV promoter, represented in figure 2.3 and listed on table 6. Alternatively, PAECs were treated with a non-targeting shRNA as control, henceforth referred to as "scrambled".

Lentiviral particles were used at the pooled concentration of 30 MOI (Multiplicity Of Infection), where MOI is the ratio between the lentiviral transducing units (TU) used to cells seeded. Lentivirus was diluted in media in the presence of DEAE-Dextran hydrochloride diluted 6 µg/ml to facilitate interaction between lentiviral particles and cells surface. PAECs were incubated with lentivirus overnight, then lentiviral particles were replaced by complete media and cells were exposed to flow at a magnitude of 4 dyn/cm^2 and a frequency of 0.5 Hz to represent low oscillating shear stress. Shear stress condition were applied for 72h. Then, to evaluate transduction efficiency PAECs were collected for protein or RNA analysis as previously described.

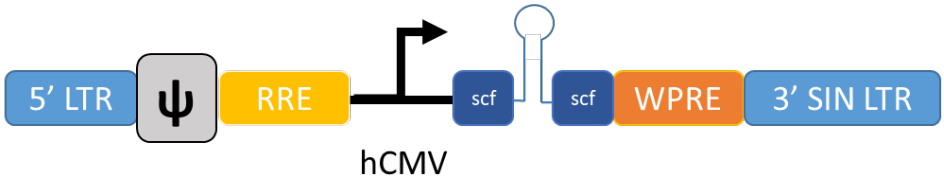

Vector Element	Description
5' LTR	5' Long Terminal
Ψ	Psi packaging sequence
PRRE	Rev Response Element
hCMV	Human Cytomegalovirus promoter
scf	SMARTvector universal scaffold enclosing the mature microRNA sequence
WPRE	Woodchuck Hepatitis Post-transcriptional Regulatory Element
3' SIN LTR	3' Self-inactivating Long Terminal Repeat

Figure 2.3 Lentiviral construct example and components description.

Three shRNA sequences were selected for lentiviral mediated HIF2-α gene silencing in endothelial cells. Human sequences were blasted onto sus scrofa HIF2-α sequence and confirmed for 100% match. Human cytomegalovirus (CMV) promoter was chosen for delivering the shRNAs. The sequence was flanked by a long terminal repeat (LTR) in 5’ and 3’ and the construct was integrated with a 3’ Self-Inactivating sequence (3’SIN) to reduce risk of viral replication after transduction into target cells. WPRE sequence supported gene delivery by viral vector. Image adapted from https://horizondiscovery.com

Proliferation quantification and senescence morphology assessment

PAECs were fixed using 4% PFA for 12 minutes to study cell cycle protein level (Ki67) using immunofluorescence staining. PAECs were incubated with 20% goat serum in 1XPBST for 1h and then stained for Ki67 overnight at 4°C. A secondary antibody conjugated to AF568 and diluted 6.6 µg/ml in 5 % goat serum 1XPBST solution was applied for 5h at room temperature. Images were taken directly onto the 6-well plate using a non-confocal microscope, Leica DMI4000B with a 20x magnification objective.

To study the morphology of ECs exposed to low WSS for cellular senescence, a prelaminar analysis was performed under the brightfield illumination. As opposed to cobblestone-shaped replicative ECs, senescent ECs are characterised by a peculiar morphology that includes an

enlarged cytoplasm, the presence of multi nuclei and possibly the absence of cell/cell contact (Hernandez-Segura, Nehme and Demaria, 2018). Thus, observation of cellular morphology at the brightfield together with the subsequent evaluation of the staining using the DAPI (nuclear) channel were engaged to preliminary define senescent cells. Cells that reflected such phenotype were counted as senescence and a percentage of the ratio between the positive cells counted and the number of cells per field of view was then calculated.

Mitochondria content and morphology

To identify mitochondrial content and morphology, PAECs were incubated with 200 nM Mitotracker Red CMXRos reagent for 40 mins at 37°C in FBS-free media. Then, PAECs were fixed using pre-warmed 3.7% PFA in FBS-free media for 15 mins at 37°C. All procedures were performed protected from light. Glass coverslips were mounted onto microscopy slides using an antifade reagent, ProLong™Gold. Samples were imaged by Olympus FV1000 confocal microscope.

Confocal images were analysed using ImageJ (FIJI) software. Mitotracker CMXRos quantification was performed by analysis of total mean fluorescent intensity (MFI) of Mitotracker staining and by identification of mitochondrial morphology. The latter was analysed by adapting a macro for Fiji generated by (Dagda *et al.*, 2009), henceforth referred to it as "F11" macro. A macro was generated for automatizing images preparation and correction prior to applying F11 analysis.

Prior to commencing the analysis all the images were split into individual channels: channel 0 for DAPI (blue), channel 1 for BODIPY (green), channel 2 for Mitotracker (red) and channel 3 for PECAM-1 (grey).

To correctly threshold the images for mitochondrial analysis, the first step of the protocol was to remove the background derived from the nuclei from the Mitotracker channel. Therefore, nuclei were delineated by a mask on channel 0 (DAPI), and exported to channel 2 (Mitotracker). Nuclei area were selected and filled in order to set the background as black and numerically as 0. Images were analysed at 8 bit and the scale set as "global", with pixel at 1 μm ratio. Then, threshold was applied to Mitotracker channel and individual cells were analysed by polygon selection. In order to identify the border of a cell, polygon selection was built on the channel 3 (PECAM-1) and exported on channel 2 (Mitotracker) for F11 analysis. A total of 40-50 cells were

analysed over three different field of view for each condition. Mitochondrial data were heterogeneously distributed in a non-gaussian curve, therefore data were analysed and presented by using geometric mean values.

The analysis generated the following outputs:

- **Count**= Number of mitochondria particle counted
- **Area**= Area occupied by mitochondria expressed in μm^2
- **Perimeter**= Perimeter covered by mitochondria expressed in μm
- **Minor axis**= Minor axis of mitochondria
- **Major axis**= Major axis of mitochondria
- **Mitochondrial content**= % of cytosol occupied by mitochondria within a defined ROI
- **Solidity**= Fraction of pixel in the smallest convex polygon that are also mitochondrial pixel

Geometrical parameters were used to further calculate :

- **Mitochondrial interconnectivity**, calculated as the ratio between area and perimeter and expressed in μm.
- **Circularity**, calculated using the following formula: $\frac{4*Area}{\pi*[major\ axis]^2}$, where the area of a circle is $A = \pi r^2$ and by definition a perfect circle has value of 1, whilst a line as representative of absence of circularity has value 0. Therefore, the inverse of circularity is index of elongation.
- Geometric analysis of the **swelling** included normalising the area- perimeter ratio values to minor axis or circularity value.

Inclusion criteria and limitations:

i. In order to identify mitochondrial morphology, PAEC presenting an incorrect threshold (Figure 2.4, left panel) were excluded from the analysis. All the cells presenting an adequate threshold that delineated the morphology of the mitochondria (Figure 2.4, right panel) were selected for F11 analysis.

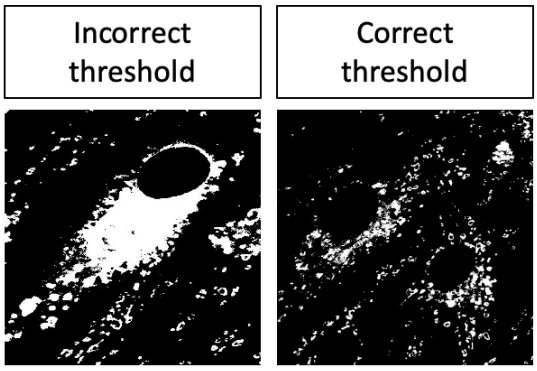

Figure 2.4 Examples of mitochondria after binarization of the image.

Left panel picture shows endothelial cells with a threshold of mitochondrial staining unsuitable for the analysis and therefore excluded. In the right panel, endothelial cells with correct characterisation of the mitochondria morphology after thresholding process and therefore included in the analysis are shown.

ii. To delineate correctly the cell border, ROI was drawn in channel 3 using polygon selection and all cells at the edges of the image with incomplete or undefined borders assessed by PECAM-1 staining were excluded from the analysis.

iii. To minimise technical artefacts, images that presented uneven planar distribution were carefully examined to allow selection of ROIs on cells on the sample plane. The cells excluded usually corresponded to the cells with incorrect threshold as described at point *i*.

Transcriptional analysis

RNA isolation and quantification

RNA was isolated by using RNA Mini kit, following the manufacturer's instruction. RNA was eluted on a column with 35-50 µL of RNA and DNA free water, supplied within the kit. RNA purity and quantification were assessed by Nanodrop spectrophotometer (Thermo Scientific) using 1 µL of sample. RNA concentration was measured as the absorption at 260 nm (A260 nm), while sample purity from DNA, protein and other contaminants were calculated as ratio

of the absorbance at A260/A280 nm and A260/A230 nm. Commonly high standard samples have expected ratio between 1.8 and 2.2.

cDNA preparation

Reverse transcription was performed by iScript cDNA Synthesis Kit (Bio-Rad). Reverse transcription reaction was followed as per the product's protocol, for a total volume of 20 µL per single reaction. RNA input required was between 100 fg–1 µg of total RNA. cDNA synthesis reaction was performed in a thermal cycler (Veriti-96 well Thermal Cycler, Applied Biosystem) with the following protocol: Priming (5 min at 25°C), Reverse transcription (RT) (1 min at 95°C), RT inactivation (20 min at 46°C), and finally sample was kept in a hold stage at 4°C at the end of the procedure.

Real Time-qPCR

In order to assess the expression of the targeted gene of interest, a selection of primers was designed by comparing the appropriate transcript sequence on an ensemble tool (http://www.ensembl.org/index.html). Then selected exons were copied onto the NCBI tool using the following settings: GC% optimum 50 and product size 70-150 base pair (https://www.ncbi.nlm.nih.gov/tools/primer-blast) . Target selectivity was confirmed by NCBI BLAST tool. Primers were ordered from Integrated DNA technologies (IDT) see table 7, with standard desalting process and 25 nmole DNA oligo settings. Primers were kept as a 100 µM stock at -20 °C. 10 µM was used as the working concentration for following procedures.

In order to evaluate transcript expression of selected genes, quantitative real-time Polymerase Chain Reaction has been performed using the Syber Green system (SsoAdvanced SYBER Green Supermix (Biorad)). cDNA samples were diluted to 1 ng/µL and following the manufacturer instructions, 4.4 ng were loaded in each well onto a 384 well plate. cDNA was combined with SsoAdvanced Superrmix and a mix of forward and reverse primers. Analysis was performed in triplicate for each sample. CFX384 Real-Time system (Bio-rad) was used with the following settings: hot start for 3 minutes at 95°C, followed by 40 amplification cycles at 95°for 5 seconds and 30 seconds at 60°C for annealing and extension.

Gene expression analysis was performed by the ΔΔCt method. This evaluates the relative quantity of a transcript, normalizing each sample to a housekeeping gene. The porcine sample

to Beta-2-microglobulin (B2M). The ΔCt was calculated from the housekeeper normalization, and then each ΔCt was further analyzed versus a control sample (untreated or reference sample, endogenous control). Hence, ΔΔCt in its linear expression (reported as $2^{-\Delta\Delta Ct}$) is shown as fold change of the sample. Primers are listed on the table 5.

Microarray

RNA samples were labelled and hybridised to a Porcine Genome array (Affymetrix). Then generated data were analysed using Transcriptome Analysis Console software (Affymetrix) and by Dr. Mark Dunning at the Bionfomatic core of the University of Sheffield. A list of differentially expressed gene was then interrogated onto the molecular signature database (MSigDB) tool of the gene set enrichment analysis (GSEA). The enriched pathway emerged from then analysis were the base for the following functional investigation *in vitro.*

Western blotting

For the present section all buffer composition and reagents are listed in tables 8 and following tables 9, 10 and 11. Cells were collected in sample buffer and boiled at 100°C for 5 mins followed by few minutes of cooling before western blotting. Western blotting was performed with 4-20% Mini-PROTEAN® TGX™ Precast Gels (BioRad). Samples were loaded, alongside a protein ladder dual colour as size reference for protein migration. Run was performed at 100 Volts for 1h in running buffer.

Gels were then prepared for transfer to membranes. Before assembly of the transfer unit, each membrane (Millipore) was activated by immersion in methanol for 3 mins. Transfer was assembled as a sandwich and submerged in transfer buffer. Transfer was performed with a cooling unit, for 80 minutes at 60V. Membranes were then blocked with 5% milk in TBST for 30 min.

After blocking, each membrane was inserted into a falcon tube with the appropriate primary antibody of interest or control diluted in 4% BSA in TBST, and kept overnight at 4°C. After the incubation with primary antibody membranes were washed and then incubated for 45 min at room temperature with secondary antibody 1 µg/ml. Membranes were then washed 5 times for 2 minutes in TBST. To reveal proteins, membranes were incubated with ECL for 2 minutes, and then imaged with a Biorad Chemidoc XRS+, using ImageLab software set for analysis on

"no filter" mode and "Chemi Hi-resultion" setting. Band intensities were analysed using Fiji Software.

Mouse studies

All animal experiments involving the study of murine aorta from high fat fed mice, obese (ob/ob) mice, streptozotocin and sulforaphane injected mice were approved under the coverage of the Institutional Animal Care and Use Committee licence (IACUC -161122), and performed at the laboratory of metabolic medicine at the Singapore Bio-imaging Consortium Institute, SBIC (Singapore). Whilst, experiments involving C57Black6/J mice, *HIF2-α$^{fl/fl}$*;*CDH5*-CreER^{T} mice and PCSK9 injected mice were compliant with the UK Home Office Animals (Scientific Procedures) Act 1986 (licence number P5395C858) and performed at The University of Sheffield (United Kingdom). All mice were fed *ad libitum* ,kept on 12h light/dark cycle caged in group of five unless otherwise stated.

C57BL6 wild type mice

To study the expression of HIF2-α at the endothelium of murine aorta, C57Black6/J were fed on a standard chow diet and sacrificed between 6-8 weeks of age. Animal sacrifice was performed with anaesthetic overdose via intraperitoneal injection in the posterior quadrant of the abdomen, using pentobarbital. When required, blood was taken by cardiac puncture in presence of heparin and centrifuged at 350 g for 5 minutes to obtain plasma.

To collect the aorta, mouse chest was opened and the heart was revealed and perfused with 10 ml of 1X PBS from the lower extremity of the left ventricle using a syringe. To reduce organ swelling the heart was snipped on the right atrium using scissors. To follow, heart was perfused with 10 ml of 4% PFA. Fixation was confirmed by visual inspection of tail and legs movement reflexes during PFA perfusion. The thorax was dissected, placed into 2% PFA for 1h and then kept in PBS at 4°C until the aortic cleaning was performed.

To study the effect of obesity and hyperglycaemia in the murine vasculature C57Black/6N mice were housed in groups of five and fed *ad libitum* with a high fat diet (HFD). Mice were fed with a rodent diet containing 60% of kcal from fat for 25 weeks (diet 1, table12). Littermate control mice were kept on a standard chow diet under the same housing condition and food accessibility for all the length of the experiment.

In addition, to assess the response of HIF2-α in diet-induced obesity mice to a natural antioxidant compound and to observe Its effect on vascular endothelium, HFD-mice were injected with sulforaphane once daily for three days and on the fourth day mice were injected 4h prior to sacrifice.

Blood glucose

Blood glucose levels were evaluated under 16h fasting condition using Accucheck glucometer strips coupled to the correspondent glucometer (Roche Diagnostics). Resting glucose levels were registered prior to animal sacrifices.

Leptin deletion model (ob/ob)

To study the effect of overt obesity in murine aorta, leptin null mice (*o*b/ob) were purchased from Jackson laboratory (JAX stock number: #000632). Homozygous ob/ob mice were sub-fertile, thus breeding strategy was to cross heterozygous mice (ob-/+) and genotyping was performed as previously published (Ellett *et al.*, 2009). Ob/Ob mice were fed on a standard chow diet for all the course of experiment. To study weight gain, body weight was recorded every week after weaning for 20 weeks. Ob/ob mice are characterised by fluctuating glycaemic levels over their life therefore, blood glucose levels was assessed after 16 hours-fasting in 12 weeks old mice and 6 months old mice.

Streptozotocin injections

Male C57BL6/J mice were fasted for 5 hour prior to intraperitoneal injections with 150mg/kg streptozotocin (STZ). STZ solution was prepared within 15 min for injections in 0.1M sodium citrate buffered with citric acid to final pH of 4.5. Buffered solution only was used as a control injection for vehicle group mice. After treatment mice were housed in separated cages and fed *ad libitum* for all the length of the experiment. All mice were weighed before injection and STZ volume adjusted accordingly. Animals with glucose >10 mmol/l were considered to have developed experimental diabetes. Thereafter, random glucose level was recorded at days 2, 8, 12 after injection to determine fluctuations and weight loss. With the aim to keep glucose levels between 15 to 18 mM, mice that didn't reach sufficient glycaemia to progress the experiment were administered with second dose of 100mg/kg STZ after at least 3 hour fasting. Glucose levels were than tested 48h after the second injection to confirm overt diabetes. At

termination of the experiment, mice were injected with 0.1 mg/g body weight of ketamine/xylazin mix. Blood was collected by cardiac puncture into a vacutainer containing heparin, centrifuged at 350 G for 5 minutes to obtain plasma and stored at -80°C until biochemical analysis was required. Tissue harvesting was performed as described for C57Black6/J mice.

Mice blood pressure

To study the effect of obesity on mice blood pressure, C57BL6/N mice exposed to a HFD for 7 months and chow diet controls and ob/ob mice or littermate controls were screened for changes in systolic and diastolic blood pressure. Mice were placed into a plastic restrainer-tube covered by a warm pad (37^{o}C) and left undisturbed for five minutes. Blood pressure measurements were performed using the non-invasive plethysmograph CODA (Kent Scientific). Blood pressure measurement was performed as instructed by the manufacturer, an O-ring cuff and VCR were placed on the mouse tail and blocked together with a plastic support, as illustrated on figure 2.5. Mice were trained for 5 to 7 consecutive days before perform final measurements. For each mouse, a minimum of 5 readings per session were annotated. All measurements were performed in a separated procedure room between 2-5pm.

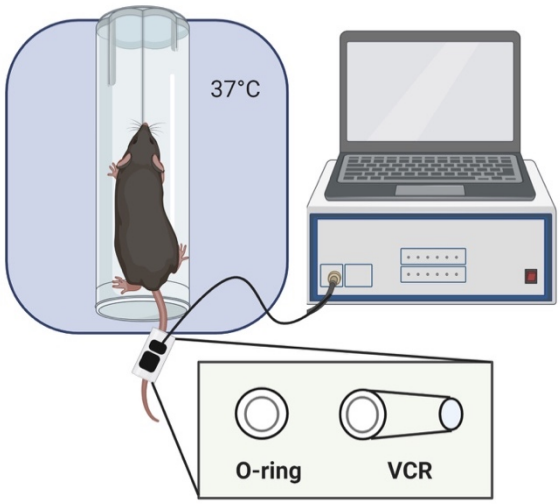

Figure 2.5 Mice blood pressure procedure

Mice were placed into a tube sat on a warm pad for acclimatization to the new environment. A tail cuff composed of two sections, O-ring and VCR was applied. Mice were trained for a minimum of five consecutive days prior to assessment. Mice that positively respond to the training by giving consistent reading over the training period, they were then used for final assessment and systolic, diastolic and mean blood pressure value were recorded. Image created using Biorenders.

Cholesterol assay

Plasma collected from chow diet fed, HFD mice, HFD mice treated with sulforaphane and ob/ob was analysed for total cholesterol level, high density lipoprotein (HDL), low and very low density lipoproteins (LDL and VLDL, respectively) contents. A quantitative colorimetric assay was performed using a cholesterol assay kit from Abcam (ab65390) that through cholesterol oxidase enzyme react with the cholesterol to generate a chemical that react with a probe and emits colour at wavelength of 570nm. A standard curve with six serial dilutions of cholesterol was generated and measured together with the sample. To separate HDL and LDL/VLDL, part of the plasma sample was mixed with sample buffer supplied by manufacturer and incubated for 10 mins. Sample were then centrifuged for 10 mins at 2000 g and the supernatant fraction was kept for HDL analysis. To obtain LDL/VLDL fraction, centrifugation was repeated and the supernatant discarded, while the pellet containing the lower lipoproteins fraction was resuspended in sample buffer. Samples and cholesterol standard curve were loaded onto a 96 well plate and incubated for 60 mins at 37^{o}C with total cholesterol reaction mix in accordance

with the manufacturer's instructions. Plate was then quickly analysed using a microplate reader (Berthold Technologies).

Generation of HIF2-α endothelial KO mice

To study the function of HIF2-α in endothelial cells, mice carrying the VE-Cadherin (CDH5)-CreER^{T} mutation were crossed with mice carrying the flox/flox allele targeting the exon 2 of HIF2-α, following the breeding scheme on figure 2.6A. Mice carrying the flox allele were kindly donated by Prof. Randall S. Johnson (Cambridge University, UK).

To obtain experimental mice, female *HIF2-α$^{fl/fl}$* mice were crossed with male *HIF2-α$^{fl/+}$;Cdh5*-CreER$^{T+/-}$ mice. The resulting progeny were predictably composed of 25% of *HIF2-α$^{fl/fl}$;Cdh5*-CreER$^{T-/-}$ mice used as controls and 25% *HIF2-α$^{fl/+}$;Cdh5*-CreER$^{T-/-}$ mice used as controls, 25% of *HIF2-α$^{fl/+}$;Cdh5*-CreER$^{T+/-}$ heterozygous mice and 25% of *HIF2-α$^{fl/fl}$;Cdh5*-CreER$^{T+/-}$ mutant mice.

To delete *HIF2-α*, six weeks old mice were treated with tamoxifen. Tamoxifen was administered once daily for a period of one week followed by a week of rest to allow gene deletion.

To identify mouse genotype, earclips from 14 days old mice or tamoxifen injected mice were collected and lysed using 50 µL of lysis buffer with 1.5% (v/v) proteinase K (composition listed in table 12) and incubated overnight on a heat block at 56°C. To inactivated enzymatic digestion samples were boiled at 100°C for 10 mins and resuspended in 350 µL nuclease free water. Genotyping analysis was performed as described by Gruber et al.2007. A set of three primers was used to distinguish wild type allele, floxed allele and the deleted allele after tamoxifen injections (Primer1-5'-CAGGCAGTATGCCTGGCTAATTCCAGTT-3'; Primer2-5'-CTTCTTCCATCATCTGGGATCTGGGACT-3'; Primer3–5'-GCTAACACTGTACTGTCTGAAAGAGTAGC-3'). As illustrated in figure 2.6B, the amplicon generated by primers 1 and 2 allowed us to distinguish between wild type (410bp) and flox alleles (444bp), while the amplicon generated by the reaction between primers 1 and 3 distinguished for the mutant mice with activated Cre and therefore amplified the band of the deleted allele (340bp). The PCR was carried out using 5 µL of DNA input diluted 1:2 with nuclease free water. PCR reaction mix was composed of 10 µL of diluted DNA, 1x PCR buffer,

100 µM dNTPs, 0.24 µM of primer mix and 0.75 units Taq DNA polymerase. The PCR reaction was then incubated using a thermal cycler (Veriti^{TM} 96-well Thermal Cycler, Thermo Fisher Scientific) at 95°C for 5 min, followed by 35 cycles composed by a first segment of 95°C for 30 sec, followed by the second segment of annealing at 63°C or 56°C for 30 seconds (genotyping HIF2-α or Cre respectively) and a third segment of extension at 72°C for 1 min. To inactivate the reaction samples were finally incubated at 72°C for 10 min and stored at 4°C. To analyse the PCR products a 2% Agarose gel was made up in 1XTAE buffer, table 12. 10 µL of the intercalating agent ethidium bromide were added to the gel prior to solidification. PCR products were loaded onto the gel using a blue loading dye alongside a reference quick-Load Purple Low Molecular Weight DNA Ladder and run at 85V for 70 min. The gel was then imaged by a Biorad Chemidoc XRS+, using ImageLab software set for nucleic acid analysis on "filter 1" mode. Band sizes were analysed using Image Lab software.

All reagents used in this section and not included in formulation are further listed in table 13.

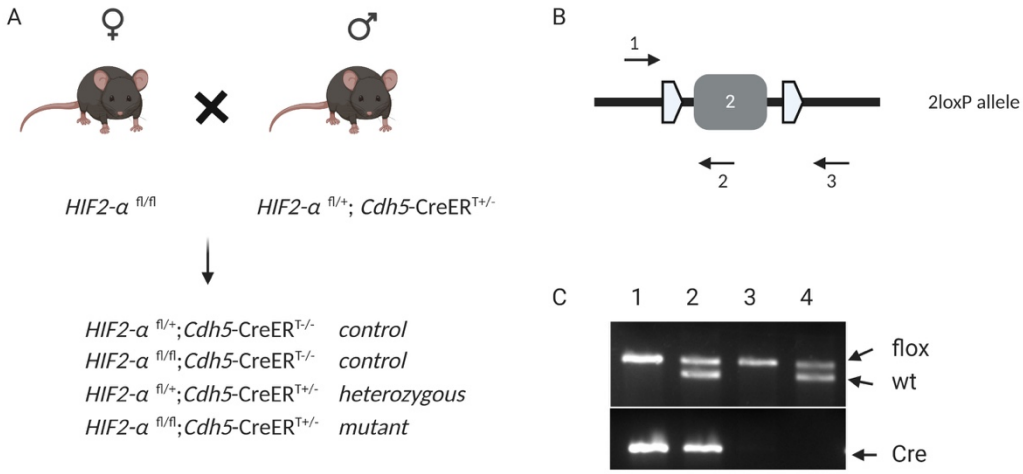

Figure 2.6 Generation of HIF2-α EC^{KO} mice

A) Female mice carrying the flox allele were crossed with male heterozygous mice expressing Cdh5-CreER$^{T+/-}$. The genotype of the obtained progeny was equally divide onto HIF2-α$^{fl/+}$;Cdh5-CreER$^{T-/-}$ (control), HIF2-α$^{fl/fl}$;Cdh5-CreER$^{T-/-}$ (control), HIF2-α$^{fl/+}$;Cdh5-CreER$^{T+/-}$ (heterozygous), HIF2-α$^{fl/fl}$;Cdh5-CreER$^{T+/-}$ (mutant). B) 2 loxP sites flanked the exon 2 of HIF2-α gene and a multiple PCR with a set of three primers was used to identify mutants from controls mice. C) DNA gel shows in lane 1 a HIF2-α$^{fl/fl}$;Cdh5-CreER$^{T+/-}$ mutant mouse, in lane 2 an heterozygous mouse with HIF2-α$^{fl/+}$;Cdh5-CreER$^{T+/-}$ genotype, lane3 shows HIF2-α$^{fl/fl}$;Cdh5-CreER$^{T-/-}$ mouse and lane 4 HIF2-α$^{fl/+}$;Cdh5-CreER$^{T-/-}$ used as experimental controls. . Image created using Biorenders.

PCSK9 model of atherosclerosis

Two weeks after tamoxifen-induced HIF2-α deletion, experimental controls (HIF2-α$^{fl/fl}$;Cdh5-CreER$^{T-/-}$ and HIF2-α$^{fl/+}$;Cdh5-CreER$^{T-/-}$) and endothelial specific HIF2-α KO mice (HIF2-α$^{fl/fl}$;Cdh5-CreER$^{T+/-}$) were injected with Adeno Associated Virus (AAV) type 8 encoding a gain of function of proprotein convertase subtilisin/kexin type 9 (PCSK9) to increase cholesterol levels. AAV was prepared by UNC Vectore Core (Chapel Hill, NC) in HEK293 cells starting with a plasmid carrying the D377Y mutation for PCSK9. pAAV/D377Y-m PCSK9 was a gift from Jacob Bentzon (Addgene plasmid #58376) (Bjorklund *et al.*, 2014). 6*10^{11} viral particle were injected in a single dose to each experimental mouse. To achieve and accelerate atherosclerosis, mice

injected with PCSK9 mutant were fed *ad libitum* a high fat diet (diet2, table 12) for 8 weeks. At termination of the experiment, blood plasma was collected and heart and aorta were perfused fixed and processed as previously described.

Dissection of fixed tissues

Fixed thoraces were cleaned by sliding forceps underneath the ribcage to remove the aorta from the spine. Heart and other peripheral organs, such as lungs, oesophagus, vena cava and trachea, were removed by dissection under the microscope. Aortae were further trimmed by removing fat and connective tissue alongside the vessel. Intercostal vessels were removed from the base by spring scissors, and the adventitial layer was removed carefully by peeling off with fine forceps. A portion of the aortic root was kept for future work. To analyse the presence of plaque at the aortic sinus, dissected hearts were cut below the atriums and aortic root was submerged in 2% PFA and incubated overnight in cold room. Following fixation the aortic root was placed into 30% sucrose until sunk, then placed and stored in optimal cutting temperature compound (OCT) frozen under liquid N_2 vapour.

Oil Red O staining

Aortae were stored overnight in 4% PFA and then processed for oil red O (ORO) staining. A stock solution of ORO at 0.3% (w/v) in isopropanol was prepared and filtered through Whatman number1 filter paper and 0.22 µm filter. A working solution was prepared by diluting ORO stock solution to 60% using deionised water. Briefly, aortae were rinsed with distilled water and submerged in 60% isopropanol for 2 mins. Then tissue were submerged for 15 mins in a solution of 60% ORO followed by a wash in 60% isopropanol and then in deionised water. Finally tissues were pinned open onto a wax coated dish, with the lumen facing upward. Images were taken using Canon PowerShot A650 IS digital camera mounted onto a Stemi 2000 C microscope (Zeiss). Plaque quantification was performed using NIS-Elements BR (Nikon).

En face staining

Tissue preparation

Mouse thoraces were cleaned as previously described into the section "dissection of fixed tissue". To perform *en face* staining, aortae were cut at two different areas of the 1st Arch, to identify HSS and LSS respectively, and at the descending aorta. The latter is a well-known atheroprotected region exposed to HSS while ostiae of the intercostal arteries are site of LSS. Open sections are shown in figure 2.7.

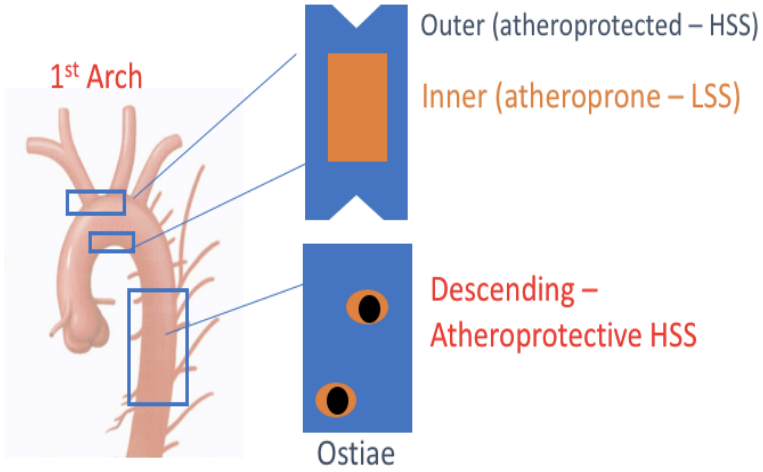

Figure 2.7 Mice aorta sections for immunofluorescent staining

Murine aortas were dissected at the first arch and at the descending aorta. Section were open along the outer curvature to reveal the area of HSS (outer curvature) and LSS (inner curvature) of the first arch, and the descending aorta with the associated ostiae.

Staining procedure

Harvested aortic tissues were sectioned into two different regions: the aortic arch and the descending aorta. To assess HIF2-α distribution in murine ECs, mouse aortic sections were stained with HIF2-α, CD31, and TO-PRO-3 antibodies (table 14). Samples were permeabilised overnight at 4°C with 20% Goat serum in 1XPBST. Then, tissues were immersed into 6.6 µg/ml of HIF2-α primary antibody in 3% BSA in 1X PBST, and incubated protected by light overnight.

After two quick washes in 1X PBST, samples were stained with secondary antibody (Goat anti Rabbit AF568) diluted 1:150 in 3% BSA in 1X PBST for 8h covered from light. Samples were then washed twice in 1X PBST and submerged in CD31 antibody conjugated to AlexaFluor®488 diluted 10 μg/ml in 3% BSA in 1X PBST for overnight. Finally, samples were washed twice in 1X PBST and counterstained for TO-PRO-3 (nuclear staining) for 45 mins. Samples were mounted using 10μL ProLong™Gold reagent onto a coverslip with endothelial cells facing down and then transferred on a microscope slide. Samples were left under a weight to dry overnight at 4 C before imaging by confocal microscopy.

Confocal microscopy imaging

Microscopy slides were imaged using Nikon Eclipse T*i*2 confocal microscope during the time of placement in Singapore. Alternatively, tissues and glass coverslips were imaged using Olympus FV1000 confocal and Zeiss LSM510 NLO inverted microscopes at the University of Sheffield. At least three images per region of interest were taken from each sample and condition. To capture fluorescent signals from Alexa Fluor fluorophores a set of lasers with emission wavelengths at 405nm, 488nm, 561nm and 640nm were used to image DAPI, AF568/Mitotracker, BODIPY and TO-PRO-3/AF647 signals respectively. For experiments performed at the Nikon centre of the Laboratory of Metabolic Medicine (LMM), A*Star, Singapore, the Nikon Eclipse T*i*2 microscope was set up using an Apochromat 60X/1.4 oil lens. The final image was the result of the average of scanning 4 images per channel, with size and frame set as XY 2048. Optical slice was optimized at 0.9 μm.

The Olympus FV1000 confocal was set up with a 60X/1.42 Oil lens in a 2 phase virtual channel setting. Zeiss LSM510 NLO inverted microscope was set for imaging using a plain apochromat 63X/1.4 oil lens. The resulting image was an average 4 line mean scanning per channel with size and frame set as XY 2048. Optical slice was optimized at 0.9 μm.

When imaging Mitotracker or HIF2-α, the red channel for imaging Alexa Fluor 568 and the far red channel for imaging Alexa Fluor 647 were split into two difference phases to avoid interferences between the two wavelengths. Size and frame were set as XY2048, averaging 2 line mean scanning in presence of Kalman filter mode. Optical slice was optimised at 0.9 μm. Gain was set as 1.

Staining analysis

Confocal images were analysed using ImageJ (FIJI) software. To perform the analysis of the antibody of interest, images were split into 3 or 4 channels, depending on the assay. Nuclear analysis was perform by highlighting nuclei by the free hand selection tool and saving them to the ROI manager to create a mask. Then, the created mask was applied to the channel of interest and analysis was performed by using the measurement tool on ImageJ. All measurements were performed as mean fluorescence intensity (MFI), unless otherwise stated. The nuclear MFI of the IgG control was subtracted from the experimental reading of the nuclear MFI of the HIF2-α staining.

Statistical analysis

All statistical analysis was performed using Graph Pad Prism 8 Software (La Jolla, California, USA) with $P<0.05$ considered as statistically significant. The statistical tests used are described according to each set of data. A minimum of three independent biological replicates was performed for each experiment and averaged mean value with the standard error of the mean was presented. To analyse qRT-PCR and western blot data, samples were normalised to high WSS regions. Whilst, when analysing data of qRT-PCR data from *in vitro HIF2-α* knock-down experiments, lentiviral HIF2-α shRNA samples were presented relative to their scrambled shRNA control. T-test, one-Way ANOVA and two-Way ANOVA were applied according to each dataset, and as described in the relevant results sections.

Chapter 3. HIF2-α responses to shear stress

Introduction

HIF transcription factors have emerged as essential regulators of vascular physiology, from their requirement for embryonic vasculogenesis to their role in post-natal angiogenesis. Furthermore, HIFs are critical regulator of glycolytic and lipid metabolism and they are widely expressed in response to hypoxia and in cancer cells. HIF2-α expression is known to be enriched at highly vascularised tissue, such as placenta, kidney, liver and endothelium. Activation of HIF isoforms upon hypoxic stimuli was previously demonstrated *in vitro* in both arterial and venous vascular endothelial cells (Bartoszewski *et al.*, 2019). Despite their well characterised roles in vascular development and homeostasis, the role of HIFs in vascular disease is only partially understood.

Arterial wall shear stress (WSS) modulates endothelial cell physiology (Davies *et al.*, 2013). It primes ECs for atherogenesis at sites of low WSS, whereas ECs exposed to high WSS are protected. Ultimately, activation of transcription factors mediates adaptative response to WSS frictional forces (Dai *et al.*, 2004; Passerini *et al.*, 2004; Jing Zhou, Yi-Shuan Li, 2014; Souilhol *et al.*, 2018). HIF1-α was shown to be activated by low WSS, where it regulates glycolytic enzymes and mediates proinflammatory responses leading to enhanced atherogenesis (Akhtar *et al.*, 2015; Feng *et al.*, 2017; Wu *et al.*, 2017).

Similarly to HIF1-α, also HIF2-α was observed to be activated by low WSS in human aortic endothelial cells exposed for 24h to disturbed flow (Wu *et al.*, 2017). However, the function of HIF2-α in this context has not been investigated yet.

Hypothesis and aim

Recent work from Evans's lab, together with other groups, demonstrated that HIF1-α was regulated by low WSS. Despite the response of HIF2-α to shear stress being previously reported, its role in murine and porcine aortic endothelial cells has never been studied. Therefore, here I hypothesised that WSS differentially regulates the expression of HIF2-α in vascular endothelial cells, and this may lead to altered endothelial cells responses.

Aims

The following aims were assessed:

- To quantify the expression level of HIF2-α in vascular endothelial cells at low and high WSS sites of healthy mice.
- To assess whether WSS regulates HIF2-α in cultured porcine aortic endothelial cells (PAECs) using an *in vitro* flow system.
- To study the transcript expression of HIF2-α in porcine aorta at sites of low and high WSS.

Results

HIF2-α expression in healthy murine vascular endothelium

To investigate the spatial distribution of HIF2-α protein at the murine vascular endothelium, *en face* staining was performed in healthy mice and three regions of the aorta were selected for the study. The outer curvature of the aortic arch, the inner curvature of the aortic arch and the descending aorta; sites of high WSS, low WSS and high WSS respectively. Chow-fed 6-8 weeks old C57BL6/J mice were selected for this study.

To identify endothelium, murine aortas were stained using green fluorescent CD31 (i.e. PECAM-1) antibody, which was already conjugated to AF488 fluorophore. Representative images show endothelial cells rearrangement at different site of the aorta (Figure 3.1A). ECs exposed to high WSS were elongated and aligned with the direction of the blood flow. In contrast, ECs exposed to low WSS exhibited disorganised arrangement and cobblestone shape.

Then, HIF2-α levels were investigated. In a healthy murine vascular endothelium, *en face* staining revealed increased HIF2-α levels at the low WSS site (inner curvature) compared to the HSS (outer curvature) of the aortic arch (Figure 3.1A). Interestingly, analysis of the thoracic descending aorta showed a high level of HIF2-α protein. In order to exclude any specific antibody binding on the aortic tissue, a quality control was performed using an IgG antibody matching the HIF2-α antibody species (Figure 3.1B).

Using *en face* staining I showed that HIF2-α can localise to both the cytoplasm and the nuclei of endothelial cells. When HIF2-α is observed in the nucleus it is assumed to be in its active form, and as it is a transcription factor, HIF2-α needs to translocate into the nucleus to exert its functions. Therefore, cytoplasmic and nuclear levels were quantified and compared for all three regions studied. At every site investigated, quantification showed that HIF2-α levels were significantly increased into the nucleus (Figure 3.1C). Then, nuclear levels of HIF2-α were compared between regions and quantification confirmed activation of HIF2-α at site of low WSS when compared to the high WSS site of the arch, whilst the highest HIF2-α levels were measured at the nuclei of the descending aorta, which is a site of high WSS (Figure 3.1D).

Taken together these data suggest that HIF2-α expression and activation (as assessed by nuclear localisation) is likely under the control of both shear stress and anatomical site (i.e. embryonic origin).

A

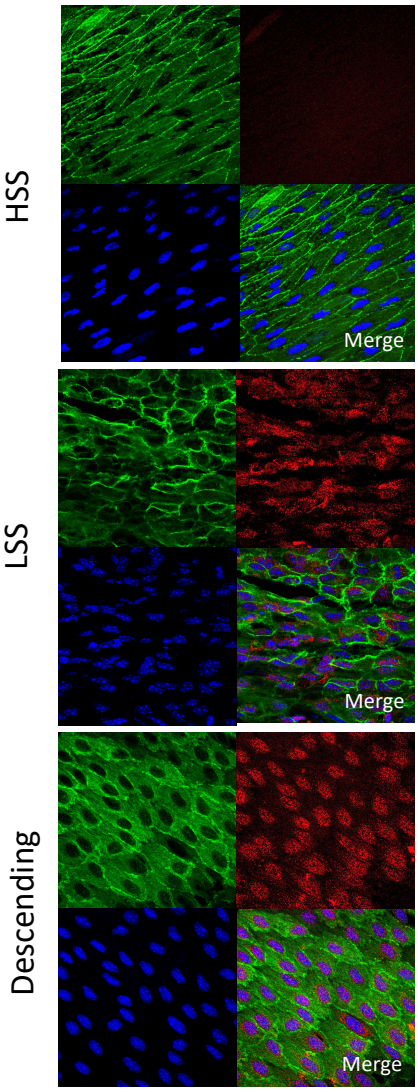

CD31, HIF2-α, TO-PRO 3

B

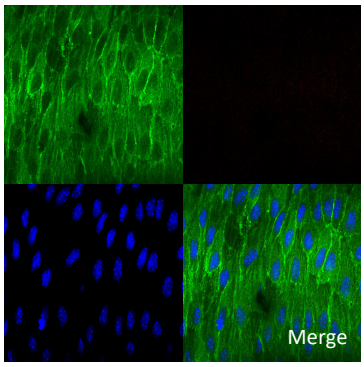

CD31, IgG, TO-PRO 3

C

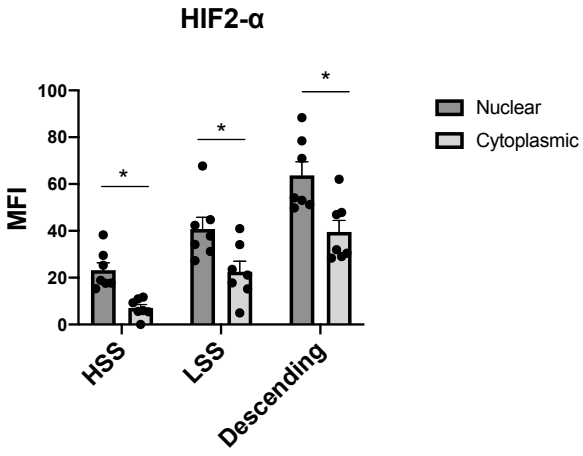

D

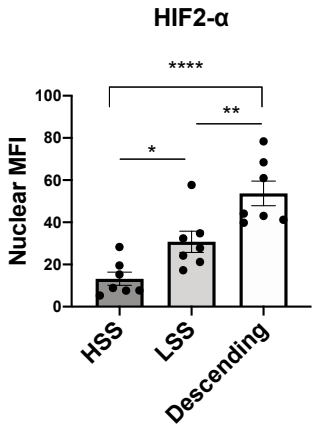

Figure 3. 1 Expression of HIF-2a in murine aortic endothelium.

Levels of HIF2-α in ECs were assessed by *en face* staining of low oscillatory WSS (LSS) or high WSS (HSS) of the aortic arch and the descending thoracic aorta of C57BL/6 mice (red). ECs were identified by co-staining with anti-CD31 antibodies conjugated to Alexa Fluor 488 (green). Cell nuclei were identified using To-Pro-3 (DNA, blue). A) Representative images are shown. B) Representative images of IgG control are shown. C) Nuclear and cytoplasmic levels of HIF2-α levels +/- SEM are shown for n=7 mice. D) Mean levels of nuclear HIF2-α. Differences between means were analysed using a one-way ANOVA and two-way ANOVA, in D and C respectively. * $p<0.05$; ** $p<0.01$;**** $p<0.0001$.

Generation of HIF2-α endothelial KO mice and antibody validation.

To understand the role of HIF2-α in vascular endothelial cells, mice carrying the floxed allele (fl) targeting the exon 2 were bred with transgenic mice carrying a VE-cadherin (CDH5) driven $CreER^{T2}$. The resultant mice were identified as: fl/fl, Cre positive mice (designated as knock-out, KO) and fl/+, Cre positive (heterozygous mice) or Cre negative mice, carrying either fl/+ and fl/fl alleles, designated as controls. To induce activation of Cre and deletion of exon 2, mice were injected with tamoxifen. Cre positive heterozygous and fl/fl mice presented the 340bp band representative of the deleted allele, hereafter referred to as Δ. On the contrary, the genome of Cre negative mice (controls) remained unaffected by tamoxifen injections. A representative image of genotyping PCR is shown in (Figure 3.2A).

Tamoxifen injected mice were sacrificed at 8 weeks of age and the descending aorta was studied to test the specificity of the HIF2-α antibody. *En face* staining of descending aortic tissue revealed that HIF2-α protein level was proportionally decreased with the loss of *hif2-α* in Cre-activated mice (Figure 3.2B). HIF2-α levels were determined by nuclear quantification normalised to the background fluorescence of the appropriate IgG control and it was shown that HIF2-α protein expression significantly decreased in KO mice (Figure 3.2C).

Collectively, these data validated the specificity of the antibody for HIF2-α protein in murine endothelium and together with the genotyping analysis, it corroborated the evidence of generation of a vascular endothelial *hif2-α* model.

A

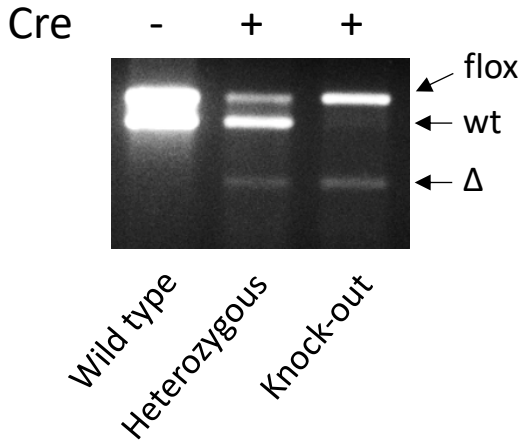

B

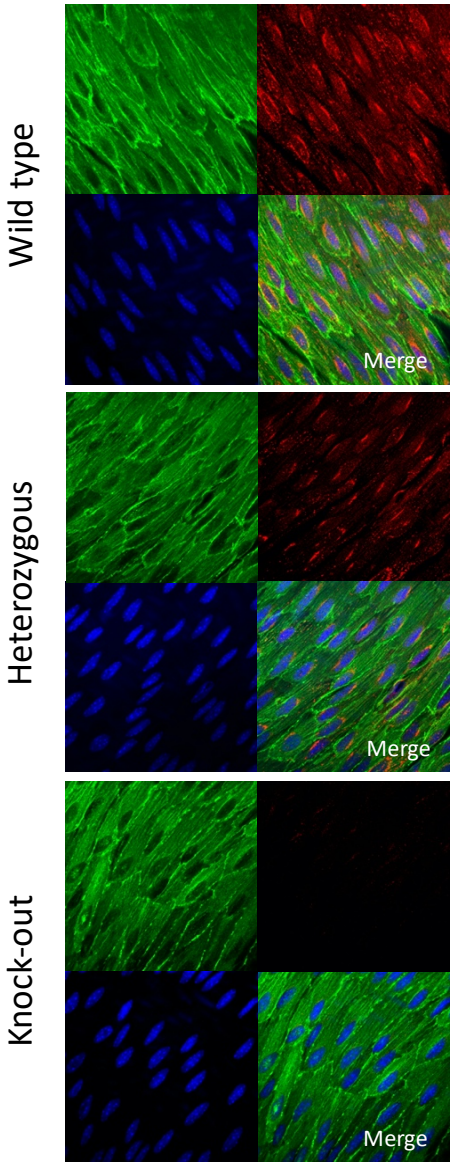

CD31, HIF2-α, TO-PRO 3

C

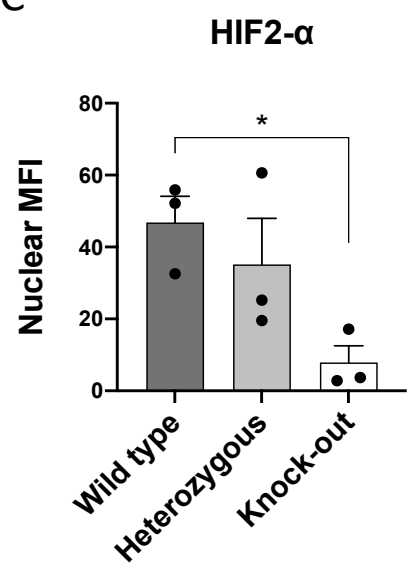

Figure 3. 2 Generation and validation of of HIF2-α endothelial cells knock-out mice.

Vascular endothelial HIF2-α was knocked out using Ve-cadherin-Cre driven recombination between loxP site of exon 2. A) Example PCR genotyping after Cre activation via tamoxifen injection in mice. Lane 1 shows genotyping of a HIF2-α flox/+, Cre negative mouse (wild type), lane 2 of a HIF2-α flox/wt, Cre positive mouse (heterozygous), and lane 3 of a HIF2-α flox/flox, Cre positive mouse (knock-out). Levels of HIF2-α in the endothelium were assessed by en face staining at the descending aorta of wild type C57Black6/J mice, wild type (N=3), heterozygous mice (N=3) or HIF2-α mutant mice, KO (N=3). HIF2-α was identified by red colour, endothelium by CD31 antibody (green) and nuclei by TO-PRO-3 staining (blue). Representative images of HIF2-α staining are shown (B). Nuclear HIF2-α level was assessed by quantification of the mean fluorescent intensity (MFI) using Fiji software. In all quantifications presented, the nuclear MFI of IgG control sample was subtracted from the experimental reading of HIF2-α nuclear MFI. C) Mean levels of HIF2-α +/- SEM are shown. Differences between means were analysed using a One-way ANOVA test. *$p<0.05$.

HIF2-α expression in PAECs exposed to flow

Isolated PAECs express endothelial markers by flow cytometry

To identify whether HIF2-α responses to shear stress were conserved in other mammals, I investigated the level of HIF2-α in porcine endothelium. Porcine endothelial cells were isolated by enzymatic digestion from two sites of the aortic tissue, the whole aortic arch (containing cells from both outer and inner curvatures) and the descending aorta. PAECs were then sub-cultured and kept as distinct cell lines.

Isolated PAECs were screened for endothelial enrichment by staining with anti-PECAM-1 antibody combined with a FITC-labelled secondary antibody and analysed by flow cytometry. Each sample was divided into three sub-fractions to analyse the full population as unlabelled control, cells incubated with secondary antibody only as negative control and cells incubated with PECAM-1 and secondary fluorescent antibody. Live to death discrimination was performed using TO-PRO-3 iodide. FlowJo analysis was performed, the entire cell population of living cells was identified using the unlabelled sample. Then, background fluorescence was gated out using the secondary antibody control and finally, any cells from the third sample with fluorescence above the background threshold was identified as PECAM1 positive, thus, endothelial cells (Supplementary figure 7.1).

Histograms were generated for PAECs isolated from the aortic arch and the descending aorta (Figure 3.3A and 3.3B). The percentage of ECs in a sample was calculated as the percentage of PECAM-1 positive cells over the entire living population of any given sample. The overall range of endothelial cells purity in isolated PAECs was estimated between 89.4% up to 96.6%, which was deemed to be sufficiently pure. Both, PAECs from aortic arch and descending aorta showed a comparable percentage of endothelial cell identity (Figure 3.3C).

The PAECs I isolated had high enough percentage of endothelial cells and thereafter they were used to study the response of HIF2-α to shear stress.

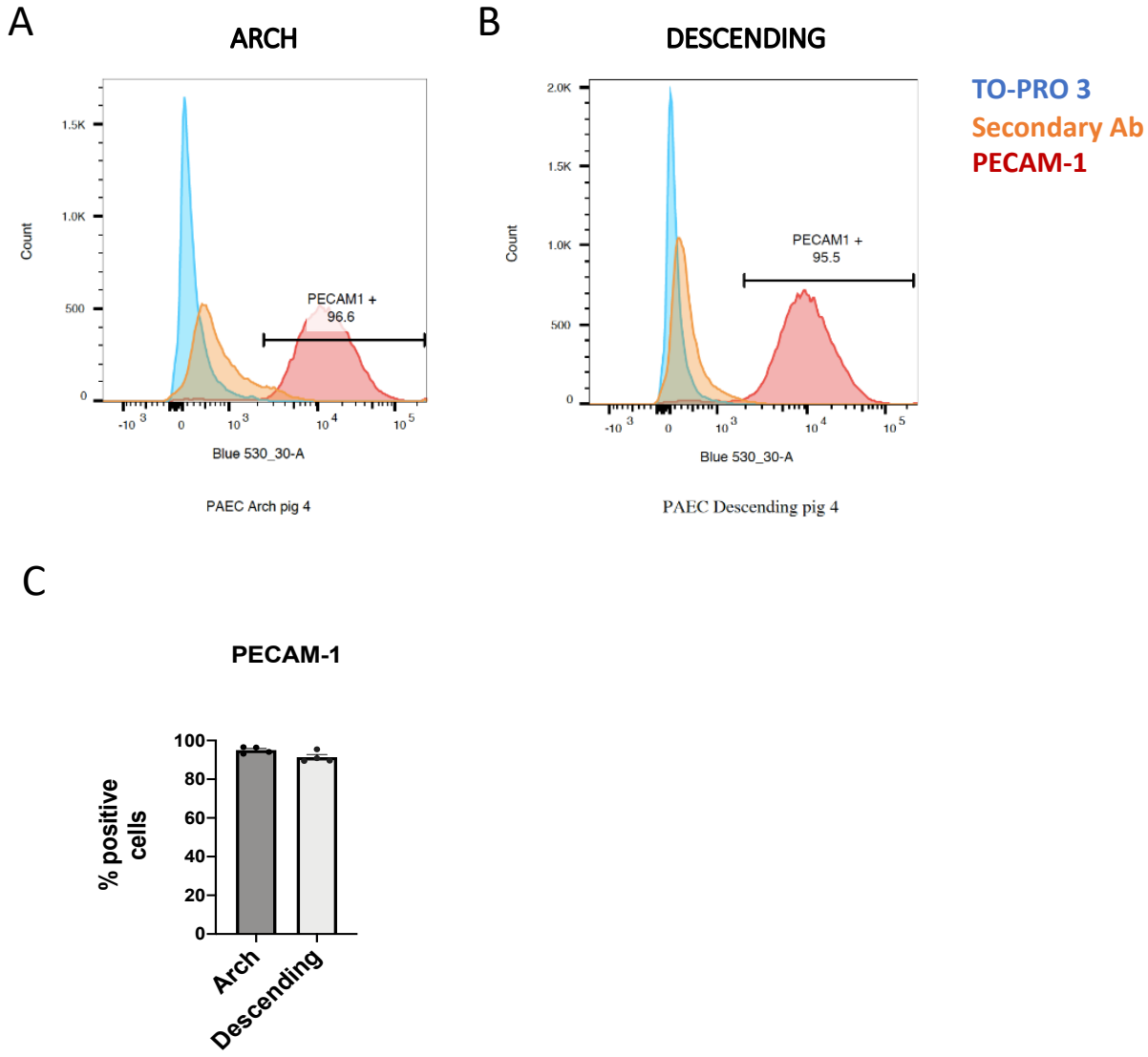

Figure 3. 3 Flow cytometry analysis confirmed endothelial cell marker enrichment in isolated PAECs.

Isolated PAECs from arch and descending aorta were tested for PECAM-1 enrichment by flow cytometry analysis. Viable PAECs were gated by TO-PRO-3 discrimination (blue), non-specific binding were identified using secondary antibody only (orange), PAECs population above the secondary antibody threshold were considered positive to PECAM-1 (red). A) Representative histograms for PAECs from arches. B) Representative histogram for PAECs from descending aortae. C) Mean levels of PECAM1 % +/- SEM are shown (N=4).

In vitro, HIF2-α levels respond to low oscillatory wall shear stress and to high wall shear stress depending on the anatomical site.

To identify whether the different expression of HIF2-α protein observed in murine aortic arch and descending aorta was also conserved in porcine aorta, responses of HIF2-α to shear stress were studied in PAECs. PAECs derived from the aortic arches or descending aortae were exposed to shear stress using the Ibidi pump system for 72h. To activate HIF2-α and avoid protein degradation during cell lysis, PAECs were exposed to 4h of DMOG pre-treatment. Given that DMOG was added at the same dose and time in all conditions, any differences in HIF2-α could be attributed to the cell responses to flow and not to DMOG itself.

As expected, all DMOG-treated cells showed stabilisation of HIF2-α (Figure 3). Interestingly, the analysis of PAECs from aortic arches revealed that compared with high and low WSS, there was a significant enrichment of HIF2-α protein in cells exposed to low oscillatory shear stress (LOSS), (Figure 3.4A). Quantification of total protein confirmed increased HIF2-α protein level at the LOSS when compared to HSS and LSS, N=4 (Figure 3.4B).

Next, HIF2-α levels were also tested in PAECs derived from descending aorta and exposed to high, low and low oscillatory WSS. Intriguingly, western blotting analysis revealed that in these ECs, HIF2-α protein was activated upon high wall shear stress (HSS), which is consistent with the *en face* experiment in murine aortas. Moreover, I found that low and low oscillatory WSS induced variable responses (Figure 3.4C). Quantification of multiple blots showed increased HIF2-α protein level at the HSS, when compared to the HIF2-α levels in PAECs exposed to LSS or LOSS N=4 (Figure 3.4D).

Therefore, these findings suggest that the expression of DMOG-induced HIF2-α could be further modulated by opposite shear stress magnitudes depending on the anatomical site of the endothelium.

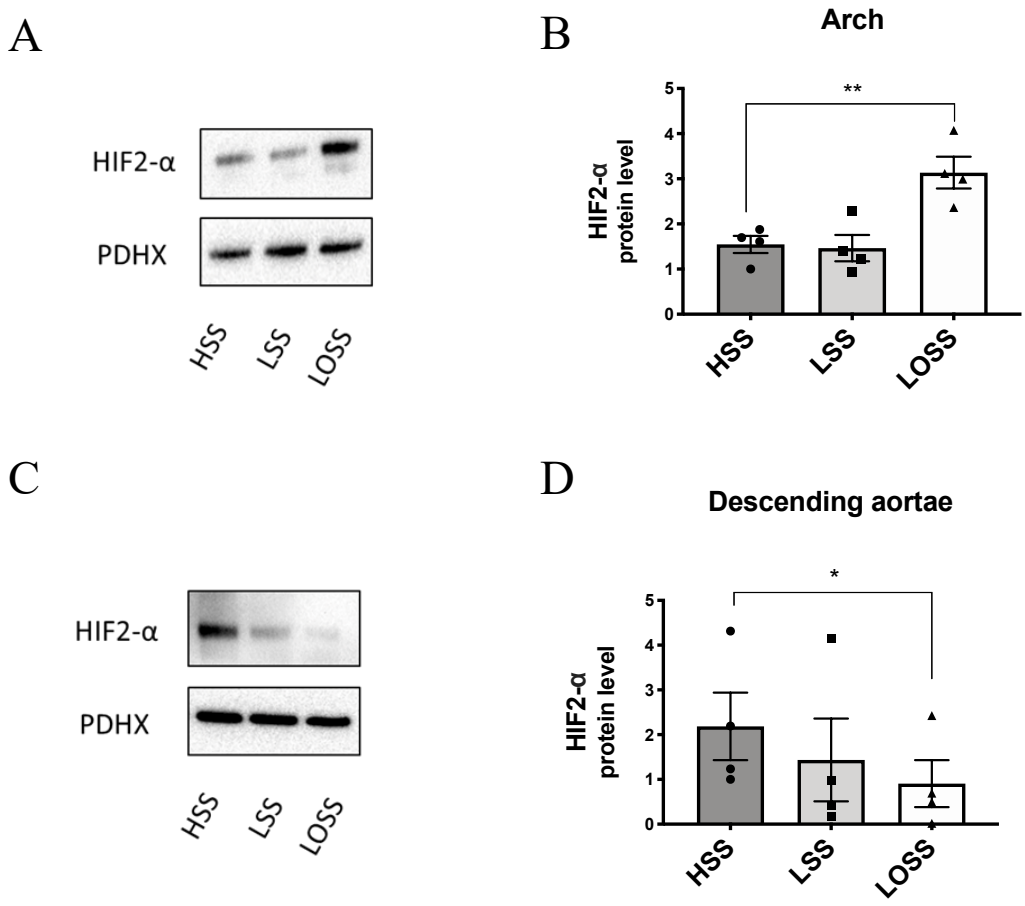

Figure 3. 4 HIF2-α expression to shear stress depend on anatomical site.

PAECs isolated from aortic arch or descending aorta were exposed to shear stress for 72h using the Ibidi pump system and treated with DMOG for 4h prior collection. HIF2-α protein analysis was carried out by western blotting. Western blots were analysed using Image Lab software. A) Representative western blotting image of HIF2-α protein level in PAECs from arch. B) Mean HIF2-α protein level +/- SEM in PAECs from arch relative to the loading control PDHX (N=4). C) Representative western blotting images HIF2-α protein level in PAECs from descending aortae . D) Mean HIF2-α protein level +/- SEM in PAECs from descending aortae relative to the loading control PDHX (N=4). Differences between means were analysed using a one-way ANOVA. * $p<0.05$;** $p<0.01$.

Shear stress did not regulate HIF2-α mRNA level or levels of downstream transcripts in porcine endothelial cells.

To test whether HIF2-α was regulated at the transcriptional level, porcine aortas were dissected and endothelial cell-derived RNA was isolated from the outer curvature, the inner curvature of the first arch. All transcriptional analysis were performed against a housekeeping control gene, Beta-2-microglobulin (B2M).

A quality control was carried out on the isolated samples, specifically enrichment for the endothelial marker CD31 was studied against smooth muscle actin (SMA) expression. CD31 expression was significantly higher than SMA (Figure 3.5A), suggesting that the isolated RNA was mainly endothelial derived with little smooth muscle cells contamination. Furthermore, to identify the regions of high WSS and low WSS, the expression of two known markers for those regions was assessed. As expected (Topper *et al.*, 1996; Bao, Lu and Frangos, 1999), eNOS expression was enriched at regions of high WSS, whereas the expression of the pro-inflammatory marker MCP1 was enriched at regions of low WSS (Figure 3.5B).

The expression of HIF2-α mRNA in porcine endothelium were then assessed. HIF2-α expression did not significantly differ between regions of high and low WSS (Figure 3.5C). To determine whether HIF2-α activity was differentially regulated in these two sites, I quantified the expression of HIF-α transcriptional downstream targets at the different WSS sites. For this I examined, adrenomedullin (ADM), tyrosine-protein kinase receptor (Tie-2), vascular endothelial growth factor (VEGF) and angiopoietin-like 4 (ANGPTL4), which were previously shown to be activated by both HIF1-α and HIF2-α (Ema *et al.*, 1997; Tian, Mcknight and Russell, 1997; Hu *et al.*, 2007; Zhang *et al.*, 2012). Interestingly, expression level of HIF2-α downstream targets were not significantly enriched at site of low WSS, when compared to high WSS samples (Figure 3.5D).

Collectively, this data suggested that HIF2-α mRNA expression and transcriptional activity may not be under the control of shear stress in porcine aortas *in vivo*.

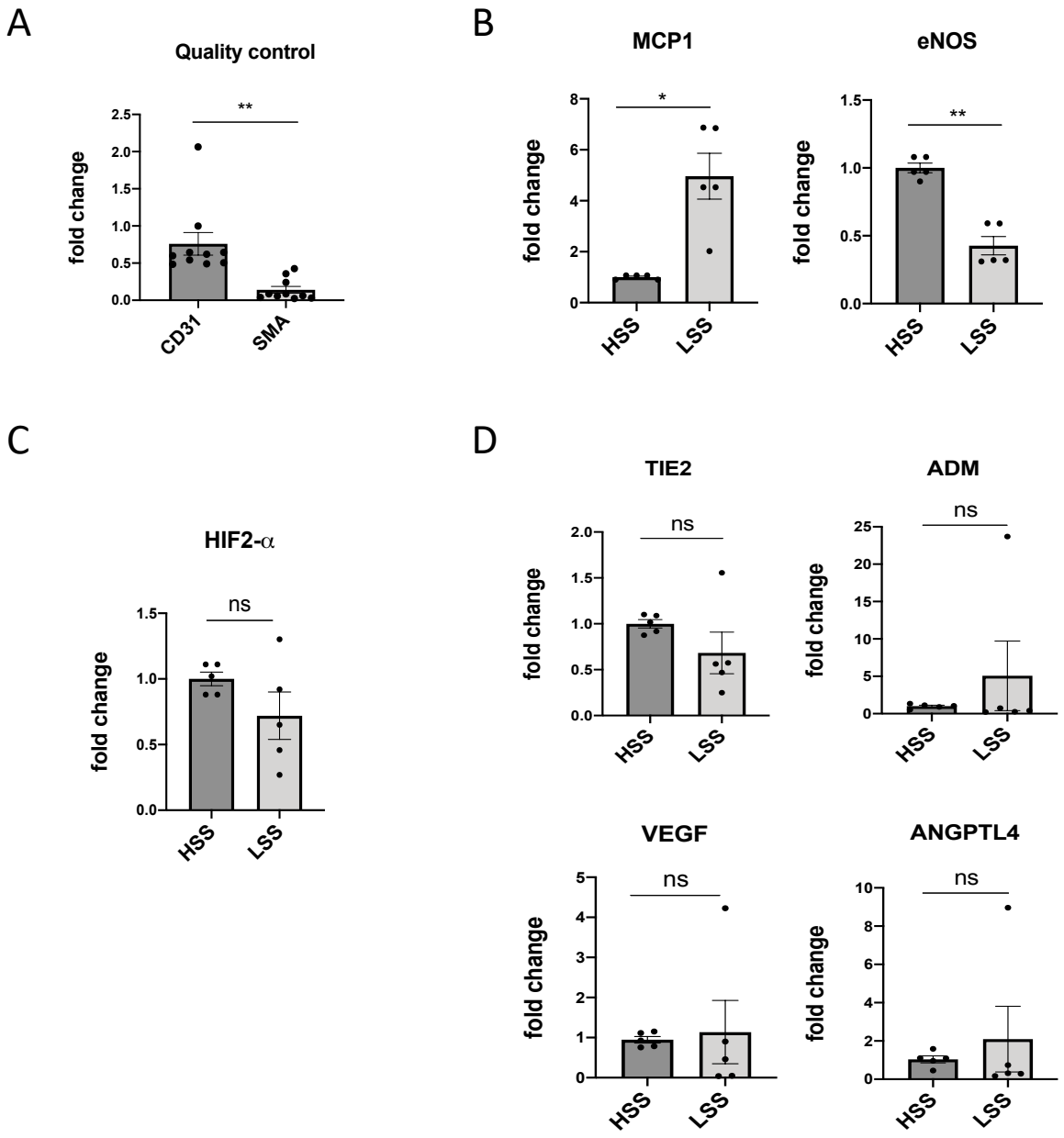

Figure 3. 5 Shear stress did not regulate HIF2-α mRNA.

Gene expression analysis was carried out by qRT-PCR. A) RNA isolated from EC was analysed for the expression of CD31 and SMA markers (N=10). B) MCP1 and eNOS were analysed as quality control of the shear stress sites (N=5). C) Expression of HIF2-α at the site of HSS and LSS of the porcine aorta (N=5). (A-C) Mean levels of $2^{-\Delta\Delta Ct}$ +/- SEM are shown. The expression of VEGF, TIE-2, ANGPTL4 and ADM was assessed in five pigs (D). Mean levels +/- SEM are shown. Differences between means of $2^{-\Delta Ct}$ were analysed using a paired T-TEST (A-D). * $p<0.05$;** $p<0.01$.

Conclusions

In this chapter I have shown that:

- HIF2-α is a mechanosensitive gene and can be differentially expressed in response to wall shear stress.
- High WSS drives the expression of HIF2-α at the descending aortic site, whereas low WSS drives the expression of HIF2-α at the aortic arch.
- *In vitro*, site specific regulation of HIF2-α by shear stress is conserved in porcine endothelial cells.
- However, the transcriptional analysis suggested that shear stress may not regulate HIF2-α mRNA expression *in vivo*.

Discussion

Endothelial cells are a structural component of the inner layer of vessels. ECs are constantly exposed to different oxygen levels depending on haemodynamic effects (Santilli *et al.*, 1995). In dog carotid arteries, low oxygen tension was observed at the bifurcation site exposed to low WSS when compared to anatomical site exposed to high WSS. Activation of HIFs is canonically associated with low oxygen tension and with its reduced proteasomal degradation (Wang *et al.*, 1995; Ivan and Kaelin, 2001; Schofield and Ratcliffe, 2005).

Furthermore, *in vitro*, primary endothelial cells respond to hypoxic stimuli via stabilising HIFs in a time dependent manner (Bartoszewski *et al.*, 2019). This pattern of expression is conserved in multiple primary cells lines originated from both vein and arterial bed. During hypoxia, HIFs regulated endothelial angiogenesis and silencing of either HIF1-α or HIF2-α in immortalised microvascular endothelial cells reduced angiogenic signals (Hahne *et al.*, 2018). Nevertheless, multiple works have recognised HIF1-α as one of several transcription factors activated by blood flow frictional forces (Feng *et al.*, 2017; Wu *et al.*, 2017).

Mechanical regulation of HIF2-α protein levels.

Our lab previously demonstrated expression of HIF1-α at sites of low WSS (Feng *et al.*, 2017). This finding was supported by a second group which also identified HIF2-α activated by low WSS (Wu *et al.*, 2017). In this chapter, I have shown activation of HIF2-α at site of low WSS in the porcine and murine aortic arch. Both immunofluorescence and western blotting analysis were in agreement also on confirming stabilisation of HIF2-α at sites of high WSS within the descending aorta. Thus, while HIF2-α may be activated by low WSS in the aortic arch, a paradox exists with unexpected activation of HIF2-α by high WSS in the descending aorta.

WSS magnitudes vary within the aortic vessel, thus it is possible that activation of HIF2-α requires a restricted range of shear stress magnitudes and that high WSS at the descending aorta is intermediate between the lowest WSS and the highest WSS of the aortic arch (Figure 3.6).

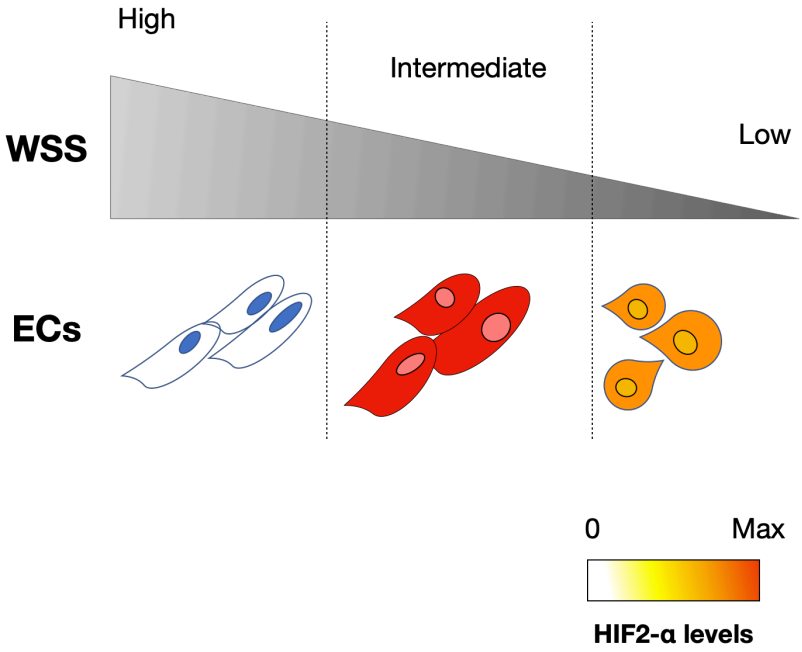

Figure 3. 6 HIF2-α activation by wall shear stress.

Endothelial cells in response to flow activate transcriptional responses to modulate adaptive responses to external stimuli. HIF2-α is activated by low WSS at the aortic arch and by high WSS exclusively at the descending aortic site. The outer curvature of the aortic arch is also exposed to high WSS, nevertheless HIF2-α levels are rarely detectable at this site. I hypothesised that very high intensity WSS in the arch inhibits HIF2-α expression whereas intermediate and low WSS in the arch and intermediate WSS in the descending aorta can activate it.

In agreement with this hypothesis, wall shear stress maps of BL6J mice showed that the outer curvature regions of aortic arch are exposed to a higher WSS than the region of the descending aorta (Van Doormaal *et al.*, 2012). Similarly, a dichotomous response to high WSS was observed in another transcription factors response to mechanical forces. A recent work on Notch1 showed that *in vitro*, very high WSS (26 dyne/cm2) activated Notch1, whereas intermediate high WSS (10 dyne/cm2) reduced it (Mack *et al.*, 2017).

Alternatively, another theory suggests that the endothelial cells that make up the descending aorta and those that make the arch come from different embryonic origins (Paffett-Lugassy *et al.*, 2013). During embryogenesis ECs of the aortic vessel derives from a mosaic of lineages, where somite precursors populate the roof and the side of the vessel, while the floor of the aorta derives from the splachnopleaural mesoderm (Pardanaud *et al.*, 1996). Interestingly, pharyngeal arch arteries contribute in a cranio-caudal sequence to the development of carotid, aorta and pulmonary arteries (Paffett-Lugassy *et al.*, 2013). Here, a common cardiac

transcription factor (nkx2.5)-mediated vasculogenesis showed a non-overlapping contribution between the dorsal and the ventral aortic sites. Similarly, the smooth muscle cells layer has different embryological origin that maps the aorta in a mosaic that distinguish the arch from the dorsal descending aorta (Majesky, 2007). If the cells are indeed from different origins one could speculate that a different epigenetic and/or genetic mechanisms may influence the levels of HIF2-α.

A technical caveat should be considered to interpret the porcine data. To detect HIF2-α by western blotting in lysates of PAECs sheared using ibidi pump system, treatment of cells for 4h with 1mM DMOG was employed to activate HIFs stabilisation and therefore prevents proteasomal degradation. In the absence of DMOG, it was not possible to detect HIF2-α protein by western blotting. In addition to activating HIFs via PHDs-mediated mechanisms, DMOG also activates NF-κB, Adenosine monophosphate-activated protein kinase (AMPK) and inhibits Jumonji C Domain-Containing Histone Demethylase (JHDM) (Cummins *et al.*, 2006; Hamada *et al.*, 2009; Yan *et al.*, 2012). Furthermore, it was previously demonstrated that DMOG has an inhibitory effect on mitochondrial function in a HIF-independent manner (Zhdanov *et al.*, 2015). Therefore, DMOG could be involve in a cellular metabolic-reprogramming that is independent and possibly uncoupled with the timing of HIFs activation. For example, in an in-vitro model of cancer cells, PHDs-independent activation of HIFs by DMOG-driven metabolic adaptation was observed at shorter time points of treatment (e.g.30 mins) (Zhdanov *et al.*, 2015). Nevertheless, after 4h of treatment with DMOG, the main effect of DMOG on cells it is to activate HIFs via inhibition of PHDs activity (Zhdanov *et al.*, 2015). It is possible that DMOG acts independently by PHDs to activate HIFs both via metabolic reprogramming of cells or via the activation of others direct HIFs regulators (e.g. NF-κB). The western blot loading control used in this project was the Pyruvate Dehydrogenase Complex Component X (PDHX). Due to PHDX being a mitochondrial protein and showing no differences between the three shear stress conditions, it is unlikely that the difference in HIF2-α protein levels were directly regulated by a known DMOG-induced metabolic reprogramming. However, it cannot be ruled out whether other factors may have had directly activated HIFs in this assay.

In conclusion, this work identified a site-specific activation of HIF2-α at both aortic arch and descending aortic endothelial beds. However, to further elucidate the variation of responses of HIF2-α to shear stress, the analysis of other endothelial sites (e.g. carotid arteries) should also be assessed.

Regulation of HIFs at site of low WSS.

Interestingly, *in vivo* analysis revealed that HIF2-α was detectable at both cytoplasmic and nuclear compartments; however the highest levels were shown within the nuclei, thereby suggesting that HIF2-α is present in its active form. Protein stabilisation is controlled by proteasomal degradation, mostly by activity of PHDs enzyme that target HIFs for ubiquitination. At site of low WSS, our previous work showed that a de-ubiquinating enzyme called Cezanne regulates HIF1-α protein levels and NF-κB its transcriptional activation (Feng *et al.*, 2017). Furthermore, other researchers have identified HIF1-α is also regulated by NOX4 (Wu *et al.*, 2017) or by a microRNA (miR-19a) during atherosclerosis (Akhtar *et al.*, 2015). Whether Cezanne, miR-19a or NOX4 also regulate HIF2-α at sites of low WSS is currently unknown.

Intriguingly, if considering our work on both HIF1-α and HIF2-α, it could be speculated that both major HIF isoforms co-exist at site of low WSS. Both HIF1-α and HIF2-α staining at sites of low WSS showed mosaic expression, suggesting that not all the ECs exposed to low WSS expressed HIF1-α or HIF2-α to the same extent. Thus, it could be hypothesised a mosaic distribution of the protein with a cluster of ECs solely expressing one of the two isoforms while others co-expressing both HIFs (Figure 3.7).

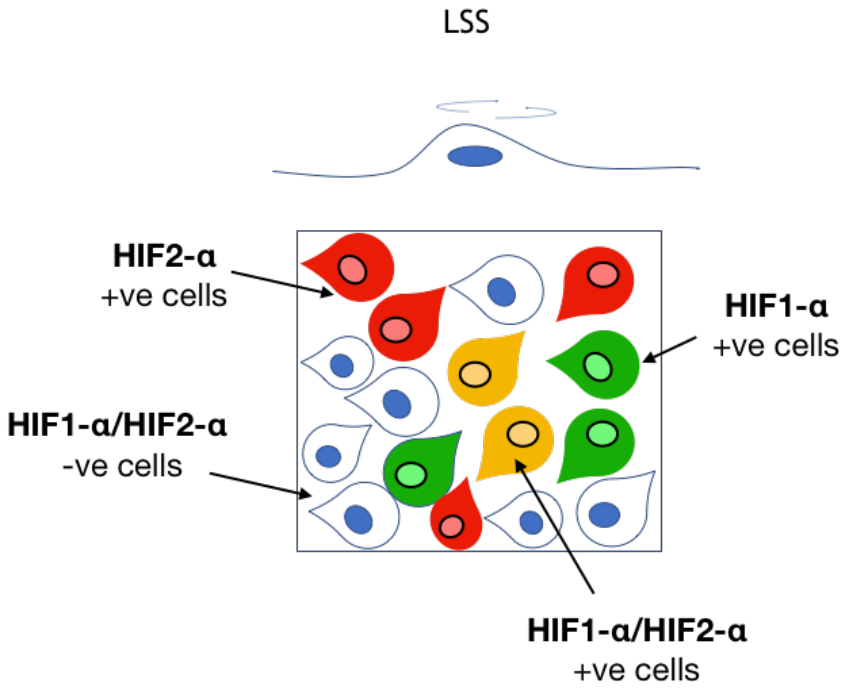

Figure 3. 7 Mosaic expression of the HIFs.

HIF1-α and HIF2-α are activated by low WSS, nevertheless not all ECs exposed to low WSS were positive to HIF1-α (Feng *et al.*, 2017) or HIF2-α antibody. Representation of a hypothetical immunofluorescent co-staining using HIF1-α and HIF2-α antibodies, conjugated to two fluorophores (green and red, respectively). This experiment could conclusively reveal the distribution of the HIFs in endothelial cells.

Despite not being assessed in this PhD project, investigating the spatial distribution of HIFs proteins by co-staining of inner curvature of aortic arches could give a further insight on the understanding of their regulation and function in endothelium. Furthermore, since HIF1-α and HIF2-α have been previously shown to activate different transcriptional responses (Hu *et al.*, 2006; Ratcliffe, 2007; Keith, Johnson and Simon, 2011; Downes *et al.*, 2018), the hypothesised mosaic distribution of HIF2-α/HIF1-α proteins could correlate with activation of distinct transcriptional response to mechanical forces. In addition, it could be also hypothesised that cells co-expressing both HIF1-α and HIF2-α isoform possess a redundancy of function for activation of common downstream targets (e.g. angiogenesis).

Reproducing physiological shear stress using *in vitro* models.

To assess the effect of shear stress *in vitro*, several approaches have been developed over the years. Parallel plate, cone system and the orbital shaker are the most widespread systems.

With the Ibidi® system I applied a high WSS (12 dyne/cm^2), low WSS (4 dyne/cm^2 ± 0.5 Hz) and low oscillatory WSS (4 dyne/cm^2) on the PAECs comparable to what was observed in pig thoracic aorta using computational fluid dynamics (CFD) analysis (Serbanovic-canic *et al.*, 2016). In comparison, in human studies, CFD analysis showed a wide range of WSS intensities across the thoracic aorta with value between 10 to 50 dyne/cm^2 (Cheng, Herfkens and Taylor, 2003a, 2003b; Callaghan and Grieve, 2018). Anatomical differences related to age and gender are fundamental parameters that alters CFD predictions and WSS maps. In addition, while pigs and human haemodynamic are more closely related, a 20 fold change in WSS maps was calculated between mice and human (Weinberg and Ross Ethier, 2007). Thus, a series of considerations must be taken into account when exposing cultured endothelial cells to shear stress. A limitation of my study is that the Ibidi system does not generate realistic waveforms of flow, and therefore future research could confirm my observations using more accurate flow bioreactors, e.g. cone-and-plate (Nagel *et al.*, 1994).

Furthermore, Pyruvate Dehydrogenase Complex Component X (PDHX), was used as loading control in western blotting assay. PDHX is located in the mitochondrial matrix and acts on the transition between pyruvate into acetyl coenzyme A. This protein was chosen as control because of its stability between the different shear stress conditions applied on endothelial cells. Similarly, no effects were observed under HIF2-α shRNA treatment, suggesting that HIF2-α does not regulate PDHX in endothelial cells. In addition, future work could employ multiple loading control proteins (e.g. β-actin and/or Calnexin).

Similarly, the analysis of gene expression was performed using the method of the $2^{-\Delta\Delta Ct}$ using a single housekeeping gene. Beta-2-microglobin (B2M) gene encodes for a protein of the major histocompatibility complex (MHC) and it is expressed in all nucleated cells. Previous works from Paul Evans's lab showed that B2M was not altered by shear stress, it was a stable and highly expressed in porcine aortic endothelial cells. For these reasons B2M was employed in this thesis as housekeeping control gene. Nevertheless, to corroborate qPCR analysis, future works will take into account the analysis of multiple housekeeping genes.

Mechanical regulation of HIF2-α transcriptional expression.

To investigate shear stress-mediated transcriptional regulation *in vivo*, HIF2-α was assessed in endothelial cells isolated from porcine aortae at sites of high and low WSS. Pigs are larger mammals providing an excellent model for studying haemodynamic forces closer to the human magnitude. Nevertheless, anatomical differences exist between pigs and human. The aortic arch in pigs presents only two bifurcation sites (the brachiocephalic artery and the left subclavian artery), whilst in humans and mice the aortic arch presents three bifurcations (brachiocephalic trunk, left common carotid artery, left subclavian artery) thus generating a possible confounding factor for haemodynamic forces. Furthermore, due to the aforementioned differences, when extrapolating from the pig to human, it is worth being careful, since some of the results might not directly translate.

However, several technical advantages are offered by working with pigs. As an example, when compared to mice, pigs offer the possibility to work with larger area and allow an easier identification of high and low WSS sites, resulting in a higher yield of isolated RNA. Furthermore, analysis of porcine aortae was previously employed to study mechano-sensing gene expression profile at site of high and low WSS (Passerini *et al.*, 2004; Lamack *et al.*, 2010; Serbanovic-canic *et al.*, 2016). HIF1-α expression was shown to be enriched at the low WSS sites; Paul Evans's group has performed a microarray on porcine endothelial cells collected from LSS and HSS sites of the aortic arch. None of the known binding partners regulating HIF2/α at the post-translational level were found differentially expressed in the array. Furthermore, within the same dataset, there was no differentially expressed microRNAs. However, several other binding partners of HIF2-α were found at the LSS, where also HIF2/α mRNA was expressed. The mediator of RNA polymerase II transcription subunit 24-like (MED24) was also expressed at site of LSS. The interaction of this protein with HIF2-α was previously shown in melanoma cells, however there are no evidence to prove the direct interaction between HIF2-α and MED24 in endothelial cells (Steunou *et al.*, 2013). Nevertheless, with the analysis conducted here, it was not possible to fully elucidate whether mechanical forces regulate HIF2-α at the transcriptional level. Using porcine aortic samples, it was not possible to observe any enrichment for HIF2-α mRNA expression at site of high or low WSS within the aortic arch. However, regulation of HIF2-α at the descending aorta site has not been assessed in this work.

Further investigation might be required to understand the regulation of HIF2-α by high shear stress.

It is likely that HIF2-α mRNA and protein levels are not coupled because of its post translational regulation, however the inconsistency in the regulation of mRNA and protein by shear stress, could also be explained by both technical and biological factors which may have cause a sub-optimal analysis of the mRNA level.

As an example, while Isolated PAECs, generated for tissue culture work were characterised by flow cytometry analysis using a CD31 marker, the quality control in cells isolated for RNA analysis was performed by RT-qPCR. Therefore, with this type of analysis, it was impossible to establish the real extent of SMC contamination in the sample (i.e. percentage of cells). To improve this quality control, RNA from undigested tissue remaining from the isolation (media and adventitia layers) could be used to evaluate the real enrichment of endothelial cells/SMC ratio within the sample. This approach was used in other work isolating RNA from mice carotid arteries (Nam *et al.*, 2009). Furthermore, collection of pig aortas revealed anatomical differences between samples that could be associated with differences in weight and age of the animals.

Furthermore, there is an increasing number of works investigating the ECs biology using single cell-RNA sequencing tool, which can generate a deeper insight on ECs heterogeneity and transcriptional identity characterising the vasculature (Kalluri *et al.*, 2019; Engelbrecht *et al.*, 2020; Zhao *et al.*, 2020). Interestingly, one paper using single-cell dataset of mice aorta, identified three distinct populations of ECs (Kalluri *et al.*, 2019). The transcriptional patterns of those populations identified the ECs as enriched for canonical endothelial profile marker expression (sub-population1), lipid transport and angiogenesis (sub-population 2) and lymphatic endothelial cells (sub-population 3). The gene encoding for HIF2A, *HIF2-α* gene, was highly expressed in all the three subsets of ECs, whereas the expression of *HIF1a* seemed restricted at the endothelial cells cluster 1. Thus, possibly suggesting that metabolic and angiogenetic signals in ECs from the sub-population 2 could be mediated exclusively by *HIF2-α*. Despite the depth of information given by single cells analysis, this work did not account for the distinct ECs transcriptional pattern observed in response to WSS, while here, it refers to the whole aortic endothelial cells population. Nevertheless, ECs heterogeneity could establish an alternative model for uncertain transcriptional expression.

In conclusion, taken together the data generated in this chapter suggest that HIF2-α could be regulated at the protein level and that is activated within the arch by low WSS. The exact mechanism by which high and low WSS activated HIF2-α at different region of the aorta is currently unknown.

Future works:

To improve the understanding of spatial distribution and functionality of HIF2-α at different region of the aorta, the following experiments could be engaged:

- To understand the correlation between high shear stress and HIF2-α protein level, both western blotting or immunofluorescence staining for HIF2-α antibody could be assessed in PAECs exposed to shear stress using a Y-slide of the Ibidi system that generates a gradient of shear stress across the slide.
- Analysis of HIF2-α levels in mice exposed to altered shear stress pattern via a constrictive cuff at the carotid artery.
- Protein lysates from PAECs exposed to shear stress using ibidi could be further analysed for protein regulating HIFs degradation (e.g. PHD2, PHD3, VHL).
- To study whether nuclear staining of HIF2-α correlated with its activity, HIF1-β levels could be assessed by enface staining of mouse aorta.
- Proximity ligation assays could be employed to study HIF1- α and HIF2-α interaction, as well as for HIF2-α and HIF-β interaction.
- To study HIF2-α activity under high or low WSS, ChIP-seq analysis could be performed on cellular lysate of PAECs exposed to WSS. To further clarify the functionality of the HIFs under shear stress, this analysis could be also performed in cells treated with DMOG. The differences between the two analyses would conclusively identify whether DMOG treatment for studying protein level under shear stress had generated any bias.

Chapter 4. Effect of pro-atherogenic factors on HIF2-α expression in the aorta

Introduction

In the previous chapter, I have demonstrated that HIF2-α levels are enriched in EC at the inner curvature of the aortic arch which is exposed to LSS but HIF2-α is not expressed in the outer part of the arch which is exposed to HSS. By contrast, the descending aorta, which is exposed to HSS, exhibited high expression of HIF2-α. The duality of HIF2-α levels at both atheroprone and atheroprotected sites is unprecedented. This unusual pattern of HIF2-α expression suggested that this transcription factor may be activated by HSS or LSS forces and this depends on anatomical context.

Diabetes clusters together with other abnormalities, including obesity, to define a complex multiorgan pathology named metabolic syndrome. Obesity and diabetes were previously shown to be highly interconnected with HIF expression in multiple organs. For example, diabetes, a risk factor for atherosclerosis, acts as a negative regulator for HIF1-α expression and for its angiogenic function (Catrina *et al.*, 2004). As a further example, in adipose tissue HIF1-α participates in obesity and insulin resistance (Zhang *et al.*, 2010; Matsuura *et al.*, 2013; Lee *et al.*, 2015). On the contrary, HIF2-α controls hypothalamic regulation of body weight (Zhang *et al.*, 2011) and hepatic glycaemic control through repression of glucagon release (Ramakrishnan *et al.*, 2016).

From the perspective of endothelial cells, obesity and diabetes participate in atherosclerosis by exacerbating endothelial dysfunction through multiple mechanisms, including increased production of ROS and other inflammatory signals, as well as reduction of protective factors such as eNOS (Du *et al.*, 2000; Beckman, Creager and Libby, 2002; Wendt *et al.*, 2006; Lopez-Quintero *et al.*, 2013; Shah and Brownlee, 2016). However, the direct influence of obesity and diabetes on endothelial levels of HIF2-α has never been investigated and is a focus of the work presented in this chapter.

Hypothesis and Aims

Given that HIF-α isoforms are involved in both lipid and glucose metabolism in multiple organs, I hypothesised that endothelial HIF2-α levels may be affected by dyslipidaemia and other risk factor for atherosclerosis, such as diabetes.

To address this hypothesis the following aims were assessed:

- To assess whether hyperlipidaemia was affecting HIF2-α levels in murine aortic endothelium, I generated two mouse models of obesity, one based on genetic mutation of the leptin gene (ob/ob) and the other based on high-fat diet feeding.
- To investigate whether hyperglycaemia affects HIF2-α levels in endothelium, I generated mice with high glucose levels by injecting them with streptozotocin (STZ).
- To investigate whether the two risk factors considered, hyperglycaemia and obesity, work synergistically or independently on HIF2-α levels in the murine aorta.
- To assess whether HIF2-α endothelial levels correlate with arterial blood pressure.
- To investigate whether dyslipidaemia, hyperglycaemia and HIF2-α expression levels are regulated by the antioxidant compound, sulforaphane.

Results

High fat feeding model

High fat feeding mimics metabolic syndrome in BL6 mice.

C57Black/6N mice were fed a HFD containing 60% fat for 25 weeks. To evaluate the effect of HFD on mouse physiology I firstly measured body weight. Mice exposed to HFD showed a significantly increase in body weight when compared to control mice exposed to a chow diet (Figure 4.1A).

I then investigated whether HFD induced changes in glycaemic levels. Glycaemic level in HFD and chow diet mice were evaluated after 16h fasting and in resting condition. Fasting glucose concentration revealed increased glycaemic level of HFD mice when compared to the chow diet controls (Figure 4.1B). Resting glycaemia also confirmed higher blood glucose level in HFD mice when compared to their chow diet controls (Figure 4.1C), these results indicate that in addition to increased body weight the mice also experience an elevation of both their fasting and resting glucose levels. Hence, glucose level is a confounding factor in the study and understanding the contribution of fat and glucose will be important to assess.

I then examined whether increased dietary intake of fat affects blood lipid profiles in my model. Thus, I investigated triglycerides and cholesterol levels of HFD when compared with chow diet fed mice. Triglyceride levels were increased in mice exposed to HFD when compared to chow diet fed controls (Figure 4.1D). Similarly, HFD increased total cholesterol levels of mice, as well as their LDL/VLDL blood content (Figure 4.1E). However, HDL content was not affected by HFD and blood titre remained comparable between HFD and chow diet mice (Figure 4.1E). Systolic and diastolic blood pressure were also investigated. Unlike systolic blood pressure (SAP), HFD caused a significant increase in diastolic blood pressure (DAP; Figure 4.1F). Mean blood pressure (MAP) was also presented, however, no significant changes were induced by HFD on MAP.

Taken together, these data provide a foundation for using the model of HFD-fed mice by showing that it promotes hyperlipidaemia, hyperglycaemia and increased DAP and to test their effects on HIF2-α expression.

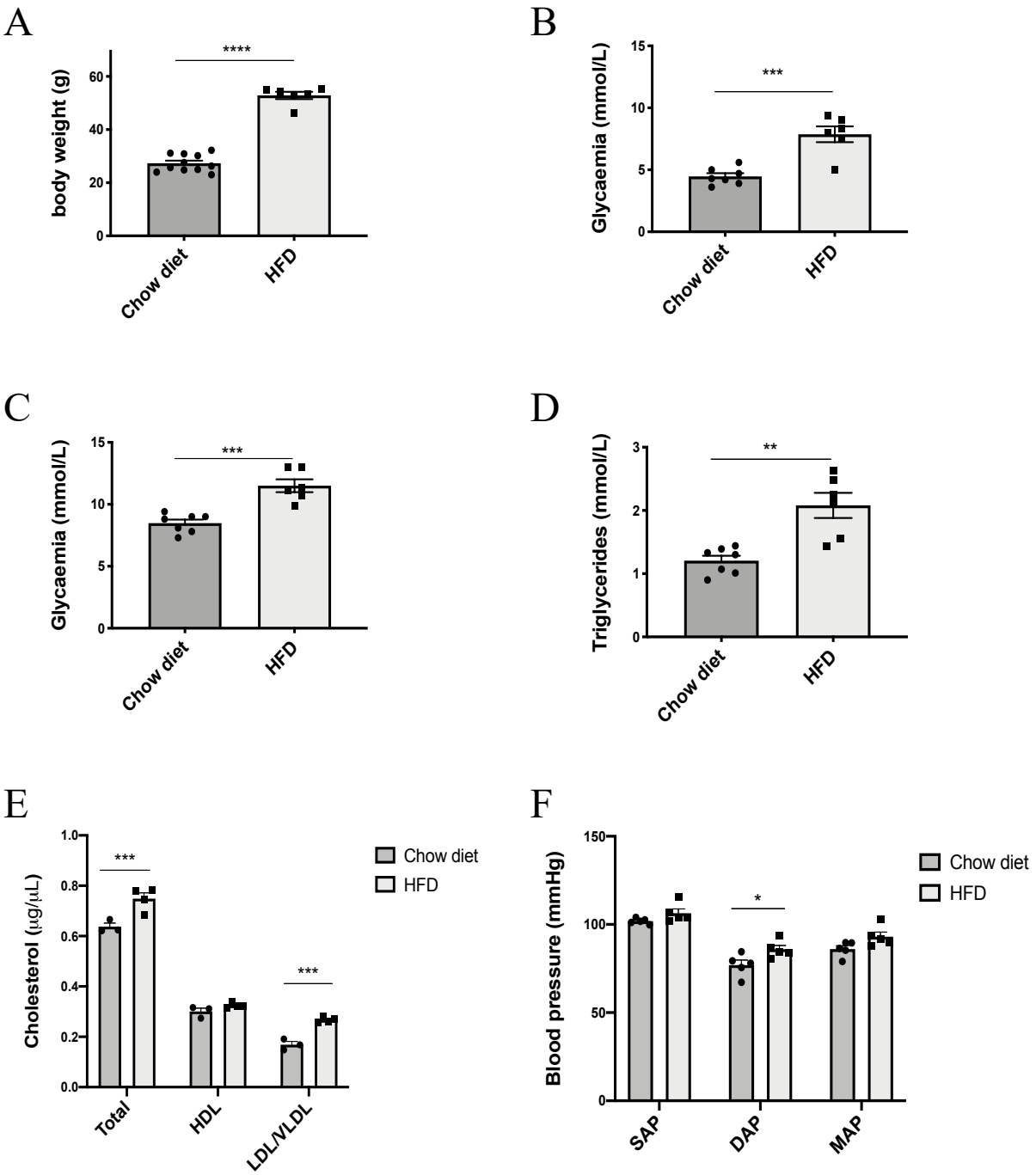
A
body weight (g)
****
Chow diet
HFD
B
Glycaemia (mmol/L)
***
Chow diet
HFD
C
Glycaemia (mmol/L)
***
Chow diet
HFD
D
Triglycerides (mmol/L)
**
Chow diet
HFD
E
Cholesterol (µg/µL)
***
***
Total
HDL
LDL/VLDL
Chow diet
HFD
F
Blood pressure (mmHg)
*
SAP
DAP
MAP
Chow diet
HFD

Figure 4. 1 HFD causes metabolic syndrome phenotype in BL6 mice.

C57Black6/N mice were exposed to 25 weeks HFD or chow diet. A) Body weight difference between chow diet mice (N=11) and HFD mice (N=6). B) Fasting glycaemic level of HFD mice (N=6) compared to chow diet mice (N=7). C) Resting glycaemic level of HFD mice (N=6) compared to chow diet mice (N=7). D) Triglycerides level of HFD mice (N=6) compared to chow diet mice (N=7). E) Total Cholesterol, HDL and LDL/VLDL cholesterol levels of HFD mice (N=4) and chow diet mice (N=3). F) Measurements of systolic (SAP), diastolic (DAP) or mean (MAP) blood pressure of HFD mice (N=5) compared to chow diet mice (N=5). Differences between means were analysed using a two-way ANOVA test (E,F) and by unpaired T-test (A,B,C,D). * $p<0.05$; ** $p<0.01$; *** $p<0.001$; **** $p<0.0001$.

High fat feeding reduced HIF2-α protein levels at the LSS site of mice aorta.

It was demonstrated that HIF2-α protein levels are enriched at sites of LSS within the aortic arch and at the descending aorta (Chapter 3). High fat diet is a well-known tool to induce dyslipidaemia and to favour the development of atherosclerosis in mice (Getz and Reardon, 2006). Glycaemic and lipid levels of mice exposed to 25 weeks of HFD, suggested a pro-atherogenic profile. To investigate the effect HFD feeding on HIF2-α levels in vascular endothelial cells, *en face* staining was conducted on the aortae of C57Black6/N mice exposed to 25 weeks of HFD. Portions of the aorta were stained with HIF2-α antibody, together with CD31, marker of endothelial cells and TO-PRO 3 to delineate nuclei and imaged by confocal microscopy.

Three regions of the aorta were analysed: the inner curvature (exposed to LSS), the outer curvature (exposed to HSS), and the descending aorta (exposed to HSS). Representative images of immunostaining are shown in Figure 4.2A. *En face* staining revealed a reduction of HIF2-α protein at the atheroprone region of the inner curvature of the arch of HFD fed mice when compared to their controls kept on standard chow diet (Figure 4.2B). On the contrary, levels of HIF2-α at the outer curvature were not affected by HFD treatment (Figure 4.2B). Similarly, levels of HIF2-α at the descending aorta, an additional HSS region, were also not affected by HFD (Figure 4.2B). Nuclear expression of HIF2-α at the HSS region of descending aorta remained highly expressed and much higher than the levels observed at the HSS region of the outer curvature, both on chow and HFD mice.

Collectively these experiments suggest that HFD reduces HIF2-α expression specifically at the inner curvature of the aorta which is an atheroprone LSS site.

A

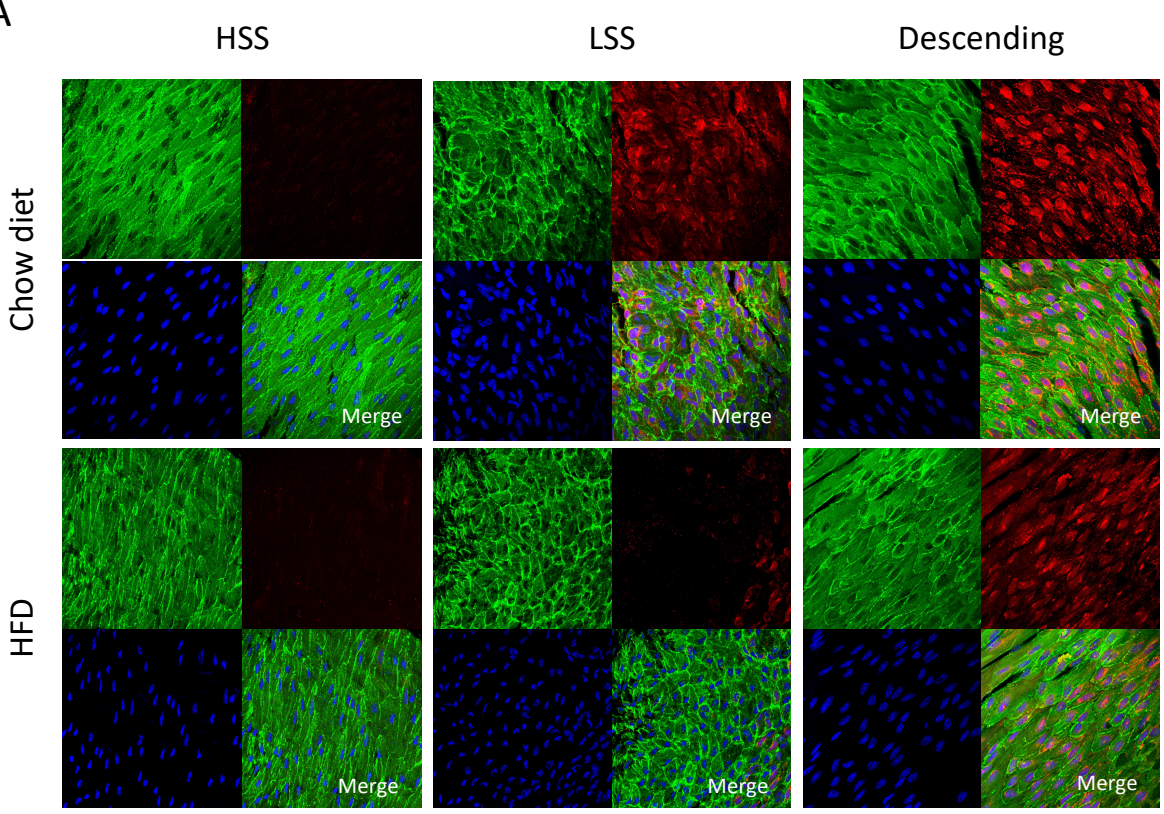
HSS
LSS
Descending
Chow diet
HFD
Merge
Merge
Merge
Merge
Merge
Merge
CD31, HIF2-α, TO-PRO 3

B

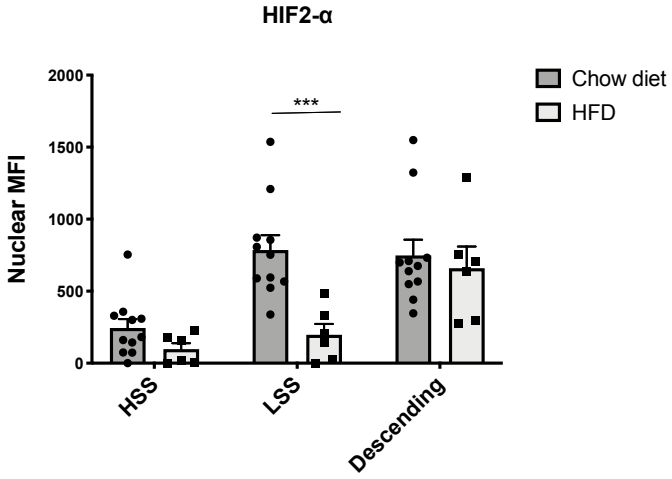
HIF2-α
Nuclear MFI
2000
1500
1000
500
0
***
HSS
LSS
Descending
Chow diet
HFD

Figure 4. 2 HFD reduces endothelial HIF2-α level at site of low shear stress.

Levels of HIF2-α in endothelium were assessed by *en face* staining of LSS and HSS regions of the first arch and at the descending aorta of C57Black/6N mice exposed to 25 weeks HFD (N=6) or chow diet (N=11). HIF2-α was identified by red colour, endothelium by CD31 antibody (green) and nuclei by TO-PRO-3 staining (blue). Representative images of HIF2-α staining are shown (A). Nuclear HIF2-α level was assessed by quantification of the mean fluorescent intensity (MFI) using Fiji software. The nuclear MFI of IgG control sample was subtracted from the experimental reading of HIF2-α nuclear MFI. B) Mean levels of nuclear HIF2-α +/- SEM are shown for controls chow diet mice or HFD mice. Differences between means were analysed using a two-way ANOVA test. *** $p<0.001$.

Leptin deletion model

Leptin deletion causes obesity and transient hyperglycaemia.

I used the leptin deletion model (ob/ob) to complement my studies using high fat feeding. Leptin is a central regulator of food intake and energy metabolism. Spontaneous mutation of the leptin gene in mice led to increase in food intake (hyperphagia), thereby leading to obesity. To monitor the extent of weight gain in wild type, heterozygous or ob/ob mice, fed on a standard rodent chow diet, body weight was measured every week after the weaning age. A body weight chart from the 3rd week until the 20th week is shown in Figure 4.3. Ob/ob mice were indistinguishable from their wild type and heterozygous littermates control until the 5th week of life. Young ob/ob mice gained weight rapidly after weaning and their severely overweight phenotype becomes obvious at the 6th week of age. Ob/ob increasingly gained weight throughout their lives, while the body weight of heterozygous mice remained comparable to that of the wild type controls.

It is known that obesity in ob/ob is linked to hyperglycaemia only until the 16th week of age (Coleman and Hummel, 1973), while after that stage, ob/ob mice reverted to euglycaemia (normal glucose levels). To confirm this phenotype, resting glycaemia was measured at 14 and 22 weeks of age. As predicted, 14 weeks old ob/ob mice presented hyperglycaemia, while heterozygous littermate controls remained euglycaemic (Figure 4.4A). On the contrary, despite the presence of obesity in ob/ob mice, 22 weeks old mice were not hyperglycaemic and the level of blood glucose were comparable between wild type, heterozygous and ob/ob mice (Figure 4.4B).

Furthermore, obesity is commonly associated with dyslipidaemia. Therefore, triglycerides levels were investigated at both ages. Despite the absence of statistically significant differences between the groups, ob/ob mice at both time points, presented a clear trend towards an increase in triglycerides level (Figure 4.4C,D). Ob/ob mice at 22 weeks of age showed increased total cholesterol levels (Figure 4.4E). HDL cholesterol level remained unchanged. Finally, LDL/VLDL cholesterol content was also investigated and it was revealed that ob/ob mice had increased LDL/VLDL content when compared to their wild type littermate controls.

Furthermore, in humans, raised blood pressure (hypertension) is a component of the metabolic syndrome. To investigate blood pressure in obese mice, 14 and 22 weeks old ob/ob

and wild type mice were trained for over one week to tolerate blood pressure measurement. Fourteen weeks old ob/ob mice showed a significant reduction of both systolic (SAP) and diastolic (DAP) blood pressure (Figure 4.4F). Median blood pressure (MAP) was also reduced in ob/ob mice. Interestingly, reduction of blood pressure seemed to be exacerbated at 22 weeks old ob/ob mice. Reduction of SAP, DAP and MAP values reached a higher significance at 22 weeks of age (Figure 4.4G), thus suggesting that blood pressure in ob/ob mice was not positively correlated with obesity and of hyperglycaemia.

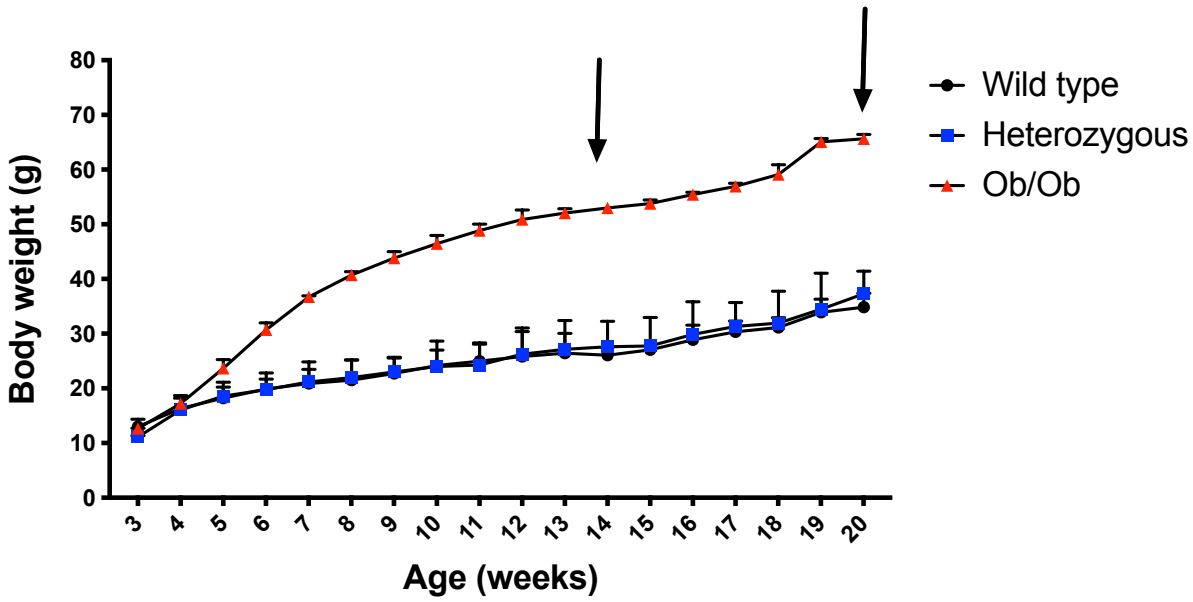

Figure 4. 3 Leptin knock-out mice develop obesity.

The effect of leptin deletion on body weight were studied in wild type, heterozygous (ob/+) and homozygous (ob/ob) mice. Body weight was recorded every week from the weaning at three weeks of age until the twenty weeks of age. Body weight difference between wild type mice (represented with black dots), heterozygous mice (represented with blue squares) and ob/ob mice (represented in red triangles) are shown in the graph. Each group, and at every time point, contains a minimum of three mice and it is represented by the mean value +/- SEM. Two ages were selected for the study of HIF2-α protein level in endothelium, 14 weeks and 20-22 weeks, and pointed on the graph using black arrows.

A

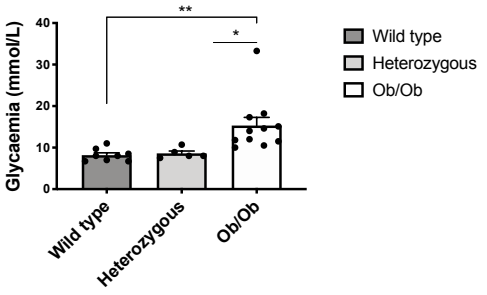
14 weeks old
Glycaemia (mmol/L)
**
*
Wild type
Heterozygous
Ob/Ob
Wild type
Heterozygous
Ob/Ob

B

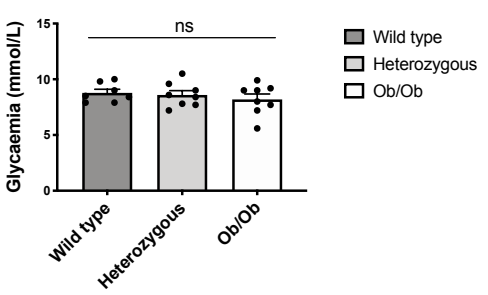
22 weeks old
Glycaemia (mmol/L)
ns
Wild type
Heterozygous
Ob/Ob
Wild type
Heterozygous
Ob/Ob

C

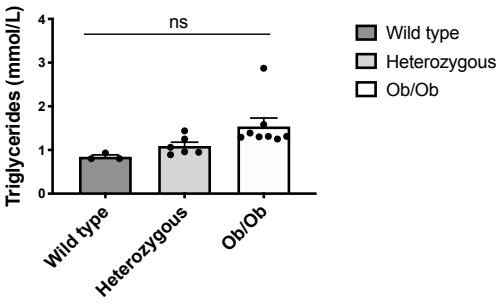
14 weeks old
Triglycerides (mmol/L)
ns
Wild type
Heterozygous
Ob/Ob
Wild type
Heterozygous
Ob/Ob

D

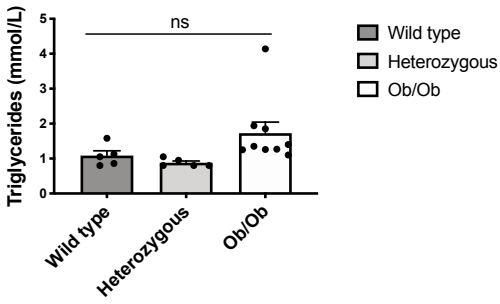
22 weeks old
Triglycerides (mmol/L)
ns
Wild type
Heterozygous
Ob/Ob
Wild type
Heterozygous
Ob/Ob

E

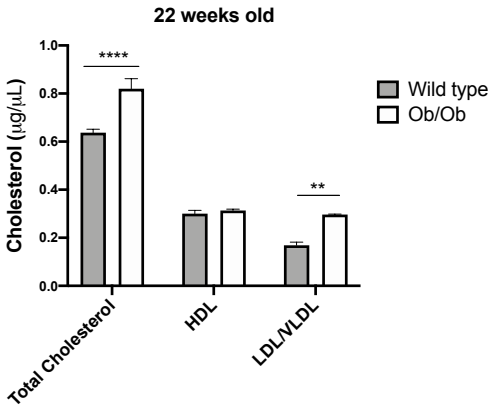
22 weeks old
Cholesterol (μg/μL)
****
**
Wild type
Ob/Ob
Total Cholesterol
HDL
LDL/VLDL

F

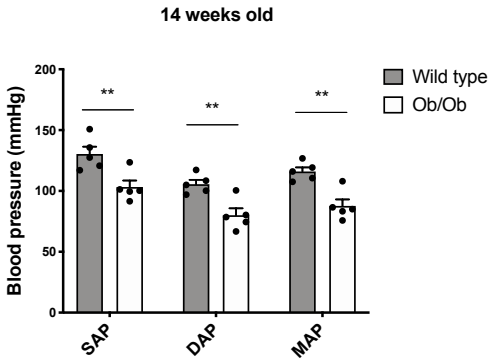
14 weeks old
Blood pressure (mmHg)
**
**
**
Wild type
Ob/Ob
SAP
DAP
MAP

G

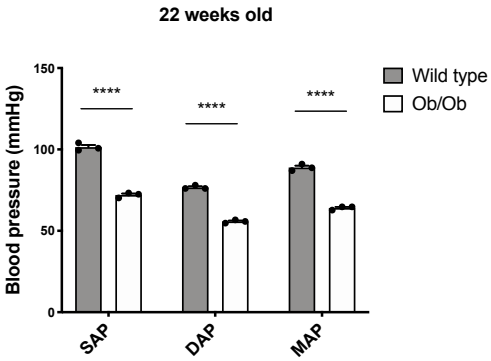
22 weeks old
Blood pressure (mmHg)
****
****
****
Wild type
Ob/Ob
SAP
DAP
MAP

Figure 4. 4 Ob/ob mice develop dyslipidaemia and transient hyperglycaemia.

Wild type, heterozygous and ob/ob mice were exposed to standard chow diet. A) Resting glycaemic level of ob/ob mice (N=11) compared to their wild type (N=8) or heterozygous (N=5) littermate controls at 14 weeks of age. B) Resting glycaemic level of ob/ob mice (N=8) compared to their wild type (N=7) or heterozygous (N=8) littermate controls at 22 weeks of age. C) Triglycerides level of ob/ob mice (N=8) compared to their wild type (N=3) or heterozygous (N=6) littermate controls at 14 weeks of age. D) Triglycerides level of ob/ob mice (N=9) compared to their wild type (N=5) or heterozygous (N=5) littermate controls at 22 weeks of age. E) Total Cholesterol, HDL and LDL/VLDL cholesterol levels of ob/ob mice (N=3) compared to wild type controls (N=3). F) Measurements of systolic (SAP), diastolic (DAP) or mean (MAP) blood pressure of wild type (N=5) and ob/ob mice (N=5) at 14 weeks of age. G) Measurements of SAP, DAP and MAP blood pressure of wild type (N=3) and ob/ob mice (N=3) at 22 weeks of age. Differences between means were analysed using a one-way ANOVA test (A,B,C,D) and two-way ANOVA test (E,F,G). * $p<0.05$; ** $p<0.01$; **** $p<0.0001$.

Obesity without hyperglycaemia reduced endothelial HIF2-α level at atheroprone site.

To assess whether elements of the metabolic syndrome altered endothelial protein level of HIF2-α, *en face* staining of aorta of leptin null mice and their littermate controls was carried out at 14 weeks of age and 20-22 weeks of age. From each mouse three regions of the aorta were analysed: the inner curvature (exposed to LSS), the outer curvature (exposed to HSS), and the descending aorta (exposed to HSS).

In wild-type mice of both age groups, HIF2-α expression in endothelial cells was observed at the inner curvature of the aortic arch and descending aorta but was not observed at the outer part of the arch, thereby confirming my previous observations (Figure 4.5). In mice aged 14 weeks, HIF2-α expression at the inner curvature and descending aorta was similar between wild type mice, heterozygous and ob/ob mice. In contrast, in mice aged 20-22 weeks, ob/ob mice exhibited a drastically reduced nuclear HIF2-α expression level at the inner curvature whereas levels between wild type mice and heterozygous mice were similar (Figure 4.5). On the contrary, the outer curvature, region of HSS remained unaltered. Furthermore, nuclear HIF2-α level in the descending aorta site showed no significant changes between the three groups. Quantification of the fluorescence confirmed a significant reduction of HIF2-α at sites of LSS in ob/ob mice when compared to wild type and heterozygous littermate controls (Figure 4.5C).

These data suggest that prolonged obesity causes a reduction in endothelial expression of HIF2-α specifically at the atheroprone LSS region of the aortic arch, which is likely independent of the glucose status of the animals.

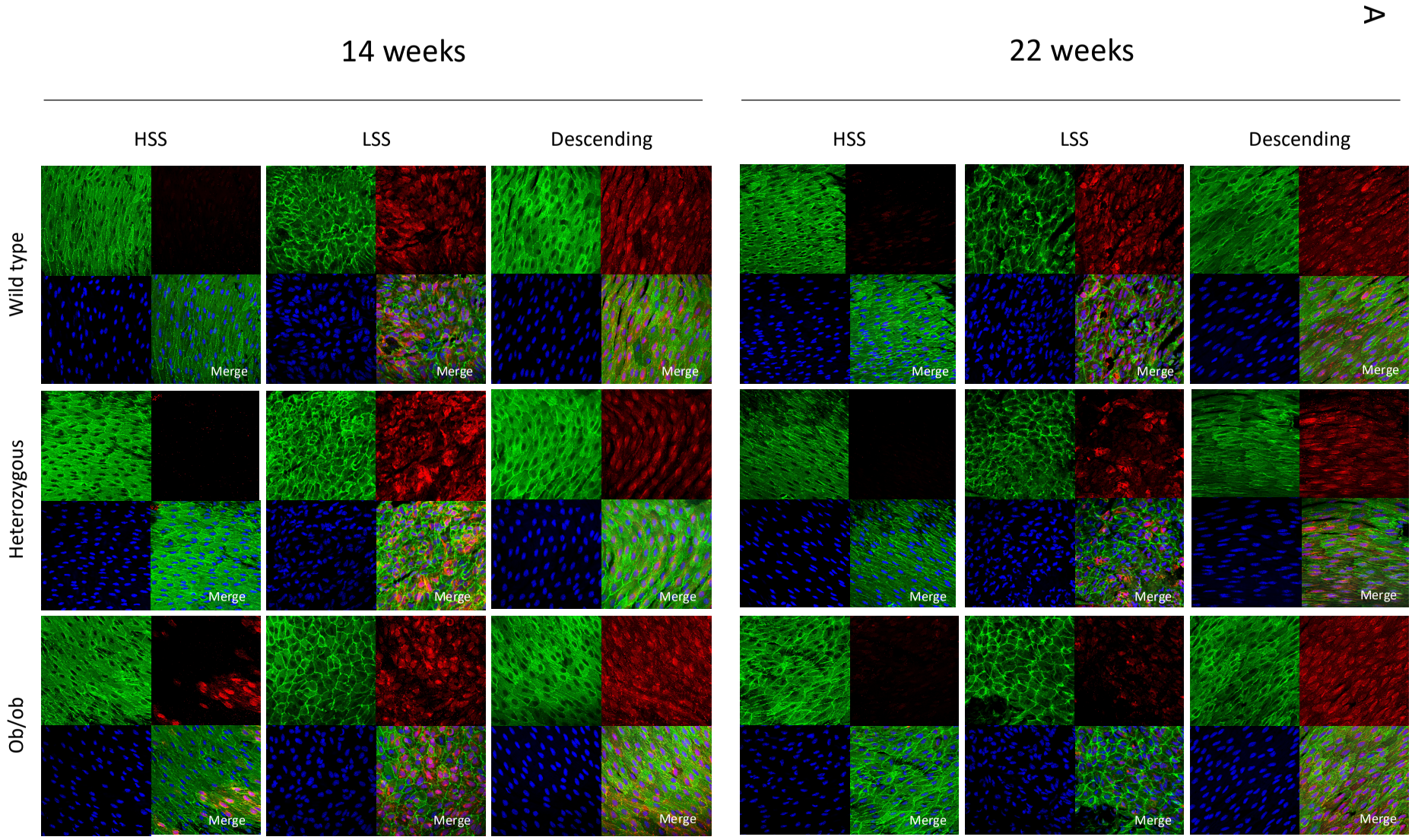
A
14 weeks
22 weeks
HSS
LSS
Descending
HSS
LSS
Descending
Wild type
Heterozygous
Ob/ob
Merge
CD31, HIF2-α, TO-PRO 3

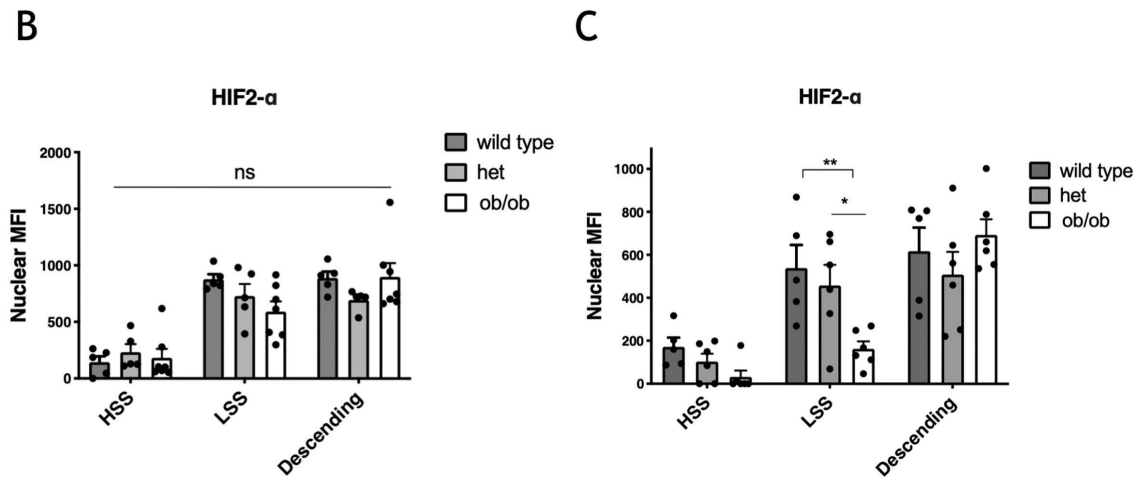

Figure 4. 5 Obesity reduced aortic endothelial HIF2-α levels at site of LSS.

Level of HIF2-α in endothelium were assessed by *en face* staining of LSS and HSS regions of the first arch and at the descending aorta of wild type, heterozygous and ob/ob mice exposed to chow diet. HIF2-α was identified by red colour, endothelium by CD31 antibody (green) and nuclei by TO-PRO-3 staining (blue). Representative images of HIF2-α staining for mice at 14 weeks of age are shown in A (lower panel) while representative images of HIF2-α staining for mice at 22 weeks of age are shown in A (upper panel). Nuclear HIF2-α level was assessed by quantification of the mean fluorescent intensity (MFI) using Fiji software. In all quantifications presented, the nuclear MFI of IgG control sample was subtracted from the experimental reading of HIF2-α nuclear MFI. B) Mean level of HIF2-α +/- SEM are shown for controls wild type and heterozygous or ob/ob mice at 14 weeks of age. C) Mean level of HIF2-α +/- SEM are shown for controls wild type and heterozygous or ob/ob mice at 22 weeks of age Differences between means were analysed using a two-way ANOVA test. * $p<0.05$;** $p<0.01$.

Single injection of STZ induced diabetes in BL6/J mice.

I observed a reduction of HIF2-α levels at the inner curvature of the aortic arch in mice exposed to HFD. The pro-atherogenic profile of HFD mice included increased body weight and an increase of both fasting and resting glycaemia and altered lipid profiles. In the ob/ob mice at 22 weeks of age, I observed reduced HIF2-α in presence of normal glucose levels. To further uncouple the contribution of hyperglycaemia from other factors, I induced type 1 diabetes mellitus in C57Black6/J mice receiving a standard chow diet.

To achieve dysregulation of glycaemic level, pancreatic injury was induced by a single dose (150mg/kg) injection of steptozotocin (STZ), whereas control mice were injected with citrate buffer (hereafter referred to as vehicle). Damage to the pancreatic tissue is expected to impair the ability of β-cells to produce insulin and hence lead to diabetic state. Glucose levels were then monitored for 14 days until the termination of the experiment. STZ is a highly toxic antibiotic and a reduction in body weight in mice injected with mild or high doses of STZ (>200 mg/kg) has been reported (Bloch *et al.*, 2006; Deeds *et al.*, 2011). In contrast, multiple low-dose STZ injections (50 mg/kg) are not associated with loss in body weight and they are commonly used to study type-2 diabetes mellitus and atherosclerosis in combination with a HFD (Kunjathoor, Wilson and Leboeuf, 1996).

I therefore recorded body weight before STZ injection and carefully monitored body weight and other signs of health after the STZ injection. Mice that developed marked weight loss, polyuria and polydipsia were humanely sacrificed before the end of the experiment. Thus, the body weight of STZ-treated mice that were used for experiments did not differ from the body weight of vehicle injected mice (Figure 4.6A).

To confirm the presence of diabetes in STZ injected mice, glycaemia was evaluated under resting conditions, prior to and 14 days after the injection of STZ. It was demonstrated that STZ injection caused hyperglycaemia, whilst mice injected with vehicle control remained euglycaemic (Figure 4.6B).

Furthermore, I investigated whether increased glycaemic levels per se would influence triglycerides levels. Triglycerides levels in chow-fed mice were not affected after 14 days from pancreatic destruction achieved by STZ injection (Figure 4.6C) suggesting that hyperglycaemia is not sufficient to cause hypertriglyceridaemia.

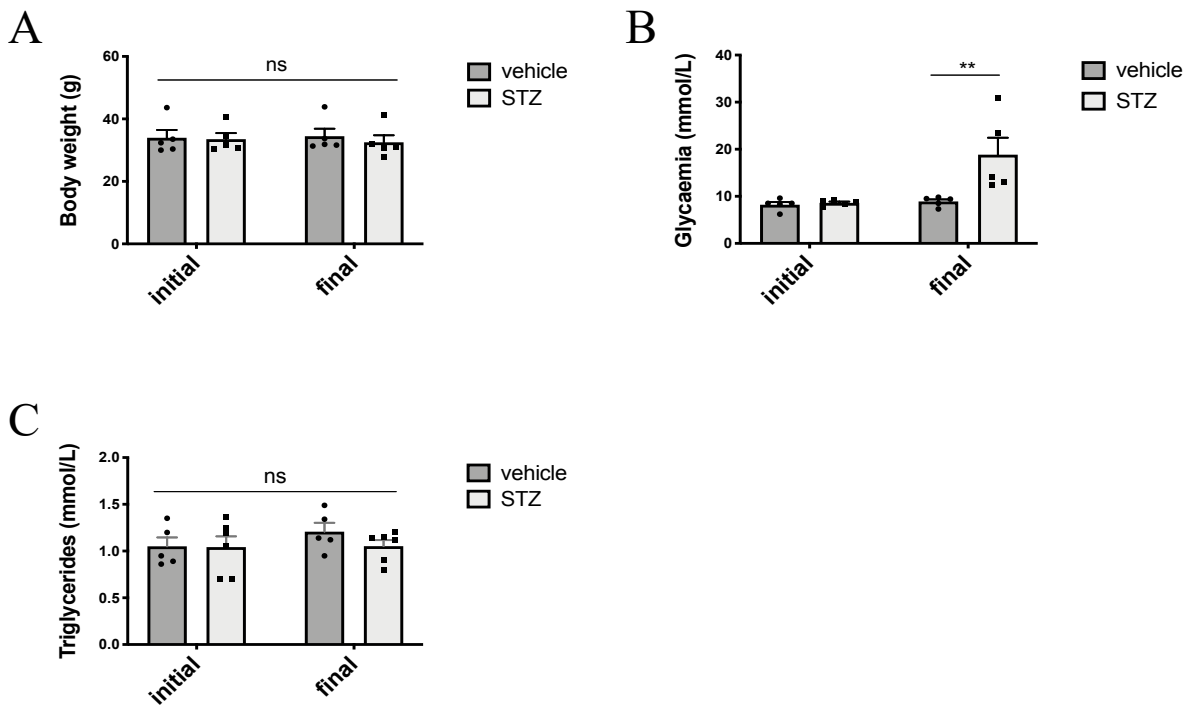

Figure 4. 6 STZ causes diabetes in BL6 mice.

C57Black6/J mice were treated with STZ 150 µg/ml (N=5) or vehicle (N=5) in single dose. A) Body weight difference before (initial) and after (final) treatment. B) Resting glycaemic level of STZ-treated mice compared to vehicle-treated mice before and after treatment. C) Triglycerides levels of STZ-treated mice compared to vehicle-treated mice before and after treatment Differences between means were analysed using a two-way ANOVA test. ** $p<0.01$.

Endothelial HIF2-α levels in the murine aorta were unaffected by STZ-induced diabetes.

Protein levels of HIF2-α were quantified in mice exposed to STZ treatment for 14 days by *en face* staining of HSS and LSS regions within the arch and the descending aorta. Aortic tissue was stained for HIF2-α antibody, together with CD31, which served as a marker of endothelial cells, and counterstained with TO-PRO 3 to delineate nuclei. Confocal microscopy revealed that HIF2-α levels were higher at site of LSS when compared to the outer curvature exposed to HSS, in both hyperglycaemic mice and euglycaemic mice, as seen in wild-type mice previously. Moreover, STZ treatment showed no effect on protein expression at the atheroprone site of LSS (Figure 4.7A). There was also no effect of STZ treatment on HIF2-α levels at the HSS region of the aortic arch or the descending aorta (Figure 4.7A and Figure 4,7B).

In conclusion, these data confirm my previous observation that HIF2-α levels are enriched at the LSS region of the aortic arch in a different cohort of mice. I also conclude that hyperglycaemia alone does not influence HIF2-α protein levels in endothelial cells of the murine aortic arch. These data suggest that hyperglycaemia *per se* is not sufficient to drive a reduction in HIF2-α levels at the LSS site.

A

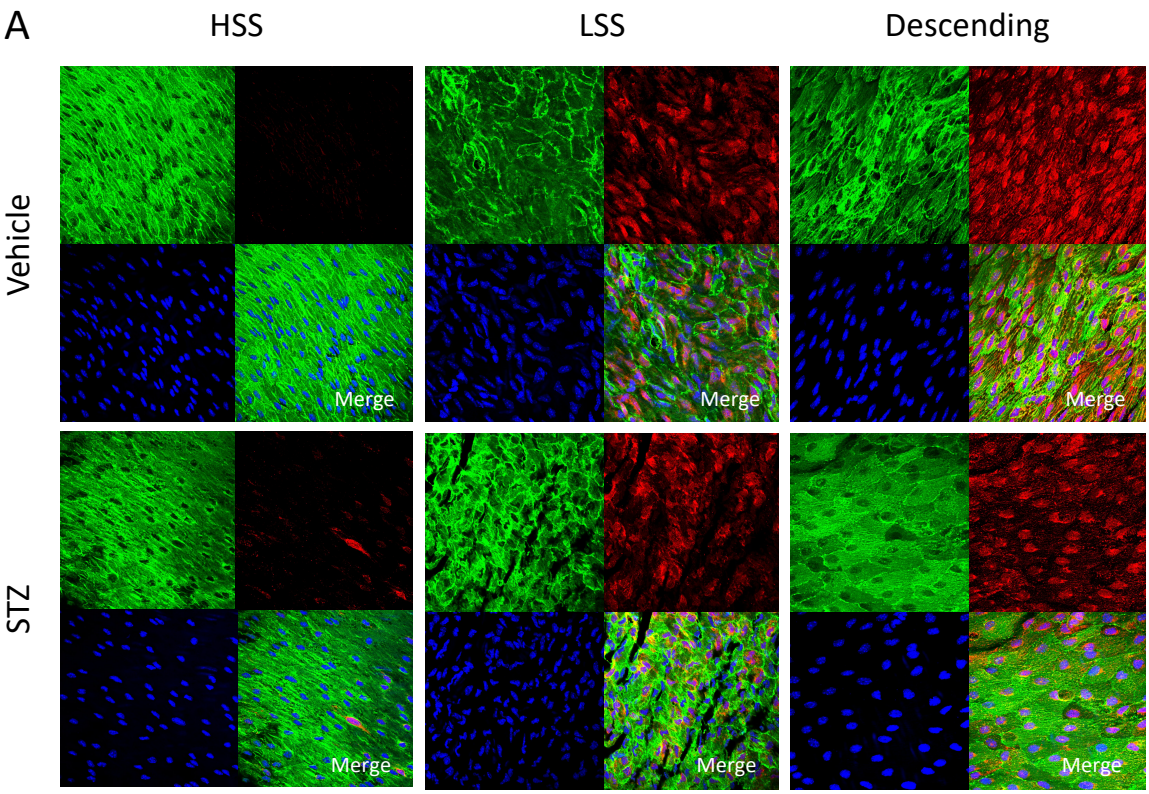

CD31, HIF2-α, TO-PRO 3

B

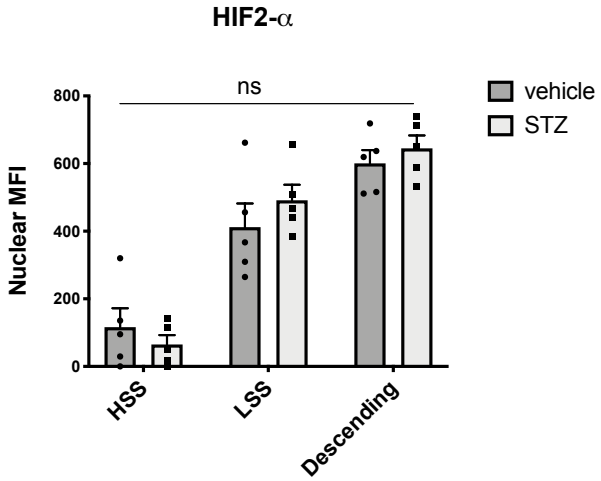

Figure 4. 7 Aortic endothelial HIF2-α levels were not regulated by STZ-induced diabetes.

Levels of HIF2-α in endothelium were assessed by *en face* staining of HSS and LSS regions of the first arch and at the descending aorta of male C57Black/6 mice treated with STZ 150 µg/ml (N=5) or vehicle (N=5). HIF2-α was identified by red colour, endothelium by CD31 antibody (green) and nuclei by TO-PRO-3 staining (blue). Representative images of HIF2-α staining are shown (A). Nuclear HIF2-α level was assessed by quantification of the mean fluorescent intensity (MFI) using Fiji software. In all quantifications presented, the nuclear MFI of IgG control sample was subtracted from the experimental reading of HIF2-α nuclear MFI. B) Mean levels of HIF2-α +/- SEM are shown. Differences between means were analysed using a two-way ANOVA test.

Sulforaphane reduces triglycerides in a model of metabolic syndrome and rescues endothelial HIF2-α

Sulforaphane ameliorates triglycerides level of HFD mice.

It was demonstrated that endothelial HIF2-α level was reduced in overweight HFD and in a model of obese mice. My data suggest that hyperglycaemia *per se* was not the driving cause of this reduction. I reasoned that obesity might lead to a low-level inflammatory state that often is associated with an increase of the reactive oxygen species (ROS). To understand whether ROS might be involved in the reduction of HIF2-α level, overweight mice exposed to HFD for 6 months were treated with sulforaphane (SFN), a natural antioxidant compound extracted from cruciferous vegetable such as broccoli and cabbage. Previously *in vitro* studies showed that sulforaphane activated atheroprotective signals, resulting in reduced ROS levels and ameliorated endothelial dysfunction in presence of hyperglycaemia (Xue *et al.*, 2008).

I firstly examined the effects of sulforaphane treatment on obesity, hyperglycaemia and dyslipidaemia in mice exposed to a HFD. Therefore, weight, glycaemic levels, triglycerides and cholesterol levels were tested pre-treatment and post-treatment in vehicle-injected controls and in SFN injected mice. Injections with SFN or vehicle control showed no effect on body weight (Figure 4.8A) or resting blood glycaemic levels (Figure 4.8B). In contrast, analysis of whole blood showed a significant reduction of triglycerides in SFN-treated mice compared to pre-treatment or to levels in control-treated mice (Figure 4.8C), demonstrating that SFN treatment ameliorates triglyceride levels in HFD mice. Unlike triglyceride levels, SFN had no effect on plasma total cholesterol content (Figure 8D). Levels of HDL and LDL/VLDL cholesterol fractions were also not affected by SFN treatment and remained similar to those of vehicle-injected controls (Figure 4.8D).

In conclusion, these data reveal that SFN treatment reduced plasma triglyceride levels without altering cholesterol levels or glycaemia in mice exposed to HFD.

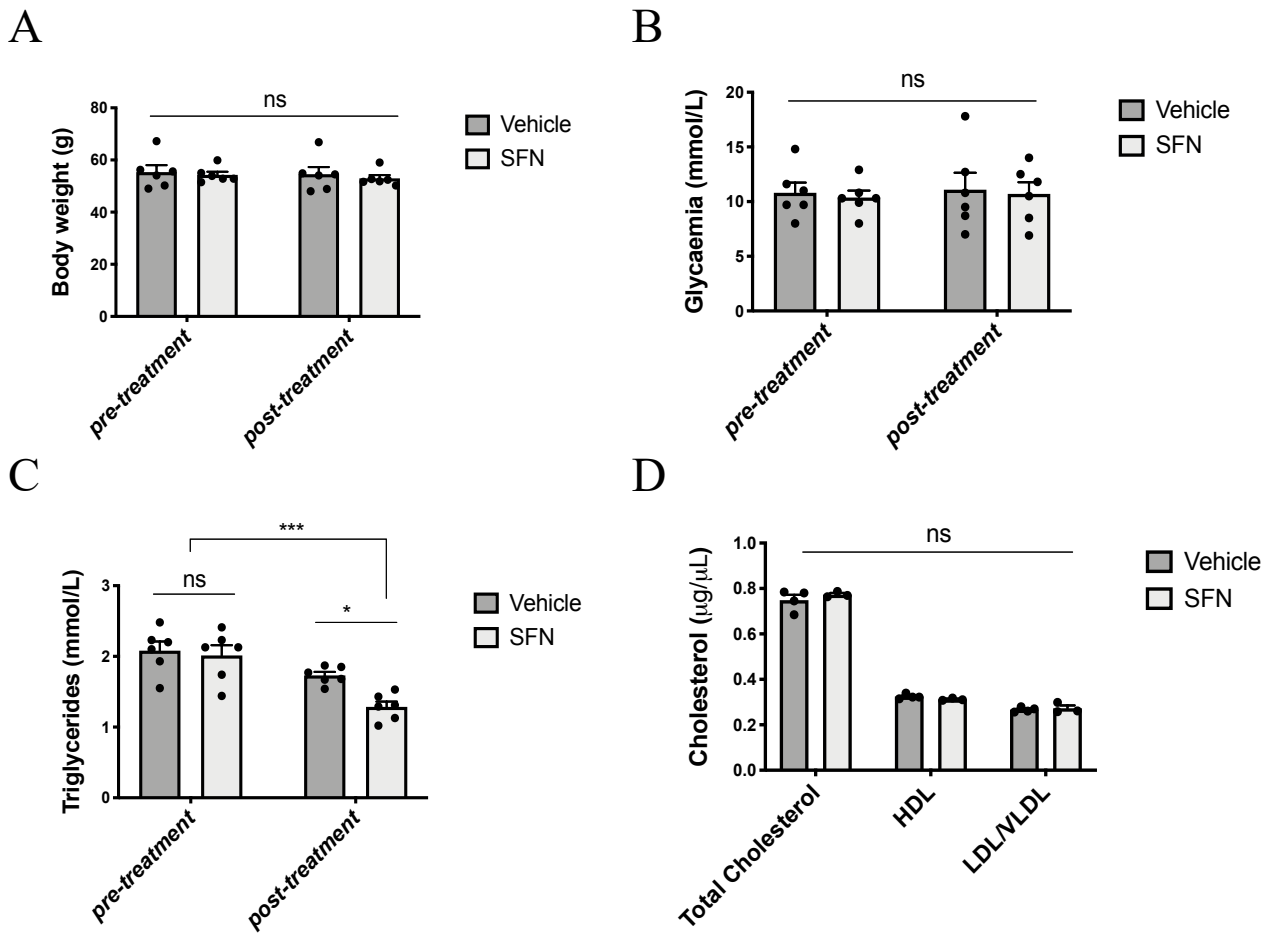

Figure 4. 8 Sulforaphane ameliorates triglyceridaemia in HFD mice.

C57Black6/N mice exposed to 6 months HFD were treated once daily with sulforaphane (SFN) 5mg/kg (N=6) or vehicle control (N=6) for 4 consecutive days. A series of physiological parameters were measured before the injections (pre-treatment) and on the last day of injection (post-treatment). A) Body weight difference between vehicle and SFN group before and after the treatment. B) Glycaemic levels were assessed before and after the treatment in vehicle-injected or SFN-injected group. C) Triglycerides levels were assessed in vehicle and SFN groups prior and post experimentation. D) Total cholesterol, HDL and LDL/VLDL levels were assessed from plasma of vehicle group mice (N=4) and SFN-treated mice (N=3). Differences between means were analysed using a two-way ANOVA test . *p<0.05, ***p<0.001

Sulforaphane rescued HIF2-α levels at atheroprone and atheroprotected sites in HFD mice.

I next determined whether SFN treatment can alter endothelial HIF2-α level in aortic endothelium of HFD mice. Mice fed on a HFD for 6 months were treated with SFN 5mg/kg for four consecutive days and aortic tissues were collected four hours after the last injection.

En face staining was performed on aortic endothelium using anti- HIF2-α antibody on the first section of the aortic arch and descending aorta. Three regions of the aorta were imaged: the inner curvature (exposed to LSS), the outer curvature (exposed to HSS), and the descending aorta (exposed to HSS).

Within the aortic arch, SFN treatment significantly enhanced nuclear HIF2-α levels at the regions of LSS but did not alter HIF2-α at the HSS region. Furthermore, the descending aorta, exposed to protective HSS, was also investigated. Intriguingly, the atheroprotected region of the descending aorta revealed an increase expression of HIF2-α level in SFN-treated mice aorta when compared to tissues harvested from their vehicle-treated controls (Figure 4.9A). Quantification of fluorescence confirmed the significant restoration of nuclear HIF2-α level at both region of LSS within the aortic arch, and at the descending aorta of SFN-injected mice (Figure 4.9B).

In conclusion, SFN treatment of mice exposed to HFD rescued HIF2-α expression at the LSS region of the aortic arch, and also enhanced HIF2-α expression in the descending aorta. Furthermore, this increment correlated with reduced triglycerides levels.

A

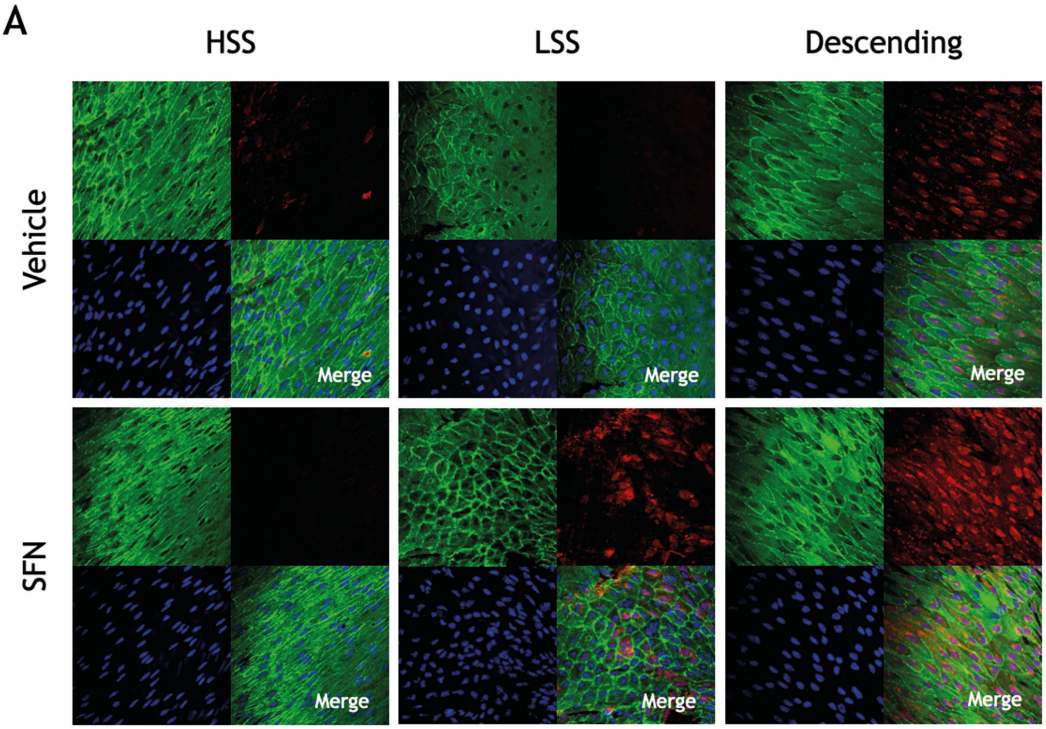

CD31, HIF2-α, TO-PRO 3

B

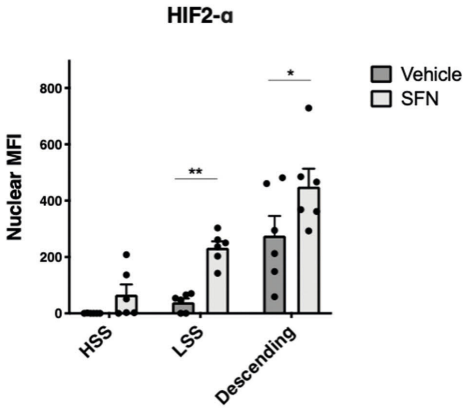

Figure 4. 9 Sulforaphane increases HIF2-α expression in aorta of HFD mice.

Level of HIF2-α in endothelium were assessed by *en face* staining of LSS and HSS regions of the first arch and at the descending aorta of C57Black/6 male mice exposed to 6 months HFD and injected with sulforaphane (SFN) at 5mg/kg (N=6) or vehicle control (N=6) for three consecutive days with the last dose administred 4h prior to tissue harvesting. HIF2-α was identified by red colour, endothelium by CD31 antibody (green) and nuclei by TO-PRO-3 staining (blue). Representative images of HIF2-α staining are shown (A). HIF2-α level was assessed by quantification of the nuclear mean fluorescent intensity (MFI) using Fiji software. The nuclear MFI of IgG control sample was subtracted from the experimental reading of HIF2-α nuclear MFI. B) Mean level of HIF2-α +/- SEM are shown for vehicle-injected mice and SFN-treated mice. Differences between means were analysed using a two-way ANOVA test . *p<0.05, **p<0.01.

Conclusions

In this chapter I demonstrated that:

- Endothelial HIF2-α levels are reduced in obese and hyperglycaemic mice at the atheroprone LSS region of the aortic arch.
- Hyperglycaemia alone is not sufficient to reduce HIF2-α expression at the atheroprone LSS region.
- Alteration in blood pressure did not correlated with changes in HIF2-α expression.
- Treatment with sulforaphane reduced triglycerides and positively regulated HIF2-α at the atheroprone region, as well as at the descending aorta, in mice exposed to HFD.

Discussion

In this chapter I have shown that endothelial levels of HIF2-α are reduced in the aorta of obese and HFD fed mice. HIF2-α protein levels were reduced exclusively at the atheroprone region of the aortic arch which is exposed to low WSS. Furthermore, treatment with sulforaphane, an antioxidant compound, reduced plasma triglyceride levels and rescued HIF2-α at the atheroprone site in mice exposed to HFD.

Obesity and high fat diet reduced endothelial HIF2-α levels independently from hypertension.

Western diet and obesity are major cardiovascular risks. Here I observed that obesity and exposure of mice to a high-fat obesogenic diet can reduce the expression of HIF2-α at an atheroprone LSS region of the aortic arch. In agreement with these findings, several studies showed that HIFs can be negatively regulated in the cardiovascular system by high fat diet and obesity. As an example, a microRNA-mediated reduction of HIF1-α was observed in coronary arteries of pigs when treated with HDL isolated from HFD-fed pigs (Ben-Aicha *et al.*, 2019). Moreover, obese diabetic mice exhibited reduced myocardial capillary density in association with the reduction of HIF1-α levels (Chen and Stinnett, 2008). Furthermore, HFD led to the reduction of HIF1-α and HIF2-α levels in murine myocardium (Zeng *et al.*, 2015). However, the majority of these studies focussed on the HIF1-α isoform and did not investigate HIF levels in the vascular endothelium.

Metabolic syndrome correlates with multiple co-morbidities, one of which is hypertension. In contrast to what is observed in human obese patients, obesity and dyslipidaemia in ob/ob mice were associated with a reduction of both systolic and diastolic pressure. These data are in agreement with previous works (Mark *et al.*, 1999) and with evidences that chronic infusion of leptin raised blood pressure via control of angiotensin converting enzyme (ACE) activity (Shek, Brands and Hall, 1998; Hilzendeger *et al.*, 2010). In contrast, mice exposed to HFD showed a mild increase diastolic blood pressure. Nevertheless, the blood pressure profiles measured in ob/ob and HFD mice suggest that hypertension is not involved in the regulation of HIF2-α in the endothelium of obese mice.

Endothelial HIF2-α levels are not regulated by glycaemia.

Hyperglycaemia is a hallmark of diabetes and triggers tissue damage in multiple organs. Whilst considering the mechanism of HIF2-α reduction in obese ob/ob mice, it should be noted that this strain is characterised by transient hyperglycaemia that reduces with age (Coleman and Hummel, 1973). Interestingly, reduction of HIF2-α level in endothelium occurred at the euglycaemic stage of 20-22 weeks of age. Nevertheless, ob/ob mice at 14 weeks of age already presented obesity. Therefore, It might also be hypothesised that HIF2-α levels were reduced with the ageing of obese mice and that hyperglycaemia may not be an essential factor.

I therefore carried out further experiments to assess directly whether hyperglycaemia could regulate the level of HIFs in aortic tissue. Pharmacological destruction of pancreatic islets causes a phenotype that resembles type-1 diabetes mellitus characterised by striking hyperglycaemia not associated with obesity. Using this approach, I showed that hyperglycaemia alone was not sufficient for HIF2-α reduction. However, it was previously demonstrated that high glucose concentrations inhibit HIF levels *in vitro* and *in vivo* (Catrina *et al.*, 2004; Botusan *et al.*, 2008). Furthermore, *in vivo* induction of diabetes in mice requires some technical considerations. Firstly, responsiveness to STZ in terms of hyperglycaemia is highly variable between mouse strains and gender (Gurley *et al.*, 2006; Hayashi, Kojima and Ito, 2006). In my experiment I used one of the most responsive strains, C57Black6/J mice, and to minimise variability I used adult male littermates as experimental animals. However, even within a closely matched group of animals it remains common to observe great variation of glycaemic levels in response to STZ treatment. Specifically, 2 mice out 5 presented in this work had very marked hyperglycaemia (20-30mmol/L) while the remaining three experimental mice maintained the glucose levels in a milder hyperglycaemic range (11-15 mmol/L). Furthermore, a potential caveat of my study is the analysis at a single time point i.e. two weeks after a single injection of STZ. It is possible that the hyperglycaemia alters HIF signalling but at later time points that have not been analysed in my research.

Furthermore, I did not measure insulin levels and therefore I cannot determine whether the injection of STZ caused an insulin-dependent diabetes mellitus (T1DM) or an insulin-independent diabetes mellitus (NIDDM). While the first one is characterised by the complete absence of insulin production, NIDDM is characterised by a combination of decreased β-cells function and insulin resistance. It was previously reported that insulin restored the activation

HIF signalling in STZ-induced diabetic rats (Katavetin *et al.*, 2006). Furthermore, insulin can activate HIF1-α in a dose dependent manner and this effect was blunted in VSMC isolated from insulin-resistant obese rats (Doronzo *et al.*, 2006). Therefore, it is possible that incomplete destruction of insulin signalling in my experiment may have led to its persistent action on peripheral tissue and endothelial cells to promote HIF2-α levels.

A further caveat for the interpretation of these results can be found in the use of different mouse strains. Both Black6/J and Black6/N mice were employed to study aortic endothelial levels of HIF2-α in the context of obesity and hyperglycaemia. HIF2-α expression is reduced in BL6/N mice exposed to HFD while in the Black6/J background, HIF2-α expression is lost in presence of obesity (22 weeks old ob/ob) but not in presence of hyperglycaemia (14 weeks old ob/ob and STZ-injected mice).

Furthermore, spatial distribution of HIF2-α expression at the aorta differed between the two mouse models. While wild-type Black6/J mice have the highest level of HIF2-α at the descending aorta (data presented in Chapter 3 and STZ-injected mice in the present Chapter); Black6/N mice failed to show increased nuclear level of HIF2-α at the descending aorta. Similarly, wild-type mice in Black6/J background obtained from the ob/ob breeding did not show increased expression of HIF2-α at the descending aortic site when compared to the inner curvature nuclear expression.

It is possible that differences in mouse strain may have introduced a confounding factor in the interpretation of these results. Black6/J ad Black6/N mice, respectively housed at the Jackson laboratory and at the National Institutes of Health, historically accumulated significant genetic variation (Bothe *et al.*, 2004; Bryant *et al.*, 2008; Matsuo *et al.*, 2010; Brown and Moore, 2012). In particular, differences in inflammatory response, metabolism and neurobehavioural/neurological function were observed between the two strains (Simon *et al.*, 2013; Ashworth *et al.*, 2015).

Thus, when interpreting these results, it must be taken into account that genetic variability between strain may cause different responses to obesity and hyperglycaemia and contribute to the variable spatial distribution at the descending aorta.

Sulforaphane ameliorated triglyceridaemia and rescued endothelial HIF2-α levels.

Reduction of HIF2-α levels at the inner curvature of HFD and ob/ob was seen with the combination of obesity and dyslipidaemia, characterised by increased triglycerides and cholesterol levels. It was previously presented that multiple risk factors for atherosclerosis can act via a common mechanism involving increased ROS. In multiple cell types, ROS promoted pro-inflammatory signals while inhibiting protective ones (Ito *et al.*, 2004; Kamata *et al.*, 2005; Enesa *et al.*, 2008). Furthermore, HIFs expression and protein level can be altered by ROS activity (Callapina *et al.*, 2005; Chang *et al.*, 2005; Guzy and Schumacker, 2006; Köhl, Zhou and Brüne, 2006; Taylor and Pouyssegur, 2007; Qutub and Popel, 2008) . Therefore, I wondered whether a natural antioxidant present in broccoli extract, could ameliorate HIF2-α loss in obese mice. Interestingly, mice injected with sulforaphane showed increased levels of HIF2-α at the atheroprone region when compare to the vehicle-injected controls, suggesting that a redox-associated mechanism could contribute to HIF2-α regulation of at this LSS site. Previous works showed that SFN activates a protective signalling mediated by the NF-E2-related factor 2 (Nrf2) (Thimmulappa *et al.*, 2002; Xue *et al.*, 2008). In endothelial cells, SFN triggers Nrf2-mediated anti-inflammatory signalling at site of LSS (Zakkar *et al.*, 2009). Consistent with these studies, my research demonstrated that SFN promoted the levels of HIF2-α in the nucleus at the atheroprone region.

Looking closely at the confocal images, although sulforaphane increased nuclear HIF2-α the mechanism does not seem to rely on translocation of HIF2-α from the nucleus (active form) to the cytoplasm (inactive form), since the staining of the latter compartment was barely detectable. Thus, I hypothesised that reduced protein degradation might be responsible for the increased level of HIF2-α in response to SFN treatment. One possibility is that SFN enhances the activity of the deubiquitinating enzyme Cezanne (Evans *et al.*, 2003) which is known to regulate the expression of HIF-α isoforms (Mader *et al.*, 2020). The deubiquitinating activity of Cezanne can be inhibited by the presence of ROS (Enesa *et al.*, 2008; Cotto-Rios *et al.*, 2012) and therefore SFN may enhance Cezanne activity. Our lab previously demonstrated that Cezanne controls HIF1-α levels under LSS (Feng *et al.*, 2017), and others found that Cezanne regulates HIF2-α at the transcriptional level (Moniz *et al.*, 2015). The potential for Cezanne to regulates HIF2-α post-translationally has not been previously studied but is

plausible. Further work is required to determine if SFN rescues HIF2-α at LSS regions of obese mice via a Cezanne dependent mechanism, for example, by analysis of Cezanne knockout mice.

Nevertheless, the mechanism by which sulforaphane could activate HIF2-α may be secondary to the activation of other proteins. As an example, *in vitro* studies have demonstrated SFN to have anti-inflammatory and anti-angiogenic effects on various cancer cell lines and on the endothelial cells (Shan *et al.*, 2010; Liu *et al.*, 2017, 2020). The protective effect of SFN on endothelial cells was ascribed to the reduction of pro-inflammatory proteins such as nuclear factor-κB (NF-κB) and intercellular adhesion molecule 1 (ICAM1), the reduction of apoptotic process via inhibition of p38 mitogen-activated protein kinases (MAPK) and c-Jun N-terminal kinase (JKN) pathways (Liu *et al.*, 2008; Shan *et al.*, 2012). In addition to this, SFN induces a plethora of genes with anti-oxidant activity, including heme oxygenase enzyme 1 (HO-1) and glutathione system, a mechanism that is partially mediated by the activation of Nrf2 (Velayutham, Babu and Petersen, 2016).

Interestingly, the treatment with sulforaphane ameliorated triglyceride levels but not cholesterol levels. Animal studies show that long term treatment with sulforaphane improves lipidemic profile by reducing triglycerides and total cholesterol levels, by ameliorating insulin responsiveness and improved glucose tolerance and by reducing endothelial dysfunction (Dixon *et al.*, 2002; De Souza *et al.*, 2016; Shehatou and Suddek, 2016; Yang, Lee and Lee, 2016; Axelsson *et al.*, 2017). Similarly my observations, treatment with SFN in rats exposed to 60% HFD for 15 weeks did not show any effect on glycaemia (Axelsson *et al.*, 2017). These data suggest that the interaction between sulforaphane and metabolic factors may depend on the length of the western diet, hence the extent of obesity, as well as the dose and the length of SFN treatment. My data suggest that plasma triglycerides are particularly sensitive to SFN treatment. Since EC can respond to triglycerides, it is plausible that SFN rescues HIF2-α expression in EC indirectly by reducing plasma triglycerides (Figure 4.10). This hypothesis is followed up experimentally in Chapter 5.

In summary, this data might also suggest that a direct link between triglycerides metabolism and interaction with endothelium could contribute to dysregulation of HIF2-α.

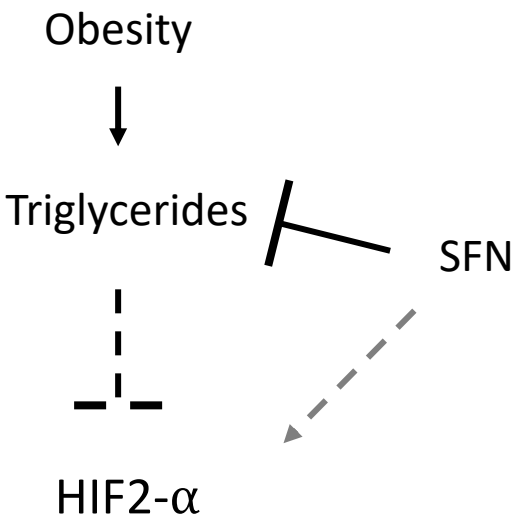

Figure 4. 10 Model of dyslipidaemia-mediated endothelial HIF2-α reduction.

Obesity induced hyperlipidaemia characterised by an increase of triglycerides and cholesterol levels. Triglycerides level correlates with the reduction of HIF2-α in endothelial cells exposed to low shear stress. SFN was shown to rescue HIF2-α level in obese mice without altering body weight, glycaemia or cholesterol levels. On contrary, SFN reduced triglycerides level. Other mechanism of HIF stabilisation mediated by SFN might exist (dashed arrow).

Future works:

The results obtained in this chapter suggested a that risk factors of atherosclerosis may inhibit HIF2-α levels. To further investigate the aspect a series of animal studies could be use:

- Aortae of STZ-induced diabetic mice could be evaluated at different time points, as an example at 1 and 3 months after induction of diabetes.
- To corroborate the correlation between triglyceride levels and HIF2-α in mouse aorta, HFD and/or ob/ob mice could be exposed to anti-dyslipidaemia treatment (e.g. fibrate) and the aorta analysed at different time points.
- Other risk factors such as cigarette smoke have not been considered in this chapter. Analysis of HIF2- α levels could be investigated in lean and obese mice after exposure to cigarette-smoke extract.

Chapter 5. Function of HIF2-α in arterial endothelium

Introduction

The hypoxia-inducible factor family has a central role in regulating the physiology of endothelial cells (ECs). ECs respond to hypoxia stimuli by activating pro-angiogenic responses, thereby facilitating vessel sprouting and rearrangement (Pugh and Ratcliffe, 2003). In addition to this, a novel role for HIF1-α in ECs physiology was identified in response to shear stress stimuli, using both *in vitro* and *in vivo* approaches (Feng *et al.*, 2017; Wu *et al.*, 2017). I have shown in this thesis that HIF2-α is also activated by shear stress forces and that HIF2-α protein levels at the atheroprone site of the aorta are reduced in mice exposed to HFD or obesity. Furthermore, inactivation of HIF2-α levels correlated with increased levels of plasma triglycerides.

Triglyceride levels are a key risk factor for cardiovascular disease (Libby, P.; Ridker, P. M.; Hansson, 2011; Wang *et al.*, 2011), nevertheless epidemiological studies reported that fasting triglyceride levels, after adjustment for total cholesterol and HDL levels, were no longer associated to cardiovascular risk (Toth, 2016). Triglycerides are carried through the lymphatic and blood streams and incorporated into apolipoproteins. Their metabolism at the peripheral tissues (e.g. muscle) converts them into free fatty acid (FFAs), that can be then utilised as a metabolic substrate for cellular energy production by mitochondria or re-converted to triglycerides. ECs buffer triglycerides levels in the blood stream by uptaking them and storing them in intracellular lipid droplets (Kuo, Lee and Sessa, 2017; Son *et al.*, 2018). Alternatively, ECs utilise FFAs for energy production through the fatty acid β-oxidation (Falkenberg *et al.*, 2019b). The balance between FFAs metabolism and glycolysis is relevant for the preservation of ECs health. Changing ECs metabolism towards fatty acid oxidation wes associated with the EndMT process, which it was implicated in atherogenesis and other endothelial-associated pathology such as pulmonary hypertension (Souilhol *et al.*, 2018; Tang *et al.*, 2018; Xiong *et al.*, 2018).

HIF2-α was identified as a regulator of fatty acid metabolism in the liver. Activation of HIF2-α in hepatocytes inhibits enzymes involved in the first step of FAs oxidation as well as enzymes involved in mitochondrial FAs import, thereby causing a mitochondrial β-oxidation defect (Rankin *et al.*, 2009). Nevertheless, the possible role of HIF2-α in fatty acid metabolism in ECs is currently unknown.

Hypothesis and Aims

I previously demonstrated that obesity and dyslipidaemia inhibit local HIF2-α levels at an atheroprone site of mouse aorta. I hypothesised that circulating triglycerides level directly inactivated HIF2-α protein in endothelial cells, thereby contributing to ECs dysfunction via metabolism maladaptation.

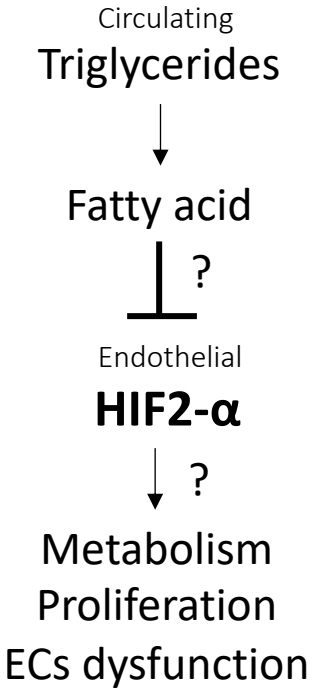

To test this hypothesis I aim to study:

- The effect of free fatty acids on HIF2-α levels in primary aortic ECs exposed to high and low WSS.
- The role of HIF2-α in mitochondrial morphology and activity using gene silencing in cultured ECs exposed to WSS,
- The role of HIF2-α on ECs proliferation under WSS using a lentiviral HIF2-α shRNA pool,
- The effect of HIF2-α on atherosclerosis by inducing plaque formation in HIF2-α-ECs knock-out mice by injection with PCSK9 adenovirus followed by exposure to high fat diet.

Results

Optimising exposure of endothelial cells to oleic acid.

I hypothesised that the local HIF2-α reduction observed in ob/ob and HFD-fed mice was directly caused by dyslipidaemia associated with an increase in triglyceride levels. Triglycerides carried through the blood flow as esterified complexes, are metabolised into free fatty acids (FFAs) and then taken up by cells. To test whether free fatty acids were affecting HIF2-α levels I investigated the effect of oleic acid (OA) overload in PAECs. Initially, to identify toxicity levels of fatty acid *in vitro*, PAECs were exposed to OA or vehicle control at a range of 125 µM-2 mM under static condition and cell viability was assessed at 24, 48 and 72h. Cell viability was expressed as cell death percentage via trypan blue counting in a haemocytometer chamber.

Oleic acid toxicity is shown on figure 5.1A. All cells started with a 100% of viability, corresponding to a 0% cell death at time 0 (0 h) corresponding to 24h after seeding. Viability test revealed that at high dosage 2mM, 1mM and 0.5mM oleic acid presented a dose-dependent amount of cell death throughout the experiment. On contrary, cell death in response to 125 µM or 250 µM oleic acid remained undistinguishable from the vehicle control.

In parallel, to test effective uptake of fatty acids by endothelial cells, PAECs were exposed for 24h to 1mM oleic acid or vehicle and lipid droplets were identified by BODIPY 493/503 staining. While vehicle treated cells expressed very few lipid droplets, exposure to OA caused a drastic increase in BODIPY staining to confirm lipid droplets accumulation in endothelium (Figure 5.1B). Furthermore, under static condition there was a suggestion for reduced PECAM-1 staining in OA-treated cells. Representative images are shown (Figure 5.1C).

In conclusion, here it was demonstrated that oleic acid induced lipid droplets formation in endothelial cells. Furthermore, It was shown that 125 µM or 250 µM of oleic acid or vehicle controls did not induce significant cell death throughout the experiment and that these concentrations should be suitable to assess ECs response to FFAs.

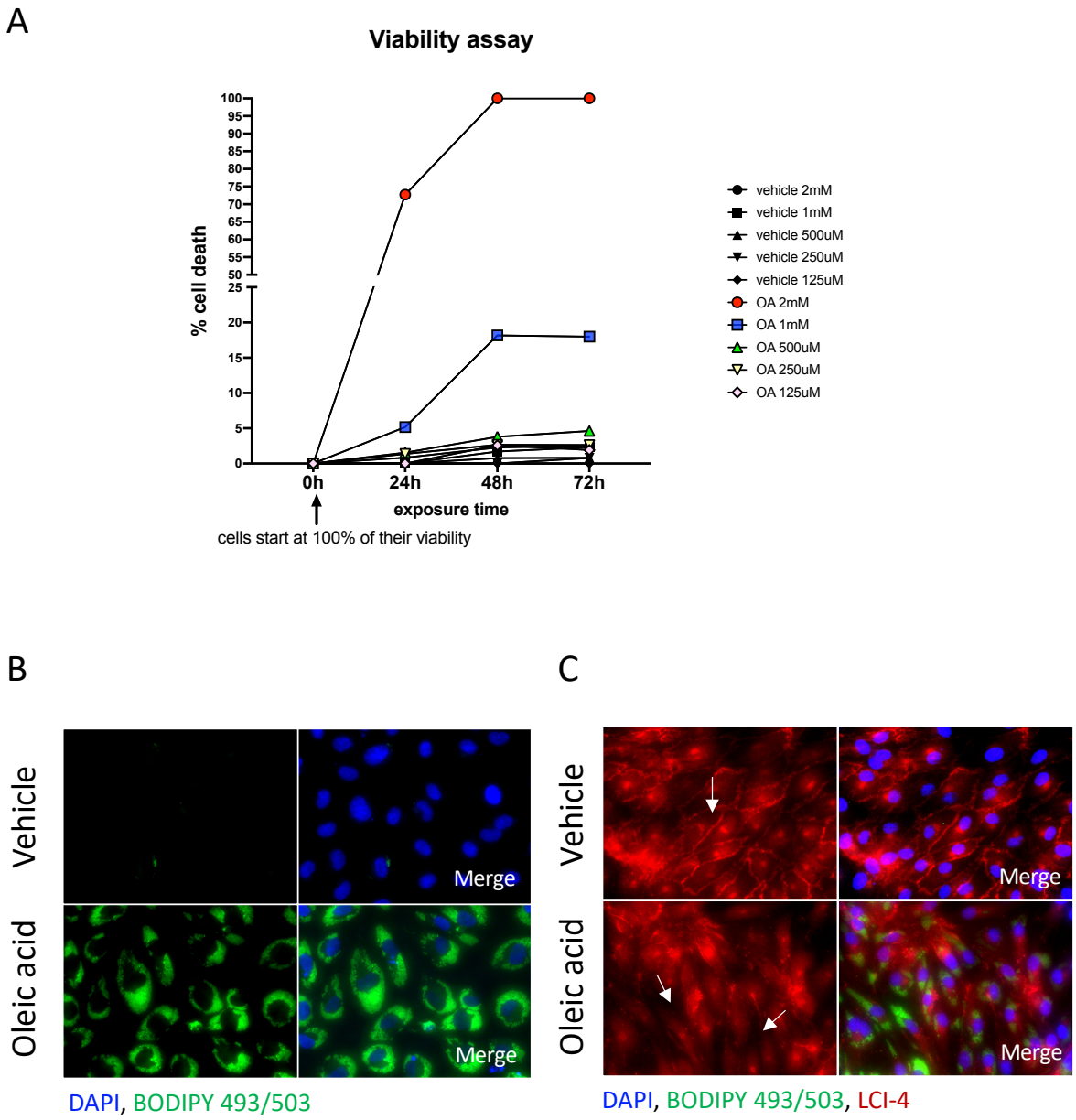

Figure 5. 1 Oleic acid induced lipid droplets formation in endothelial cells.

In vitro toxicity of oleic acid was assessed in PAECs under static condition. Oleic acid or vehicle control was supplemented to media at concentration between 125µM and 2mM for 24, 48 or 72h. Cell death was assessed using trypan blue exclusion staining and cells were counted into a haemocytometer chamber for each time point. Each measurement represents the average of two wells. A) oleic acid toxicity in PAECs, N=2. B) Lipid droplets formation was identified by staining with BODIPY 493/503 reagent. Representative images of PAECs exposed for 24h to 1mM of oleic acid or vehicle control. Lipid droplets are highlighted by FITC fluorescence channel (green) and nuclei were delineated by DAPI counterstaining (blue). C) Representative images of PAECs staining in static cells exposed to 24h of 500µM are shown. PECAM-1 (LCI-4) is highlighted in red, BODIPY staining for lipid droplets (green) and DAPI counterstaining of nuclei (blue). Junctional PECAM-1 expression is indicated by the white arrows.

Oleic acid reduced HIF2-α protein levels *in vitro*

To assess whether *in vitro* fatty acid supplementation alter the level of HIF2-α, PAECs were treated with two doses of oleic acid (125 µM and 250 µM) that were identified as non-toxic for endothelial cells or appropriate vehicle controls. Therefore, treated PAECs were exposed to 72h of shear stress using orbital shaker and protein levels of HIF2-α were investigated using fluorescence staining. Confocal images were analysed for the relative abundance of nuclear HIF2-α compared to the IgG control.

Confocal microscopy revealed that oleic acid at 125 µM concentration altered HIF2-α levels when compare to vehicle treated cells at site of low WSS. Representative images are shown (Figure 5.2A, left panel). On the contrary, HIF2-α levels in cells exposed to high WSS were unaltered by the OA supplementation. Similarly, treatment of PAECs to 72h with 250 µM oleic acid, reduced HIF2-α levels at site of low WSS but not at site of high WSS when compared to their vehicle treated controls (Figure 5.2A, right panel). Quantification of nuclear levels of HIF2-α normalised to the IgG controls (not shown) confirmed reduction of HIF2-α at site of low WSS (Figure 5.2B) for 125 µM oleic acid treatment and for 250 µM oleic acid treatment (Figure 5.2C). On contrary, quantification of HIF2-α at high WSS sites were not significantly different using both oleic acid concentrations.

In conclusion, oleic acid inhibits HIF2-α expression in endothelial cells exposed to low WSS but not in ECs exposed to an atheroprotective flow pattern.

A
125 μM
250 μM
High WSS
Low WSS
High WSS
Low WSS
Vehicle
Oleic acid
Merge
DAPI, BODIPY 493/503, HIF2-α, LCI-4

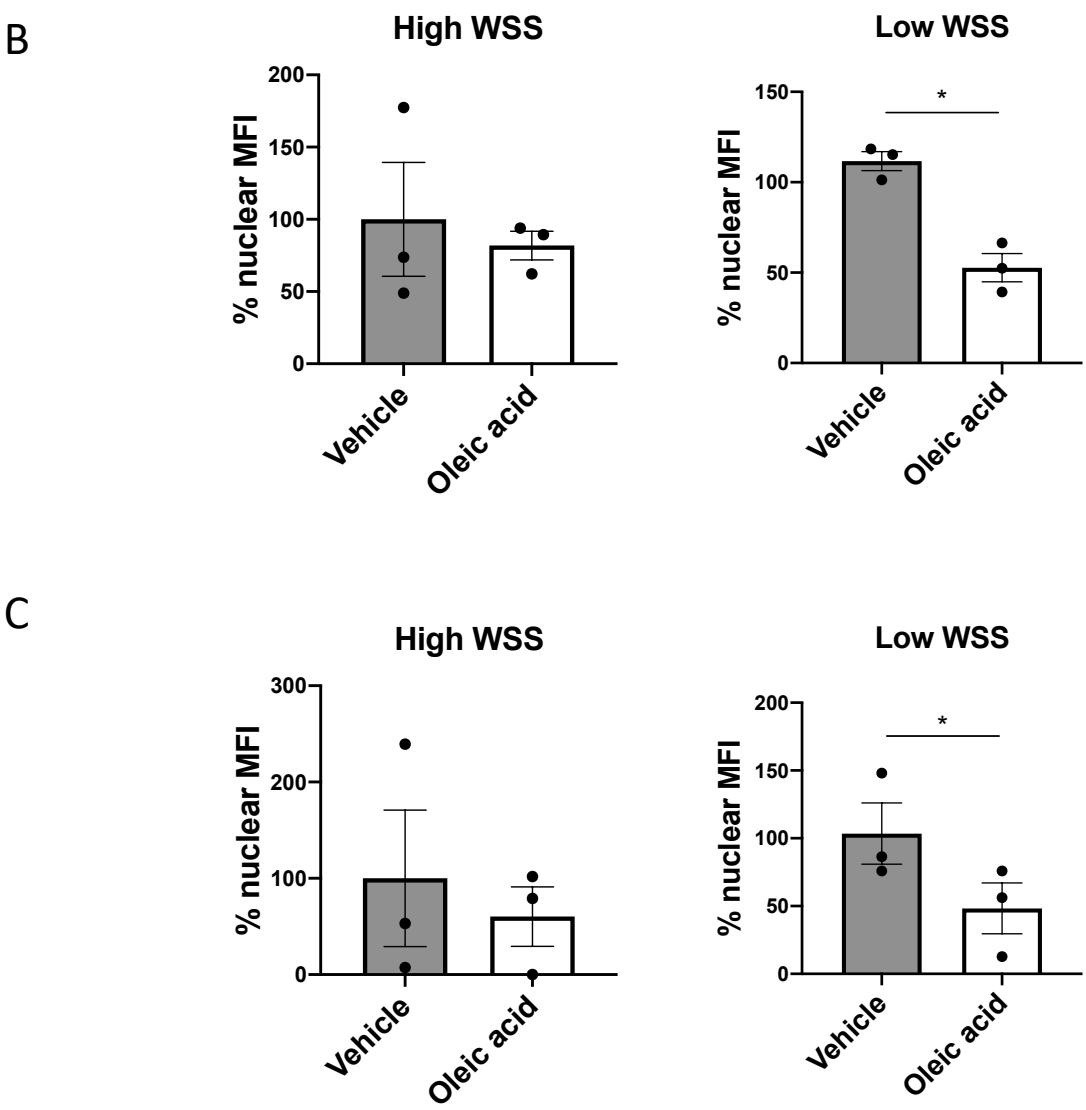

Figure 5. 2 Oleic acid reduced HIF2-α level in PAEC exposed to low WSS.

PAECs were treated with 125µM or 250µM oleic acid or vehicle control and exposed to low or high levels of shear stress using orbital shaker for 72h. HIF2-α levels were assessed using immunofluorescence staining. Confocal images represents HIF2-α in red, PECAM-1 (LCI-4) levels in grey, BOPIDY (lipid droplets) in green and DAPI counterstaining (nuclei) in blue. Nuclear mean fluorescence intensity (MFI) was analysed using ImageJ software. A) Representative images are shown. B) Quantification of nuclear MFI of 125 µM OA treated cells relative to the their vehicle-treated high WSS regions are shown. C) Quantification of nuclear MFI of 250 µM OA treated cells relative to the their vehicle-treated high WSS regions are shown. Mean levels +/- SEM are shown. Differences between means were analysed using a one-tailed paired T-test. *p<0.05

In vitro HIF2-α knock down using lentivirus transduction

To study the function of HIF2-α *in vitro*, lentiviral-shRNA knock-down against HIF2-α was carried out in PAECs. The HIF2-α gene is highly conserved between species. In order to identify compatibility between commercial human shRNA sequences and the porcine genome, lentiviral shRNA sequences were interrogated against *Sus scrofa* HIF2-α mRNA. Sequence blast revealed 100% match between three shRNAs and porcine HIF2-α sequences (Figure 5.3A). Therefore, an equimolar pool of the three shRNAs sequence was used to knock-down HIF2-A in PAECs.

To study the response to flow of PAECs deprived of HIF2-α, cells transduced with lentiviral-HIF2-α shRNAs pool or scrambled control were exposed to 72h of low oscillatory shear stress using the ibidi pump system. Western blotting was carried out to study HIF2-α protein levels. Western blotting analysis revealed reduction of HIF2-α protein in lentiviral-HIF2-α shRNAs treated samples when compared to their scrambled controls (Figure 5.3B). PAECs were further studied for reduction of HIF2-α mRNA expression after lentiviral transduction. qRT-PCR analysis revealed that lentiviral-shRNAs efficiently reduced HIF2-α transcript expression, when compared to their scrambled treated controls (Figure 5.3C).

These data indicate that lentiviral delivery of shRNA efficiently targeted HIF2-α in primary endothelial cells exposed to flow, thus making this a suitable *in vitro* model to study the function of HIF2-α.

A

5’-(1)

CGCTTAGGATCTTTAACACCTGCGAGGGCCACAGCGAAGGCAGCAGCTGCAGCCGCTACTGGTCCTGTAGCCCAGGTGCTCCG
CGTCTCAAAGGGCCACAGCGACGATGACAGCTGACAAGGAAAAGAAAAGGAGTAGCTCGGAGAGGAGGAAGGAGAAGTCC
CGGGATGCTGCCCGGTGCCGGCGGAGCAAGGAGACAGAGGTCTTCTACGAGCTGGCCCACGAGCTGCCCCTGCCCCACAGCG
TGAGCTCCCACCTGGACAAGGCCTCCATCATGCGGCTGGCCATCAGCTTCCTGCGCACACACAAGCTCCTGTCCTCAGTTTGCTC
TGAAAATGAATCTGAAGCAGAAGCTGACCAGCAGATGGACAACTTGTACCTGAAAGCCTTGGAGGGTTTCATTGCCGTAGTGA
CCCAGGATGGCGACATGATCTTTCTGTCGGAAAACATCAGCAAGTTCATGGGACTCACACAGGTGGAGCTAACAGGACACAGC
ATCTTTGACTTCACTCACCCCTGTGACCATGAGGAGATCCGTGAGAACCTCAGCCTCAAAAATGGCTCTGGTTTTGGGAAGAAA
AGCAAAGACATGTCCACCGAGCGGGACTTCTTCATGAGGATGAAGTGCACCGTCACCAACAGAGGCCGCACCGTCAACCTCAA
GTCAGCCACCTGGAAGGTCCTGCACTGCACGGGCCAGGTGAAGGTCTACAACAACTGCCCCCCTCACAGCAGTCTCTGCGGCT
GCAAGGAGCCGCTGCTGTCCTGCCTCATCATCATGTGCGAGCCCATCCAGCACCCGTCCCACATGGACATCCCCCTGGACAGCA
AGACCTTCCTGAGCCGCCACAGCATGGACATGAAGTTCACCTACTGCGACGACAGAATCACAGAACTGATTGGTTACCACCCCG
AGGAGCTGCTCGGCCGCTCAGCATATGAGTTCTACCATGCCCTGGACTCGGAGAACATGACCAAAAGTCACCAGAACTTGTGCA
CCAAAGGGCAGGTGGTCAGCGGCCAGTACCGGATGCTTGCGAAGCACGGGGGCTACGTGTGGCTGGAGACGCAGGGGACG
GTCATCTACAACCCCCGCAACCTGCAGCCTCAGTGCATCATGTGTGTCAACTACGTCCTGAGTGAGATTGAGAAGAACGACGTG
GTATTCTCCATGGACCAGACAGAGTCCCCGTTCAAGCCGCACCTGATGGCCATGAATAGCATCTTTGACAACAGTGGCAAGGTG
CCTGTGTCGGAGAAGAGCAACTTCCTGTTCACCAAGCTGAAGGAGGAACCTGAGGAGCTGGCCCAGCTGGCCCCCACCGCGG
GAGACACCATCATTTCTCTGGATTTCGGAAACCCGACCTTCGAGGAGTCCTCAGCCTATGGCAAGGCCATCC

(1400) 2865-3’

B

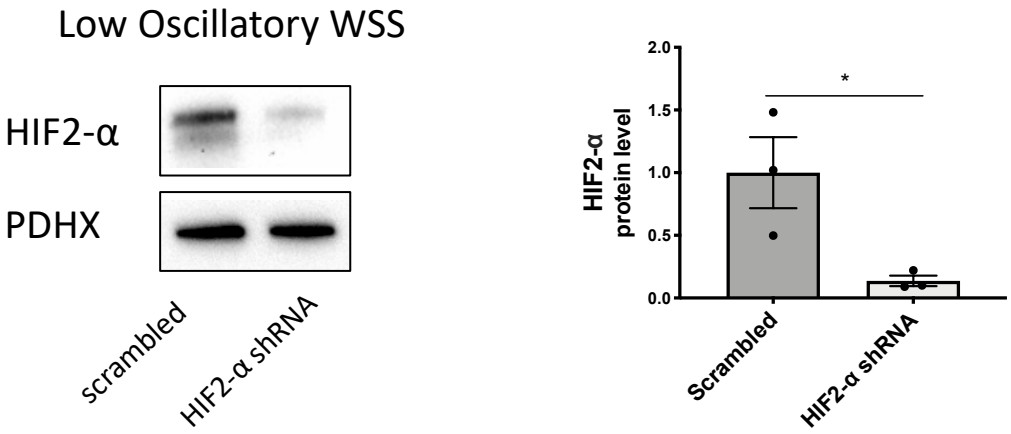

C

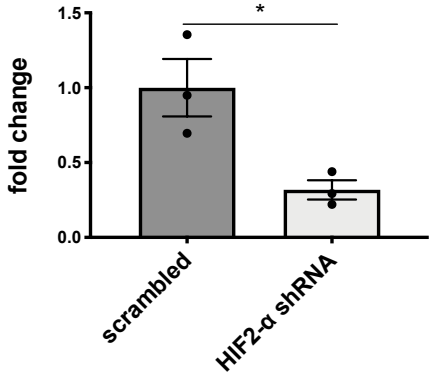

Figure 5. 3 Lentivirus-mediated HIF2-α knock-down in sheared PAECs.

HIF2-α (NM_001097420.1) sequence was interrogated for shRNA alignment. A) shRNA pool was composed of three sequences: shRNA sequence 1 (yellow), shRNA sequence 2 (red), and shRNA sequence 3 (green). PAECs from aortic arches were exposed to LOSS using ibidi pump system and were treated with non-targeting shRNA (scrambled) or HIF2-α shRNA pool at 30 MOI. Protein levels were assessed by western blotting. B) representative blot is shown, left panel, and protein quantification relative to the loading control PDHX, right panel, N=3. RNA expression level was assessed using RT-qPCR. C) Quantification of HIF2-α mRNA content, N=3. Mean levels +/- SEM are shown. Differences between means were analysed using a paired T-test. *$p<0.05$.

Transcriptional profile of HIF2-α knock-down porcine aortic endothelial cells under low WSS.

To assess the function of HIF2-α in endothelial cells exposed to low WSS, the transcriptional profiles of lentiviral treated cells transduced with HIF2-α shRNA pool or scrambled shRNA sequences were analysed using microarray analysis. PAECs from three independent donors were harvested 72h post-infection, their RNA was isolated and then hybridised against PorGene1_0 array (Affymetrix). Data were then analysed using Transcriptome Analysis Console (Affymetrix) and with the help of Dr. Mark Dunning from the Bionformatics Core Facility (Sheffield). The microarray contained more than 23000 probes, however only 126 genes were significantly different when using an unsupervised analysis with fold change threshold of 1.2 and p-value threshold of 0.05 (Figure 5.4A). Of these 126 genes, 53 gene were discontinued resulting at the end in 41 genes up-regulated and 31 genes down-regulated (tables 17 and 18).

Amongst all, the most up-regulated genes (log2FC ≥ 2) were: *DEXI*, *PSAT1* and *LOC100513296* and the down-regulated genes (log2FC ≤ -2) were: *LOC100518322* and *TRIM44*. Genes strongly significant (p-value ≤ 0.01) between the two condition were: *SLC38A1*, *LOC100152378, LOC100513296* and *PSAT1* for the up-regulated and *TCEAL2, TUSC5, LOC100513955; LOC100737189* for the down-regulated.

The differentially expressed genes (DEG) obtained from the analysis were interrogated on the molecular signature database (MSigDB) tool of the gene set enrichment analysis (GSEA) website (https://www.gsea-msigdb.org). The enriched pathway emerged from this analysis were ranked by p-value using a logarithmic scale (Figure 5.4B). The pathway enrichment analysis revealed that HIF2-α regulated genes involved in epithelial to mesenchymal transition, mTORC1-signalling pathway, cell division and KRAS pathway among others. Despite not being clustered as an enriched pathway from the GSEA analysis, several metabolic genes were differentially regulated between the scrambled and HIF2-α shRNA samples. As an example, sulfatase 1 (SULF1) , the glycosyltransferase 8 domain containing 1 (GLT8D1) and the NADH dehydrogenase (ubiquinone) 1 alpha subcomplex, 8 (NDUFA8) were down-regulated by HIF2-α knockdown, whereas the thiosulfate sulfotransferase like domain containing 3 (TSTD3) and the solute carrier family 38 member 1 (SLC38A1) genes were upregulated by HIF2-α knockdown. Of these metabolic genes, TSTD3, GLT8D1, NDUFA8 and SLC38A1 were mitochondrial genes and/or involved in mitochondrial metabolism and mitophagy.

In conclusion, this microarray analysis suggested a role for HIF2-α in endothelial cells proliferation, differentiation and metabolism.

A

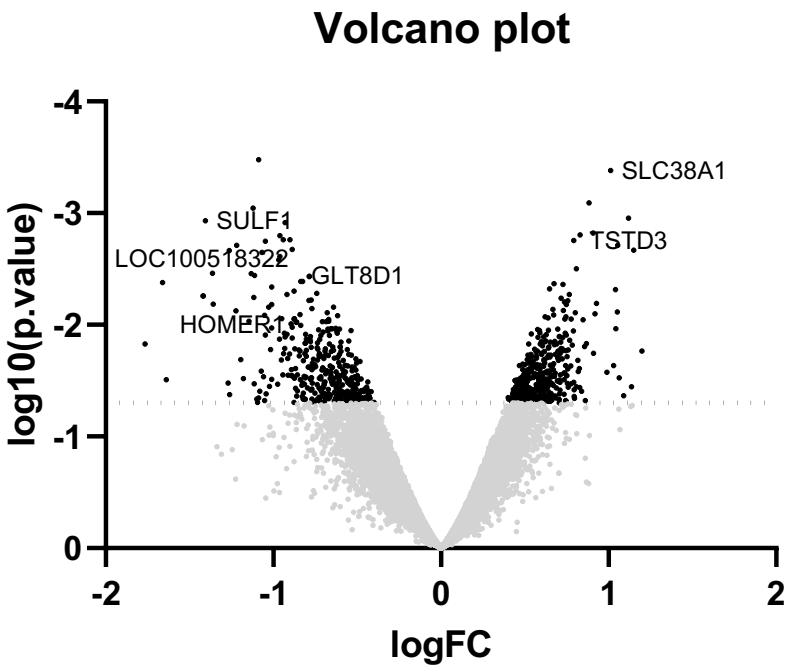

B

Pathway	Genes	-log(p-value)
Genes defining epithelial-mesenchymal transition, as in wound healing, fibrosis and metastasis.	13	5.34E+00
Genes up-regulated in response to IFNG.	10	3.32E+00
Genes up-regulated through activation of mTORC1 complex.	10	3.32E+00
Genes involved in the G2/M checkpoint, as in progression through the cell division cycle.	9	2.73E+00
Genes up-regulated by KRAS activation.	9	2.73E+00
Genes up-regulated in response to alpha interferon proteins.	6	2.65E+00
Genes down-regulated by KRAS activation.	8	2.18E+00
A subgroup of genes regulated by MYC - version 1 (v1).	8	2.18E+00
Genes involved in development of skeletal muscle (myogenesis).	8	2.18E+00
A subgroup of genes regulated by MYC - version 2 (v2).	4	2.08E+00

Figure 5. 4 HIF2-α regulates genes involved in proliferation, differentiation and metabolism.

PAECs from aortic arches were exposed to LOSS using ibidi pump system and were treated with non-targeting shRNA (Scrambled) or HIF2-α shRNA pool at 30 MOI. RNA was then extracted from three independent donors and hybridised against a microarray probes PorGene1_0 (Affymetrix). A) Volcano plot generated by unsupervised analysis using FC 1.2 and p-value 0.05. Differentially regulated genes (DEG) were identified as black dots. Genes identified in the volcano plot: Sulfatase 1 (SULF1), Centrosomal p57 (LOC100518322), Homer Scaffold Protein 1 (HOMER1), Glycosyltransferase 8 Domain Containing 1 (GLT8D1), Thiosulfate Sulfotransferase Like Domain Containing 3 (TSTD3), Solute Carrier Family 38 Member 1 (SLC38A1). B) Gene ontology analysis of enriched pathway targeted by the DEG of the microarray and ranked as –log10 scale of the p-value.

Table 17. Upregulated genes in the microarray with log2FC>1.5.

Probe ID	Log2FC	P-val	Gene Symbol	Description
15269169	2.47	0.0398	DEXI	Dexi homolog (mouse); dexamethasone-induced protein
15189350	2.37	0.0093	PSAT1	phosphoserine aminotransferase 1
15323178	2.24	0.0042	LOC100513296	transmembrane protease serine 11F
15286868	1.94	0.0031	LOC100152378	volume-regulated anion channel subunit LRRC8D
15294565	1.83	0.0024	SLC38A1	solute carrier family 38, member 1
15184635	1.82	0.0188	TSTD3	thiosulfate sulfurtransferase (rhodanese)-like domain containing 3
15202050	1.78	0.019	SUSD4	sushi domain containing 4
15275176	1.77	0.0323	MALL	mal, T-cell differentiation protein-like
15322017	1.74	0.0277	PAQR3	progestin and adipoQ receptor family member III
15201008	1.72	0.0335	LOC100515159	probable G-protein coupled receptor 158
15329787	1.71	0.0438	LOC100517485	calcineurin-binding protein cabin-1-like
15214373	1.69	0.0308	LOC100625836	heparan sulfate glucosamine 3-O-sulfotransferase 3A1
15331112	1.68	0.0258	ATP2B4	ATPase, Ca++ transporting, plasma membrane 4
15288219	1.67	0.0455	DGKA	diacylglycerol kinase, alpha 80kDa;
15328992	1.67	0.0319	LOC100511274	olfactory receptor 51I2; olfactory receptor 51I2-like
15225453	1.65	0.0239	SLC5A1	solute carrier family 5 (sodium/glucose cotransporter), member 1
15298948	1.63	0.0149	PQLC2	PQ loop repeat containing 2
15328896	1.63	0.0425	TIMM10B	translocase of inner mitochondrial membrane 10 homolog B (yeast)
15227467	1.61	0.0244	FAS	Fas cell surface death receptor
15305859	1.61	0.0494	TWSG1	twisted gastrulation BMP signaling modulator 1
15267414	1.6	0.0346	LOC100626192	sodium-dependent proline transporter-like
15273595	1.58	0.0434	CHCHD2	coiled-coil-helix-coiled-coil-helix domain containing 2
15258720	1.58	0.0367	GPR150	G protein-coupled receptor 150
15261871	1.58	0.0364	LOC106504186	olfactory receptor 5B12-like
15299269	1.58	0.0364	PIGV	phosphatidylinositol glycan anchor biosynthesis, class V;
15188926	1.57	0.0377	ERMP1	endoplasmic reticulum metallopeptidase 1
15308830	1.57	0.0421	PSMB9	proteasome subunit beta 9; proteasome subunit beta type-9
15223040	1.57	0.036	SYK	spleen tyrosine kinase; tyrosine-protein kinase SYK-like
15326519	1.56	0.0378	SLC37A2	solute carrier family 37 (glucose-6-phosphate transporter), member 2

15337705	1.55	0.0176	AMMECR1	Alport syndrome, mental retardation, midface hypoplasia and elliptocytosis chromosomal region gene 1
15214297	1.53	0.0419	MYH1	myosin, heavy chain 1, skeletal muscle, adult
15186551	1.51	0.05	PPIP5K1	diphosphoinositol pentakisphosphate kinase 1

Table 18. Downregulated genes in the microarray with log2FC>-1.5

Probe ID	Lof2FC	**P-val**	**Gene Symbol**	**Description**
15329997	-2.58	0.0201	LOC100518322	centrosomal protein of 57 kDa-like
15262423	-2.48	0.0407	TRIM44	tripartite motif containing 44
15302882	-1.98	0.0429	MIA	melanoma inhibitory activity
15334517	-1.96	0.0093	TCEAL2	transcription elongation factor A (SII)-like 2
15213132	-1.96	0.0084	TUSC5	tumor suppressor candidate 5
15237027	-1.94	0.0069	LOC100513955	asparagine synthetase domain-containing protein 1
15298041	-1.78	0.0393	LOC100516741	NACHT, LRR and PYD domains-containing protein 7
15242037	-1.77	0.0458	LOC106506441	olfactory receptor 12-like
15245366	-1.76	0.0107	UBE2QL1	ubiquitin-conjugating enzyme E2Q family-like 1
15310081	-1.76	0.0235	VEGFA	vascular endothelial growth factor A
15310586	-1.74	0.0318	CPEB1; LOC100622904	cytoplasmic polyadenylation element binding protein 1; cytoplasmic polyadenylation element-binding protein 1-like
15219836	-1.74	0.0467	IP6K2	inositol hexakisphosphate kinase 2
15307509	-1.69	0.0359	TUBB2B	tubulin, beta 2B class IIb
15335207	-1.69	0.0143	ZIC3	Zic family member 3
15319568	-1.68	0.034	LOC100155405	olfactory receptor 4K1
15275469	-1.66	0.0243	RPL31	ribosomal protein L31; 60S ribosomal protein L31
15198746	-1.64	0.03	NDUFA8	NADH dehydrogenase (ubiquinone) 1 alpha subcomplex, 8, 19kDa
15307109	-1.57	0.0284	LOC100517289	E3 ubiquitin-protein ligase RNF220
15233250	-1.56	0.0117	ALOX5	arachidonate 5-lipoxygenase
15208128	-1.56	0.0238	LOC100514982	leucine-rich repeat-containing protein 37A2-like
15324262	-1.56	0.0424	TACR3	tachykinin receptor 3
15335584	-1.53	0.0414	CMC4; MTCP1	C-x(9)-C motif containing 4
15302610	-1.52	0.0256	LOC102164889	zinc finger protein 569
15207151	-1.51	0.0178	DUSP3	dual specificity phosphatase 3

HIF2-α controls endothelial mitochondrial content.

Based on the microarray data, I hypothesized that HIF2-α regulates mitochondrial function. To assess the effect of HIF2-α knock-down on mitochondria and endothelial cells metabolism, PAECs were treated with lentiviral shRNA targeting HIF2-α or a non-targeting sequence (scrambled) and then exposed to shear stress for 72h using an orbital shaker. Lentiviral knock-down was confirmed by RT-qPCR, in samples isolated from site of high WSS and low WSS (Figure 5.5).

To investigate mitochondrial content and organisation, cells were treated with Mitotracker CMXRos Red 579/599 dye. Mitotracker dye enters healthy living cells with intact membrane potential and it is retained after paraformaldehyde fixation. Confocal images suggested that HIF2-α silencing potentially increased Mitotracker fluorescence levels at low WSS. However, quantification of Mitotracker staining showed that the differences did not reach significance. Regions exposed to high WSS were insensitive to HIF2-α silencing (Figures 5.6B).

Variation in mitochondrial staining may reflect variation in metabolic fuel availability, therefore, I also investigated the effect of HIF2-α silencing on lipid droplets formation. Quantification of lipid droplets identified by BODIPY fluorescence revealed that lipid droplets formation, in absence of external stimuli, was independent of HIF2-α activity (Figure 5.6C).

Nevertheless, MFI analysis not fully represent the mitochondria morphology and functionality. Therefore, a morphological analysis of mitochondria was carried out.

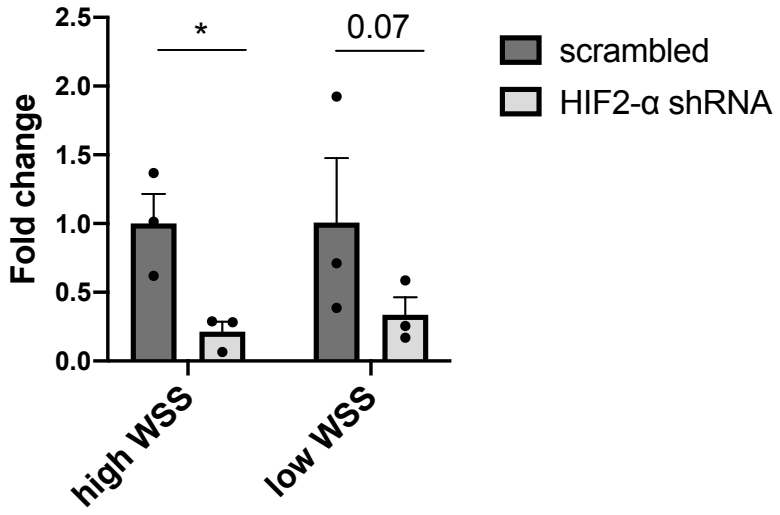

Figure 5. 5 Lentiviral HIF2-α shRNA pool caused knock-down of HIF2-α in PAECs exposed to high WSS.

PAECs were transduced with lentiviral HIF2-α shRNA pool or lentiviral non-targeting control (scrambled) at the MOI of 30. PAECs were exposed to shear stress using an orbital shaker for 72h. RNA was extracted from the periphery and the centre of the well, regions exposed to high WSS and low WSS respectively. HIF2-α expression levels were analysed using RT-qPCR. HIF2-α mRNA was normalised against a housekeeping control gene (B2M) and represented using the $2^{-\Delta\Delta Ct}$ method. Mean levels +/- SEM are shown. Statistical analysis was performed using the $2^{-\Delta Ct}$ (raw data) values. Differences between means were analysed using two-way ANOVA with Sidak's multiple comparison test. * $p<0.05$.

A

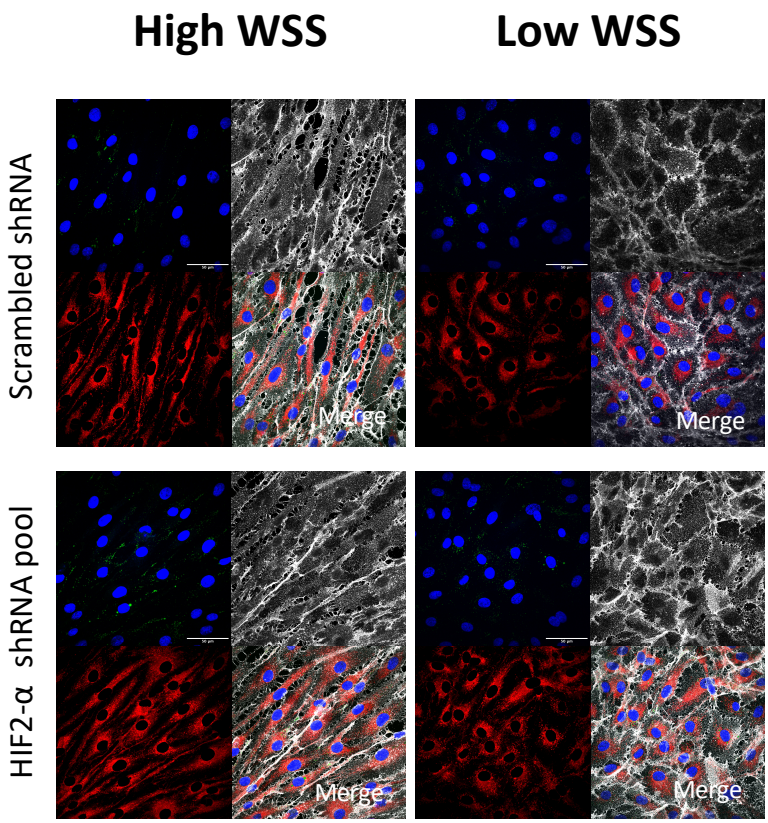

Mitotracker, BODIPY 493/503, LCI-4, DAPI

B

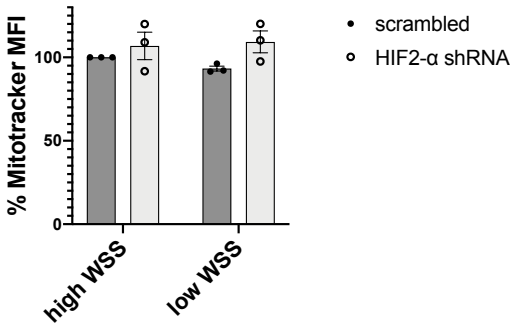

C

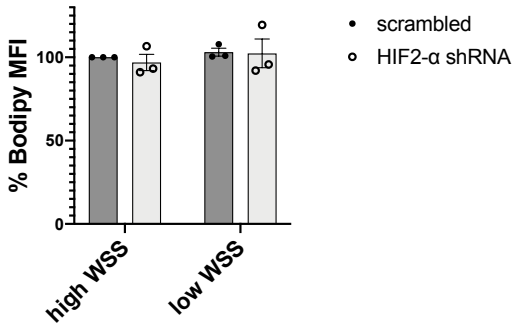

Figure 5. 6 HIF2-α did not regulate mitochondrial staining.

PAECs were transduced with lentiviral HIF2-α shRNA pool or lentiviral non-targeting control (scrambled shRNA) at the MOI of 30. PAECs were exposed to shear stress using orbital shaker for 72h. Mitochondria were identified by Mitotracker CMXRos probe (red). PAECs were further stained for PECAM-1 (LCI-4) endothelial marker (white), BODIPY 493/503 (lipid droplets, green) and DAPI (nuclei, blue). Representative images of PAECs exposed to high WSS and to low WSS are shown in A. Mitotracker and Bodipy levels were quantified using ImageJ software. B) percentage of Mitotracker MFI in HIF2-α shRNA samples relative to Mitotracker MFI of scrambled shRNA sample. C) percentage of Bodipy MFI in HIF2-α shRNA samples relative to Mitotracker MFI of scrambled shRNA sample. Mean levels +/- SEM are shown. Difference between means were analysing using two-way ANOVA with Sidak's multiple comparison test.

Mitochondria morphology analysis

To further investigate the effect of HIF2-α in endothelial mitochondrial content and organisation I initially investigated the average number of mitochondria in a cell at sites of high and low WSS. The analysis revealed that at the periphery of the well, a site of high WSS, the mitochondrial count of PAECs was unaffected by HIF2-α shRNA treatment (Figure 5.7A). In contrast, lentiviral HIF2-α shRNA treatment caused an increase in number of mitochondrial particles per cell under low WSS condition (Figure 5.7).

To understand whether the increased number of mitochondrial particles was associated with changes in morphology and organization of the mitochondria, a series of geometrical features were investigated. Specifically, analysis of perimeter, area, percentage of cytosol occupied by the mitochondria and mitochondrial elongation was carried out. The analysis revealed that at both site of high and low WSS, HIF2-α shRNA treatment did not alter the perimeter of the mitochondria (Figure 5.8A). Analysis of the area also revealed an absence of significant differences between groups (Figure 5.8B). Furthermore, the percentage of cytoplasmic area occupied by the mitochondria within a cells was also investigated. The analysis did not show any variation caused by HIF2-α shRNA treatment (Figure 5.8C). To further investigate morphology of the mitochondria, circularity was also considered. Circularity was presented as its inverse, thus, it was interpreted as an index of mitochondrial elongation. Analysis of the circularity showed no differences between groups at either sites of high or low WSS (Figure 5.8D).

To further understand the interaction between mitochondria an analysis of area/perimeter ratio was carried out. The ratio between area and perimeter was considered as an index of mitochondrial interconnectivity. Lentiviral HIF2-α treatment did not alter the interaction between mitochondria at either sites of high or low WSS (Figure 5.9A).

To investigate further morphology and spatial distribution of mitochondria, solidity and angle were analysed. Simplistically, solidity is a measurement of how much a mitochondria has a compact shape and usually solidity correlates with the tendency of mitochondria to undergo fusion (Westrate *et al.*, 2014). In this analysis, at both site of high and low WSS, the solidity parameter did not varies between conditions (Figure 5.9B). The analysis further considered the angle between minor and major axes of the mitochondria. Analysis of angle at high or low

shear stress showed that variations between HIF2-α KD cells and scrambled cells were not significant (Figure 5.9C).

Mitochondria swelling was also assessed. Analysis of swelling was performed by normalising the interconnectivity index (area/perimeter) by the minor axis. The analysis revealed not significant differences of mitochondrial volume under any condition investigated (Figure 5.9D).

In summary, morphological analysis of mitochondria showed that HIF2-α was affecting the number of mitochondria per cell at site of low WSS. Despite the extensive analysis, a clear pattern of morphological variation was not identified. Thus, suggesting that mitochondria were not changing their spatial distribution in response to shear stress or HIF2-α knock-down.

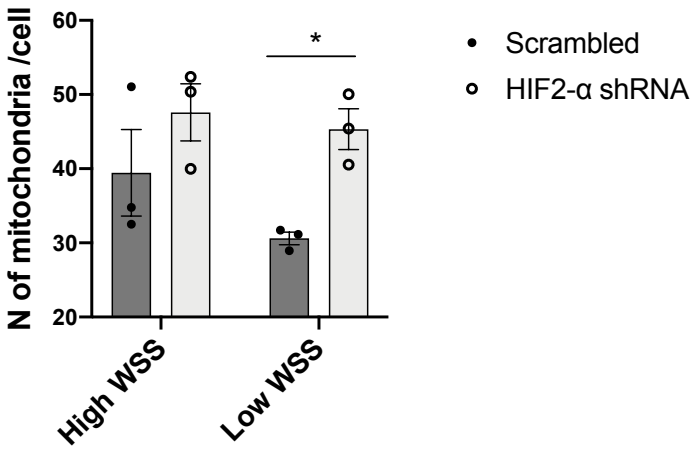

Figure 5. 7 HIF2-α regulates mitochondrial mass at site of low WSS.

PAECs were transduced with lentiviral HIF2-α shRNA pool (HIF2-α shRNA) or lentiviral non-targeting control (scrambled shRNA) at the MOI of 30 and exposed to shear stress using orbital shaker for 72h. Mitochondria were identified by Mitotracker CMXRos probe. Mitochondria morphology was studied using ImageJ software. 40-50 cells per condition were analysed for each experiment, N=3. Data represents the average number of mitochondria per cell. Difference between means are analysed using a two-way ANOVA test with Sidak's multiple comparison test. *$p<0.05$

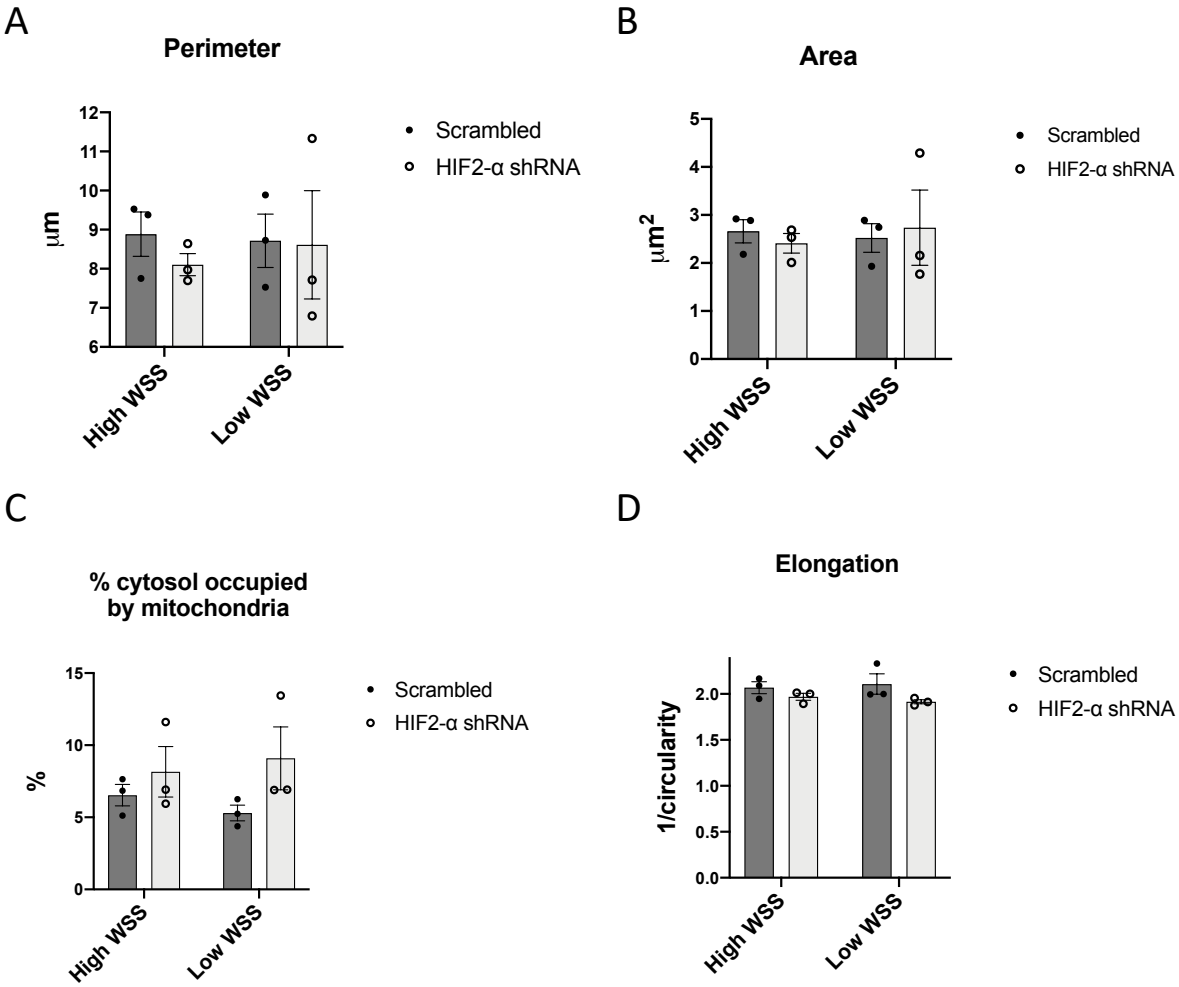

Figure 5. 8 HIF2-α did not regulate morphology of mitochondria.

PAECs were transduced with lentiviral HIF2-α shRNA pool (HIF2-α shRNA) or lentiviral non-targeting control (scrambled shRNA) at the MOI of 30. PAECs were exposed to shear stress using an orbital shaker for 72h. Mitochondria were identified by Mitotracker CMXRos probe. Mitochondria morphology was studied using ImageJ software. 40-50 cells per condition were analysed for each experiment, N=3. A) Perimeter of mitochondria. B) Area of the mitochondria. C) Percentage of cytosol occupied by the mitochondria in a given cell. D) Mitochondria elongation, calculated as 1/circularity value. Geometric mean +/- SEM are shown. Difference between means are analysed using a two-way ANOVA test with Sidak's multiple comparison test.

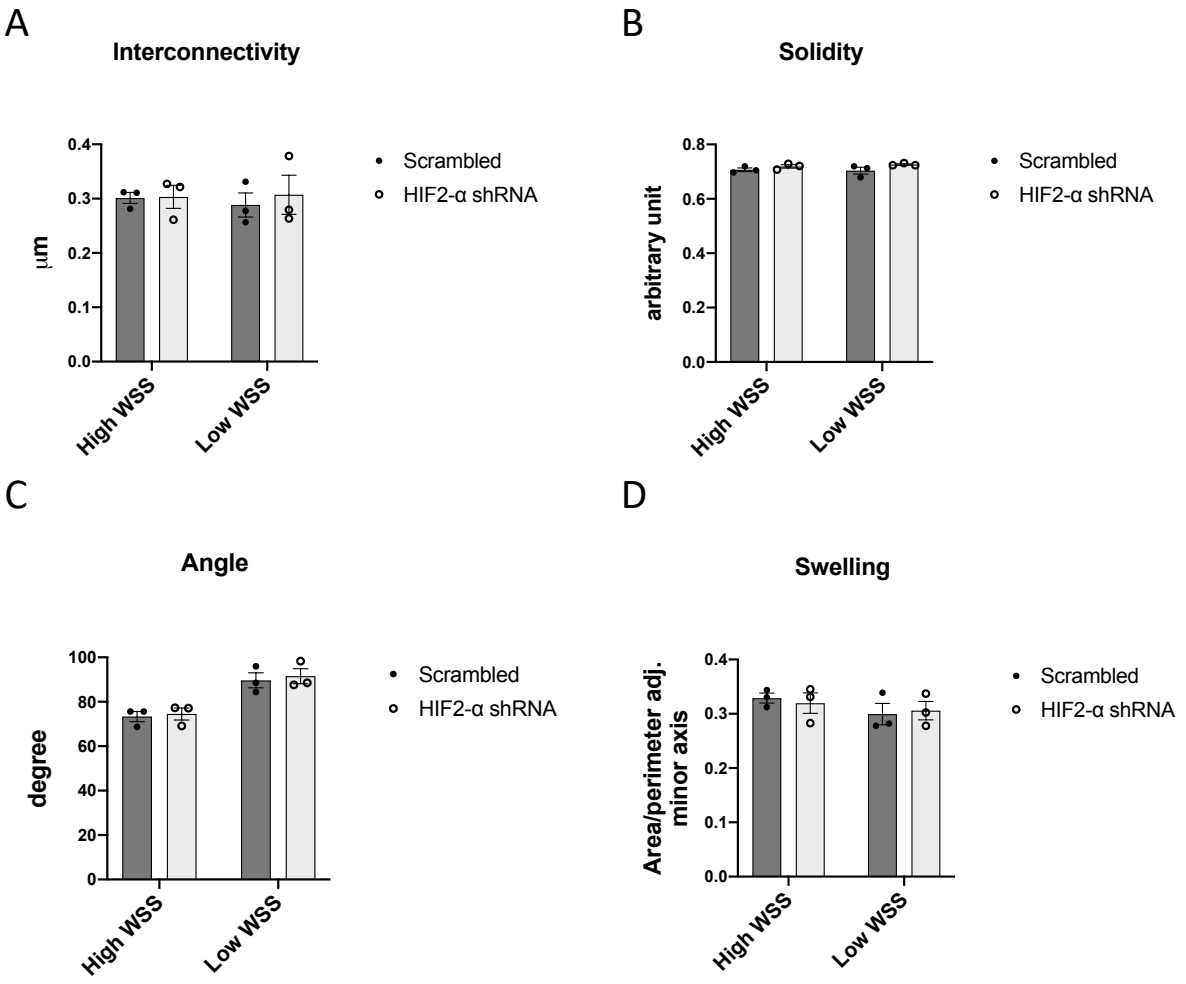

Figure 5. 9 HIF2-α did not regulate interconnectivity of mitochondria.

PAECs were transduced with lentiviral HIF2-α shRNA pool (HIF2-α shRNA) or lentiviral non-targeting control (scrambled) at the MOI of 30. PAECs were exposed to shear stress using orbital shaker for 72h. Mitochondria were identified by Mitotracker CMXRos probe. Mitochondria morphology was studied using ImageJ software. 40-50 cells per condition were analysed for each experiment, N=3. A) Interconnectivity calculated as area/perimeter. B) Solidity. C) Mitochondria angle. D) Swelling of mitochondria calculated as the adjusted value of interconnectivity to the minor axis of the mitochondria. Geometric mean +/- SEM are shown. Difference between means are analysed using a two-way ANOVA test with Sidak's multiple comparison test.

HIF2-α promotes endothelial cells proliferation

HIF2-α promotes aortic endothelial cell proliferation via a mechanism dependent of fatty acids.

To understand the influence of HIF2-α on proliferation in a context of lipid overload, PAECs were treated with HIF2-α lentiviral siRNA in the presence or absence of 250 μM oleic acid and exposed to shear stress for 24h using the orbital shaker system. Then, PAECs were analysed for proliferation by staining for Ki67 protein. Two regions were considered: the periphery and the centre of the well, exposed to high WSS and low WSS respectively. Representative images are shown in (Figure 5.10A).

Analysis of the Ki67 marker revealed that HIF2-α knock-down endothelial cells presented reduced proliferation rate at the low WSS site. In contrast, level of proliferation at the periphery were unaltered by knockdown of HIF2-α (Figure 5.10B). Interestingly, in presence of fatty acid overload the influence of HIF2-α on endothelial cells proliferation was partially increased at site of low WSS, while endothelial cells at site of high WSS remained unaffected by the oleic acid treatment (Figure 5.10C).

In conclusion, HIF2-α promote ECs proliferation and exposure of endothelial cells to an excess of fatty acid did not significantly affect proliferation.

A

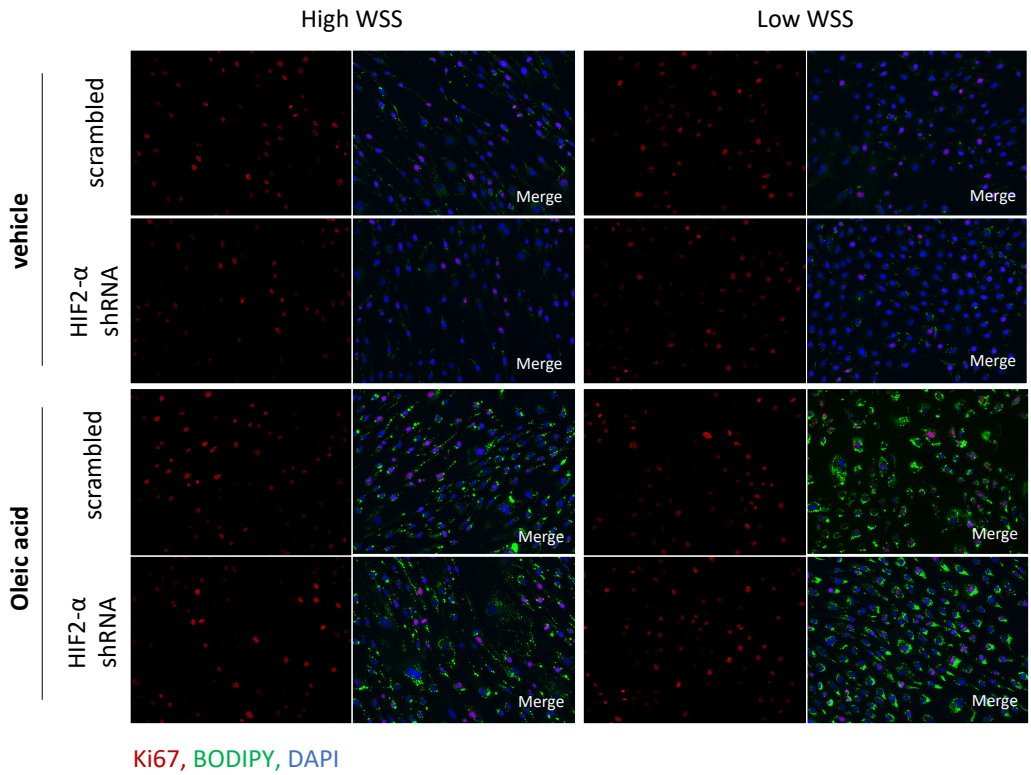
High WSS
Low WSS
vehicle
Oleic acid
scrambled
HIF2-α shRNA
Merge
Ki67, BODIPY, DAPI

B

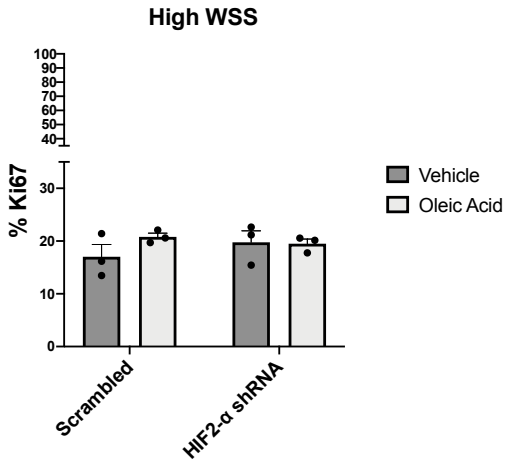
High WSS
% Ki67
Vehicle
Oleic Acid
Scrambled
HIF2-α shRNA

C

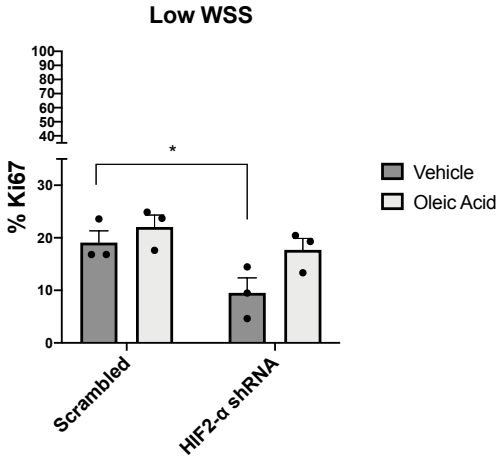
Low WSS
% Ki67
*
Vehicle
Oleic Acid
Scrambled
HIF2-α shRNA

Figure 5. 10 HIF2-α promotes aortic endothelial cell proliferation and this is partially rescued by oleic acid.

PAECs were transduced with lentiviral HIF2-α shRNA pool (HIF2-α shRNA) or lentiviral non-targeting control (scrambled) at the MOI of 30. PAECs were treated with 250μM oleic acid or vehicle control and exposed to shear stress using an orbital shaker for 24h. Proliferative level was assessed by Ki67 staining (red), lipid droplets were identified by BODIPY 499/503 (green) staining and nuclei were delineated by DAPI counterstaining (blue). Representative images are shown on panel A. Quantification of Ki67 positive cells was performed using ImageJ software at the periphery and the centre of the well, sites of high WSS and low WSS respectively. B) Quantification of percentage of Ki67 positive cells at the periphery. C) Quantification of percentage of Ki67 positive cells at the centre. Mean levels +/- SEM are shown. Difference between means were analysing using two-way ANOVA with Sidak's multiple comparison test. * $p<0.05$

HIF2-α protects the endothelium from senescence

In order to investigate further the role of HIF2-α in regulating endothelial cells proliferation, PAECs were also morphologically analysed for senescence.

Endothelial cells that undergo senescence reduced their proliferative rate, enlarge their size and increase the number of nuclei per cells (Boisen *et al.*, 2010). A study of senescence in PAECs exposed to 24h shear stress in presence or absence of oleic acid was carried out by analysing bright field images and DAPI counterstain of nuclei. Thereafter, images were analysed to identify enlarged and multi-nucleated cells (Figure 5.11A).

The percentage of senescent cells at site of high WSS was not affected by oleic acid treatment or HIF2-α silencing when compared to the scrambled control or vehicle treated samples (Figure 5.11B). On the contrary, senescence in PAECs exposed to low WSS was exacerbated by lentiviral HIF2-α KD treatment when compared to their scrambled controls in the absence of oleic acid. Whereas, treatment with oleic acid, even though statistically not-significant, partially recover endothelial cells senescence in HIF2-α knock-down endothelial cell (Figure 5.11C).

In conclusion, HIF2-α limits endothelial cells senescence under low WSS. However, it was not possible to conclusively identify whether oleic acid may have a role on regulating endothelial cells senescence in either presence of HIF2-α or in its absence.

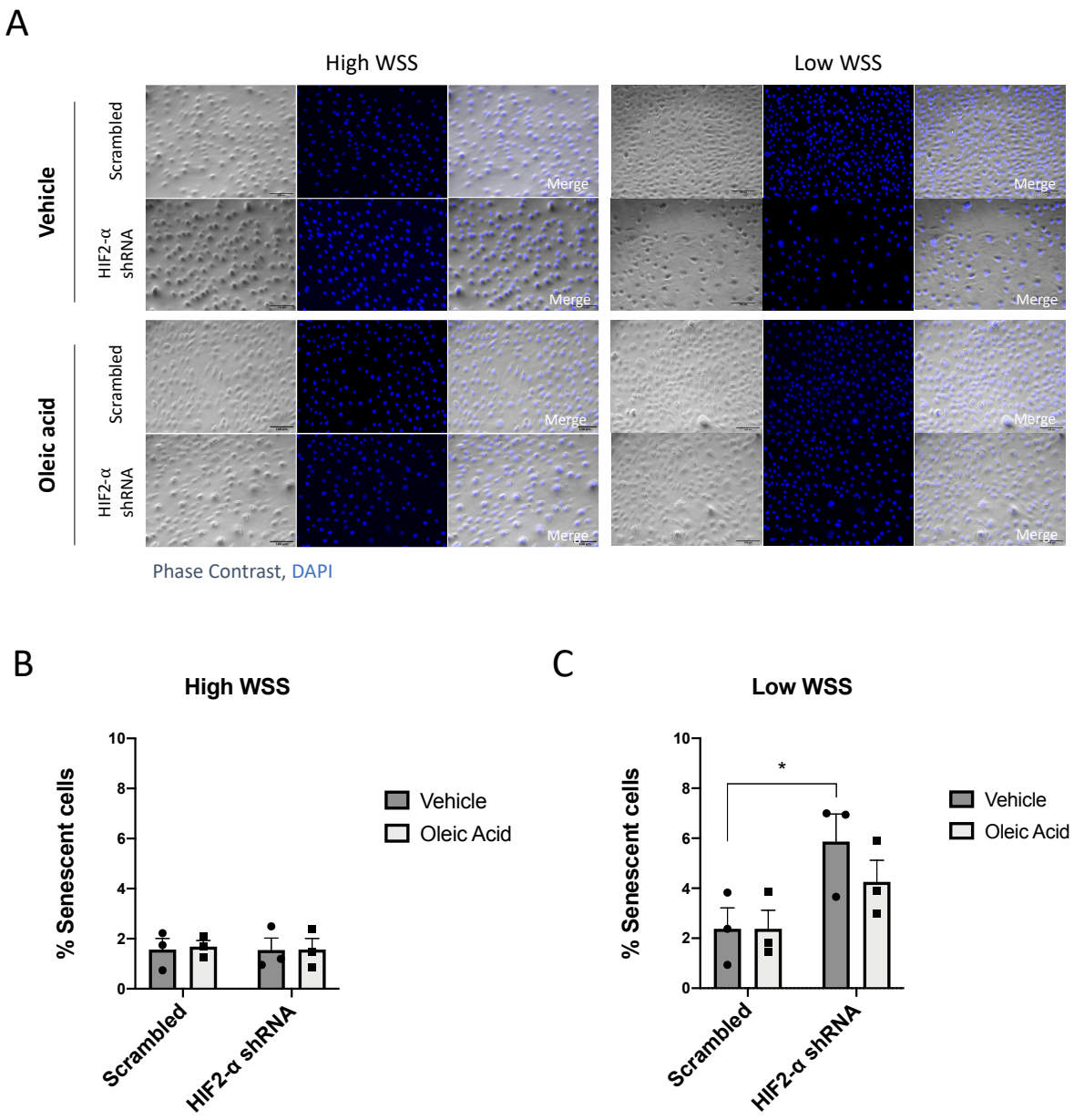

Figure 5. 11 HIF2-α reduced aortic endothelial cells senescence.

PAECs were transduced with lentiviral HIF2-α shRNA pool (HIF2-α shRNA) or lentiviral non-targeting control (scrambled) at the MOI of 30. PAECs were treated with 250µM oleic acid or vehicle control and exposed to shear stress using an orbital shaker for 24h. Senescent cells were identified by comparing phase contrast and nuclear staining using DAPI (blue). Representative images are shown on panel A, scale bar 100µm. Senescent cells were analysed using ImageJ software. Multinucleated and enlarged cells were counted as senescence. B) percentage of senescent cells at the periphery, area of high WSS. C, percentage of senescent cells at the centre, area of low WSS. Difference between means were analysing using two-way ANOVA with Sidak's multiple comparison test. * $p<0.05$

Loss of endothelial HIF2-α causes DNA damage

After showing that HIF2-α promotes proliferation while preventing senescence, I investigated a marker for DNA damage. In presence of DNA breaks, the histone H2AX becomes phosphorylated at Serine 139; this variant is also known as γ-H2AX. Increase numbers of γ-H2AX expressing foci were associated with aging in cultured cells (Sedelnikova *et al.*, 2004). Therefore, lentiviral-treated PAECs were exposed to high and low WSS using the orbital shaker system for 72h prior to quantification of γ-H2AX by immunoflurescence. Representative images are shown (Figure 5.12A).

Loss of HIF2-α did not regulate the expression of γ-H2AX at site of high WSS (Figure 5.12B,left panel). On the contrary, in agreement with the morphological changes observed at site of low WSS, PAECs at the centre of the well increased γ-H2AX expression in absence of HIF2-α (Figure 5.12B, right panel).

Thus, HIF2-α protects endothelial cells from DNA damage and cellular senescence at sites exposed to atheroprone shear stress.

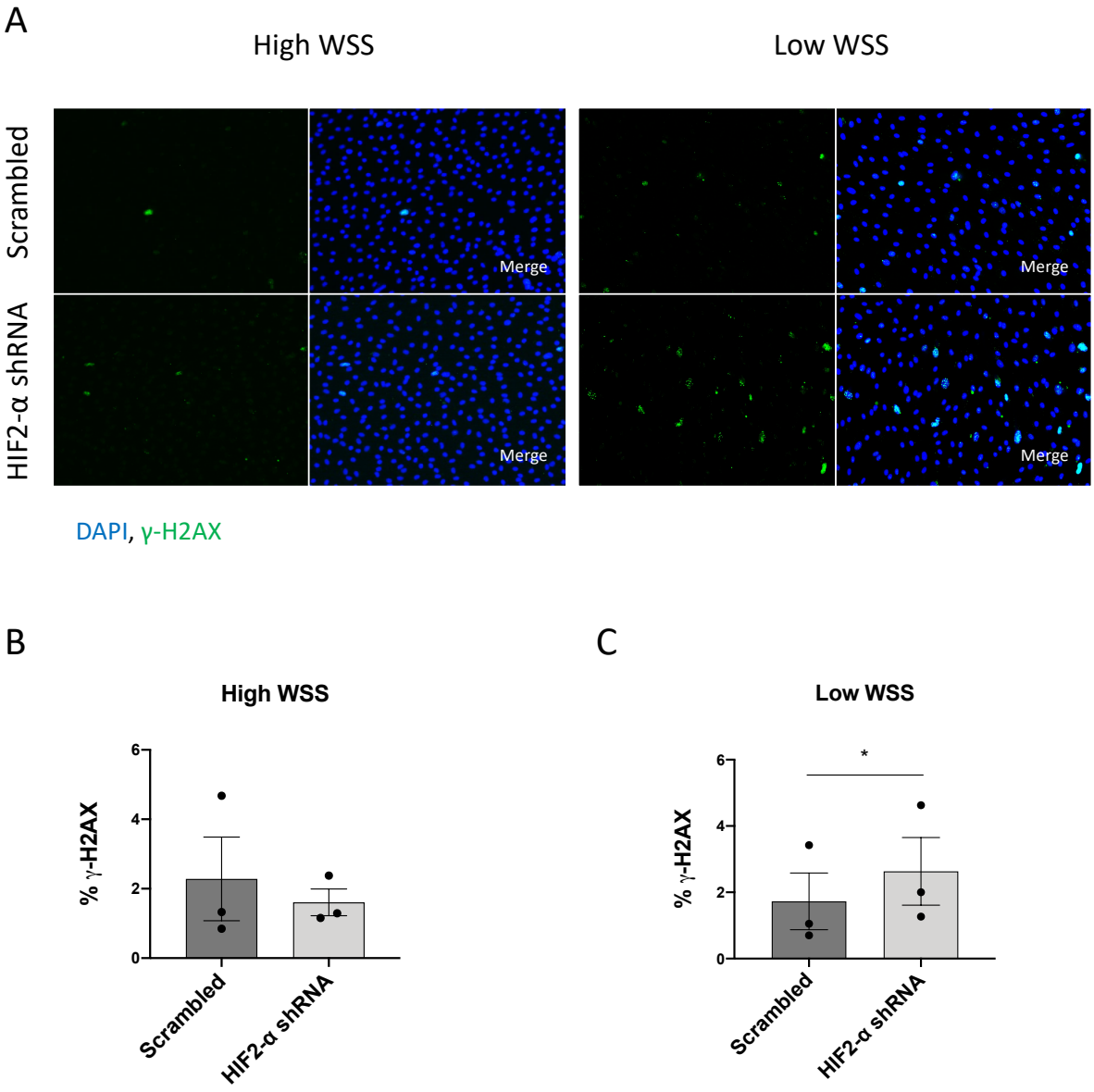

Figure 5. 12 HIF2-α protect endothelial cells from DNA damage.

PAECs were transduced with lentiviral HIF2-α shRNA pool (HIF2-α shRNA) or lentiviral non-targeting control (scrambled) at the MOI of 30. Transduced PAECs were then exposed to shear stress using orbital shaker for 72h. To identify cells with DNA damage, fixed well were stained for γ-H2AX conjugated to a secondary antibody AF488, while nuclei were counterstained with DAPI. Representative images are shown on panel A. γ-H2AX positive cells were analysed using ImageJ software. B) percentage of senescent cells at the periphery, area of high WSS. C, percentage of senescent cells at the centre, area of low WSS. Difference between means were analysing a two-tails paired T-test. * $p<0.05$

HIF2-α protects from atherosclerosis development

To determine the role of HIF2-α in endothelial cells and its contribution to atherosclerosis, responses of an endothelial specific HIF2-α null mice to a proatherogenic diet were investigated. To obtain deletion of HIF2-α from endothelial cells, mice carrying the loxP sites flanking the exon 2 of HIF2-α gene were crossed with mice with a tamoxifen-inducible $CreER^{T2}$ under the control of VE-Cadherin (Cdh5) promoter. Thus, injection with tamoxifen of mice containing HIF2-α flox/flox and Chd5-$CreER^{T2}$ sequences caused deletion of HIF2-α gene and protein in vascular endothelial cells.

When mice were 9 week old, a single PCSK9 injection was performed to achieve hypercholesterolaemia. Subsequently, mice were challenged with HFD for the following 8 weeks from the injection. Mice were then sacrificed and their blood was investigated for cholesterol and triglycerides levels. At termination of the experiments, HIF2-α^{EC-KO} mice and experimental controls were morphologically indistinguishable with no apparent differences in appearance (Figure 5.13A, left panel) or in body weight (Figure 5.13A,right panel). Furthermore, cholesterol levels were comparable between the two genotypes (Figure 5.13B). The levels of HDL and LDL were then analysed. While the HDL level was not-significantly higher in the HIF2-α^{EC-KO} mice, the LDL subfraction was unaltered (Figure 14C). Furthermore, analysis of the triglycerides levels revealed no differences between the HIF2-α^{EC-KO} mice and the experimental controls (Figure 5.13C).

Plaques were analysed using Oil Red O staining in aortae of HIF2-α^{EC-KO} mice and experimental controls. Plaque analysis revealed that aortae from HIF2-α^{EC-KO} mice displayed increased plaque area when compared to their experimental controls. Plaques developed at site of low WSS at the inner curvature of the aortic arch, at the bifurcation with the carotid arteries and also at the branching points of the intercostal arteries (also known as ostiae), (Figure 5.14A). Experimental control mice (considered as wild type) also developed plaque as predicted by the use of AAV-PCSK9.

In conclusion, this result indicates that endothelial HIF2-α is a protective transcription factor for plaque development.

A

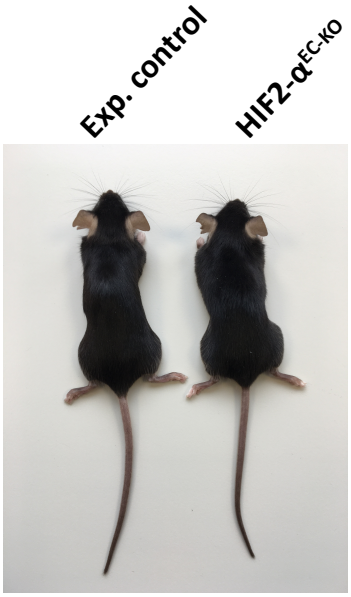
Exp. control
HIF2-α EC-KO

B

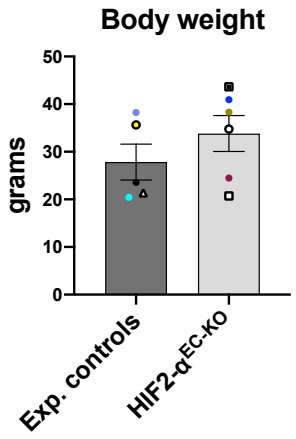
Body weight
grams
50
40
30
20
10
0
Exp. controls
HIF2-α EC-KO

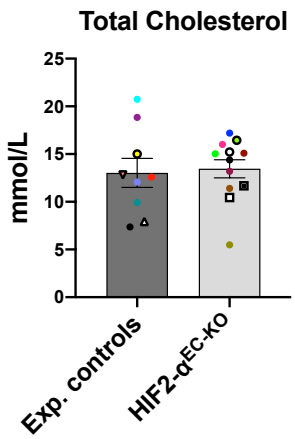
Total Cholesterol
mmol/L
25
20
15
10
5
0
Exp. controls
HIF2-α EC-KO

C

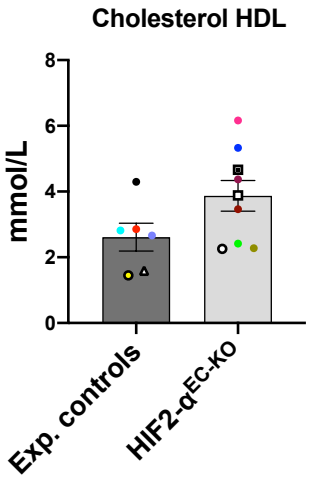
Cholesterol HDL
mmol/L
8
6
4
2
0
Exp. controls
HIF2-α EC-KO

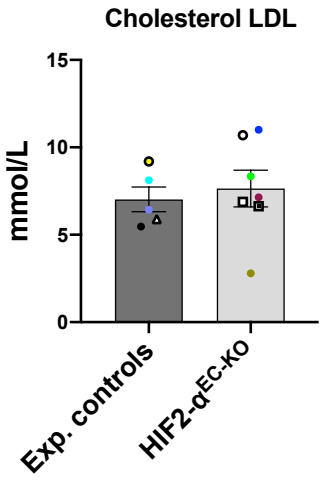
Cholesterol LDL
mmol/L
15
10
5
0
Exp. controls
HIF2-α EC-KO

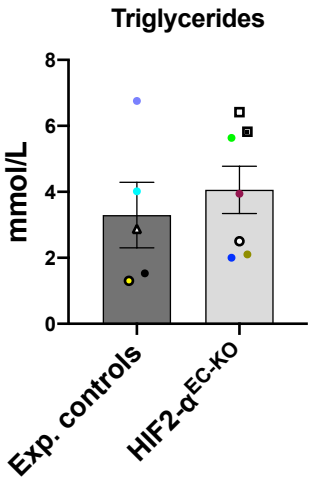
Triglycerides
mmol/L
8
6
4
2
0
Exp. controls
HIF2-α EC-KO

Figure 5. 13 Lipid profile in an atherogenic model of HIF2-α endothelial cells knock-out mice.

HIF2-α fl/fl-CDH5-Cre mice (HIF2-A^{EC-KO}) and Cre-negative littermate controls (Experimental controls) were injected with tamoxifen to delete HIF2-α expression in vascular endothelial cells. After achieving HIF2-α knock out, mice were injected with PCSK9 and exposed to HFD for 8 weeks to obtain an atherogenic lipid profile. A) Representative images of experimental control and HIF2-α^{EC-KO} mice after HFD, left panel and body weight differences of experimental controls and HIF2-A^{EC-KO} mice , right panel. B) Total cholesterol level of experimental control and HIF2-α^{EC-KO} mice after 8 weeks of HFD. C) Sub-composition of cholesterol content: HDL, LDL and triglycerides levels. Mean levels +/- SEM are shown. Difference between means are analysed using a unpaired T-test.

A

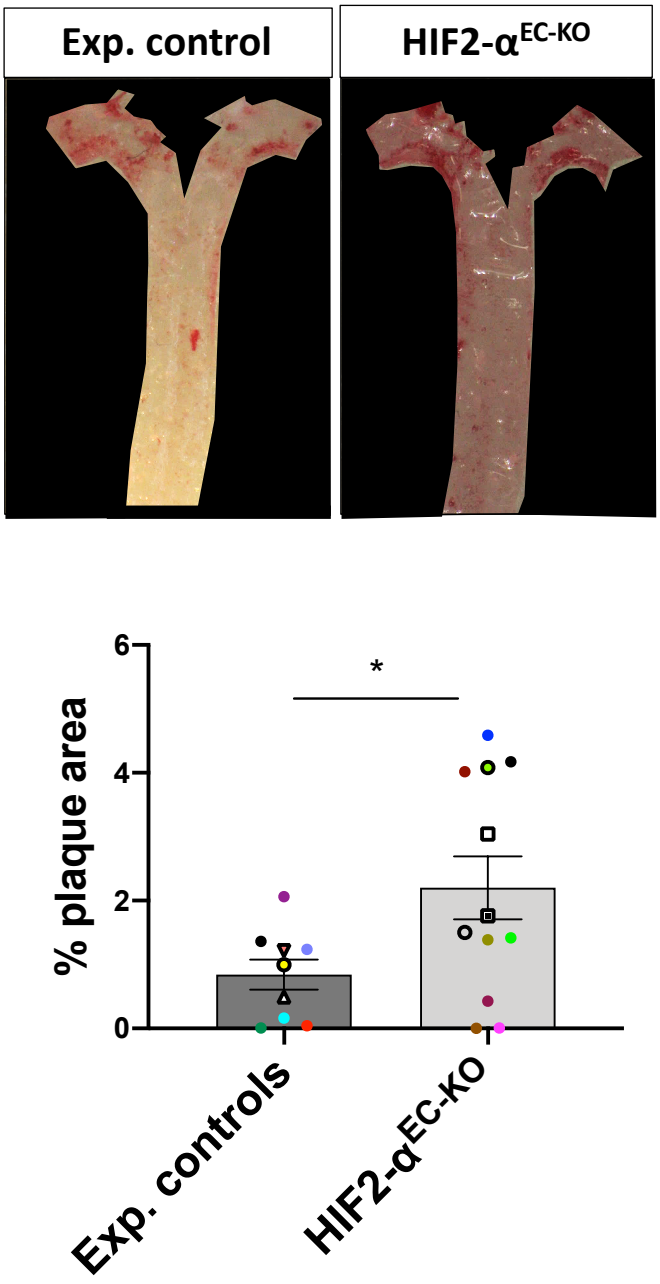

Figure 5. 14 HIF2-α protects from atherosclerosis formation.

HIF2-α fl/fl-CDH5-Cre mice (HIF2-α^{EC-KO}, N=12) and Cre-negative littermate controls (Experimental controls , N=9) were injected with PCSK9 and exposed to HFD for 8 weeks to obtain development of plaque at the aortae. Plaques were visualised by Oil Red O staining. A) Representative plaque images of experimental controls and HIF2-α^{EC-KO} mice , upper panel, and plaque quantification , lower panel. Mean levels +/- SEM are shown. Difference between means are analysed using a paired T-test. * $p<0.05$

Conclusions

In this chapter, I have demonstrated that:

- FAs supplementation reduced nuclear HIF2-α protein levels in ECs exposed to low WSS.
- HIF2-α regulates mitochondrial content without altering morphological parameters in PAECs exposed to low WSS.
- HIF2-α protects from DNA damage and senescence and concomitantly promotes proliferation in EC exposed to low WSS.
- Some of these effects are partially rescued by the OA supplementation suggesting that HIF2-α function may involve fatty acid metabolism
- HIF2-α ECs-KO mice increased plaque formation when compared to their experimental controls.

A summary model of the function of HIF2-α in arterial endothelium is represented in figure 5.15.

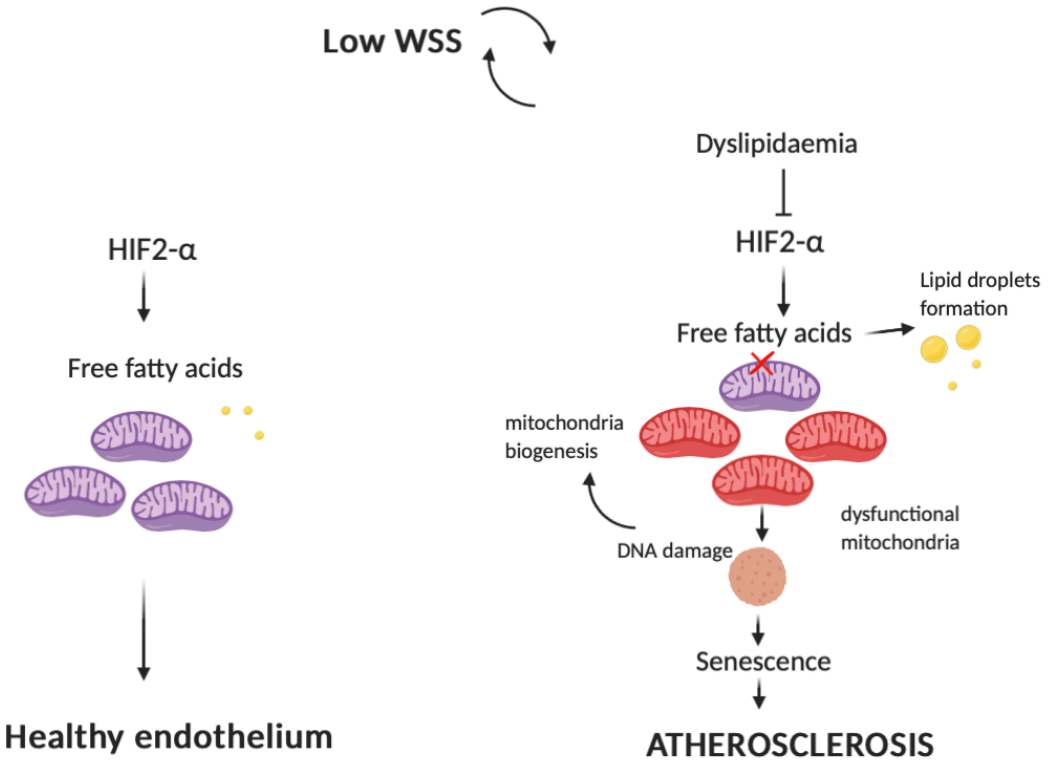

Figure 5. 15 Model of HIF2-α regulation of endothelial cells metabolism and protection from atherosclerosis.

In healthy individual HIF2-α in enriched at site of the vasculature exposed to low WSS. In this conditions HIF2-α promotes fatty acid metabolism by preserving mitochondria integrity and functionality. On the contrary, when the endothelium is exposed to risk factors, such as obesity and diabetes, comprising a state of hypertriglyceridemia; HIF2-α is reduced. Free fatty acid treatment induced lipid droplets formation. I hypothesised that DNA damage and cellular senescence could be potentially caused by the presence of dysfunctional mitochondria and an increase in ROS production. In response to such changes, on one hand, mitochondria biogenesis is activated in the attempt to repristinate functional mitochondria. Whereas, on the other hand, the increase of cellular senescence promotes atherosclerosis. Illustration created using Biorender.com.

Discussion

What is the mechanism by which fatty acids alter HIF2-α expression in endothelium?

Fatty acids enter the cell via CD36 or via plasma membrane fatty acid binding protein (FABP). Before entering into the metabolic pathway, fatty acids need to be activated to acyl-coenzyme A (CoA) esters and then enter the carnitine cycle. The latter is essential for the import of FA inside the mitochondria via carnitine palmitoyl transferase 1 and 2 (CPT1, CPT2). After entering the mitochondria, FA in the form of acyl-CoA are finally degraded by beta-oxidation. The ending product of this four steps process, the Acetyl-CoA, will fuel the tricarboxylic (TCA) cycle along with other pathways. Canonically, fatty acid oxidation (FAO) has been discussed as a supportive metabolic pathway in case of nutrient deprivation in cells; nevertheless, FAO relevance is tissue specific and it depends on energetic requirements.

Fatty acids utilisation is characteristic of cells of the peripheral tissues requiring a highly energetic substrate (e.g. muscle and heart). On the contrary ECs metabolism is mostly supported by glycolysis (Falkenberg *et al.*, 2019b) and mitochondria account only for a small portion of endothelial cells cytoplasm (Groschner *et al.*, 2012; Kluge, 2013; Kadlec *et al.*, 2016). Specifically, in PAECs, the in vitro model used in this project, by nuclear magnetic resonance (NMR) analysis it was estimated that cells obtain more than 75% of ATP from glycolysis (Culic, Gruwel and Schrader, 1997).

Nevertheless, a small amount of glycolysis-derived product can also enter the TCA cycle (De Bock *et al.*, 2013), while the largest portion of product fuelling the TCA is derived from the FA oxidation. It was suggested that TCA cycle is essential for supporting biomass production in endothelial cells and inhibition of FA within the TCA impairs vessel spouting without altering energy demand of the ECs (Schoors *et al.*, 2015). Endothelial cells proliferation is further supported by fatty acid metabolism, with an increase in FAs synthesis and an increase in long fatty acid transport protein 3 and 4 (FATP 3, FATP4) via a VEGF-β mediated mechanism (Hagberg *et al.*, 2010; Kalucka *et al.*, 2018). Thus, endothelial cells possibly use fatty acid oxidation as a vascular protective mechanism (Kalucka *et al.*, 2018).

In this chapter, I observed reduction of HIF2-α in ECs exposed to shear stress for 72h in presence of oleic acid (OA). The alteration of endothelial substrate utilization using an excess of FAs may be the cause of such inactivation, for example, by altering mitochondrial activity.

Indeed, despite oxygen being the main substrate for PHD activity, several works have implicated mitochondria as regulators of PHD activity (Hagen *et al.*, 2003; Pan *et al.*, 2007), as reviewed in (Fong and Takeda, 2008).

The possible mechanisms by which PHDs may be altered by FAs and mitochondria activity are hypothesised as follows:

- Oxidative phosphorylation (OXPHOS) rapidly reduced the oxygen concentration within the cytosol, where PHDs reside; thereby, functional mitochondria stabilised HIF by reducing PHDs substrate.
- Nitric oxide (NO) is a respiratory mitochondrial inhibitor and by inactivating cytochrome C oxidase, also known as complex IV, causes increase PHDs activity, thereby increasing HIF degradation.
- ROS production from the mitochondria may reduce PHDs activity and contribute to stabilise HIFs.
- The TCA intermediate 2-OG is an essential substrate for PHDs activity, however, TCA cycle also produce negative regulator of PHDs by generating succinate and fumarate which compete against 2-OG.

In summary, alteration of OXPHOS by excess FAs driving mitochondrial activity might alter PHDs stability and thus HIF degradation. Thus, mechanistically HIF2-α reduction in the presence of OA might be the consequence of increased activity of PHD1, PHD2 and/or 3 enzymes. Moreover there exists a multilayer interconnection between HIFs, mitochondria and hypoxia (reviewed in (Fuhrmann and Brune, 2017). On one hand, mitochondria may control HIFs stability; on the other hand, HIFs activation upon hypoxia re-programme all the components of the mitochondrial electron transport chain to adapt the cell for survival and to minimise excessive ROS production. In agreement with this, Paul Evans group previously reported that HIF1-α regulated glycolytic enzymes at site of low WSS, thus a role for the HIFs in metabolic reprogramming of the ECs may have a key role in the physiological adaptation of the vessel.

Nevertheless, a mechanism of regulation of HIF completely independent by PHDs and mitochondrial activity may take place and to this end, this aspect of the project requires further investigation.

A technical limitation to the use of OA in this work could reside in the assessment of cytotoxicity via cell death rate. Firstly, other assays evaluating cytotoxicity could have been used to refine the analysis. PAECs could have also been tested for the level of lactate dehydrogenase (LDH) and adenosine triphosphate (ATP). LDH and ATP are considered a marker of cytotoxicity. When the cellular membrane is compromised, cells release LDH in the media and its variation can be detected by colourimetric assay. Similarly, the ATP-cytotoxic assay is based on the observation that dying cells drastically reduced the production of ATP. In addition to this, toxicity may not correspond to cell death and testing the cells for markers of inflammation could have helped to understand the effect of oleic acid on endothelial cells.

HIF2-α promotes proliferative repair.

The role of the HIF subunits in proliferation and angiogenesis is well established. Nevertheless, the angiogenic state in ECs may also be involved in pathological processes. Several cancer cells type use HIF2-α to promote proliferation and invasiveness (Gnarra *et al.*, 1994; Maxwell *et al.*, 1999; Bangoura *et al.*, 2007; Shay *et al.*, 2014).

In this chapter, I investigated proliferation by assessing Ki67 staining in vitro, and it was observed that HIF2-α promotes proliferation and that OA partially co-operate to this, by promoting proliferation during the loss of HIF2-α. Ki67 identifies cells whose current cell cycle state is between late interphase (S) and the M phases. However, the relative abundance of this cells within these sub-states of the cell cycle are not determined by Ki67 staining. Whether HIF2-α KD cells are reducing the proliferative rate because of arrest in G0 phase or because of accumulation in S phase and G1 is unknown. Conventionally, a second staining with PCNA is also performed, however, in this case the use of a marker mostly expressed between S and G2 would not resolve this issue. To overcome this uncertainty, I would propose to analyse HIF2-α KD endothelial cells exposed to low WSS versus scrambled control with propidium a iodide staining using flow cytometry. This experiment would conclusively identified the current state of ECs within the cell cycle.

In the past few decades, circulating endothelial progenitor cells (EPCs) were identified to have a potential role for post-natal angiogenesis and proliferative repair of the vasculature (reviewed in (Zhang, Malik and Rehman, 2014)). Nevertheless, a major contribution to proliferative repair derived from resident endothelial cells (Hagensen *et al.*, 2012). Thereby, it could be speculated that resident endothelial cells expressing HIF2-α may have the ability to promote proliferative repair following an insult or as part of the HIF2-α -mediated transcriptional programme induced by shear stress.

Furthermore, the turnover of triglycerides into specific subset of fatty acids can determine cell viability (Ackerman *et al.*, 2018). Thus, the buffering effect of OA on proliferation seen in endothelial cells with HIF2-α KD could be possibly explained by a parallel and independent effect of OA on endothelial cells proliferation.

HIF2-α prevents endothelial cells senescence by promoting mitochondria mass.

Cellular senescence is an evolved mechanism to prevent infinite proliferation of a cell that potentially could lead to cancer development (Rodier and Campisi, 2011). Despite endothelial cells being mostly in a quiescent state within the vasculature, senescence is found in endothelial cells and it was associated with vascular diseases, including atherosclerosis (Ferrucci and Fabbri, 2018). The hallmarks of senescence are mitochondrial dysfunction, DNA damage and a pro-inflammatory phenotype (Uryga and Bennett, 2016). Endothelial cells undergo senescence by a permanent cell-cycle arrest followed by a switch in their metabolism. Morphological and structural changes are associated with senescence; endothelial cells enlarge their cytoplasm and present an increasingly polyploid nucleus (Rodier and Campisi, 2011). In this chapter, I have observed an increase of DNA damage and multinucleated and enlarged cells in HIF2-α KD PAECs and I interpreted such morphological changes as senescence. Furthermore, in agreement with what observed for the proliferation state of the cells, this phenotype was partially rescued by exposure to oleic acid overload. Suggesting that regulation of metabolic rate in ECs prevents senescence and preserves ECs functions.

However, marker of senescence or DNA damage were not found in the microarray performed in the PAECs KD of HIF2-α. Thus, at the transcriptional level HIF2-α may not be a regulator of this pathways.

In contrast to that, loss of HIF2-α was previously shown to increase p53 expression due to increased ROS level within the cell (Bertout *et al.*, 2009). In further agreement with this, dysregulation of anti-oxidant response in response to HIF2-α loss in kidney and lung cancer cells, increased the number of γ-H2AX foci (Bertout *et al.*, 2009).

Activation of senescent markers, such as p53, were previously shown upregulated in cultured endothelial cells exposed to low WSS (Warboys *et al.*, 2014). Nevertheless, other works suggested that p21, downstream effector of p53, was activated under high WSS with a final outcome leading to a quiescent state (Akimoto *et al.*, 2000). At the moment, while HIF1-α was previously link to senescence and cardiovascular disease (Alique *et al.*, 2020), the role of the HIF2-α in endothelial cell senescence is completely not-understood.

Taken together, my data suggest that endothelial HIF2-α prevented endothelial senescence. Previous studies have shown that senescent endothelial cells display increased mitochondrial mass and increase mitochondrial membrane hyperpolarization (Correia-Melo *et al.*, 2016; Fafián-Labora *et al.*, 2019). Other studies using HUVECs associated cellular senescence with a decrease in mitochondrial number and an increase mitochondrial network (Mai *et al.*, 2010).

Alteration of mitochondrial biogenesis or rearrangement processes is a determinant of cardiovascular health. As an example, endothelial cells isolated from diabetic patients had increased number of fragmented mitochondria compared to healthy donors (Shenouda *et al.*, 2011). Here I demonstrated that HIF2-α regulates the number of mitochondria in ECs but I did not observe a change in overall mitochondrial area or morphology. However, the analysis performed in this project on mitochondria do not cover all the morphological parameters. Specifically, a limitation for the mitochondrial analysis is the lack of a robust interpretation for mitochondria swelling; mechanism by which mitochondria undergo to ultrastructural changes of the inner membrane, which expand in diameter and potentially perforates the outer membrane (Blondin and Green, 1969). The release of mitochondrial content into the cytoplasm may activate an apoptotic process. In conclusion my work defined a potential rule for HIF2-α in cellular ageing and endothelial mitochondrial content at site of low WSS.

In addition, the mitochondria protein PDHX was chosen as control in the western blot analysis due to its stability to HIF2-α knockdown and to shear stress condition *in-vitro*. Controversially, in this chapter, the data suggested that HIF2-α may regulate mitochondrial density. Whether

mitochondrial density and activity were uncoupled it was not assessed in this study and future investigation should point toward this direction to reconcile this conflicting data.

A possible role for the mTORC pathway

Unfortunately, the microarray analysis performed in this project was suboptimal. Multiple factors could explain this:

- Firstly, variability between animals (age, gender) may account for the inter-variability observed between animals.
- Secondly, PAECs were isolated with different percentage of purity, thus, small difference between non-ECs (e.g. fibroblast, VSMC) contamination may reflect a higher transcriptional variability between samples.
- Thirdly, a variability between knock down efficiency may also contribute to the transcriptional profile of HIF2-α knock-down cells.

Nevertheless GSEA analysis provided a hint for investigating endothelial cells proliferation, senescence and metabolic alteration and experimental evidence confirmed them. Among other enriched pathways, it was suggested that molecules involved in the mammalian target of rapamycin complex (mTORC) pathway were regulated by HIF2-α. Possibly, activation of mTORC pathway may reconciliate the data generated in this chapter. In agreement with this observation, mTORC has a role in both mitochondrial regulation and senescence.

mTORC consists of two complexes, mTORC1 and mTORC2 which possess different sensitivity to rapamycin, where the latter is strikingly less sensitive than the former (Sabatini, 2006). Senescent cells are characterised by a multi-complex senescent-associated secretory phenotype (SAPS), and mTORC activity promotes this phenotype (Narita *et al.*, 2011; Rodier and Campisi, 2011). Inhibition of mTORC1 prevented stem cell senescence (Kolesnichenko *et al.*, 2012). Moreover, inhibiting mTORC1 was previously shown to reduce mitochondrial content *in vivo* and to prevent senescence in mice liver (Correia-Melo *et al.*, 2016). Furthermore, it was reported that HIFs are sensitive to rapamycin treatment, therefore are regulated in part by the mTORC (Hudson *et al.*, 2002; Bernardi *et al.*, 2006; Thomas *et al.*, 2006; Land and Tee, 2007).

Therefore, mTORC regulation by HIF2-α could be involved in the HIF2-a-sensitive endothelial senescence pathway described in this thesis. Further work is required in this area to unveil the role of mTORC in this process.

Endothelial HIF2-α protects mice from atherosclerosis development.

Atherosclerosis develops preferentially at branches and curvature of the aortic vessel. The inner curvature of the aortic arch and the ostiae at the descending aorta are exposed to low WSS and thus are atheroprone. On the contrary, the descending aorta and the outer curvature of the aortic arch are exposed to high WSS and generally atheroprotected. In this project, atherosclerosis was achieved in both mice lacking of HIF2-α in endothelium and experimental controls using a combination of AAV-PCSK9 and 8 weeks of HFD. HIF2-α endothelial (EC) knock-out (KO) mice developed increased aortic atherosclerosis when compared to their experimental controls. As expected, both HIF2- α EC-KO and experimental controls mice developed plaques at the aortic arch and, to a smaller extent, at the descending aorta. This data suggested a role for HIF2-α in protecting the endothelial cells from atherosclerosis development.

In the microarray performed in PAECs, it was not possible to identify a direct link between HIF2-α knockdown with lipid metabolism or senescence. Therefore at the transcriptional level it is difficult to reconcile *in-vitro* and *in-vivo* data.

Interestingly, together with the increase in plaque area in HIF2-α EC-KO mice there was no changes in lipid profile between transgenic mice and experimental controls. Thus, I reasoned that a secondary effect from other organs (e.g. fat and liver) on circulating level of lipids is unlikely to contribute to plaque formation in HIF2-α EC-KO mice. Furthermore, the ratio between HDL and LDL in HIF2-α EC-KO mice seems to favour the HDL fraction, thereby corroborating this hypothesis.

Nevertheless, the increase in plaque area in HIF2-α EC-KO may occur via other mechanisms. As I have already discussed in this thesis, it was demonstrated that activation of HIF1-α led to an increase pro-inflammatory state and that potentially promotes atherosclerosis. Thereby, a limitation to this study is that I haven't investigated HIF1-α level at the endothelium HIF2-α EC-

KO mice. A possible compensatory response between the two isoforms might be responsible for the increase plaque area in HIF2-α EC-KO mice.

Conclusively, a second model of atherosclerosis (e.g. ApoE-/-;HIF2-α EC-KO) may be considered for future work to corroborate the state of these findings.

Future works:

Experiments that could implement and corroborate these data are:

- Generating new PAECs from freshly collected pigs aorta. This will allow the increase in number of replicates for the experiments presented in this chapter.
- Studying plaque area at aortic root sites and evaluate the abundance of macrophage within the plaque and the SMCs content.
- Studying the levels of mitochondria at the low WSS site of mice aorta in HIF2-α $^{EC-KO}$ and control mice.
- Studying the effect of HIF2-α on mitochondrial metabolism by assessing the oxygen consumption rate (OCR) in PAECs using the seahorse assay for fatty acid and glycolytic metabolism.
- Studying mitochondrial morphology and defects (e.g. swelling) using electron microscopy.
- Studying other markers of senescence (e.g. p53) in PAECs treated with lentiviral shRNA targeting HIF2-α or scrambled control and exposed to low WSS.

Chapter 6. General discussion

Study summary

Over the past two decades, angiogenesis was the focus of the research on HIFs functions in endothelium. Nevertheless, recent evidences switched the research interest towards atherosclerosis. Despite angiogenesis being observed during the progression of atherosclerosis via the formation of vessel within a plaque, HIF1-α was observed at site of low WSS of healthy mice (Feng *et al.*, 2017). Mechanical activation of HIF1-α was also observed *in vitro* using human and porcine endothelial cells (Feng *et al.*, 2017; Wu *et al.*, 2017). In this project, I have shown that HIF2-α was activated by either low WSS or high WSS depending on the anatomical site, using both *in vivo* and *in vitro* models. Furthermore, at the atheroprone foci, HIF2-α was dramatically inhibited by the presence of obesity and metabolic syndrome. After showing that inhibition of HIF2-α level was not due to hyperglycaemia alone in the absence of obesity, I have shown a direct correlation between triglycerides level and HIF2-α expression at the endothelium. Injection of obese (HFD mice) with the antioxidant sulforaphane, rescued HIF2-α level at site of low WSS and concomitantly ameliorated mice triglycerides levels. Interestingly, the use of a metabolite of triglycerides, oleic acid, inhibited HIF2-α level *in vitro,* in cultured porcine aortic endothelial cells exposed to low WSS. Therefore, low shear stress induces HIF2-α and my data suggest this is prevented by obesity via triglycerides.

An *in vitro* functional analysis using microarray was performed in endothelial cells treated with lentivirus shRNA pool targeting HIF2-α sequences. The analysis revealed that HIF2-α was modulating proliferation, a mTORC1 related pathway as well as several metabolic genes.

To confirm the functional annotation emerged from the microarray, proliferation rate was studied using Ki67 staining. Results showed that HIF2-α promotes endothelial cells proliferation and further investigation revealed that the mechanism involved altered mitochondrial activity and reduced senescence. After showing how HIF2-α was altering endothelial cells physiology *in vitro*, a model of HIF2-α vascular endothelial deletion in mice was generated to study atherosclerosis. HIF2-α endothelial cells KO mice increased atherosclerosis. In conclusion, these data suggest that HIF2-α play a fundamental role in atherosclerosis development by preventing both metabolic and proliferative failure in endothelial cells. A summary model is presented in Figure 6.1.

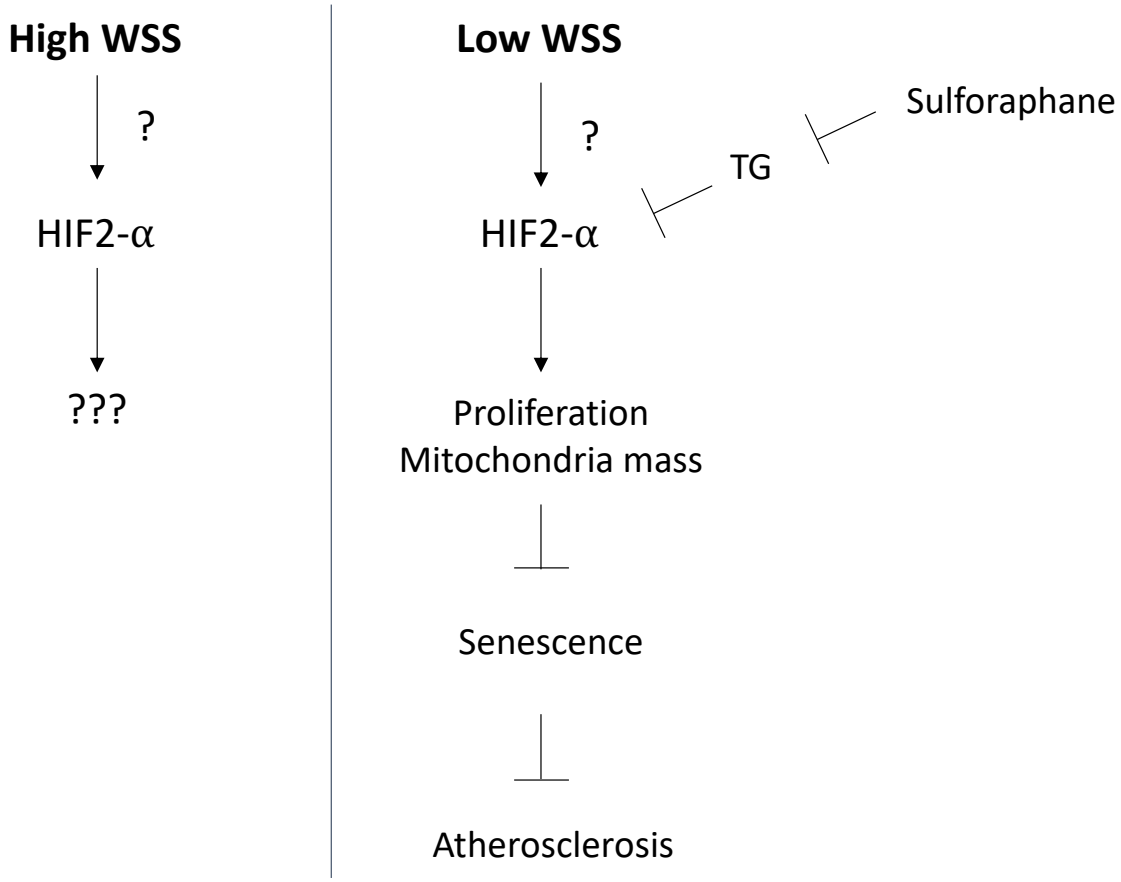

Figure 6. 1 Activation of HIF2-α by wall shear stress and its functions.

High wall shear stress (WSS) activates HIF2-α at the descending aortic site, while low WSS activate HIF2-α at the inner curvature of the aortic arch. The mechanism by which HIF2-α responds to high WSS and its function at the atheroprotected site is currently unknown. At site of Low WSS, this thesis unveil novel functions of the HIF2-α in endothelium and it identified a protective role for the development of atherosclerosis. Nevertheless, the mechanism of activation of HIF2-α by low WSS is unknown.

Therapeutic implications and future directions

This work has shown that HIF2-α might protect from atherosclerosis by preventing endothelial senescence and promoting mitochondrial activity. In contrast, it was previously demonstrated that HIF1-α promoted atherosclerosis. Despite extensive research into the activation of HIFs for therapeutic applications, very little is known about selective activation of the diverse HIF isoform. On the other hand, HIF2-α selective inhibitors were developed and they are currently undergoing clinical trials for treatment of cancer and pulmonary hypertension (Chen *et al.*, 2016; Dai *et al.*, 2018). My observations indicate that HIF2-α inhibitors should be used with caution because of the protective role of HIF2-α in endothelium at sites of low WSS. Indeed, an ideal therapeutic aim for the HIF2-α in atherosclerosis may be to achieve a selective stabilisation of the protein at atheroprone sites in order to prevent endothelial cells dysfunction.

While animal models with transgenic activation of HIF2-α in endothelium are available (Kong *et al.*, 2017), the translation of this approach towards the clinic is challenging.

Selective drug delivery to endothelium is a recent advance in cardiovascular therapy. Nanoparticles have been engineered and used as a cargo for various therapeutic agents that targeted macrophage accumulation, thrombosis, vascular inflammation, neovascularization and neointimal growth (Dahlman *et al.*, 2015; Khan *et al.*, 2018; Flores *et al.*, 2019).

Both, selective treatment toward HIF2-α over HIF1-α activation and a selective endothelial cells-delivery of a therapeutic agent require further investigation. Thus, therapeutically targeting HIF2-α for atherosclerosis establishes a novel challenge for pharmacotherapy.

Future works

Site specific regulation of HIF2-α by shear stress.

This work identified HIF2-α as a gene responsive to both high and low WSS. Furthermore, in the previous chapters I have hypothesis that the divergent results achieved on the activation of HIF2-α by high WSS could be caused by differences in high WSS magnitudes between the outer curvature of the aortic arch and the descending aorta. To elucidate this, a y-slide experiment using Ibidi® system could be perform on cells deriving from aortic arch and descending aorta. The y-slide allows to create a gradient of shear stress across the ibidi slide (e.g. 10 to 26 dyne/cm^2). Immunofluorescent staining of cells exposed to a gradient of shear stress could help to disclose the reasons behind the site specific activation of HIF2-α under high WSS stimuli.

Alternatively, an *in-vivo* model of constrictive cuff (Kuhlmann *et al.*, 2012), could corroborate the casual correlation between shear stress activation of HIF2-α in endothelium. A constrictive cuff on mouse carotid artery causes three distinct regions of flow patterns. Downstream the cuff site it generates low oscillatory shear, while upstream the cuff constriction endothelial cells are exposed to low unidirectional flow, whereas the area within the cuff is exposed to high WSS.

Mechanosensing signalling pathway upstream HIF2-α.

Future work could aim to investigate the regulatory molecules upstream HIF2-α. Protein lysates generated by the Ibidi® system or orbital shaker experiments should be investigated for PHD2, PHD3, Cezanne and VHL, biochemical protagonists of the equilibrium of the proteasomal degradation of the HIFs.

Role of HIF2-α in Endothelial to Mesenchymal (EndMT) Transition.

The link between atherosclerosis and endothelial to mesenchymal transition (EndMT) is currently of great and increasing interest in this field (Souilhol *et al.*, 2018). Experimental evidences reported that mesenchymal markers were activated at region of low WSS (Moonen

et al., 2015; Mahmoud *et al.*, 2016, 2017). Hypoxia is known to increase EndMT by a HIF1-α - mediated regulation of several biochemical signals involved in this process. Nevertheless, a role for HIF2-α in EndMT has been recognised in pulmonary hypertension (Tang *et al.*, 2018). The direct link between HIF2-α and EndMT in atherosclerosis development is currently unveil. Recent advanced in endothelial cells biology implemented the lineage tracing techniques. Mice carrying gene floxed regions and a fluorescent conjugated marker for endothelial cells (e.g. RosaTomato-CHD5CreERT2) have been used to identify cell fate during EndMT (Evrard *et al.*, 2016; Kim, Alfieri and Yutzey, 2019). To understand the contribution of HIF on endothelial cells identity during atherosclerosis mice crossed with a HIF2-α fl/fl allele and RosaTomato CDH5 CreERT2 could be treated with AAV-PSCK9 injection and exposed to HFD to achieve atherosclerosis. Immunofluorescence analysis of aortic endothelium would reveal the fate of HIF2-α endothelial cells during atherosclerosis progression.

Regulation of mitochondrial activity and ROS production by HIF2-α.

In order to understand metabolic regulation of HIF2-α in sheared endothelial cells, Seahorse analysis may be employed to study oxygen consumption rate (OCR) and glycolytic rate (ECAR). PAECs sheared for 72h using orbital shaker can be collected for seahorse analysis by removing the high WSS site (periphery) by gently scraping the 6 well plate following a shear stress map (Feng *et al.*, 2017). Cells can then be tested for Mitofuel flux assay (Agilent), using a combination of inhibitors for the mitochondrial pyruvate carrier (MCP), UK5099, the glutaminase enzyme (GLS1), BPTES, and the carnitine palmitoyl-transferase 1A (CPT1A), Etomoxir. The outcome of this assay will determine mitochondrial dependency from the energetic fuel input.

Validation of HIF2-α regulation of mitochondria *in vivo*.

To assess whether HIF2-α is altering mitochondria, DNA damage and senescence *in vivo*, aorta of HIF2-α ^{ECKO} mice could be studied using Mitotracker staining and immunostaining of DNA damage and senescence markers and confocal microscopy.

Conclusion

A countless number of works investigating HIFs in endothelial cells have been generated in the past few decades. Nevertheless, until now , very little was known about mechanical activation of HIFs in endothelium and their function in atherosclerosis. Wall shear stress drives endothelial cells physiology, by adapting different transcriptional responses at site of the vasculature exposed to high WSS or low WSS. Firstly, HIF1-α was found enriched at site low WSS, where it promoted atherosclerosis. Then, after showing HIF2-α activation at low WSS, my observations have provided evidence of a functional role for HIF2-α under low WSS conditions. In this project, I unveiled a role for HIF2-α in protecting the endothelium from atherosclerosis development, by promoting metabolic adaptation to changes in lipid content and by preventing endothelial senescence. Thus, HIF2-α might be the future therapeutic target for preventing atherosclerosis development.

Chapter 7. Appendix

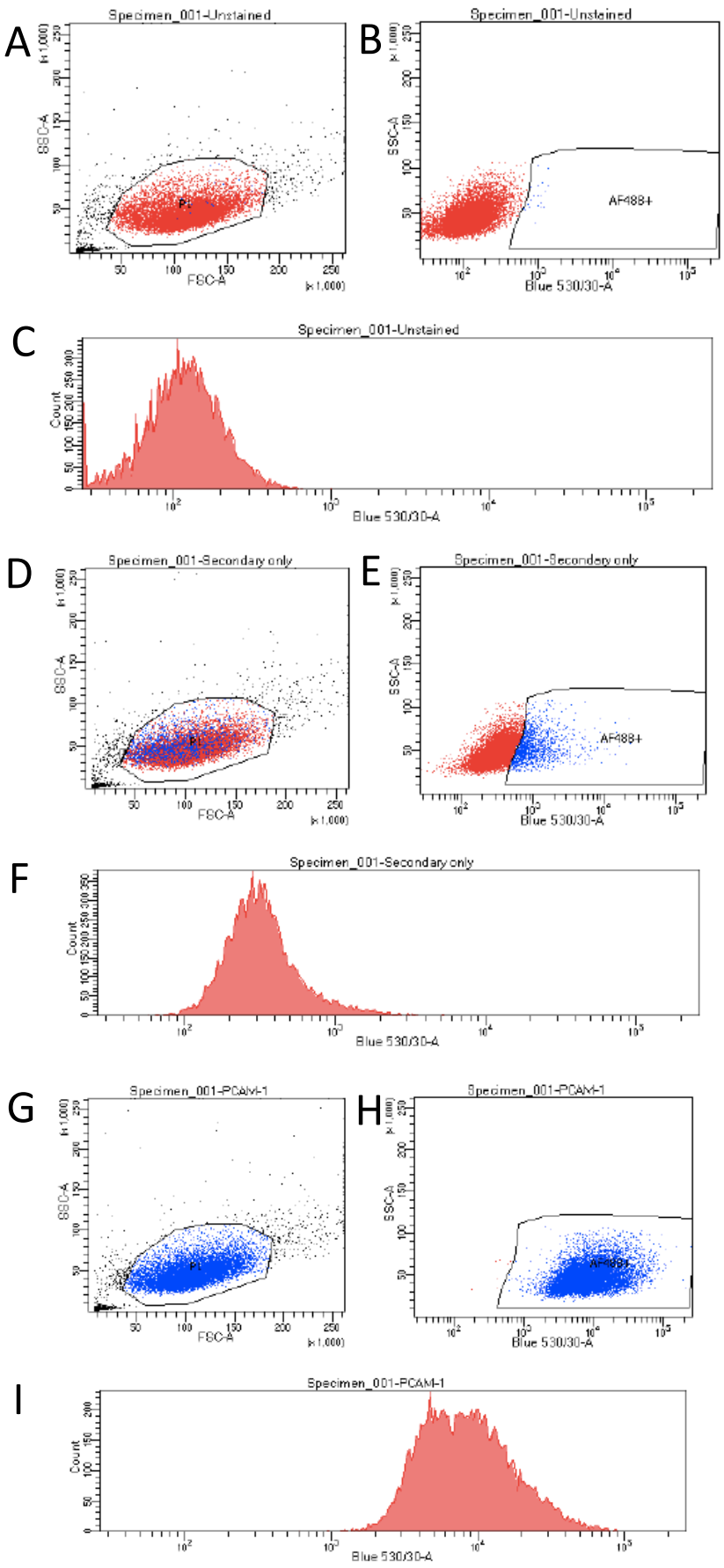
A
Specimen_001-Unstained
SSC-A
FSC-A
P1
B
Specimen_001-Unstained
SSC-A
AF488+
Blue 530/30-A
C
Specimen_001-Unstained
Count
Blue 530/30-A
D
Specimen_001-Secondary only
SSC-A
FSC-A
P1
E
Specimen_001-Secondary only
SSC-A
AF488+
Blue 530/30-A
F
Specimen_001-Secondary only
Count
Blue 530/30-A
G
Specimen_001-PCAM-1
SSC-A
FSC-A
P1
H
Specimen_001-PCAM-1
SSC-A
Blue 530/30-A
I
Specimen_001-PCAM-1
Count
Blue 530/30-A

Figure 7. 1 Gating strategy of PAECs isolation.

To determine cell purity, PAECs were labelled using anti-PECAM-1 primary antibody followed by a FITC-conjugated secondary antibody. PECAM-1 surface expression was then analysed using the BD LSRII flow cytometer. A) Unlabelled cells were analysed initially using a plot of forward (FSC-A) versus side scatter (SSC-A) to identify and gate on the cell population (red). B) Baseline fluorescence was established using the unstained cell sample with the Blue laser (488 nm) and 530/30-A filter, and a gate for positively-stained cells was set above this threshold; the fluorescence intensity histogram for this cell population is shown in C. Using the same gating strategy (D), cells incubated with the FITC-conjugated secondary antibody only were analysed to determine non-specific antibody binding (dot plot shown in E and histogram shown in F). Blue events indicate positively-stained cells with FITC-fluorescence. Finally, PAECs expressing surface PECAM-1 were identified after antibody labelling using the established parameters (G and H), where a large shift to the right in the dot plot in H and histogram in I indicated that approx. 100% of these cells were positive for this surface protein.

In vitro experiments

Table 3 Tissue culture FBS-Free media (Media A).

Reagent	Brand	Catalogue N	Final concentration
10X M199	Gibco	21180-021	1X
Sodium bicarbonate 7.5%	Sigma	S5761	0.03%
Pen/Strep	Gibco	1514-122	Pen: 10,000 U/ml Strep: 10,000 µg/ml
Amphotericin B	Fisher Bioreagents	BP2645-50	250µg/ml
Gentamycin (for PAEC only)	Gibco	15710-049	50µg/ml
L-glutamine	Gibco	25030-024	2mM
Sterile water	/	/	/

Table 4 Complete media.

Reagent	Brand	Catalogue N	Final concentration
Media A	/	/	/
ECGF	Millipore	3117593	5µg/ml
Heparin	Sigma	H3149	50µg/ml
Fetal Bovine Serum (FBS)	Labtech	FCS-SA	20%

Table 5 *In-vitro* reagents

Reagent	Brand	Catalogue number	Dilution/volume
Mitotracker CMXRos	Thermo Fisher Scientific	M7512	200 nM
Dulbecco's Modified Eagle Medium (DMEM)	Thermo Fisher Scientific	41965120	1X
Oleic acid	Sigma Aldrich	O1383	Range: 250 µM-125 µM
Trypan Blue	Gibco	15250061	/
DMOG (N-(methoxyoxoacetyl)-glycine methyl ester)	MedChemExpress	HY-15893	1 mM
RLT buffer	Qiagen	79216	/
4x Laemmeli buffer	Bio-Rad	161-0747	1x
β-mercaptoethanol	Sigma	M3148	Assay dependent
TRIzol Reagent	ThermoFischer Scientific	15596-026	/
Gelatin from Bovine Skin	Sigma	G9391	1% w/v
DEAE-Dextran	Sigma	D9885	6 µg/ml
Lentivirus	Dharmacon	V3SH7590	MOI 30
DPX mounting media	VWR	360294H	/
Collagenase type IV	Gibco	17104-019	1 mg/ml
Phosphate buffer saline	Sigma	P4417	1x
Nuclease free water	Qiagen	129115	/
Tween 20	Thermo Fisher Scientific	BP337	/

BODIPY 499/503	Thermo Fisher Scientific	D32922	0.1mg/ml
DAPI	Thermo Fisher Scientific	D1306	5 µg/ml
Goat anti-rabbit conjugated AF568	Thermo Fisher Scientific	A-11036	10 µg/ml
Pro-Long Gold	Thermo Fisher Scientific	P36930	/
LCI-4	Santacruz	80912	10 µg/ml
Goat anti-Mouse AF647	Abcam	A-21235	3.3 µg/ml
TOPRO 3 IODIDE	ThermoFisher Scientific	T3605	5µM
0.25% Trypsin-EDTA	Gibco	25200-072	/
Goat serum	Sigma	G6767	Assay dependant

Table 6 Lentiviral shRNA sequences targeting HIF2-A human and porcine sequence.

Clone ID	Target	Sequence	Titer (TU/mL)
V3SVHSHC_5189144	HIF2-α	CTCAGGACGTAGTTGACAC	2.00E+08
V3SVHSHC_8578211	HIF2-α	CCCATGAACTTGCTGATGT	1.63E+08
V3SVHSHC_8945039	HIF2-α	TCATGAAGAAGTCCCGCTC	1.77E+08
V16060303	Non-targeting	///	1.36E+09

Table 7 Primers list used in qRT-PCR experiments.

Target	Forward sequence	Reverse sequence
B2M	GGTTCAGGTTTACTCACGCCAC	CTTAACTATCTTGGGCTTATCG
HIF2-α	CAGGGGACGGTCATCTACAA	TCTCAATCTCACTCAGGACGT
MCP1	TCACCTGCTATACACTTAC	ATCACTGCTTCTTTAGGACACTTG
eNOS	CGCTACAACATTCTGGAGGA	ACTTTGGCCAGCTGGTAACT
ADM	CAGGCCAGCATTCCGGAT	CAGGCCCTGGAAGTTGTTC
TIE-2	GCTTCTATCGGTCTTCCTCCT	ACAGACCTCCTCTCAACTTCA
VEGF	TCTTCAAGCCGTCCTGTGT	GAGGTTTGATCCGCATAATCTG
ANGPTL4	ACTGCCAAGAGCTGTTTGAAGA	CCATCTGAGGTCATCTTGCAGTT
CD31	TCAATGCTCCGTGAAAGAAG	CCTGGGTGTCATTCAAAGTG
SMA	CGATGAAGGAGGGCTGGAACAGGG	CGTGACCACTGCCGAGCGTGAGAT

Western Blotting

Table 8 Reagents.

Reagent	Brand	Catalogue N	Final concentration
Precision Plus- Dual colour Protein Ladder	BioRad	1610374	/
Milk powder	Sigma	70166	5-10% in TBST
Secondary antibody HRP-conjugated	DAKO	P0449	Assay dependent
ECL	GE Healthcare	RPN2106	/
BSA	Sigma	A9418	Assay dependent

Table 9 Running buffer.

Reagent	Brand	Catalogue N	Final concentration
Tris Base	Sigma	T1503	25mM
Glycine	Fisher Scientific	G/0800/060	190mM
SDS	GE Healthcare	17-1313-01	3.5mM
Deionised water	/	/	/

Table 10 Transfer buffer.

Reagent	Brand	Catalogue N	Final concentration
Tris Base	Sigma	T1503	45mM
Glycine	Fisher Scientific	G/0800/060	40mM
SDS	GE Healthcare	17-1313-01	20 %
Methanol	Fisher Scientific	M/4000/17	20%
Deionised water	/	/	/

Table 11 TBST buffer

Reagent	Brand	Catalogue N	Final concentration
Tris Base	Sigma	T1503	25mM
NaCl	Fluorochem	094554	140mM
KCl	Sigma	P9333	3mM
Tween 20	Fisher Scientific	BP337	0.05%
Deionised water	/	/	/

In-vivo reagents and buffers

Table 12 *in-vivo* reagents.

Reagent	Brand	Catalogue number	Dilution/volume
Western Diet Diet1-Singapore	Reasearchdiets	D12492i	Ad libitum
Western Diet Diet2-Sheffield	Special Diet Services (SDS)	829100	Ad libitum
rAAAV8/mPCSK9	UNC Vector Core	//	6*10^11 Virus particle
Plasmid D3777Y-PCSK9	Addgene	58376	/
Tamoxifen	Sigma	T5648	40mg/ml
Sulforaphane	CaymanChem	10496	5mg/kg
Corn Oil	Sigma	C8267	90%
Ethanol	VWR	20821.330	10%
Streptozotocin	Sigma	S1030	150mg/kg

Sodium citrate	Sigma	PHR1416	0.1M
Citric acid	Sigma	251275	2% (w/v)
Saline solution	Braun	361-1639	/
Oil Red O	Sigma	O0625	0.3%

Table 13 Genotyping buffer and reagent.

Reagent	Brand	Catalogue N	Final concentration
Tris-HCl	Sigma	T3253	1M
Tween 20	Fisher Scientific	BP337	10%
EDTA	Sigma	EDS	0.5M
Proteinase K	Thermo Fisher Scientific	EO0491	300 µg/ml

Table 14 Genotyping gel and running buffer.

Reagent	Brand	Catalogue N	Final concentration
Agarose	SLS	BIO-41025	2% w/v
Ethidium Bromide	Sigma	E1510	0.05% v/v
TAE buffer 50x	National diagnostics	EC-782	1x

Table 15 Genotyping reagents not included in formulations

Reagent	Brand	Catalogue N	Final concentration

Loading buffer	ThermoFisher	R0611	1x
Low molecular weight ladder	New England BioLabs	N0557S	/
10X PCR buffer	Qiagen	203203	1x
dNTP mix	ThermoFischer Scientific	R0181	100 μM
Taq DNA polymerase	Qiagen	203203	0.75U/reaction

En face staining

Table 16 Antibody list.

Antibody target	Brand	Catalogue number	Concentration
Polyclonal rabbit IgG (Sheffield)	Vector	I-1000	6.6 μg/ml
Monoclonal rat IgG (Sheffield)	Biolegend	400401	10 μg/ml
Rabbit polyclonal anti-HIF2-α	Abcam	199	6.6 μg/ml
Polyclonal rabbit IgG (Singapore)	Millipore	12-370	6.6 μg/ml
Mouse monoclonal anti-PECAM-1 conjugated AF488	Biolegend	MEC13.3 (102501)	10 μg/ml
Goat anti-rabbit conjugated AF568	Thermo Fisher	A-11036	6.6-10 μg/ml
Goat anti-rat conjugated AF568	Thermo Fisher	A-11077	10 μg/ml
Goat anti-rabbit AF488	Thermo Fisher	A-11034	10 μg/ml
Goat anti-Mouse AF647	Abcam	A-21235	3.3 μg/ml
Mouse monoclonal anti-PECAM-1 (LCI-4)	Santacruz	SC-80912	6.6 μg/ml
Rat monoclonal anti-Ki67	Thermo Fisher Scientific	14/5698/82	10 μg/ml
Γ-H2AX	Millipore	05-636	10 μg/ml

Table 19 Differentially regulated genes in PAECs microarray.

Affymetrix Probe ID	Fold Change	P-val	Gene Symbol	Description
15275645	-2.61	0.0431		
15329997	-2.58	0.0201	LOC100518322	centrosomal protein of 57 kDa-like
15262423	-2.48	0.0407	TRIM44	tripartite motif containing 44
15327929	-2.22	0.0455		
15333968	-2.2	0.0088		
15328353	-2	0.0426		
15302882	-1.98	0.0429	MIA	melanoma inhibitory activity
15334517	-1.96	0.0093	TCEAL2	transcription elongation factor A (SII)-like 2
15213132	-1.96	0.0084	TUSC5	tumor suppressor candidate 5
15237027	-1.94	0.0069	LOC100513955; LOC100737189	asparagine synthetase domain-containing protein 1
15296373	-1.83	0.0447		
15298041	-1.78	0.0393	LOC100516741	NACHT, LRR and PYD domains-containing protein 7
15242037	-1.77	0.0458	LOC106506441; LOC100524176	olfactory receptor 12-like
15245366	-1.76	0.0107	UBE2QL1	ubiquitin-conjugating enzyme E2Q family-like 1
15310081	-1.76	0.0235	VEGFA	vascular endothelial growth factor A
15310586	-1.74	0.0318	CPEB1; LOC100622904	cytoplasmic polyadenylation element binding protein 1
15219836	-1.74	0.0467	IP6K2	inositol hexakisphosphate kinase 2
15234087	-1.74	0.0257		
15267675	-1.71	0.0215		
15301316	-1.71	0.0393		
15342707	-1.7	0.0484		
15307509	-1.69	0.0359	TUBB2B	tubulin, beta 2B class IIb
15335207	-1.69	0.0143	ZIC3	Zic family member 3
15319568	-1.68	0.034	LOC100155405	olfactory receptor 4K1

15343873	-1.67	0.03		
15275469	-1.66	0.0243	RPL31; LOC100520127	ribosomal protein L31; 60S ribosomal protein L31
15342359	-1.66	0.0444		
15351083	-1.66	0.0471		
15198746	-1.64	0.03	NDUFA8	NADH dehydrogenase (ubiquinone) 1 alpha subcomplex, 8, 19kDa
15245171	-1.64	0.0303		
15307109	-1.57	0.0284	LOC100517289	E3 ubiquitin-protein ligase RNF220
15342905	-1.57	0.0272		
15345503	-1.57	0.0278		
15218367	-1.57	0.0247		
15233250	-1.56	0.0117	ALOX5	arachidonate 5-lipoxygenase
15208128	-1.56	0.0238	LOC100514982	leucine-rich repeat-containing protein 37A2-like
15324262	-1.56	0.0424	TACR3	tachykinin receptor 3
15349839	-1.55	0.044		
15267742	-1.55	0.0194		
15335584	-1.53	0.0414	CMC4; MTCP1	C-x(9)-C motif containing 4; mature T-cell proliferation 1
15302610	-1.52	0.0256	LOC102164889; ZNF527	zinc finger protein 569
15207151	-1.51	0.0178	DUSP3	dual specificity phosphatase 3
15194396	-1.5	0.0341		
15198797	-1.5	0.0399		
15263897	-1.49	0.0355	PRAM1	PML-RARA regulated adaptor molecule 1
15314508	-1.48	0.0486	LOC100519492	olfactory receptor 12D2-like
15341275	-1.48	0.0315		
15205707	-1.48	0.0196		
15350589	-1.47	0.0315		
15347665	-1.47	0.0429		
15327718	-1.47	0.0415		
15348465	-1.46	0.0477		
15330400	-1.45	0.0264	ZPR1	ZPR1 zinc finger
15344369	-1.45	0.045		
15346589	-1.45	0.0433		

15316861	-1.44	0.0419	ANPEP	alanyl (membrane) aminopeptidase
15200163	-1.44	0.0267	CFH	complement factor H
15319813	-1.43	0.0165		
15192434	-1.42	0.0414	CCDC28A	coiled-coil domain containing 28A
15315742	-1.4	0.036	LOC106507682	uncharacterized LOC106507682
15257209	-1.37	0.034	IER2	immediate early response 2
15219497	-1.37	0.0497		
15229768	-1.37	0.0402		
15254942	-1.36	0.0457		
15262170	-1.36	0.0457		
15224830	1.29	0.0364	CABP1	calcium binding protein 1
15255025	1.32	0.0425	TSPAN18	tetraspanin 18
15227951	1.37	0.0454	ZFYVE27	zinc finger, FYVE domain containing 27
15269638	1.4	0.0282	LOC100521004	SPRY domain-containing SOCS box protein 3-like
15199637	1.4	0.0312		
15347123	1.42	0.0487		
15190287	1.44	0.0291	PAPPA	pregnancy-associated plasma protein A, pappalysin 1
15302800	1.44	0.0441		
15191786	1.46	0.0287	RNF208	ring finger protein 208
15346509	1.46	0.0271		
15216254	1.47	0.0366		
15245012	1.47	0.0391		
15274208	1.49	0.0171	ABCC1	ATP-binding cassette, sub-family C (CFTR/MRP), member 1
15215108	1.49	0.0448	LOC100738134	zinc finger protein 501
15302975	1.49	0.0246	PRR19	proline rich 19
15348399	1.5	0.0312		
15340247	1.5	0.018		
15186551	1.51	0.05	PPIP5K1	diphosphoinositol pentakisphosphate kinase 1

15214297	1.53	0.0419	MYH1; LOC106505524	myosin, heavy chain 1, skeletal muscle, adult; myosin-1-like
15337705	1.55	0.0176	AMMECR1	Alport syndrome, mental retardation, midface hypoplasia and elliptocytosis chromosomal region gene 1
15326519	1.56	0.0378	SLC37A2	solute carrier family 37 (glucose-6-phosphate transporter), member 2
15188926	1.57	0.0377	ERMP1	endoplasmic reticulum metallopeptidase 1
15308830	1.57	0.0421	PSMB9; LOC100520085	proteasome subunit beta 9; proteasome subunit beta type-9
15223040	1.57	0.036	SYK; LOC102164599	spleen tyrosine kinase; tyrosine-protein kinase SYK-like
15273595	1.58	0.0434	CHCHD2	coiled-coil-helix-coiled-coil-helix domain containing 2
15258720	1.58	0.0367	GPR150	G protein-coupled receptor 150
15261871	1.58	0.0364	LOC106504186; LOC100628183	olfactory receptor 5B12-like
15299269	1.58	0.0364	PIGV; LOC100624784	phosphatidylinositol glycan anchor biosynthesis, class V
15230062	1.58	0.0414		
15267414	1.6	0.0346	LOC100626192	sodium-dependent proline transporter-like
15346963	1.6	0.0412		
15227467	1.61	0.0244	FAS	Fas cell surface death receptor
15305859	1.61	0.0494	TWSG1	twisted gastrulation BMP signaling modulator 1
15298948	1.63	0.0149	PQLC2	PQ loop repeat containing 2
15328896	1.63	0.0425	TIMM10B	translocase of inner mitochondrial membrane 10 homolog B (yeast)

15288320	1.63	0.027		
15225453	1.65	0.0239	SLC5A1	solute carrier family 5 (sodium/glucose cotransporter), member 1
15288219	1.67	0.0455	DGKA; LOC100626461; LOC106504273	diacylglycerol kinase, alpha 80kDa; diacylglycerol kinase alpha-like
15328992	1.67	0.0319	LOC100511274; LOC100739702	olfactory receptor 51I2; olfactory receptor 51I2-like
15331112	1.68	0.0258	ATP2B4	ATPase, Ca++ transporting, plasma membrane 4
15214373	1.69	0.0308	LOC100625836	heparan sulfate glucosamine 3-O-sulfotransferase 3A1
15329787	1.71	0.0438	LOC100517485	calcineurin-binding protein cabin-1-like
15201008	1.72	0.0335	LOC100515159; LOC100622098	probable G-protein coupled receptor 158
15322017	1.74	0.0277	PAQR3	progestin and adipoQ receptor family member III
15347967	1.75	0.0442		
15275176	1.77	0.0323	MALL	mal, T-cell differentiation protein-like
15202050	1.78	0.019	SUSD4	sushi domain containing 4
15243839	1.78	0.0481		
15184635	1.82	0.0188	TSTD3	thiosulfate sulfurtransferase (rhodanese)-like domain containing 3
15294565	1.83	0.0024	SLC38A1	solute carrier family 38, member 1
15347435	1.87	0.0136		
15347259	1.88	0.0417		
15306496	1.88	0.0445		
15286868	1.94	0.0031	LOC100152378	volume-regulated anion channel subunit LRRC8D
15323178	2.24	0.0042	LOC100513296	transmembrane protease serine 11F

15281342	2.27	0.0079		
15189350	2.37	0.0093	PSAT1	phosphoserine aminotransferase 1
15269169	2.47	0.0398	DEXI; LOC100739750	Dexi homolog (mouse); dexamethasone-induced protein
15351517	2.61	0.0415		
15318076	2.89	0.0208		
15273578	4.19	0.0194		

Chapter 8. Bibliography

Aarup, A. *et al.* (2016) 'Hypoxia-inducible factor-1α expression in macrophages promotes development of atherosclerosis', *Arteriosclerosis, Thrombosis, and Vascular Biology*, 36(9), pp. 1782–1790. doi: 10.1161/ATVBAHA.116.307830.
Ackerman, D. *et al.* (2018) 'Triglycerides Promote Lipid Homeostasis during Hypoxic Stress by Balancing Fatty Acid Saturation.', *Cell reports*, 24(10), pp. 2596-2605.e5. doi: 10.1016/j.celrep.2018.08.015.
Akhtar, S. *et al.* (2015) 'Endothelial Hypoxia-Inducible Factor-1α Promotes Atherosclerosis and Monocyte Recruitment by Upregulating MicroRNA-19a', *Hypertension*, 66(6), pp. 1220–1226. doi: 10.1161/HYPERTENSIONAHA.115.05886.
Akimoto, S. *et al.* (2000) 'Laminar shear stress inhibits vascular endothelial cell proliferation by inducing cyclin-dependent kinase inhibitor p21(Sdi1/Cip1/Waf1).', *Circulation research*. United States, 86(2), pp. 185–190. doi: 10.1161/01.res.86.2.185.
Alique, M. *et al.* (2020) 'Hypoxia-Inducible Factor-1α: The Master Regulator of Endothelial Cell Senescence in Vascular Aging', *Cells*, 9(1), p. 195. doi: 10.3390/cells9010195.
Alva, J. A. *et al.* (2006) 'VE-cadherin-cre-recombinase transgenic mouse: A tool for lineage analysis and gene deletion in endothelial cells', *Developmental Dynamics*, 235(3), pp. 759–767. doi: 10.1002/dvdy.20643.
Di Angelantonio, E. *et al.* (2009) 'Major lipids, apolipoproteins, and risk of vascular disease.', *JAMA*, 302(18), pp. 1993–2000. doi: 10.1001/jama.2009.1619.
Araldi, E. and Suárez, Y. (2015) 'MicroRNAs as regulators of endothelial cell functions in cardiometabolic diseases', *Biochimica et Biophysica Acta - Molecular and Cell Biology of Lipids*. Elsevier B.V., 1861(12), pp. 2094–2103. doi: 10.1016/j.bbalip.2016.01.013.
ARIAS-STELLA, J. and KRUGER, H. (1963) 'PATHOLOGY OF HIGH ALTITUDE PULMONARY EDEMA.', *Archives of pathology*. United States, 76, pp. 147–157.
Ashworth, A. *et al.* (2015) 'Comparison of Neurological Function in Males and Females from Two Substrains of C57BL/6 Mice.', *Toxics*, 3(1), pp. 1–17. doi: 10.3390/toxics3010001.
Athyros, V. G. *et al.* (2018) 'Diabetes and lipid metabolism', *Hormones*. Hormones, 17(1), pp. 61–67. doi: 10.1007/s42000-018-0014-8.
Axelsson, A. S. *et al.* (2017) 'Sulforaphane reduces hepatic glucose production and improves glucose control in patients with type 2 diabetes', *Science Translational Medicine*, 9(394), pp. 1–13. doi: 10.1126/scitranslmed.aah4477.
Bäck, M. and Hansson, G. K. (2015) 'Anti-inflammatory therapies for atherosclerosis', *Nature Reviews Cardiology*. Nature Publishing Group, a division of Macmillan Publishers Limited. All Rights Reserved., 12, p. 199. Available at: https://doi.org/10.1038/nrcardio.2015.5.
Bangoura, G. *et al.* (2007) 'Prognostic significance of HIF-2alpha/EPAS1 expression in hepatocellular carcinoma.', *World journal of gastroenterology : WJG*, 13(23), pp. 3176–82. Available at: http://www.pubmedcentral.nih.gov/articlerender.fcgi?artid=4436602&tool=pmcentrez&rendertype=abstract.
Bansal, S. *et al.* (2007) 'Fasting compared with nonfasting triglycerides and risk of cardiovascular events in women.', *JAMA*. United States, 298(3), pp. 309–316. doi: 10.1001/jama.298.3.309.
Banskota, N. K. *et al.* (1989) 'Insulin, insulin-like growth factor I and platelet-derived growth factor interact additively in the induction of the protooncogene c-myc and cellular proliferation in cultured bovine aortic smooth muscle cells.', *Molecular endocrinology (Baltimore, Md.)*. United States, 3(8), pp. 1183–1190. doi: 10.1210/mend-3-8-1183.
Bao, X., Lu, C. and Frangos, J. A. (1999) 'Temporal gradient in shear but not steady shear stress induces PDGF-A and MCP-1 expression in endothelial cells: Role of NO, NFκB, and

egr-1', *Arteriosclerosis, Thrombosis, and Vascular Biology*, 19(4), pp. 996–1003. doi: 10.1161/01.ATV.19.4.996.
Bartoszewski, R. *et al.* (2019) 'Primary endothelial-specific regulation of hypoxiainducible factor (HIF)-1 and HIF-2 and their target gene expression profiles during hypoxia', *FASEB Journal*, 33(7), pp. 7929–7941. doi: 10.1096/fj.201802650RR.
Beall, C. M. *et al.* (2010) 'Natural selection on EPAS1 (HIF2α) associated with low hemoglobin concentration in Tibetan highlanders', *Proceedings of the National Academy of Sciences of the United States of America*, 107(25), pp. 11459–11464. doi: 10.1073/pnas.1002443107.
Beckman, J. A., Creager, M. A. and Libby, P. (2002) 'Diabetes and atherosclerosis: epidemiology, pathophysiology, and management.', *JAMA*. United States, 287(19), pp. 2570–2581.
Bell, D. S. H. (2003) 'Heart failure: the frequent, forgotten, and often fatal complication of diabetes.', *Diabetes care*. United States, 26(8), pp. 2433–2441.
Ben-Aicha, S. *et al.* (2019) 'HDL remodelled in hypercholesterolemic blood induce epigenetically driven downregulation of endothelial HIF-1alpha expression in a preclinical animal model.', *Cardiovascular research*. England. doi: 10.1093/cvr/cvz239.
Ben-Shoshan, J. *et al.* (2009) 'HIF-1alpha overexpression and experimental murine atherosclerosis', *Arteriosclerosis, Thrombosis, and Vascular Biology*, 29(5), pp. 665–670. doi: 10.1161/ATVBAHA.108.183319.
Bergheanu, S. C. (2017) 'Pathophysiology and treatment of atherosclerosis Current view and future perspective on lipoprotein modification treatment', pp. 231–242. doi: 10.1007/s12471-017-0959-2.
Bernardi, R. *et al.* (2006) 'PML inhibits HIF-1alpha translation and neoangiogenesis through repression of mTOR.', *Nature*. England, 442(7104), pp. 779–785. doi: 10.1038/nature05029.
Berra, E. *et al.* (2003) 'HIF prolyl-hydroxylase 2 is the key oxygen sensor setting low steady-state levels of HIF-1alpha in normoxia.', *The EMBO journal*. England, 22(16), pp. 4082–4090. doi: 10.1093/emboj/cdg392.
Bertout, J. A. *et al.* (2009) 'HIF2alpha inhibition promotes p53 pathway activity, tumor cell death, and radiation responses.', *Proceedings of the National Academy of Sciences of the United States of America*. United States, 106(34), pp. 14391–14396. doi: 10.1073/pnas.0907357106.
Biddlestone, J. *et al.* (2018) 'Sinhcaf/fam60a and sin3a specifically repress hif-2α expression', *Biochemical Journal*, 475(12), pp. 2073–2090. doi: 10.1042/BCJ20170945.
Bishop, T. and Ratcliffe, P. J. (2020) 'Genetic basis of oxygen sensing in the carotid body: HIF2α and an isoform switch in cytochrome c oxidase subunit 4', *Science Signaling*, 13(615), pp. 3–5. doi: 10.1126/scisignal.aba1302.
Bjorklund, M. M. *et al.* (2014) 'Induction of atherosclerosis in mice and hamsters without germline genetic engineering.', *Circulation research*. United States, 114(11), pp. 1684–1689. doi: 10.1161/CIRCRESAHA.114.302937.
Blanco-Cedres, L. *et al.* (2002) 'Relation of cigarette smoking to 25-year mortality in middle-aged men with low baseline serum cholesterol: the Chicago Heart Association Detection Project in Industry.', *American journal of epidemiology*. United States, 155(4), pp. 354–360. doi: 10.1093/aje/155.4.354.
Bloch, K. *et al.* (2006) 'Improved activity of streptozotocin-selected insulinoma cells following microencapsulation and transplantation into diabetic mice.', *Cell biology international*. England, 30(2), pp. 138–143. doi: 10.1016/j.cellbi.2005.08.012.
Blondin, G. A. and Green, D. E. (1969) 'Mechanism of mitochondrial swelling. III. Two forms of energized swelling', *Archives of Biochemistry and Biophysics*, 132(2), pp. 509–523. doi: 10.1016/0003-9861(69)90395-6.

De Bock, K. *et al.* (2013) 'Role of PFKFB3-driven glycolysis in vessel sprouting.', *Cell*. United States, 154(3), pp. 651–663. doi: 10.1016/j.cell.2013.06.037.
Boisen, L. *et al.* (2010) 'Evaluation of endothelial cell culture as a model system of vascular ageing', *Experimental Gerontology*, 45(10), pp. 779–787. doi: 10.1016/j.exger.2010.06.003.
Bonello, S. *et al.* (2007) 'Reactive oxygen species activate the HIF-1α promoter via a functional NFκB site', *Arteriosclerosis, Thrombosis, and Vascular Biology*, 27(4), pp. 755–761. doi: 10.1161/01.ATV.0000258979.92828.bc.
Bothe, G. W. M. *et al.* (2004) 'Genetic and behavioral differences among five inbred mouse strains commonly used in the production of transgenic and knockout mice.', *Genes, brain, and behavior*. England, 3(3), pp. 149–157. doi: 10.1111/j.1601-183x.2004.00064.x.
Botusan, I. R. *et al.* (2008) 'Stabilization of HIF-1 is critical to improve wound healing in diabetic mice', *Proceedings of the National Academy of Sciences*, 105(49), pp. 19426–19431. doi: 10.1073/pnas.0805230105.
Bouloumie, A. *et al.* (1998) 'Leptin, the product of Ob gene, promotes angiogenesis.', *Circulation research*. United States, 83(10), pp. 1059–1066.
Branco-Price, C. *et al.* (2012) 'Endothelial cell HIF-1?? and HIF-2?? differentially regulate metastatic success', *Cancer Cell*, 21(1), pp. 52–65. doi: 10.1016/j.ccr.2011.11.017.
Brandes, R. P., Fleming, I. and Busse, R. (2005) 'Endothelial aging.', *Cardiovascular research*. England, 66(2), pp. 286–294. doi: 10.1016/j.cardiores.2004.12.027.
Brown, S. D. M. and Moore, M. W. (2012) 'Towards an encyclopaedia of mammalian gene function: the International Mouse Phenotyping Consortium.', *Disease models & mechanisms*, pp. 289–292. doi: 10.1242/dmm.009878.
Brusselmans, K. *et al.* (2003) 'Heterozygous deficiency of hypoxia-inducible factor-2α protects mice against pulmonary hypertension and right ventricular dysfunction during prolonged hypoxia', *Journal of Clinical Investigation*, 111(10), pp. 1519–1527. doi: 10.1172/JCI200315496.
Bryant, C. D. *et al.* (2008) 'Behavioral differences among C57BL/6 substrains: implications for transgenic and knockout studies.', *Journal of neurogenetics*, 22(4), pp. 315–331. doi: 10.1080/01677060802357388.
Callaghan, F. M. and Grieve, S. M. (2018) 'Translational Physiology: Normal patterns of thoracic aortic wall shear stress measured using four-dimensional flow MRI in a large population', *American Journal of Physiology - Heart and Circulatory Physiology*, 315(5), pp. H1174–H1181. doi: 10.1152/ajpheart.00017.2018.
Callapina, M. *et al.* (2005) 'NO restores HIF-1alpha hydroxylation during hypoxia: role of reactive oxygen species.', *Free radical biology & medicine*. United States, 39(7), pp. 925–936. doi: 10.1016/j.freeradbiomed.2005.05.009.
Camps, C. *et al.* (2014) 'Integrated analysis of microRNA and mRNA expression and association with HIF binding reveals the complexity of microRNA expression regulation under hypoxia.', *Molecular cancer*, 13, p. 28. doi: 10.1186/1476-4598-13-28.
Cancel, L. M. and Tarbell, J. M. (2010) 'The role of apoptosis in LDL transport through cultured endothelial cell monolayers', *Atherosclerosis*, 208(2), p. 335. doi: 10.1016/j.atherosclerosis.2009.07.051.The.
Cancel, L. M. and Tarbell, J. M. (2011) 'The role of mitosis in LDL transport through cultured endothelial cell monolayers.', *American journal of physiology. Heart and circulatory physiology*, 300(3), pp. H769-76. doi: 10.1152/ajpheart.00445.2010.
Cao, Y. *et al.* (2020) 'Comparison of Carotid Atherosclerosis between Patients at High Altitude and Sea Level: A Chinese Atherosclerosis Risk Evaluation Study', *Journal of Stroke and Cerebrovascular Diseases*. Elsevier Inc., 29(2), pp. 1–8. doi: 10.1016/j.jstrokecerebrovasdis.2019.104448.
Capehorn, M. S., Haslam, D. W. and Welbourn, R. (2016) 'Obesity Treatment in the UK

Health System', *Current obesity reports*. Current Obesity Reports, 5(3), pp. 320–326. doi: 10.1007/s13679-016-0221-z.
CARO, C. G., FITZ-GERALD, J. M. and SCHROTER, R. C. (1969) 'Arterial Wall Shear and Distribution of Early Atheroma in Man', *Nature*, 223(5211), pp. 1159–1161. doi: 10.1038/2231159a0.
Catrina, S.-B. *et al.* (2004) 'Hyperglycemia regulates hypoxia-inducible factor-1alpha protein stability and function.', *Diabetes*. United States, 53(12), pp. 3226–3232.
Chan, M. C. *et al.* (2016) 'Pharmacological targeting of the HIF hydroxylases - A new field in medicine development', *Molecular Aspects of Medicine*. Elsevier Ltd, 47–48, pp. 54–75. doi: 10.1016/j.mam.2016.01.001.
Chan, S. Y. *et al.* (2009) 'MicroRNA-210 controls mitochondrial metabolism during hypoxia by repressing the iron-sulfur cluster assembly proteins ISCU1/2.', *Cell metabolism*. United States, 10(4), pp. 273–284. doi: 10.1016/j.cmet.2009.08.015.
Chang, T. C. *et al.* (2005) 'Stabilization of hypoxia-inducible factor-1α by prostacyclin under prolonged hypoxia via reducing reactive oxygen species level in endothelial cells', *Journal of Biological Chemistry*, 280(44), pp. 36567–36574. doi: 10.1074/jbc.M504280200.
Chaudhury, H. *et al.* (2010) 'C-Jun N-terminal kinase primes endothelial cells at atheroprone sites for apoptosis', *Arteriosclerosis, Thrombosis, and Vascular Biology*, 30(3), pp. 546–553. doi: 10.1161/ATVBAHA.109.201368.
Chen, J. X. and Stinnett, A. (2008) 'Ang-1 gene therapy inhibits hypoxia-inducible Factor-1α (HIF-1α)-prolyl-4-hydroxylase-2, stabilizes HIF-1α expression, and normalizes immature vasculature in db/db mice', *Diabetes*, 57(12), pp. 3335–3343. doi: 10.2337/db08-0503.
Chen, P. Y. *et al.* (2015) 'Endothelial-to-mesenchymal transition drives atherosclerosis progression', *Journal of Clinical Investigation*, 125(12), pp. 4514–4528. doi: 10.1172/JCI82719.
Chen, W. *et al.* (2016) 'Targeting renal cell carcinoma with a HIF-2 antagonist.', *Nature*, 539(7627), pp. 112–117. doi: 10.1038/nature19796.
Cheng, C. *et al.* (2006) 'Atherosclerotic lesion size and vulnerability are determined by patterns of fluid shear stress.', *Circulation*. United States, 113(23), pp. 2744–2753. doi: 10.1161/CIRCULATIONAHA.105.590018.
Cheng, C. P., Herfkens, R. J. and Taylor, C. A. (2003a) 'Abdominal aortic hemodynamic conditions in healthy subjects aged 50-70 at rest and during lower limb exercise: In vivo quantification using MRI', *Atherosclerosis*, 168(2), pp. 323–331. doi: 10.1016/S0021-9150(03)00099-6.
Cheng, C. P., Herfkens, R. J. and Taylor, C. A. (2003b) 'Comparison of abdominal aortic hemodynamics between men and women at rest and during lower limb exercise', *Journal of Vascular Surgery*, 37(1), pp. 118–123. doi: 10.1067/mva.2002.107.
Chiba, T. *et al.* (2008) 'Leptin deficiency suppresses progression of atherosclerosis in apoE-deficient mice', 196, pp. 68–75. doi: 10.1016/j.atherosclerosis.2007.01.040.
Chien, S. (2008) 'Role of shear stress direction in endothelial mechanotransduction.', *Molecular & cellular biomechanics : MCB*. United States, 5(1), pp. 1–8.
Cho, H. *et al.* (2016) 'On-target efficacy of a HIF-2α antagonist in preclinical kidney cancer models', *Nature Publishing Group*. Nature Publishing Group, 539(7627), pp. 107–111. doi: 10.1038/nature19795.
Christoph, M. *et al.* (2014) 'Local inhibition of hypoxia-inducible factor reduces neointima formation after arterial injury in ApoE-/- mice', *Atherosclerosis*. Elsevier Ltd, 233(2), pp. 641–647. doi: 10.1016/j.atherosclerosis.2014.01.048.
Coleman, D. L. and Hummel, K. P. (1973) 'The influence of genetic background on the expression of the obese (ob) gene in the mouse', *Diabetologia*, 9(4), pp. 287–293. doi: 10.1007/BF01221856.

Collins, C. and Tzima, E. (2011) 'Hemodynamic forces in endothelial dysfunction and vascular aging.', *Experimental gerontology*, 46(2–3), pp. 185–188. doi: 10.1016/j.exger.2010.09.010.
Comino-Méndez, I. *et al.* (2013) 'Tumoral EPAS1 (HIF2A) mutations explain sporadic pheochromocytoma and paraganglioma in the absence of erythrocytosis', *Human Molecular Genetics*, 22(11), pp. 2169–2176. doi: 10.1093/hmg/ddt069.
Compernolle, V. *et al.* (2002) 'Loss of HIF-2alpha and inhibition of VEGF impair fetal lung maturation, whereas treatment with VEGF prevents fatal respiratory distress in premature mice.', *Nature medicine*. United States, 8(7), pp. 702–710. doi: 10.1038/nm721.
Conrad, P. W. *et al.* (1999) 'EPAS1 trans-Activation during Hypoxia Requires p42/p44 MAPK*', *Journal of Biological Chemistry*, 274(47), pp. 33709–33713. doi: https://doi.org/10.1074/jbc.274.47.33709.
Coon, B. G. *et al.* (2015) 'Intramembrane binding of VE-cadherin to VEGFR2 and VEGFR3 assembles the endothelial mechanosensory complex.', *The Journal of cell biology*. United States, 208(7), pp. 975–986. doi: 10.1083/jcb.201408103.
Correia-Melo, C. *et al.* (2016) 'Mitochondria are required for pro-ageing features of the senescent phenotype', *The EMBO Journal*, 35(7), pp. 724–742. doi: 10.15252/embj.201592862.
Cotto-Rios, X. M. *et al.* (2012) 'Deubiquitinases as a Signaling Target of Oxidative Stress', *Cell Reports*, 2(6), pp. 1475–1484. doi: 10.1016/j.celrep.2012.11.011.
Cowburn, A. S. *et al.* (2016) 'HIF2α-Arginase axis is essential for the development of pulmonary hypertension', *Proceedings of the National Academy of Sciences of the United States of America*, 113(31), pp. 8801–8806. doi: 10.1073/pnas.1602978113.
Creager, M. A. *et al.* (2011) 'Effect of Hypoxia-Inducible Factor-1 ␣ Gene Therapy Intermittent Claudication'. doi: 10.1161/CIRCULATIONAHA.110.009407.
Crews, S. T. (1998) 'Control of cell lineage-specefic development and transcription by bHLH-PAS proteins', *Genes Dev.*, (919), pp. 607–620. doi: 10.1101/gad.12.5.607.
Cruzeiro, G. A. V. *et al.* (2018) 'HIF1A is Overexpressed in Medulloblastoma and its Inhibition Reduces Proliferation and Increases EPAS1 and ATG16L1 Methylation.', *Current cancer drug targets*. Netherlands, 18(3), pp. 287–294. doi: 10.2174/1568009617666170315162525.
Cui, J. *et al.* (2016) 'MBD3 mediates epigenetic regulation on EPAS1 promoter in cancer.', *Tumour biology : the journal of the International Society for Oncodevelopmental Biology and Medicine*. United States, 37(10), pp. 13455–13467. doi: 10.1007/s13277-016-5237-1.
Culic, O., Gruwel, M. L. and Schrader, J. (1997) 'Energy turnover of vascular endothelial cells.', *The American journal of physiology*. United States, 273(1 Pt 1), pp. C205-13. doi: 10.1152/ajpcell.1997.273.1.C205.
Cummins, E. P. *et al.* (2006) 'Prolyl hydroxylase-1 negatively regulates IκB kinase-β, giving insight into hypoxia-induced NFκB activity', *Proceedings of the National Academy of Sciences*, 103(48), pp. 18154 LP – 18159. doi: 10.1073/pnas.0602235103.
Cybulsky, M. I. and Gimbrone, M. A. J. (1991) 'Endothelial expression of a mononuclear leukocyte adhesion molecule during atherogenesis.', *Science (New York, N.Y.)*. United States, 251(4995), pp. 788–791.
Dagda, R. K. *et al.* (2009) 'Loss of PINK1 function promotes mitophagy through effects on oxidative stress and mitochondrial fission', *Journal of Biological Chemistry*, 284(20), pp. 13843–13855. doi: 10.1074/jbc.M808515200.
Dahia, P. L. M. (2014) 'Pheochromocytoma and paraganglioma pathogenesis: Learning from genetic heterogeneity', *Nature Reviews Cancer*. Nature Publishing Group, 14(2), pp. 108–119. doi: 10.1038/nrc3648.
Dahlman, J. E. *et al.* (2015) 'NIH Public Access', 9(8), pp. 648–655. doi:

10.1038/nnano.2014.84.In.
Dai, G. *et al.* (2004) 'Distinct endothelial phenotypes evoked by arterial waveforms derived from atherosclerosis-susceptible and -resistant regions of human vasculature.', *Proceedings of the National Academy of Sciences of the United States of America*, 101(41), pp. 14871–14876. doi: 10.1073/pnas.0406073101.
Dai, Z. *et al.* (2016) 'Prolyl-4 Hydroxylase 2 (PHD2) deficiency in endothelial cells and hematopoietic cells induces obliterative vascular remodeling and severe pulmonary arterial hypertension in mice and humans through hypoxia-inducible factor-2??', *Circulation*, 133(24), pp. 2447–2458. doi: 10.1161/CIRCULATIONAHA.116.021494.
Dai, Z. *et al.* (2018) 'Therapeutic Targeting of Vascular Remodeling and Right Heart Failure in Pulmonary Arterial Hypertension with a HIF-2α Inhibitor.', *American journal of respiratory and critical care medicine*, 198(11), pp. 1423–1434. doi: 10.1164/rccm.201710-2079OC.
Davies, P. F. *et al.* (1986) 'Turbulent fluid shear stress induces vascular endothelial cell turnover in vitro.', *Proceedings of the National Academy of Sciences of the United States of America*, 83(7), pp. 2114–7. doi: 10.1073/pnas.83.7.2114.
Davies, P. F. *et al.* (2013) 'The atherosusceptible endothelium: Endothelial phenotypes in complex haemodynamic shear stress regions in vivo', *Cardiovascular Research*, 99(2), pp. 315–327. doi: 10.1093/cvr/cvt101.
Deeds, M. C. *et al.* (2011) 'Single dose streptozotocin-induced diabetes: Considerations for study design in islet transplantation models', *Laboratory Animals*, 45(3), pp. 131–140. doi: 10.1258/la.2010.010090.
Dejana, E. ; Corada, M. ; Lampugnani, M. G. (1995) 'Endothelial cell-to-cell junctions', *FASEB journal : official publication of the Federation of American Societies for Experimental Biology*, 9(10), pp. 910–918.
Dixon, J. L. *et al.* (2002) 'Increased atherosclerosis in diabetic dyslipidemic swine: protection by atorvastatin involves decreased VLDL triglycerides but minimal effects on the lipoprotein profile', *Journal of Lipid Research*, 43(10), pp. 1618–1629. doi: 10.1194/jlr.M200134-JLR200.
Van Doormaal, M. a *et al.* (2012) 'Haemodynamics in the mouse aortic arch computed from MRI-derived velocities at the aortic root.', *Journal of the Royal Society, Interface / the Royal Society*, 9(76), pp. 2834–44. doi: 10.1098/rsif.2012.0295.
Doronzo, G. *et al.* (2006) 'Insulin activates hypoxia-inducible factor-1α in human and rat vascular smooth muscle cells via phosphatidylinositol-3 kinase and mitogen-activated protein kinase pathways: Impairment in insulin resistance owing to defects in insulin signalling', *Diabetologia*, 49(5), pp. 1049–1063. doi: 10.1007/s00125-006-0156-0.
Downes, N. L. *et al.* (2018) 'Differential but Complementary HIF1α and HIF2α Transcriptional Regulation', *Molecular Therapy*, 26(7), pp. 1735–1745. doi: 10.1016/j.ymthe.2018.05.004.
Du, X. L. *et al.* (2000) 'Hyperglycemia-induced mitochondrial superoxide overproduction activates the hexosamine pathway and induces plasminogen activator inhibitor-1 expression by increasing Sp1 glycosylation.', *Proceedings of the National Academy of Sciences of the United States of America*. United States, 97(22), pp. 12222–12226. doi: 10.1073/pnas.97.22.12222.
Duan, L. J., Zhang-Benoit, Y. and Fong, G. H. (2005) 'Endothelium-intrinsic requirement for Hif-2α during vascular development', *Circulation*, 111(17), pp. 2227–2232. doi: 10.1161/01.CIR.0000163580.98098.A3.
Dumont, D. J. *et al.* (1995) 'Vascularization of the mouse embryo: a study of flk-1, tek, tie, and vascular endothelial growth factor expression during development.', *Developmental dynamics : an official publication of the American Association of Anatomists*. United States,

203(1), pp. 80–92. doi: 10.1002/aja.1002030109.
Ellett, J. D. *et al.* (2009) 'A rapid PCR-based method for the identification of ob mutant mice', *Obesity*, 17(2), pp. 402–404. doi: 10.1038/oby.2008.443.
Ema, M. *et al.* (1997) 'A novel bHLH-PAS factor with close sequence similarity to hypoxia-inducible factor 1α regulates the VEGF expression and is potentially involved in lung and vascular development', *Proceedings of the National Academy of Sciences of the United States of America*, 94(9), pp. 4273–4278. doi: 10.1073/pnas.94.9.4273.
Ema, M. *et al.* (1999) 'Molecular mechanisms of transcription activation by HLF and HIF1alpha in response to hypoxia: their stabilization and redox signal-induced interaction with CBP/p300.', *The EMBO journal*, 18(7), pp. 1905–1914. doi: 10.1093/emboj/18.7.1905.
Endler, A. *et al.* (2013) 'Int6/eIF3e silenced HIF2α stabilization enhances migration and tube formation of HUVECs via IL-6 and IL-8 signaling', *Cytokine*. Elsevier Ltd, 62(1), pp. 115–122. doi: 10.1016/j.cyto.2013.01.021.
Enesa, K. *et al.* (2008) 'Hydrogen peroxide prolongs nuclear localization of NF-κB in activated cells by suppressing negative regulatory mechanisms', *Journal of Biological Chemistry*, 283(27), pp. 18582–18590. doi: 10.1074/jbc.M801312200.
Engelbrecht, E. *et al.* (2020) 'Sphingosine 1-phosphate-regulated transcriptomes in heterogenous arterial and lymphatic endothelium of the aorta', *eLife*, 9, pp. 1–37. doi: 10.7554/eLife.52690.
Epstein, A. C. *et al.* (2001) 'C. elegans EGL-9 and mammalian homologs define a family of dioxygenases that regulate HIF by prolyl hydroxylation.', *Cell*. United States, 107(1), pp. 43–54.
Evans, P. C. *et al.* (2003) 'A novel type of deubiquitinating enzyme.', *The Journal of biological chemistry*. United States, 278(25), pp. 23180–23186. doi: 10.1074/jbc.M301863200.
Evrard, S. M. *et al.* (2016) 'Endothelial to mesenchymal transition is common in atherosclerotic lesions and is associated with plaque instability', *Nature Communications*, 7(May). doi: 10.1038/ncomms11853.
Ezzati, M. *et al.* (2005) 'Role of smoking in global and regional cardiovascular mortality', *Circulation*, 112(4), pp. 489–497. doi: 10.1161/CIRCULATIONAHA.104.521708.
Faeh, D., Gutzwiller, F. and Bopp, M. (2009) 'Lower mortality from coronary heart disease and stroke at higher altitudes in Switzerland', *Circulation*, 120(6), pp. 495–501. doi: 10.1161/CIRCULATIONAHA.108.819250.
Faergeman, O. *et al.* (2009) 'Plasma triglycerides and cardiovascular events in the Treating to New Targets and Incremental Decrease in End-Points through Aggressive Lipid Lowering trials of statins in patients with coronary artery disease.', *The American journal of cardiology*. United States, 104(4), pp. 459–463. doi: 10.1016/j.amjcard.2009.04.008.
Fafián-Labora, J. *et al.* (2019) 'FASN activity is important for the initial stages of the induction of senescence', *Cell Death and Disease*, 10(4). doi: 10.1038/s41419-019-1550-0.
Falkenberg, K. D. *et al.* (2019a) 'The metabolic engine of endothelial cells', *Nature Metabolism*. Springer US, 1(10), pp. 937–946. doi: 10.1038/s42255-019-0117-9.
Falkenberg, K. D. *et al.* (2019b) 'The metabolic engine of endothelial cells', *Nature Metabolism*. Springer US, 1(10), pp. 937–946. doi: 10.1038/s42255-019-0117-9.
Favier, J. *et al.* (1999) 'Cloning and expression pattern of EPAS1 in the chicken embryo: Colocalization with tyrosine hydroxylase', *FEBS Letters*, 462(1–2), pp. 19–24. doi: 10.1016/S0014-5793(99)01476-3.
Favier, J. *et al.* (2001) 'Coexpression of endothelial PAS protein 1 with essential angiogenic factors suggests its involvement in human vascular development', *Developmental Dynamics*, 222(3), pp. 377–388. doi: 10.1002/dvdy.1207.
Feng, S. *et al.* (2017) 'Mechanical Activation of Hypoxia-Inducible Factor 1alpha Drives

Endothelial Dysfunction at Atheroprone Sites.', *Arteriosclerosis, thrombosis, and vascular biology*. United States, 37(11), pp. 2087–2101. doi: 10.1161/ATVBAHA.117.309249.
Ferrucci, L. and Fabbri, E. (2018) 'Inflammageing: chronic inflammation in ageing, cardiovascular disease, and frailty', *Nature Reviews Cardiology*. Springer US, 15(9), pp. 505–522. doi: 10.1038/s41569-018-0064-2.
Fielding, J. W. *et al.* (2018) 'PHD2 inactivation in Type I cells drives HIF-2α-dependent multilineage hyperplasia and the formation of paraganglioma-like carotid bodies.', *The Journal of physiology*, 596(18), pp. 4393–4412. doi: 10.1113/JP275996.
Flores, A. M. *et al.* (2019) 'Nanoparticle Therapy for Vascular Diseases', *Arteriosclerosis, thrombosis, and vascular biology*, 39(4), pp. 635–646. doi: 10.1161/ATVBAHA.118.311569.
Fong, G. H. *et al.* (1995) 'Role of the Flt-1 receptor tyrosine kinase in regulating the assembly of vascular endothelium.', *Nature*. England, 376(6535), pp. 66–70. doi: 10.1038/376066a0.
Fong, G. H. and Takeda, K. (2008) 'Role and regulation of prolyl hydroxylase domain proteins', *Cell Death and Differentiation*, 15(4), pp. 635–641. doi: 10.1038/cdd.2008.10.
Forsythe, J. A. *et al.* (1996) 'Activation of vascular endothelial growth factor gene transcription by hypoxia-inducible factor 1.', *Molecular and cellular biology*. United States, 16(9), pp. 4604–4613.
Foteinos, G. and Xu, Q. (2009) 'Immune-mediated mechanisms of endothelial damage in atherosclerosis.', *Autoimmunity*. England, 42(7), pp. 627–633.
Frede, S. *et al.* (2006) 'Bacterial lipopolysaccharide induces HIF-1 activation in human monocytes via p44/42 MAPK and NF-κB', *Biochemical Journal*, 396(3), pp. 517–527. doi: 10.1042/BJ20051839.
Freiberg, J. J. *et al.* (2008) 'Nonfasting triglycerides and risk of ischemic stroke in the general population.', *JAMA*. United States, 300(18), pp. 2142–2152. doi: 10.1001/jama.2008.621.
Fuchs, F. D. and Whelton, P. K. (2020) 'High Blood Pressure and Cardiovascular Disease.', *Hypertension (Dallas, Tex. : 1979)*. United States, 75(2), pp. 285–292. doi: 10.1161/HYPERTENSIONAHA.119.14240.
Fuhrmann, D. C. and Brune, B. (2017) 'Mitochondrial composition and function under the control of hypoxia', *Redox Biology*. Elsevier B.V., 12(January), pp. 208–215. doi: 10.1016/j.redox.2017.02.012.
Gao, L. *et al.* (2017) 'Gene expression analyses reveal metabolic specifications in acute O2-sensing chemoreceptor cells', *Journal of Physiology*, 595(18), pp. 6091–6120. doi: 10.1113/JP274684.
Gareus, R. *et al.* (2008) 'Endothelial cell-specific NF-kappaB inhibition protects mice from atherosclerosis.', *Cell metabolism*. United States, 8(5), pp. 372–383. doi: 10.1016/j.cmet.2008.08.016.
Getz, G. S. and Reardon, C. A. (2006) 'Diet and murine atherosclerosis', *Arteriosclerosis, Thrombosis, and Vascular Biology*, 26(2), pp. 242–249. doi: 10.1161/01.ATV.0000201071.49029.17.
Ghesquière, B. *et al.* (2014) 'Metabolism of stromal and immune cells in health and disease', *Nature*, 511(7508), pp. 167–176. doi: 10.1038/nature13312.
Gimbrone, M. A. J. *et al.* (2000) 'Endothelial dysfunction, hemodynamic forces, and atherogenesis.', *Annals of the New York Academy of Sciences*. United States, 902, pp. 230–240.
Gnarra, J. R. *et al.* (1994) 'Mutations of the VHL tumour suppressor gene in renal carcinoma', *Nature Genetics*, 7(1), pp. 85–90. doi: 10.1038/ng0594-85.
Goldstein, J. L. and Brown, M. S. (1977) 'Atherosclerosis: the low-density lipoprotein receptor hypothesis.', *Metabolism: clinical and experimental*. United States, 26(11), pp. 1257–1275.

Gong, H. *et al.* (2015) 'HIF2?? signaling inhibits adherens junctional disruption in acute lung injury', *Journal of Clinical Investigation*, 125(2), pp. 652–664. doi: 10.1172/JCI77701.
González, E. L. M. *et al.* (2009) 'Trends in the prevalence and incidence of diabetes in the UK: 1996-2005.', *Journal of epidemiology and community health*. England, 63(4), pp. 332–336. doi: 10.1136/jech.2008.080382.
Gordan, J. D. *et al.* (2007) 'HIF-2alpha promotes hypoxic cell proliferation by enhancing c-myc transcriptional activity.', *Cancer cell*. United States, 11(4), pp. 335–347. doi: 10.1016/j.ccr.2007.02.006.
Groschner, L. N. *et al.* (2012) 'Endothelial mitochondria--less respiration, more integration.', *Pflugers Archiv : European journal of physiology*. Germany, 464(1), pp. 63–76. doi: 10.1007/s00424-012-1085-z.
Gruber, M. *et al.* (2007) 'Acute postnatal ablation of Hif-2alpha results in anemia.', *Proceedings of the National Academy of Sciences of the United States of America*, 104(7), pp. 2301–6. doi: 10.1073/pnas.0608382104.
Gu, Y. Z. *et al.* (1998) 'Molecular characterization and chromosomal localization of a third alpha-class hypoxia inducible factor subunit, HIF3alpha.', *Gene expression*. United States, 7(3), pp. 205–213.
Gurley, S. B. *et al.* (2006) 'Impact of genetic background on nephropathy in diabetic mice', *American Journal of Physiology - Renal Physiology*, 290(1), pp. 214–222. doi: 10.1152/ajprenal.00204.2005.
Gustafsson, E. *et al.* (2001) 'Tie-1-directed expression of Cre recombinase in endothelial cells of embryoid bodies and transgenic mice', *Journal of Cell Science*, 114(4), pp. 671–676.
Guzy, R. D. and Schumacker, P. T. (2006) 'Oxygen sensing by mitochondria at complex III: the paradox of increased reactive oxygen species during hypoxia.', *Experimental physiology*. England, 91(5), pp. 807–819. doi: 10.1113/expphysiol.2006.033506.
Hagberg, C. E. *et al.* (2010) 'Vascular endothelial growth factor B controls endothelial fatty acid uptake', *Nature*, 464(7290), pp. 917–921. doi: 10.1038/nature08945.
Hagen, T. *et al.* (2003) 'Redistribution of intracellular oxygen in hypoxia by nitric oxide: effect on HIF1alpha.', *Science (New York, N.Y.)*. United States, 302(5652), pp. 1975–1978. doi: 10.1126/science.1088805.
Hagensen, M. K. *et al.* (2012) 'Circulating endothelial progenitor cells do not contribute to regeneration of endothelium after murine arterial injury', *Cardiovascular Research*, 93(2), pp. 223–231. doi: 10.1093/cvr/cvr278.
Hahne, M. *et al.* (2018) 'Unraveling the role of hypoxia-inducible factor (HIF)-1α and HIF-2α in the adaption process of human microvascular endothelial cells (HMEC-1) to hypoxia: Redundant HIF-dependent regulation of macrophage migration inhibitory factor.', *Microvascular research*. United States, 116, pp. 34–44. doi: 10.1016/j.mvr.2017.09.004.
Hamada, S. *et al.* (2009) 'Synthesis and activity of N-oxalylglycine and its derivatives as Jumonji C-domain-containing histone lysine demethylase inhibitors.', *Bioorganic & medicinal chemistry letters*. England, 19(10), pp. 2852–2855. doi: 10.1016/j.bmcl.2009.03.098.
Hansson, G. K. *et al.* (1985) 'Aortic endothelial cell death and replication in normal and lipopolysaccharide-treated rats.', *The American journal of pathology*, 121(1), pp. 123–127.
Hayashi, K., Kojima, R. and Ito, M. (2006) 'Strain differences in the diabetogenic activity of streptozotocin in mice', *Biological and Pharmaceutical Bulletin*, 29(6), pp. 1110–1119. doi: 10.1248/bpb.29.1110.
Hegele, R. A. *et al.* (2014) 'The polygenic nature of hypertriglyceridaemia: implications for definition, diagnosis, and management.', *The lancet. Diabetes & endocrinology*, 2(8), pp. 655–666. doi: 10.1016/S2213-8587(13)70191-8.
Hernandez-Segura, A., Nehme, J. and Demaria, M. (2018) 'Hallmarks of Cellular

Senescence', *Trends in Cell Biology*. Elsevier Ltd, 28(6), pp. 436–453. doi: 10.1016/j.tcb.2018.02.001.
Hilzendeger, A. M. *et al.* (2010) 'Leptin regulates ACE activity in mice', *Journal of Molecular Medicine*, 88(9), pp. 899–907. doi: 10.1007/s00109-010-0649-7.
Ho, J. J. D. *et al.* (2012) 'Functional importance of dicer protein in the adaptive cellular response to hypoxia', *Journal of Biological Chemistry*, 287(34), pp. 29003–29020. doi: 10.1074/jbc.M112.373365.
Hu, C.-J. *et al.* (2006) 'Differential regulation of the transcriptional activities of hypoxia-inducible factor 1 alpha (HIF-1alpha) and HIF-2alpha in stem cells.', *Molecular and cellular biology*. United States, 26(9), pp. 3514–3526. doi: 10.1128/MCB.26.9.3514-3526.2006.
Hu, C.-J. *et al.* (2007) 'The N-terminal transactivation domain confers target gene specificity of hypoxia-inducible factors HIF-1alpha and HIF-2alpha.', *Molecular biology of the cell*, 18(11), pp. 4528–4542. doi: 10.1091/mbc.e06-05-0419.
Huang, L. *et al.* (2019) 'HHS Public Access', 569(7757), pp. 565–569. doi: 10.1038/s41586-019-1140-4.SR-B1.
Hudson, C. C. *et al.* (2002) 'Regulation of hypoxia-inducible factor 1alpha expression and function by the mammalian target of rapamycin.', *Molecular and cellular biology*, 22(20), pp. 7004–7014. doi: 10.1128/mcb.22.20.7004-7014.2002.
Hussein, K., Percy, M. and McMullin, M. F. (2012) 'Clinical utility gene card for: Familial erythrocytosis', *European Journal of Human Genetics*. Nature Publishing Group, 20(5), p. 593. doi: 10.1038/ejhg.2011.252.
Iliopoulos, O. *et al.* (1996) 'Negative regulation of hypoxia-inducible genes by the von Hippel-Lindau protein.', *Proceedings of the National Academy of Sciences of the United States of America*, 93(20), pp. 10595–10599. doi: 10.1073/pnas.93.20.10595.
Iorga, A. *et al.* (2017) 'The protective role of estrogen and estrogen receptors in cardiovascular disease and the controversial use of estrogen therapy.', *Biology of sex differences*, 8(1), p. 33. doi: 10.1186/s13293-017-0152-8.
Ito, K. *et al.* (2004) 'Oxidative stress reduces histone deacetylase 2 activity and enhances IL-8 gene expression: Role of tyrosine nitration', *Biochemical and Biophysical Research Communications*, 315(1), pp. 240–245. doi: 10.1016/j.bbrc.2004.01.046.
Ivan, M. and Kaelin, W. G. J. (2001) 'The von Hippel-Lindau tumor suppressor protein.', *Current opinion in genetics & development*. England, 11(1), pp. 27–34.
Janaszak-Jasiecka, A. *et al.* (2016) 'miR-429 regulates the transition between Hypoxia-Inducible Factor (HIF)1A and HIF3A expression in human endothelial cells.', *Scientific reports*. Nature Publishing Group, 6, p. 22775. doi: 10.1038/srep22775.
Jiang, G. *et al.* (2007) 'RNA interference for HIF-1?? inhibits foam cells formation in vitro', *European Journal of Pharmacology*, 562(3), pp. 183–190. doi: 10.1016/j.ejphar.2007.01.066.
Jiang, X. *et al.* (2019) 'Endothelial Hypoxia-Inducible Factor-2 Is Required for the Maintenance of Airway Microvasculature', *Circulation*, 139(4), pp. 502–517. doi: 10.1161/CIRCULATIONAHA.118.036157.
Jing Zhou, Yi-Shuan Li, and S. C. (2014) 'Shear stress-initiated signaling and its regulation of endothelial function', *Arterioscler Thromb Vasc Biol.*, 71(11), pp. 3831–3840. doi: 10.1158/0008-5472.CAN-10-4002.BONE.
Kadlec, A. O. *et al.* (2016) 'Mitochondrial signaling in the vascular endothelium: beyond reactive oxygen species.', *Basic research in cardiology*, 111(3), p. 26. doi: 10.1007/s00395-016-0546-5.
Kalluri, A. S. *et al.* (2019) 'Single-Cell Analysis of the Normal Mouse Aorta Reveals Functionally Distinct Endothelial Cell Populations', *Circulation*, 140(2), pp. 147–163. doi: 10.1161/CIRCULATIONAHA.118.038362.
Kalucka, J. *et al.* (2018) 'Quiescent Endothelial Cells Upregulate Fatty Acid β-Oxidation for

Vasculoprotection via Redox Homeostasis', *Cell Metabolism*, 28(6), pp. 881-894.e13. doi: 10.1016/j.cmet.2018.07.016.
Kamata, H. *et al.* (2005) 'Reactive oxygen species promote TNFα-induced death and sustained JNK activation by inhibiting MAP kinase phosphatases', *Cell*, 120(5), pp. 649–661. doi: 10.1016/j.cell.2004.12.041.
Kang, J.-G. *et al.* (2016) 'Low ambient oxygen prevents atherosclerosis.', *Journal of molecular medicine (Berlin, Germany)*, 94(3), pp. 277–286. doi: 10.1007/s00109-016-1386-3.
Kannel, W. B. and McGee, D. L. (1979) 'Diabetes and cardiovascular disease. The Framingham study.', *JAMA*. United States, 241(19), pp. 2035–2038.
Kapitsinou, P. P. *et al.* (2014) 'Endothelial HIF-2 mediates protection and recovery from ischemic kidney injury.', *The Journal of clinical investigation*, 124(6), pp. 2396–2409. doi: 10.1172/JCI69073.
Kapitsinou, P. P. *et al.* (2016) 'Factor 2 Axis Regulates Pulmonary Artery Pressure in Mice', *Molecular and Cellular Biology*, 36(10), pp. 1584–1594. doi: 10.1128/MCB.01055-15.Address.
Karshovska, E. *et al.* (2007) 'Expression of HIF-1 in Injured Arteries Controls SDF-1 Mediated Neointima Formation in Apolipoprotein E Deficient Mice', *Arteriosclerosis, Thrombosis, and Vascular Biology*, 27(12), pp. 2540–2547. doi: 10.1161/ATVBAHA.107.151050.
Katavetin, P. *et al.* (2006) 'High glucose blunts vascular endothelial growth factor response to hypoxia via the oxidative stress-regulated hypoxia-inducible factor/hypoxia-responsible element pathway', *Journal of the American Society of Nephrology*, 17(5), pp. 1405–1413. doi: 10.1681/ASN.2005090918.
Kawachi, I. *et al.* (1994) 'Smoking cessation and time course of decreased risks of coronary heart disease in middle-aged women.', *Archives of internal medicine*. United States, 154(2), pp. 169–175.
Keith, B., Johnson, R. S. and Simon, M. C. (2011) 'HIF1alpha and HIF2alpha: sibling rivalry in hypoxic tumour growth and progression.', *Nature reviews. Cancer*. England, 12(1), pp. 9–22. doi: 10.1038/nrc3183.
Kennedy, A. J. *et al.* (2010) 'Mouse models of the metabolic syndrome.', *Disease models & mechanisms*. England, 3(3–4), pp. 156–166. doi: 10.1242/dmm.003467.
Khan, O. F. *et al.* (2018) 'Endothelial siRNA delivery in nonhuman primates using ionizable low–molecular weight polymeric nanoparticles', *Science Advances*, 4(6), pp. 1–11. doi: 10.1126/sciadv.aar8409.
Kim, A. J., Alfieri, C. M. and Yutzey, K. E. (2019) 'Endothelial Cell Lineage Analysis Does Not Provide Evidence for EMT in Adult Valve Homeostasis and Disease.', *Anatomical record (Hoboken, N.J. : 2007)*, 302(1), pp. 125–135. doi: 10.1002/ar.23916.
Kluge, M. A. (2013) 'Mitochondria and Endothelial Function', *Bone*, 23(1), pp. 1–7. doi: 10.1038/jid.2014.371.
Köhl, R., Zhou, J. and Brüne, B. (2006) 'Reactive oxygen species attenuate nitric-oxide-mediated hypoxia-inducible factor-1alpha stabilization.', *Free radical biology & medicine*. United States, 40(8), pp. 1430–1442. doi: 10.1016/j.freeradbiomed.2005.12.012.
Kolesnichenko, M. *et al.* (2012) 'Attenuation of TORC1 signaling delays replicative and oncogenic RAS-induced senescence.', *Cell cycle (Georgetown, Tex.)*, 11(12), pp. 2391–2401. doi: 10.4161/cc.20683.
Kolodgie, F. D. *et al.* (2004) 'The accumulation of specific types of proteoglycans in eroded plaques: A role in coronary thrombosis in the absence of rupture', *Current Opinion in Lipidology*, 15(5), pp. 575–582. doi: 10.1097/00041433-200410000-00012.
Kolodgie FD, Burke AP, Farb A, Gold HK, Yuan J, Narula J, F. A. (2001) 'The thin-cap

fibroatheroma: a type of vulnerable plaque: the major precursor lesion to acute coronary syndromes.', *Curr Opin Cardiol.*, 16, pp. 285–292.
Kong, K. H. *et al.* (2017) 'Selective tubular activation of hypoxia-inducible factor-2α has dual effects on renal fibrosis', *Scientific Reports*. Springer US, 7(1), pp. 1–12. doi: 10.1038/s41598-017-11829-2.
Konstantinides, S. *et al.* (2001) 'Leptin-dependent platelet aggregation and arterial thrombosis suggests a mechanism for atherothrombotic disease in obesity.', *The Journal of clinical investigation*. United States, 108(10), pp. 1533–1540. doi: 10.1172/JCI13143.
Kuboki, K. *et al.* (2000) 'Regulation of endothelial constitutive nitric oxide synthase gene expression in endothelial cells and in vivo : a specific vascular action of insulin.', *Circulation*. United States, 101(6), pp. 676–681.
Kuhlmann, M. T. *et al.* (2012) 'Implantation of a carotid cuff for triggering shear-stress induced atherosclerosis in mice.', *Journal of visualized experiments : JoVE*, (59). doi: 10.3791/3308.
Kunjathoor, V. V, Wilson, D. L. and Leboeuf, R. C. (1996) 'Increased atherosclerosis in streptozotocin- induced diabetic mice . Find the latest version ':, 97(7), pp. 1767–1773.
Kuo, A., Lee, M. Y. and Sessa, W. C. (2017) 'Lipid Droplet Biogenesis and Function in the Endothelium.', *Circulation research*, 120(8), pp. 1289–1297. doi: 10.1161/CIRCRESAHA.116.310498.
Lakatta, E. G. and Levy, D. (2003) 'Arterial and cardiac aging: major shareholders in cardiovascular disease enterprises: Part I: aging arteries: a "set up" for vascular disease.', *Circulation*. United States, 107(1), pp. 139–146. doi: 10.1161/01.cir.0000048892.83521.58.
Lamack, J. A. *et al.* (2010) 'Endothelial gene expression in regions of defined shear exposure in the porcine iliac arteries', *Annals of Biomedical Engineering*, 38(7), pp. 2252–2262. doi: 10.1007/s10439-010-0030-6.
Land, S. C. and Tee, A. R. (2007) 'Hypoxia-inducible factor 1alpha is regulated by the mammalian target of rapamycin (mTOR) via an mTOR signaling motif.', *The Journal of biological chemistry*. United States, 282(28), pp. 20534–20543. doi: 10.1074/jbc.M611782200.
Lando, D. *et al.* (2002) 'FIH-1 is an asparaginyl hydroxylase enzyme that regulates the transcriptional activity of hypoxia-inducible factor.', *Genes & development*. United States, 16(12), pp. 1466–1471. doi: 10.1101/gad.991402.
Law, M. R., Morris, J. K. and Wald, N. J. (2009) 'Use of blood pressure lowering drugs in the prevention of cardiovascular disease: meta-analysis of 147 randomised trials in the context of expectations from prospective epidemiological studies.', *BMJ (Clinical research ed.)*, 338, p. b1665. doi: 10.1136/bmj.b1665.
Lee, F. S. and Percy, M. J. (2011) 'The HIF Pathway and Erythrocytosis', *Annual Review of Pathology: Mechanisms of Disease*, 6(1), pp. 165–192. doi: 10.1146/annurev-pathol-011110-130321.
Lee, Y. S. *et al.* (2015) 'Increased Adipocyte O2 Consumption Triggers HIF-1α Causing Inflammation and Insulin Resistance in Obesity', *Cell*, 157(6), pp. 1339–1352. doi: 10.1016/j.cell.2014.05.012.Increased.
Libby, P.; Ridker, P. M.; Hansson, G. K. (2011) 'Progress and challenges in translating the biology of atherosclerosis', *Nature*, 473, pp. 317–325. doi: 10.1038/nature10146.
Libby, P. (2012) 'Inflammation in atherosclerosis', *Arteriosclerosis, Thrombosis, and Vascular Biology*, 32(9), pp. 2045–2051. doi: 10.1161/ATVBAHA.108.179705.
Lin, K. *et al.* (2000) 'Molecular mechanism of endothelial growth arrest by laminar shear stress', *Proceedings of the National Academy of Sciences*, 97(17), pp. 9385–9389. doi: 10.1073/pnas.170282597.
Liu, J. *et al.* (2020) 'Acute antioxidant and cytoprotective effects of sulforaphane in brain

endothelial cells and astrocytes during inflammation and excitotoxicity', *Pharmacology Research and Perspectives*, 8(4), pp. 1–11. doi: 10.1002/prp2.630.
Liu, P. *et al.* (2017) 'Sulforaphane exerts anti-angiogenesis effects against hepatocellular carcinoma through inhibition of STAT3/HIF-1α/VEGF signalling', *Scientific Reports*. Springer US, 7(1), pp. 1–11. doi: 10.1038/s41598-017-12855-w.
Liu, Y.-C. *et al.* (2008) 'Sulforaphane inhibition of monocyte adhesion via the suppression of ICAM-1 and NF-kappaB is dependent upon glutathione depletion in endothelial cells.', *Vascular pharmacology*. United States, 48(1), pp. 54–61. doi: 10.1016/j.vph.2007.11.006.
Loffreda, S. *et al.* (1998) 'Leptin regulates proinflammatory immune responses.', *FASEB journal : official publication of the Federation of American Societies for Experimental Biology*. United States, 12(1), pp. 57–65.
Lopez-Quintero, S. V *et al.* (2013) 'High glucose attenuates shear-induced changes in endothelial hydraulic conductivity by degrading the glycocalyx.', *PloS one*. United States, 8(11), p. e78954. doi: 10.1371/journal.pone.0078954.
Lorenzo, F. R. *et al.* (2014) 'A genetic mechanism for Tibetan high-altitude adaptation', *Nature Genetics*, 46(9), pp. 951–956. doi: 10.1038/ng.3067.
Lutgens, E. *et al.* (1999) 'Biphasic pattern of cell turnover characterizes the progression from fatty streaks to ruptured human atherosclerotic plaques.', *Cardiovascular research*. England, 41(2), pp. 473–479.
Ma, X. *et al.* (2017) 'Hypoxia-inducible factor 2 (HIF-2) promotes colon cancer growth by potentiating Yes-associated protein 1 (YAP1) activity', *Journal of Biological Chemistry*, 292(41), pp. 17046–17056. doi: 10.1074/jbc.M117.805655.
Maas, A. H. E. M. and Appelman, Y. E. A. (2010) 'Gender differences in coronary heart disease.', *Netherlands heart journal : monthly journal of the Netherlands Society of Cardiology and the Netherlands Heart Foundation*, 18(12), pp. 598–602. doi: 10.1007/s12471-010-0841-y.
Macias, D. *et al.* (2018) 'Correction: HIF-2α is essential for carotid body development and function', *eLife*, 7, pp. 1–26. doi: 10.7554/elife.38781.
Mack, J. J. *et al.* (2017) 'NOTCH1 is a mechanosensor in adult arteries.', *Nature communications*. England, 8(1), p. 1620. doi: 10.1038/s41467-017-01741-8.
Mack, J. J. and Iruela-Arispe, M. L. (2018) 'NOTCH regulation of the endothelial cell phenotype.', *Current opinion in hematology*. United States, 25(3), pp. 212–218. doi: 10.1097/MOH.0000000000000425.
Mader, J. *et al.* (2020) 'Oxygen-dependent asparagine hydroxylation of the ubiquitin-associated (UBA) domain in Cezanne regulates ubiquitin binding', *Journal of Biological Chemistry*, 295(8), pp. 2160–2174. doi: 10.1074/jbc.RA119.010315.
Mahmoud, M. M. *et al.* (2016) 'TWIST1 Integrates Endothelial Responses to Flow in Vascular Dysfunction and Atherosclerosis.', *Circulation research*. United States, 119(3), pp. 450–462. doi: 10.1161/CIRCRESAHA.116.308870.
Mahmoud, M. M. *et al.* (2017) 'Shear stress induces endothelial-To-mesenchymal transition via the transcription factor Snail', *Scientific Reports*, 7(1), pp. 1–12. doi: 10.1038/s41598-017-03532-z.
Mai, S. *et al.* (2010) 'Decreased expression of Drp1 and Fis1 mediates mitochondrial elongation in senescent cells and enhances resistance to oxidative stress through PINK1', *Journal of Cell Science*, 123(6), pp. 917–926. doi: 10.1242/jcs.059246.
Majesky, M. W. (2007) 'Developmental basis of vascular smooth muscle diversity', *Arteriosclerosis, Thrombosis, and Vascular Biology*, 27(6), pp. 1248–1258. doi: 10.1161/ATVBAHA.107.141069.
Marcelo, K. K. L., Goldie, L. C. L. and Hirschi, K. K. K. (2013) 'Regulation of Endothelial Cell Differentiation and Specification', *Circulation research*, 112(9), pp. 1272–1287. doi:

10.1161/CIRCRESAHA.113.300506.Regulation.
Mark, A. L. *et al.* (1999) 'Contrasting blood pressure effects of obesity in leptin-deficient ob/ob mice and agouti yellow obese mice', *Journal of Hypertension*, 17(12 SUPPL.), pp. 1949–1953. doi: 10.1097/00004872-199917121-00026.
Masson, N. and Ratcliffe, P. J. (2014) 'Hypoxia signaling pathways in cancer metabolism: the importance of co-selecting interconnected physiological pathways.', *Cancer & metabolism*, 2(1), p. 3. doi: 10.1186/2049-3002-2-3.
Matsuo, N. *et al.* (2010) 'Behavioral profiles of three C57BL/6 substrains.', *Frontiers in behavioral neuroscience*, 4, p. 29. doi: 10.3389/fnbeh.2010.00029.
Matsuura, H. *et al.* (2013) 'Prolyl hydroxylase domain protein 2 plays a critical role in diet-induced obesity and glucose intolerance', *Circulation*, 127(21), pp. 2078–2087. doi: 10.1161/CIRCULATIONAHA.113.001742.
Maxwell, P. H. *et al.* (1993) 'Identification of the renal erythropoietin-producing cells using transgenic mice', *Kidney International*. Elsevier Masson SAS, 44(5), pp. 1149–1162. doi: 10.1038/ki.1993.362.
Maxwell, P. H. *et al.* (1999) 'The tumour suppressor protein VHL targets hypoxia-inducible factors for oxygen-dependent proteolysis.', *Nature*, 399(6733), pp. 271–275. doi: 10.1038/20459.
Mehta, V. and Tzima, E. (2016) 'Cardiovascular disease: A turbulent path to plaque formation.', *Nature*. England, 540(7634), pp. 531–532. doi: 10.1038/nature20489.
Michael A., G. J. and Guillermo, G.-C. (2016) 'Endothelial cell dysfunction and the pathobiology of atherosclerosis.', *Circulation Research*, 176(1), pp. 139–148. doi: 10.1016/j.physbeh.2017.03.040.
Michiels, C. (2003) 'Endothelial cell functions', *Journal of Cellular Physiology*, 196(3), pp. 430–443. doi: 10.1002/jcp.10333.
Mohlin, S. *et al.* (2015) 'PI3K-mTORC2 but not PI3K-mTORC1 regulates transcription of HIF2A/EPAS1and vascularization in neuroblastoma', *Cancer Research*, 75(21), pp. 4617–4628. doi: 10.1158/0008-5472.CAN-15-0708.
Moniz, S. *et al.* (2015) 'Cezanne regulates E2F1-dependent HIF2alpha expression.', *Journal of cell science*. England, 128(16), pp. 3082–3093. doi: 10.1242/jcs.168864.
Moonen, J. R. A. J. *et al.* (2015) 'Endothelial-to-mesenchymal transition contributes to fibro-proliferative vascular disease and is modulated by fluid shear stress', *Cardiovascular Research*, 108(3), pp. 377–386. doi: 10.1093/cvr/cvv175.
Morello, E. *et al.* (2018) 'Hypoxia-inducible factor 2α drives nonalcoholic fatty liver progression by triggering hepatocyte release of histidine-rich glycoprotein', *Hepatology*, 67(6), pp. 2196–2214. doi: 10.1002/hep.29754.
Moreno-Domínguez, A. *et al.* (2020) 'Acute O2 sensing through HIF2α-dependent expression of atypical cytochrome oxidase subunits in arterial chemoreceptors', *Science Signaling*, 13(615). doi: 10.1126/scisignal.aay9452.
Mortimer, E. A. J., Monson, R. R. and MacMahon, B. (1977) 'Reduction in mortality from coronary heart disease in men residing at high altitude.', *The New England journal of medicine*. United States, 296(11), pp. 581–585. doi: 10.1056/NEJM197703172961101.
van Mourik, J. A. *et al.* (1985) 'Vascular endothelial cells synthesize a plasma membrane protein indistinguishable from the platelet membrane glycoprotein IIa', *Journal of Biological Chemistry*, 260(20), pp. 11300–11306.
Mylonis, I. *et al.* (2006) 'Identification of MAPK phosphorylation sites and their role in the localization and activity of hypoxia-inducible factor-1alpha.', *The Journal of biological chemistry*. United States, 281(44), pp. 33095–33106. doi: 10.1074/jbc.M605058200.
Mylonis, I. *et al.* (2008) 'Atypical CRM1-dependent Nuclear Export Signal Mediates Regulation of Hypoxia-inducible Factor-1α by MAPK*', *Journal of Biological Chemistry*,

283(41), pp. 27620–27627. doi: https://doi.org/10.1074/jbc.M803081200.
Nagel, T. *et al.* (1994) 'Shear stress selectively upregulates intercellular adhesion molecule-1 expression in cultured human vascular endothelial cells.', *The Journal of clinical investigation*. United States, 94(2), pp. 885–891. doi: 10.1172/JCI117410.
Nakano, D. *et al.* (2005) 'Chronic hypoxia accelerates the progression of atherosclerosis in apolipoprotein E-knockout mice', *Hypertension Research*, 28(10), pp. 837–845. doi: 10.1291/hypres.28.837.
Nakata, M. *et al.* (1999) 'Leptin promotes aggregation of human platelets via the long form of its receptor.', *Diabetes*. United States, 48(2), pp. 426–429.
Nakazawa, M. S. *et al.* (2016) 'Epigenetic re-expression of HIF-2α suppresses soft tissue sarcoma growth', *Nature Communications*. Nature Publishing Group, 7. doi: 10.1038/ncomms10539.
Nam, D. *et al.* (2009) 'Partial carotid ligation is a model of acutely induced disturbed flow, leading to rapid endothelial dysfunction and atherosclerosis.', *American journal of physiology. Heart and circulatory physiology*. United States, 297(4), pp. H1535-43. doi: 10.1152/ajpheart.00510.2009.
Narita, Masako *et al.* (2011) 'Spatial coupling of mTOR and autophagy augments secretory phenotypes.', *Science (New York, N.Y.)*, 332(6032), pp. 966–970. doi: 10.1126/science.1205407.
Nerem, R. M. (1993) 'Hemodynamics and the vascular endothelium.', *Journal of biomechanical engineering*, 115(4B), pp. 510–4. doi: 10.1115/1.2895532.
Nigro, J. *et al.* (2006) 'Insulin Resistance and Atherosclerosis', 27(3), pp. 242–259. doi: 10.1210/er.2005-0007.
North, B. J. and Sinclair, D. A. (2012) 'The intersection between aging and cardiovascular disease.', *Circulation research*, 110(8), pp. 1097–1108. doi: 10.1161/CIRCRESAHA.111.246876.
Oldendorf, W. H., Cornford, M. E. and Brown, W. J. (1977) 'The large apparent work capability of the blood-brain barrier: a study of the mitochondrial content of capillary endothelial cells in brain and other tissues of the rat.', *Annals of neurology*. United States, 1(5), pp. 409–417. doi: 10.1002/ana.410010502.
Paffett-Lugassy, N. *et al.* (2013) 'Heart field origin of great vessel precursors relies on nkx2.5-mediated vasculogenesis.', *Nature cell biology*. Nature Publishing Group, 15(11), pp. 1362–9. doi: 10.1038/ncb2862.
Pan, Y. *et al.* (2007) 'Multiple Factors Affecting Cellular Redox Status and Energy Metabolism Modulate Hypoxia-Inducible Factor Prolyl Hydroxylase Activity In Vivo and In Vitro', *Molecular and Cellular Biology*, 27(3), pp. 912–925. doi: 10.1128/mcb.01223-06.
Pangou, E. *et al.* (2016) 'HIF-2α phosphorylation by CK1δ promotes erythropoietin secretion in liver cancer cells under hypoxia', *Journal of Cell Science*, 129(22), pp. 4213–4226. doi: 10.1242/jcs.191395.
Parathath, S. *et al.* (2011) 'Hypoxia is present in murine atherosclerotic plaques and has multiple adverse effects on macrophage lipid metabolism.', *Circulation research*. United States, 109(10), pp. 1141–1152. doi: 10.1161/CIRCRESAHA.111.246363.
Pardanaud, L. *et al.* (1996) 'Two distinct endothelial lineages in ontogeny , one of them related to hemopoiesis', 1371, pp. 1363–1371.
Parmar, K. M. *et al.* (2005) 'Statins exert endothelial atheroprotective effects via the KLF2 transcription factor', *Journal of Biological Chemistry*, 280(29), pp. 26714–26719. doi: 10.1074/jbc.C500144200.
Passerini, A. G. *et al.* (2004) 'Coexisting proinflammatory and antioxidative endothelial transcription profiles in a disturbed flow region of the adult porcine aorta.', *Proceedings of the National Academy of Sciences of the United States of America*, 101(8), pp. 2482–7. doi:

10.1073/pnas.0305938101.
Peng, J. *et al.* (2000) 'The transcription factor EPAS-1/hypoxia-inducible factor 2alpha plays an important role in vascular remodeling.', *Proceedings of the National Academy of Sciences of the United States of America*. United States, 97(15), pp. 8386–8391. doi: 10.1073/pnas.140087397.
Peng, Y. *et al.* (2017) 'Down-regulation of EPAS1 transcription and genetic adaptation of tibetans to high-altitude hypoxia', *Molecular Biology and Evolution*, 34(4), pp. 818–830. doi: 10.1093/molbev/msw280.
Pugh, C. W. and Ratcliffe, P. J. (2003) 'Regulation of angiogenesis by hypoxia: role of the HIF system.', *Nature medicine*, 9(6), pp. 677–684. doi: 10.1038/nm0603-677.
Qi, D. *et al.* (2017) 'GW28-e0958 Hypoxia-Inducible Factor-2α Activation in Vascular Smooth Muscle Cells Accelerates Atherogenesis in ApoE-/- Mice', *Journal of the American College of Cardiology*. Elsevier, 70(16), p. C36. doi: 10.1016/j.jacc.2017.07.123.
Qu, A. *et al.* (2011) 'Hypoxia-inducible transcription factor 2α promotes steatohepatitis through augmenting lipid accumulation, inflammation, and fibrosis', *Hepatology*, 54(2), pp. 472–483. doi: 10.1002/hep.24400.
Qutub, A. A. and Popel, A. S. (2008) 'Reactive Oxygen Species Regulate Hypoxia-Inducible Factor 1α Differentially in Cancer and Ischemia', *Molecular and Cellular Biology*, 28(16), pp. 5106–5119. doi: 10.1128/mcb.00060-08.
Rahtu-Korpela, L. *et al.* (2014) 'HIF prolyl 4-hydroxylase-2 inhibition improves glucose and lipid metabolism and protects against obesity and metabolic dysfunction', *Diabetes*, 63(10), pp. 3324–3333. doi: 10.2337/db14-0472.
Rahtu-Korpela, L. *et al.* (2016) 'Hypoxia-Inducible Factor Prolyl 4-Hydroxylase-2 Inhibition Protects Against Development of Atherosclerosis', *Arteriosclerosis, Thrombosis, and Vascular Biology*, 36(4), pp. 608–617. doi: 10.1161/ATVBAHA.115.307136.
Ramakrishnan, S. K. *et al.* (2016) 'HIF2α Is an essential molecular brake for postprandial hepatic glucagon response independent of insulin signaling', *Cell Metabolism*. Elsevier Ltd, 23(3), pp. 505–516. doi: 10.1016/j.cmet.2016.01.004.
Rankin, E. B. *et al.* (2007) 'Regulates Hepatic Erythropoietin in Vivo', *The Journal of Clinical Investigation*, 117(4), pp. 1068–1077. doi: 10.1172/JCI30117.1068.
Rankin, E. B. *et al.* (2009) 'Hypoxia-Inducible Factor 2 Regulates Hepatic Lipid Metabolism', *Molecular and Cellular Biology*, 29(16), pp. 4527–4538. doi: 10.1128/MCB.00200-09.
Ratcliffe, P. J. (2007) 'HIF-1 and HIF-2: Working alone or together in hypoxia?', *Journal of Clinical Investigation*, 117(4), pp. 862–865. doi: 10.1172/JCI31750.
Richard, D. E. *et al.* (1999) 'p42/p44 Mitogen-activated Protein Kinases Phosphorylate Hypoxia-inducible Factor 1α (HIF-1α) and Enhance the Transcriptional Activity of HIF-1*', *Journal of Biological Chemistry*, 274(46), pp. 32631–32637. doi: https://doi.org/10.1074/jbc.274.46.32631.
Rius, J. *et al.* (2008) 'NF-kappaB links innate immunity to the hypoxic response through transcriptional regulation of HIF-1alpha.', *Nature*. England, 453(7196), pp. 807–811. doi: 10.1038/nature06905.
Rodier, F. and Campisi, J. (2011) 'Four faces of cellular senescence.', 192(4), pp. 547–556. doi: 10.1083/jcb.201009094.
Rosenson, R. S. *et al.* (2014) 'Genetics and causality of triglyceride-rich lipoproteins in atherosclerotic cardiovascular disease.', *Journal of the American College of Cardiology*. United States, 64(23), pp. 2525–2540. doi: 10.1016/j.jacc.2014.09.042.
Sabatini, D. M. (2006) 'mTOR and cancer: insights into a complex relationship.', *Nature reviews. Cancer*. England, pp. 729–734. doi: 10.1038/nrc1974.
Sahlgren, C. *et al.* (2008) 'Notch signaling mediates hypoxia-induced tumor cell migration

and invasion.', *Proceedings of the National Academy of Sciences of the United States of America*. United States, 105(17), pp. 6392–6397. doi: 10.1073/pnas.0802047105.
Salahuddin, S., Prabhakaran, D. and Roy, A. (2012) 'Pathophysiological Mechanisms of Tobacco-Related CVD.', *Global heart*. England, 7(2), pp. 113–120. doi: 10.1016/j.gheart.2012.05.003.
Saldana, M. J., Salem, L. E. and Travezan, R. (1973) 'High altitude hypoxia and chemodectomas.', *Human pathology*. United States, 4(2), pp. 251–263. doi: 10.1016/s0046-8177(73)80012-7.
Sang, N. *et al.* (2003) 'MAPK Signaling Up-regulates the Activity of Hypoxia-inducible Factors by Its Effects on p300*', *Journal of Biological Chemistry*, 278(16), pp. 14013–14019. doi: https://doi.org/10.1074/jbc.M209702200.
Santilli, S. M. *et al.* (1995) 'Transarterial wall oxygen gradients at the dog carotid bifurcation', *American Journal of Physiology - Heart and Circulatory Physiology*, 268(1), pp. H155–H161. Available at: http://ajpheart.physiology.org/content/268/1/H155.abstract.
Sato, M. *et al.* (2004) 'The PAI-1 gene as a direct target of endothelial PAS domain protein-1 in adenocarcinoma A549 cells', *American Journal of Respiratory Cell and Molecular Biology*, 31(2 I), pp. 209–215. doi: 10.1165/rcmb.2003-0296OC.
Sato, T. N. *et al.* (1995) 'Distinct roles of the receptor tyrosine kinases Tie-1 and Tie-2 in blood vessel formation', *Nature*, 376(6535), pp. 70–74. Available at: http://dx.doi.org/10.1038/376070a0.
Satta, S. *et al.* (2017) 'The Role of Nrf2 in Cardiovascular Function and Disease', *Oxidative Medicine and Cellular Longevity*. Hindawi, 2017. doi: 10.1155/2017/9237263.
Savransky, V. *et al.* (no date) 'Chronic Intermittent Hypoxia Induces Atherosclerosis'. doi: 10.1164/rccm.200612-1771OC.
Schober, A., Nazari-Jahantigh, M. and Weber, C. (2015) 'MicroRNA-mediated mechanisms of the cellular stress response in atherosclerosis', *Nat Rev Cardiol*, 12(6), pp. 361–374. doi: 10.1038/nrcardio.2015.38.
Schofield, C. J. and Ratcliffe, P. J. (2005) 'Signalling hypoxia by HIF hydroxylases', *Biochemical and Biophysical Research Communications*, 338(1), pp. 617–626. doi: 10.1016/j.bbrc.2005.08.111.
Schoors, S. *et al.* (2015) 'Fatty acid carbon is essential for dNTP synthesis in endothelial cells', *Nature*, 520(7546), pp. 192–197. doi: 10.1038/nature14362.
Schuster, S. J. *et al.* (1989) 'Stimulation of erythropoietin gene transcription during hypoxia and cobalt exposure.', *Blood*. United States, 73(1), pp. 13–16.
Schwartz, M. A. and DeSimone, D. W. (2008) 'Cell adhesion receptors in mechanotransduction.', *Current opinion in cell biology*. England, 20(5), pp. 551–556. doi: 10.1016/j.ceb.2008.05.005.
Scortegagna, M. *et al.* (2003) 'Multiple organ pathology, metabolic abnormalities and impaired homeostasis of reactive oxygen species in Epas1-/- mice.', *Nature genetics*. United States, 35(4), pp. 331–340. doi: 10.1038/ng1266.
Scortegagna, M. *et al.* (2005) 'HIF-2α regulates murine hematopoietic development in an erythropoietin-dependent manner', *Blood*, 105(8), pp. 3133–3140. doi: 10.1182/blood-2004-05-1695.
Sedelnikova, O. A. *et al.* (2004) 'Senescing human cells and ageing mice accumulate DNA lesions with unrepairable double-strand breaks.', *Nature cell biology*. England, 6(2), pp. 168–170. doi: 10.1038/ncb1095.
Semenza, G. L. *et al.* (1996) 'Assignment of the hypoxia-inducible factor 1alpha gene to a region of conserved synteny on mouse chromosome 12 and human chromosome 14q.', *Genomics*. United States, 34(3), pp. 437–439. doi: 10.1006/geno.1996.0311.
Semenza, G. L. (2019) 'Pharmacologic Targeting of Hypoxia-Inducible Factors'.

Serbanovic-canic, J. *et al.* (2016) 'A zebrafish model for functional screening of flow-responsive genes', 44(0), pp. 1–27.
Serocki, M. *et al.* (2018) 'miRNAs regulate the HIF switch during hypoxia: a novel therapeutic target', *Angiogenesis*. Springer Netherlands, 21(2), pp. 183–202. doi: 10.1007/s10456-018-9600-2.
Shah, M. S. and Brownlee, M. (2016) 'Molecular and Cellular Mechanisms of Cardiovascular Disorders in Diabetes.', *Circulation research*. United States, 118(11), pp. 1808–1829. doi: 10.1161/CIRCRESAHA.116.306923.
Shalaby, F. *et al.* (1995) 'Failure of blood-island formation and vasculogenesis in Flk-1-deficient mice', *Nature*, 376(6535), pp. 62–66. Available at: http://dx.doi.org/10.1038/376062a0.
Shan, Y. *et al.* (2010) 'Protective effect of sulforaphane on human vascular endothelial cells against lipopolysaccharide-induced inflammatory damage', *Cardiovascular Toxicology*, 10(2), pp. 139–145. doi: 10.1007/s12012-010-9072-0.
Shan, Y. *et al.* (2012) 'Sulphoraphane inhibited the expressions of intercellular adhesion molecule-1 and vascular cell adhesion molecule-1 through MyD88-dependent toll-like receptor-4 pathway in cultured endothelial cells.', *Nutrition, metabolism, and cardiovascular diseases : NMCD*. Netherlands, 22(3), pp. 215–222. doi: 10.1016/j.numecd.2010.06.013.
Shay, J. E. S. *et al.* (2014) 'Inhibition of hypoxia-inducible factors limits tumor progression in a mouse model of colorectal cancer.', *Carcinogenesis*. England, 35(5), pp. 1067–1077. doi: 10.1093/carcin/bgu004.
Shehatou, G. S. G. and Suddek, G. M. (2016) 'Sulforaphane attenuates the development of atherosclerosis and improves endothelial dysfunction in hypercholesterolemic rabbits', *Experimental Biology and Medicine*, 241(4), pp. 426–436. doi: 10.1177/1535370215609695.
Shek, E. W., Brands, W. and Hall, J. E. (1998) 'Chronic infusion of leptin increases arterial pressure', *Hypertension*.
Shenouda, S. M. *et al.* (2011) 'Altered mitochondrial dynamics contributes to endothelial dysfunction in diabetes mellitus', *Circulation*, 124(4), pp. 444–453. doi: 10.1161/CIRCULATIONAHA.110.014506.
Simon, M. M. *et al.* (2013) 'A comparative phenotypic and genomic analysis of C57BL/6J and C57BL/6N mouse strains.', *Genome biology*, 14(7), p. R82. doi: 10.1186/gb-2013-14-7-r82.
Skuli, N., Liu, L., Runge, A., Wang, T., Yuan, L., Patel, S., Iruela-Arispe, L., *et al.* (2009) 'Endothelial deletion of hypoxia-inducible factor-2alpha (HIF-2alpha) alters vascular function and tumor angiogenesis.', *Blood*. United States, 114(2), pp. 469–477. doi: 10.1182/blood-2008-12-193581.
Skuli, N., Liu, L., Runge, A., Wang, T., Yuan, L., Patel, S., Iruela-arispe, L., *et al.* (2009) 'Endothelial deletion of hypoxia-inducible factor – 2 alfa (HIF-2alfa) alters vascular function and tumor angiogenesis', *Blood*, 114(2), pp. 469–477. doi: 10.1182/blood-2008-12-193581.
Skuli, N. *et al.* (2012) 'Endothelial HIF-2alpha regulates murine pathological angiogenesis and revascularization processes.', *The Journal of clinical investigation*. United States, 122(4), pp. 1427–1443. doi: 10.1172/JCI57322.
Sluimer, J. C. *et al.* (2008) 'Hypoxia, Hypoxia-Inducible Transcription Factor, and Macrophages in Human Atherosclerotic Plaques Are Correlated With Intraplaque Angiogenesis', *Journal of the American College of Cardiology*, 51(13), pp. 1258–1265. doi: 10.1016/j.jacc.2007.12.025.
Sluimer, J. C. and Daemen, M. J. (2009) 'Novel concepts in atherogenesis: angiogenesis and hypoxia in atherosclerosis.', *The Journal of pathology*. England, 218(1), pp. 7–29. doi: 10.1002/path.2518.
Son, N.-H. *et al.* (2018) 'Endothelial cell CD36 optimizes tissue fatty acid uptake.', *The*

Journal of clinical investigation, 128(10), pp. 4329–4342. doi: 10.1172/JCI99315.
Souilhol, C. *et al.* (2018) 'Endothelial-mesenchymal transition in atherosclerosis', *Cardiovascular Research*, 114(4), pp. 565–577. doi: 10.1093/cvr/cvx253.
De Souza, C. G. *et al.* (2016) 'Sulforaphane ameliorates the insulin responsiveness and the lipid profile but does not alter the antioxidant response in diabetic rats', *Food and Function*. Royal Society of Chemistry, 7(4), pp. 2060–2065. doi: 10.1039/c5fo01620g.
Stavik, B. *et al.* (2016) 'EPAS1/HIF-2 alpha-mediated downregulation of tissue factor pathway inhibitor leads to a pro-thrombotic potential in endothelial cells', *Biochimica et Biophysica Acta - Molecular Basis of Disease*. Elsevier B.V., 1862(4), pp. 670–678. doi: 10.1016/j.bbadis.2016.01.017.
Stenmark, K. R., Fagan, K. A. and Frid, M. G. (2006) 'Hypoxia-induced pulmonary vascular remodeling: Cellular and molecular mechanisms', *Circulation Research*, 99(7), pp. 675–691. doi: 10.1161/01.RES.0000243584.45145.3f.
Steunou, A. L. *et al.* (2013) 'Identification of the hypoxia-inducible factor 2α nuclear interactome in melanoma cells reveals master proteins involved in melanoma development', *Molecular and Cellular Proteomics*, 12(3), pp. 736–748. doi: 10.1074/mcp.M112.020727.
Stratton, I. M. *et al.* (2000) 'Association of glycaemia with macrovascular and microvascular complications of type 2 diabetes (UKPDS 35): prospective observational study.', *BMJ (Clinical research ed.)*. England, 321(7258), pp. 405–412.
Tabas, I. (2010) 'Macrophage death and defective inflammation resolution in atherosclerosis.', *Nature reviews. Immunology*, 10(1), pp. 36–46. doi: 10.1038/nri2675.
Tabas, I., Williams, K. J. and Borén, J. (2007) 'Subendothelial lipoprotein retention as the initiating process in atherosclerosis: Update and therapeutic implications', *Circulation*, 116(16), pp. 1832–1844. doi: 10.1161/CIRCULATIONAHA.106.676890.
Takeda, N. *et al.* (2004) 'Endothelial PAS domain protein 1 gene promotes angiogenesis through the transactivation of both vascular endothelial growth factor and its receptor, Flt-1', *Circulation Research*, 95(2), pp. 146–153. doi: 10.1161/01.RES.0000134920.10128.b4.
Tan, Q. *et al.* (2013) 'Erythrocytosis and pulmonary hypertension in a mouse model of human HIF2A gain of function mutation', *Journal of Biological Chemistry*, 288(24), pp. 17134–17144. doi: 10.1074/jbc.M112.444059.
Tang, H. *et al.* (2018) 'Endothelial HIF-2α contributes to severe pulmonary hypertension due to endothelial-to-mesenchymal transition', *American Journal of Physiology - Lung Cellular and Molecular Physiology*, 314(2), pp. L256–L275. doi: 10.1152/ajplung.00096.2017.
Tang, N. *et al.* (2004) 'Loss of HIF-1alpha in endothelial cells disrupts a hypoxia-driven VEGF autocrine loop necessary for tumorigenesis.', *Cancer cell*. United States, 6(5), pp. 485–495. doi: 10.1016/j.ccr.2004.09.026.
Taniguchi, C. M. *et al.* (2013) 'Cross-talk between hypoxia and insulin signaling through Phd3 regulates hepatic glucose and lipid metabolism and ameliorates diabetes.', *Nature medicine*. United States, 19(10), pp. 1325–1330. doi: 10.1038/nm.3294.
Taylor, C. T. and Pouyssegur, J. (2007) 'Oxygen, hypoxia, and stress', *Annals of the New York Academy of Sciences*, 1113, pp. 87–94. doi: 10.1196/annals.1391.004.
Thimmulappa, R. K. *et al.* (2002) 'Identification of Nrf2-regulated genes induced by the chemopreventive agent sulforaphane by oligonucleotide microarray', *Cancer Research*, 62(18), pp. 5196–5203.
Thomas, G. V *et al.* (2006) 'Hypoxia-inducible factor determines sensitivity to inhibitors of mTOR in kidney cancer.', *Nature medicine*. United States, 12(1), pp. 122–127. doi: 10.1038/nm1337.
Tian, H. *et al.* (1998) 'The hypoxia-responsive transcription factor EPAS1 is essential for catecholamine homeostasis and protection against heart failure during embryonic development.', *Genes & development*. United States, 12(21), pp. 3320–3324.

Tian, H., Mcknight, S. L. and Russell, D. W. (1997) ‘ndothelial PAS domain protein 1 . y EPAS1), a transcription factor selectively expressed in endothelial cells’, pp. 72–82. doi: 10.1101/gad.11.1.72.
Toledo, R. A. *et al.* (2013) ‘In vivo and in vitro oncogenic effects of HIF2A mutations in pheochromocytomas and paragangliomas’, *Endocrine-Related Cancer*, 20(3), pp. 349–359. doi: 10.1530/ERC-13-0101.
Topper, J. N. *et al.* (1996) ‘Identification of vascular endothelial genes differentially responsive to fluid mechanical stimuli: cyclooxygenase-2, manganese superoxide dismutase, and endothelial cell nitric oxide synthase are selectively up-regulated by steady laminar shear stress.’, *Proceedings of the National Academy of Sciences of the United States of America*, 93(19), pp. 10417–10422. doi: 10.1073/pnas.93.19.10417.
Toth, P. P. (2016) ‘Triglyceride-rich lipoproteins as a causal factor for cardiovascular disease’, *Vascular Health and Risk Management*, 12, pp. 171–183. doi: 10.2147/VHRM.S104369.
Treins, C. *et al.* (2002) ‘Insulin Stimulates Hypoxia-inducible Factor 1 through a Phosphatidylinositol 3-Kinase/Target of Rapamycin-dependent Signaling Pathway*’, *Journal of Biological Chemistry*, 277(31), pp. 27975–27981. doi: https://doi.org/10.1074/jbc.M204152200.
Triantafyllou, A. *et al.* (2006) ‘Cobalt induces hypoxia-inducible factor-1α (HIF-1α) in HeLa cells by an iron-independent, but ROS-, PI-3K- and MAPK-dependent mechanism’, *Free Radical Research*. Taylor & Francis, 40(8), pp. 847–856. doi: 10.1080/10715760600730810.
Tzima, E. *et al.* (2005) ‘A mechanosensory complex that mediates the endothelial cell response to fluid shear stress’, *Nature*, 437(7057), pp. 426–431. doi: Doi 10.1038/Nature03952.
van Uden, P., Kenneth, N. S. and Rocha, S. (2008) ‘Regulation of hypoxia-inducible factor-1alpha by NF-kappaB.’, *The Biochemical journal*. England, 412(3), pp. 477–484. doi: 10.1042/BJ20080476.
Uryga, A. K. and Bennett, M. R. (2016) ‘Ageing induced vascular smooth muscle cell senescence in atherosclerosis’, *Journal of Physiology*, 594(8), pp. 2115–2124. doi: 10.1113/JP270923.
Vasa, M. *et al.* (2000) ‘Nitric oxide activates telomerase and delays endothelial cell senescence.’, *Circulation research*. United States, 87(7), pp. 540–542. doi: 10.1161/01.res.87.7.540.
Vecchione, C. *et al.* (2009) ‘Pressure-induced vascular oxidative stress is mediated through activation of integrin-linked kinase 1/betaPIX/Rac-1 pathway.’, *Hypertension (Dallas, Tex. : 1979)*. United States, 54(5), pp. 1028–1034. doi: 10.1161/HYPERTENSIONAHA.109.136572.
Velayutham, P., Babu, A. and Petersen, C. (2016) ‘Sulforaphane and atherosclerosis’, *Glucosinolates*. doi: 10.1007/978-3-319-26479-0.
Vink, A. *et al.* (2007) ‘HIF-1 alpha expression is associated with an atheromatous inflammatory plaque phenotype and upregulated in activated macrophages.’, *Atherosclerosis*. Ireland, 195(2), pp. e69-75. doi: 10.1016/j.atherosclerosis.2007.05.026.
Vizán, P. *et al.* (2009) ‘Characterization of the metabolic changes underlying growth factor angiogenic activation: Identification of new potential therapeutic targets’, *Carcinogenesis*, 30(6), pp. 946–952. doi: 10.1093/carcin/bgp083.
Van Der Wal, A. C. *et al.* (1994) ‘Site of intimal rupture or erosion of thrombosed coronary atherosclerotic plaques is characterized by an inflammatory process irrespective of the dominant plaque morphology’, *Circulation*, 89(1), pp. 36–44. doi: 10.1161/01.CIR.89.1.36.
Wallace, E. M. *et al.* (2016) ‘A Small-Molecule Antagonist of HIF2 a Is Ef fi cacious in Preclinical Models of Renal Cell Carcinoma’, pp. 5491–5501. doi: 10.1158/0008-5472.CAN-

16-0473.
Walpola, P. L. *et al.* (1995) 'Expression of ICAM-1 and VCAM-1 and monocyte adherence in arteries exposed to altered shear stress.', *Arteriosclerosis, thrombosis, and vascular biology*. United States, 15(1), pp. 2–10.
Wang, C. *et al.* (2013) 'Endothelial cell sensing of flow direction', *Arteriosclerosis, Thrombosis, and Vascular Biology*. doi: 10.1161/ATVBAHA.113.301826.
Wang, G. L. *et al.* (1995) 'Hypoxia-inducible factor 1 is a basic-helix-loop-helix-PAS heterodimer regulated by cellular 02 tension', *Genetics*, 92(June), pp. 5510–5514. doi: 10.1073/pnas.92.12.5510.
Wang, G. L. and Semenza, G. L. (1993) 'Characterization of hypoxia-inducible factor 1 and regulation of DNA binding activity by hypoxia.', *The Journal of biological chemistry*. United States, 268(29), pp. 21513–21518.
Wang, L. *et al.* (2016) 'Integrin-YAP/TAZ-JNK cascade mediates atheroprotective effect of unidirectional shear flow.', *Nature*. England, 540(7634), pp. 579–582. doi: 10.1038/nature20602.
Wang, Y. I. *et al.* (2011) 'Endothelial inflammation correlates with subject triglycerides and waist size after a high-fat meal', *American Journal of Physiology - Heart and Circulatory Physiology*, 300(3). doi: 10.1152/ajpheart.01036.2010.
Warboys, C. M. *et al.* (2014) 'Disturbed flow promotes endothelial senescence via a p53-dependent pathway', *Arteriosclerosis, Thrombosis, and Vascular Biology*, 34(5), pp. 985–995. doi: 10.1161/ATVBAHA.114.303415.
Weinberg, P. D. and Ross Ethier, C. (2007) 'Twenty-fold difference in hemodynamic wall shear stress between murine and human aortas', *Journal of Biomechanics*, 40(7), pp. 1594–1598. doi: 10.1016/j.jbiomech.2006.07.020.
Wendt, T. *et al.* (2006) 'RAGE modulates vascular inflammation and atherosclerosis in a murine model of type 2 diabetes', *Atherosclerosis*, 185(1), pp. 70–77. doi: 10.1016/j.atherosclerosis.2005.06.013.
Westrate, L. M. *et al.* (2014) 'Mitochondrial morphological features are associated with fission and fusion events', *PLoS ONE*, 9(4). doi: 10.1371/journal.pone.0095265.
Whicher, C. A., O'Neill, S. and Holt, R. I. G. (2020) 'Diabetes in the UK: 2019.', *Diabetic medicine : a journal of the British Diabetic Association*. England, 37(2), pp. 242–247. doi: 10.1111/dme.14225.
White, S. J. *et al.* (2011) 'Characterization of the differential response of endothelial cells exposed to normal and elevated laminar shear stress', *Journal of Cellular Physiology*, 226(11), pp. 2841–2848. doi: 10.1002/jcp.22629.
White, S. J., Newby, A. C. and Johnson, T. W. (2016) 'Endothelial erosion of plaques as a substrate for coronary thrombosis', *Thrombosis and Haemostasis*, 115(3), pp. 509–519. doi: 10.1160/TH15-09-0765.
WHO (no date) *https://www.who.int/cardiovascular_diseases/publications/atlas_cvd/en/*.
Widder, J. D. *et al.* (2009) 'Attenuation of angiotensin II-induced vascular dysfunction and hypertension by overexpression of Thioredoxin 2.', *Hypertension (Dallas, Tex. : 1979)*, 54(2), pp. 338–344. doi: 10.1161/HYPERTENSIONAHA.108.127928.
Wolf, M. B. and Baynes, J. W. (2007) 'Cadmium and mercury cause an oxidative stress-induced endothelial dysfunction.', *Biometals : an international journal on the role of metal ions in biology, biochemistry, and medicine*. Netherlands, 20(1), pp. 73–81. doi: 10.1007/s10534-006-9016-0.
Wu, C.-C. *et al.* (2006) 'Shear stress regulation of Krüppel-like factor 2 expression is flow pattern-specific', *Biochemical and Biophysical Research Communications*, 341(4), pp. 1244–1251. doi: 10.1016/j.bbrc.2006.01.089.
Wu, D. *et al.* (2017) 'HIF-1alpha is required for disturbed flow-induced metabolic

reprogramming in human and porcine vascular endothelium.', *eLife*. England, 6. doi: 10.7554/eLife.25217.
Wu, K. K. *et al.* (2005) 'Increased hypercholesterolemia and atherosclerosis in mice lacking both ApoE and leptin receptor', *Atherosclerosis*, 181(2), pp. 251–259. doi: 10.1016/j.atherosclerosis.2005.01.029.
Xia, G. *et al.* (2001) 'Regulation of vascular endothelial growth factor transcription by endothelial PAS domain protein 1 (EPAS1) and possible involvement of EPAS1 in the angiogenesis of renal cell carcinoma.', *Cancer*. United States, 91(8), pp. 1429–1436.
Xiong, J. *et al.* (2018) 'A Metabolic Basis for Endothelial-to-Mesenchymal Transition', 69(4), pp. 689–698. doi: 10.1016/j.molcel.2018.01.010.A.
Xue, M. *et al.* (2008) 'Activation of NF-E2-related factor-2 reverses biochemical dysfunction of endothelial cells induced by hyperglycemia linked to vascular disease', *Diabetes*, 57(10), pp. 2809–2817. doi: 10.2337/db06-1003.
Xue, X. *et al.* (2012) 'Hypoxia-inducible factor-2α activation promotes colorectal cancer progression by dysregulating iron homeostasis', *Cancer Research*, 72(9), pp. 2285–2293. doi: 10.1158/0008-5472.CAN-11-3836.
Yamagishi, S. I. *et al.* (2001) 'Leptin induces mitochondrial superoxide production and monocyte chemoattractant protein-1 expression in aortic endothelial cells by increasing fatty acid oxidation via protein kinase A.', *The Journal of biological chemistry*. United States, 276(27), pp. 25096–25100. doi: 10.1074/jbc.M007383200.
Yamaguchi, Y. *et al.* (2000) 'Evidence of modified LDL in the plasma of hypercholesterolemic WHHL rabbits injected with aqueous extracts of cigarette smoke', *Environmental Toxicology and Pharmacology*, 8(4), pp. 255–260. doi: 10.1016/S1382-6689(00)00050-8.
Yamashita, T. *et al.* (2008) 'The microenvironment for erythropoiesis is regulated by HIF-2ά through VCAM-1 in endothelial cells', *Blood*, 112(4), pp. 1482–1492. doi: 10.1182/blood-2007-11-122648.
Yan, H. *et al.* (2012) 'Activation of the prolyl-hydroxylase oxygen-sensing signal cascade leads to AMPK activation in cardiomyocytes.', *Journal of cellular and molecular medicine*, 16(9), pp. 2049–2059. doi: 10.1111/j.1582-4934.2011.01500.x.
Yang, G., Lee, H. E. and Lee, J. Y. (2016) 'A pharmacological inhibitor of NLRP3 inflammasome prevents non-alcoholic fatty liver disease in a mouse model induced by high fat diet', *Scientific Reports*. Nature Publishing Group, 6(March), pp. 1–11. doi: 10.1038/srep24399.
Yang, M.-H. *et al.* (2008) 'Direct regulation of TWIST by HIF-1alpha promotes metastasis.', *Nature cell biology*. England, 10(3), pp. 295–305. doi: 10.1038/ncb1691.
Zakkar, M. *et al.* (2009) 'Activation of Nrf2 in endothelial cells protects arteries from exhibiting a proinflammatory state', *Arteriosclerosis, Thrombosis, and Vascular Biology*, 29(11), pp. 1851–1857. doi: 10.1161/ATVBAHA.109.193375.
Zarkesh-Esfahani, H. *et al.* (2001) 'High-dose leptin activates human leukocytes via receptor expression on monocytes.', *Journal of immunology (Baltimore, Md. : 1950)*. United States, 167(8), pp. 4593–4599.
Zeng, H. *et al.* (2015) 'High-fat diet induces cardiac remodelling and dysfunction: Assessment of the role played by SIRT3 loss', *Journal of Cellular and Molecular Medicine*, 19(8), pp. 1847–1856. doi: 10.1111/jcmm.12556.
Zhang, H. *et al.* (2011) 'Hypoxia-inducible factor directs POMC gene to mediate hypothalamic glucose sensing and energy balance regulation', *PLoS Biology*, 9(7), pp. 1–16. doi: 10.1371/journal.pbio.1001112.
Zhang, H. *et al.* (2012) 'HIF-1-dependent expression of angiopoietin-like 4 and L1CAM mediates vascular metastasis of hypoxic breast cancer cells to the lungs.', *Oncogene*, 31(14),

pp. 1757–1770. doi: 10.1038/onc.2011.365.
Zhang, M., Malik, A. B. and Rehman, J. (2014) 'Endothelial progenitor cells and vascular repair.', *Current opinion in hematology*, 21(3), pp. 224–228. doi: 10.1097/MOH.0000000000000041.
Zhang, X. *et al.* (2010) 'Adipose tissue-specific inhibition of hypoxia-inducible factor 1α induces obesity and glucose intolerance by impeding energy expenditure in mice', *Journal of Biological Chemistry*, 285(43), pp. 32869–32877. doi: 10.1074/jbc.M110.135509.
Zhang, X. *et al.* (2019) 'Adipocyte Hypoxia-Inducible Factor 2α Suppresses Atherosclerosis by Promoting Adipose Ceramide Catabolism', *Cell Metabolism*. Elsevier Inc., 30(5), pp. 937-951.e5. doi: 10.1016/j.cmet.2019.09.016.
Zhao, G. *et al.* (2020) 'Single cell RNA sequencing reveals the cellular heterogeneity of aneurysmal infrarenal abdominal aorta.', *Cardiovascular research*. doi: 10.1093/cvr/cvaa214.
Zhdanov, A. V. *et al.* (2015) 'A novel effect of DMOG on cell metabolism: Direct inhibition of mitochondrial function precedes HIF target gene expression', *Biochimica et Biophysica Acta - Bioenergetics*. Elsevier B.V., 1847(10), pp. 1254–1266. doi: 10.1016/j.bbabio.2015.06.016.
Zhou, G. *et al.* (2012) 'Brief report Endothelial Kruppel-like factor 4 protects against atherothrombosis in mice', 122(12), pp. 4727–4731. doi: 10.1172/JCI66056DS1.
Zhou, T. *et al.* (2016) 'Single cell transcriptome analysis of mouse carotid body glomus cells', *Journal of Physiology*, 594(15), pp. 4225–4251. doi: 10.1113/JP271936.
Zhou, Z. *et al.* (2011) 'Lipoprotein-derived lysophosphatidic acid promotes atherosclerosis by releasing CXCL1 from the endothelium.', *Cell metabolism*. United States, 13(5), pp. 592–600. doi: 10.1016/j.cmet.2011.02.016.
Zhuang, Z. *et al.* (2012) 'Somatic HIF2A gain-of-function mutations in paraganglioma with polycythemia', *New England Journal of Medicine*, 367(10), pp. 922–930. doi: 10.1056/NEJMoa1205119.